

Institute of Experimental and Clinical Pharmacology and Toxicology  
Faculty of Medicine  
Saarland University

**Pharmacological Modulation of Ca<sup>2+</sup> Leak through  
Sec61 Complexes of the Endoplasmic Reticulum**

**Dissertation for obtaining the university degree of**

**Doctor rerum naturalium**

**Igor Gamayun**

Born on 9<sup>th</sup> March 1987  
Kyiv, Ukraine

2017



*Dedicated to my family*

**Table of contents**

Table of contents.....	4
Abbreviations.....	7
List of Figures.....	10
List of Tables.....	11
1 Summary.....	12
2 Introduction.....	15
2.1 Ca <sup>2+</sup> in the organism.....	15
2.2 Ca <sup>2+</sup> homeostasis in the cell.....	15
2.2.1 Ca <sup>2+</sup> channels in the plasma membrane.....	17
2.2.2 Intracellular Ca <sup>2+</sup> channels.....	18
2.2.3 Ca <sup>2+</sup> pumps.....	19
2.2.4 Mitochondria.....	21
2.2.5 Endoplasmic reticulum.....	21
2.2.6 Theoretical modeling of Ca <sup>2+</sup> homeostasis.....	22
2.3 Sec61 complex.....	24
2.4 Human diseases related to the endoplasmic reticulum.....	29
2.5 Aims of the work.....	32
3 Materials and methods.....	33
3.1 Chemicals.....	33
3.2 Cell lines.....	34
3.2.1 HEK and HeLa cell lines.....	34
3.2.2 Cell culture.....	34
3.2.3 Preparation of cells for Ca <sup>2+</sup> imaging.....	34
3.3 Plasmids.....	35
3.3.1 D1ER.....	35
3.3.2 GFP analogue markers.....	36
3.3.3 Plasmid amplification.....	36
3.4 Analysis of protein expression levels.....	37
3.4.1 Rough microsomes.....	37
3.4.2 Primary and secondary antibodies.....	37
3.4.3 Western blot analysis.....	38
3.5 Generation of cell lines stably expressing D1ER.....	40
3.5.1 General principles of transfection.....	40
3.5.2 Transfection of D1ER pcDNA3.....	40

---

3.6	Selection of cell clones stably expressing D1ER .....	41
3.6.1	Analysis of D1ER fluorescence levels.....	41
3.6.2	FACS.....	41
3.6.3	Sub-cloning and clonal expansion .....	41
3.6.4	Culture of D1ER cell lines .....	42
3.6.5	ER stress check in generated cell lines stably expressing D1ER.....	42
3.7	Gene silencing .....	43
3.7.1	General principles for gene silencing .....	43
3.7.2	“Small interference” RNA oligonucleotides.....	46
3.7.3	Silencing of <i>SEC61A1</i> .....	47
3.7.4	Silencing of <i>ERj3</i> and <i>ERj6</i> co-chaperones .....	48
3.8	Silencing efficiency.....	49
3.9	Recording solutions.....	50
3.10	Chemical compounds and cell treatment.....	52
3.10.1	Compounds .....	52
3.10.2	“Online” treatment protocol.....	53
3.10.3	“Offline” treatment protocol .....	54
3.11	Single cell calcium imaging .....	54
3.11.1	Ratiometric measurements of cytosolic Ca <sup>2+</sup> with FURA-2.....	54
3.11.2	Principles of FRET-based measurements of ER Ca <sup>2+</sup> with D1ER .....	56
3.12	Imaging setup .....	60
3.12.1	iMIC microscope and illumination system.....	60
3.12.2	Optical filters .....	62
3.12.3	Software control.....	62
3.13	Simultaneous measurement of FURA-2 and D1ER signals.....	63
3.13.1	Spectral overlap of FURA-2 and D1ER fluorescence .....	63
3.13.2	Bleed through.....	65
3.13.3	Calibration of FURA-2 signals .....	68
3.13.4	Calibration of D1ER signals .....	69
3.14	Analysis and Ca <sup>2+</sup> imaging data .....	75
3.15	Statistical analysis.....	77
4	Results.....	78
4.1	Analysis of endoplasmic reticulum Ca <sup>2+</sup> efflux .....	78
4.2	Effects of protein synthesis inhibitors on Ca <sup>2+</sup> homeostasis.....	83
4.3	Effect of Sec61 $\alpha$ silencing on endoplasmic reticulum Ca <sup>2+</sup> leak.....	90
4.4	Effect of Calmodulin and UPR on ER Ca <sup>2+</sup> leak .....	93

---

4.5	Summarizing analysis of endoplasmic reticulum $\text{Ca}^{2+}$ leak through Sec61 complexes .....	96
4.6	Cytosolic-endoplasmic reticulum $\text{Ca}^{2+}$ relationship of $\text{Ca}^{2+}$ leak through Sec61 complexes .....	102
4.7	Endoplasmic reticulum $\text{Ca}^{2+}$ leak mediated by luminal co-chaperones .....	111
4.8	Mycolactone and endoplasmic reticulum $\text{Ca}^{2+}$ homeostasis.....	113
4.9	Effect of eeyarestatin 1 and its analogues on $\text{Ca}^{2+}$ homeostasis .....	120
5	Discussion.....	131
5.1	The direct measurement of the $\text{Ca}^{2+}$ concentration in the ER gives the better insight of the functioning of this organelle about the $\text{Ca}^{2+}$ homeostasis .....	131
5.2	The correct estimation of the ER $\text{Ca}^{2+}$ content and dynamics remains to be a challenge for every cell line.....	133
5.3	The analysis of the ER $\text{Ca}^{2+}$ leak kinetics gives important numbers .....	134
5.4	The main point of my study was to determine the leak through Sec61 $\alpha$ complex in the ER membrane.....	136
5.5	The cells should deal with Sec61 $\alpha$ -mediated $\text{Ca}^{2+}$ leak.....	139
5.6	Two compounds mycolactone and eeyarestatin with previously unknown action on Sec61 $\alpha$ were tested in the present study .....	140
5.7	The conclusions of this study can be presented as a model of $\text{Ca}^{2+}$ leak during secretory and membrane protein biosynthesis .....	141
6	References.....	143
7	Publications.....	152
8	Acknowledgements.....	153

## Abbreviations

°C	degree Celsius
μ	micro-
Å	angstrom
AM	acetoxymethylester
AMPS	2-Acrylamido-2-methylpropane sulfonic acid
ATP	adenosine triphosphate
avg	average
BAPTA	1,2-bis( <i>o</i> -aminophenoxy)ethane- <i>N,N,N',N'</i> -tetraacetic acid
Bcl-2	B-cell lymphoma
bg	background
BiP/GRP78	binding immunoglobulin protein/glucose regulated protein 78
CaM	calmodulin
CCCP	carbonyl cyanide <i>m</i> -chlorophenyl hydrazone
CCD	charge-coupled device
CHX	cycloheximide
cyt	cytosolic
DMSO	dimethyl sulfoxide
DNA	deoxyribonucleic acid
<i>E.coli</i>	<i>Escherichia coli</i>
eCFP	enhanced cyan fluorescent protein
EGTA	ethylene glycol-bis(β-aminoethyl ether)- <i>N,N,N',N'</i> -tetraacetic acid
eIF2a	eukaryotic initiation factor 2 a
EM	electron microscopy
EME	emetine
ER	endoplasmic reticulum
ERAD	ER associated degradation
ERj	ER-associated dnaJ protein
ES	evarestatin
ext.	external
FCS	Fetal calf serum
FP	fluorescent protein
g	gramm
G418	geneticin
GECI	genetically encoded calcium indicator
GFP	green fluorescent protein
GPCR	G-protein coupled receptor
GRP170	glucose regulated protein 170
HEK	human embryonic kidney
HEPES	4-(2-hydroxyethyl)-1-piperazineethanesulfonic acid
IMM	inner mitochondrial membrane
IONO	ionomycin
IP3	inositol triphosphate

kbp	kilobasepairs
$K_D$	dissociation constant
LB medium	Lysogeny broth medium
Log-	logarithmic
m	meter
M	molar (mol per liter)
M13	truncated part of myosin light chain kinase
mA	milliampere
max	maximal
MCU	mitochondrial calcium uniporter
MEM	minimal essential medium
min	minimal
mm	millimeter
ms	milliseconds
mRNA	messenger RNA
n	nano-
n.s.	not significant
Na <sub>3</sub> -HEDTA	trisodium salt of N-(hydroxyethyl)-ethylenediaminetriacetic acid
NCX	sodium-calcium exchanger
NHDF	Nucleofector Kit for Human Dermal Fibroblasts
NTA	nitrilotriacetic acid
OMM	outer mitochondrial membrane
PAC	pactamycin
PBS	phosphate-buffered saline
pcDNA	plasmid cytomegalovirus promoter DNA Vector
PLC	phospholipase C
PDI	protein disulfide isomerase
PMCA	plasma membrane calcium ATPase
PMSF	phenylmethylsulfonyl fluoride
PUR	puromycin
PVDF	polyvinylidene fluoride
RISC	RNA induced silencing complex
RM	rough microsomes
RNA	ribonucleic acid
ROI	region of interest
RT	room temperature
RyR	ryanodine receptor
s	seconds
s.e.m.	standart error of the mean
scrRNA	scrambled RNA, negative control RNA nucleotide sequence
SDS	sodium dodecyl sulfat
SERCA	sarcoplasmic/endoplasmic reticulum calcium ATPase
siRNA	small interference RNA, silencing RNA
SPCA	secretory pathway calcium ATPase

SRP	signal recognition particle
STIM	stromal interaction molecule
TFP	trifluoperazine
TM	transmembrane domain
TUN	tunicamycin
UPR	unfolded protein response
v/v	volume to volume proportion
VDAC	voltage-dependent anion channel
w/v	weight to volume proportion
WB	western blot
wt	wild type / untransfected

## List of Figures

Figure 2.1. General scheme of Ca <sup>2+</sup> signaling in the cell. ....	16
Figure 2.2. Simplified model of the cell shows main Ca <sup>2+</sup> fluxes. ....	23
Figure 2.3. Translocation process. ....	25
Figure 2.4. Ribosome-translocon interaction. ....	27
Figure 2.5. Lateral gate opening of Sec61. ....	28
Figure 2.6. Putative Ca <sup>2+</sup> leakage through Sec61. ....	29
Figure 3.1. pcDNA3 plasmid map of Ca <sup>2+</sup> sensitive D1ER chameleon. ....	36
Figure 3.2. Morphological diversity of D1ER clones during cell line creation. ....	42
Figure 3.3. D1ER stable cell lines check, whether expression of the chameleon causes ER stress. ....	43
Figure 3.4. Transfection efficiency of siRNA in HEK cells. ....	45
Figure 3.5. Silencing efficiency with AMAXA. ....	48
Figure 3.6. Dose dependence of siRNA on silencing efficiency. ....	49
Figure 3.7. FURA-2. ....	55
Figure 3.8. Principles of Förster Resonance Energy Transfer (FRET). ....	58
Figure 3.9. Schematic structural conformation changes of the D1ER molecule upon Ca <sup>2+</sup> binding. ....	59
Figure 3.10. System used for simultaneous imaging of cytosolic and ER Ca <sup>2+</sup> . ....	61
Figure 3.11. Comparison of excitation and emission spectra of FURA-2 and fluorophores of D1ER. ....	64
Figure 3.12. Bleed-through in simultaneous measurements of cytosolic and ER Ca <sup>2+</sup> with FURA-2 and D1ER respectively. ....	67
Figure 3.13. Experimental calibration of FURA-2 on iMIC System. ....	69
Figure 3.14. Determining of the dynamic range of D1ER in HEK D1ER cells. ....	70
Figure 3.15. Analysis of extreme D1ER signal (FRET Ratio) values in HEK D1ER cells. ....	71
Figure 3.16. Obtaining of D1ER K <sub>D</sub> <i>in vivo</i> . ....	72
Figure 3.17. Correction of a FRET Ratio signal. ....	73
Figure 3.18. ER Ca <sup>2+</sup> distribution. ....	74
Figure 3.19. Correction of FURA-2 ratio signal. ....	75
Figure 3.20. FRET ratio traces smoothed by Savitzky-Goley digital filtering. ....	77
Figure 4.1. Analysis of ER Ca <sup>2+</sup> efflux. ....	81
Figure 4.2. Effect of extracellular Ca <sup>2+</sup> on thapsigargin-evoked store depletion. ....	84
Figure 4.3 Effect of protein synthesis inhibitors on Ca <sup>2+</sup> leak. ....	89
Figure 4.4 Effect of Sec61a silencing on ER Ca <sup>2+</sup> efflux. ....	91
Figure 4.5. Effect of Calmodulin and UPR on ER Ca <sup>2+</sup> leak. ....	94
Figure 4.6. Numerical approach on the normalized traces. ....	100
Figure 4.7. Estimation of ER Ca <sup>2+</sup> leakage through Sec61 complex. ....	101
Figure 4.8. Clearance mechanisms of Ca <sup>2+</sup> leak from the Sec61. ....	103
Figure 4.9. Dose-dependent effects to puromycin on Ca <sup>2+</sup> leak from ER. ....	106
Figure 4.10. Dose dependent effect of pactamycin. ....	108
Figure 4.11. Online effect of pactamycin. ....	109
Figure 4.12. Effect of ERj3 and ERj6 on intracellular Ca <sup>2+</sup> signalization. ....	112
Figure 4.13. Mycolactone 1.5 hours on HEK D1ER cells. ....	114
Figure 4.14. Mycolactone “online” on HEK D1ER cells. ....	115

Figure 4.15. Mycolactone overnight on HEK D1ER cells. ....	117
Figure 4.16. Mycolactone 6 hours on HEK D1ER cells. ....	118
Figure 4.17. Enhanced $\text{Ca}^{2+}$ leak induced by mycolactone. ....	119
Figure 4.18. Structure of eeyarestatins. ....	120
Figure 4.19. Effect of ES1 on $\text{Ca}^{2+}$ homeostasis. ....	121
Figure 4.20. Comparison of ES1, ES2 and ES24 on $\text{Ca}^{2+}$ homeostasis. ....	123
Figure 4.21. Effect of ESr35 and ES47 on $\text{Ca}^{2+}$ homeostasis. ....	124
Figure 4.22. Differential effects of ES1 at different incubation times. ....	126
Figure 4.23. Effect of silencing of Sec61 on ES1-evoked ER $\text{Ca}^{2+}$ leakage. ....	128
Figure 4.24. Effect of silencing of Sec61 on ES24-evoked ER $\text{Ca}^{2+}$ leakage. ....	129
Figure 5.1. ER $\text{Ca}^{2+}$ distribution in non-excitabile cells. ....	134
Figure 5.2. $\text{Ca}^{2+}$ fluxes during secretory and membrane protein biosynthesis. ....	142

## List of Tables

Table 2.1. Major agents of protein translocation:.....	26
Table 3.1 Chemical substances.....	33
Table 3.2 Primary and Secondary Antibodies.....	37
Table 3.3 Casting gels for Immunoblot analysis. ....	39
Table 3.4. siRNAs and their sense sequences. ....	46
Table 3.5 Experimental solutions:.....	50
Table 3.6. $\text{Ca}^{2+}$ -saturation extracellular.....	50
Table 3.7. $\text{Ca}^{2+}$ -depletion solution. ....	51
Table 3.8. Intracellular-like “0” solution. ....	51
Table 3.9. $\text{Ca}^{2+}$ calibration steps.....	52
Table 3.10. Excitation and emission of D1ER and FURA-2 during experiments.*LP- long path filter. ....	62
Table 4.1 Effect of protein synthesis inhibitors on $\text{Ca}^{2+}$ leakage. ....	88

## 1 Summary

The co-translational translocation is an essential mechanism in the biosynthesis of secretory proteins, which require targeting to the ER, and thus to the secretory pathway. The association of a ribosome-nascent chain complex with a Sec61 complex leads to conformational changes resulting in the opening of Sec61 $\alpha$ , the main gate for protein translocation on the ER membrane. Forming a large pore for polypeptide transport, Sec61 $\alpha$  also supports Ca<sup>2+</sup> leak from the ER. However, so far, the role of Sec61 $\alpha$  in the Ca<sup>2+</sup> homeostasis during protein biosynthesis remained unclear. In the present study, I quantified the Sec61 $\alpha$ -mediated Ca<sup>2+</sup> leak, its modulation during protein biosynthesis, and its contribution to the total basal ER Ca<sup>2+</sup> leak of the cell. The quantification was done using single cell Ca<sup>2+</sup> imaging performed with FURA-2 dye for cytosolic Ca<sup>2+</sup> and D1ER, a genetically encoded indicator, for ER Ca<sup>2+</sup>. For this purpose, new cell lines based on HEK293 and HeLa cells were created by introducing D1ER into the ER. Direct measurements of ER Ca<sup>2+</sup> showed that the average basal Ca<sup>2+</sup> leak rate was  $2.34 \pm 0.15$   $\mu\text{M/s}$  at rest. Treatment of the cells with small molecules (protein synthesis inhibitors, calmodulin inhibitor, N-linked glycosylation inhibitor) was done to induce states of Sec61 complexes, at which Sec61 $\alpha$  mimics natural translocation steps: occupied with polypeptide chains, releasing polypeptide chains or being free from translocation. At these extreme states of co-translational translocation, the ER Ca<sup>2+</sup> leak rate was estimated. Comparing to the basal levels at rest, it decreased to 42-59% upon occupation of Sec61 $\alpha$  with polypeptide chains and also after silencing of *SEC61A1*, the Sec61 $\alpha$  encoding gene, and conversely increased to 172-185% upon polypeptide chain releasing from the Sec61 $\alpha$ . In addition, two new compounds, mycolactone and eeyarestatin were tested. The decrease of ER Ca<sup>2+</sup> content induced by mycolactone required rather long incubation time, whereas acute application of eeyarestatin had an immediate effect in disrupting Ca<sup>2+</sup> homeostasis. The lack of eeyarestatin effects after *SEC61A1* silencing suggests that eeyarestatin directly promotes the Ca<sup>2+</sup>-permeable state of Sec61 $\alpha$ . In conclusion, Sec61 complexes support Ca<sup>2+</sup> leak in the ribosome-bound, idle state, and the fraction of Sec61 $\alpha$ -mediated Ca<sup>2+</sup> leak is 41-58% of the basal ER Ca<sup>2+</sup> leak rate, while a pharmacological modulation of Sec61 complexes could significantly increase the ER Ca<sup>2+</sup> leak rate. Taken together, this study provides a comprehensive semi-quantitative model of the Ca<sup>2+</sup> leak that is tightly bound to each step of secretory protein biosynthesis.

## Zusammenfassung

Die kotranslationale Translokation ist ein essentieller Mechanismus in der Biosynthese sekretorischer Proteine, die einen Transport ins endoplasmatische Retikulum (ER) zur Sekretion erfordern. Die Anlagerung eines Ribosom-naszierenden Kettenkomplexes an einen Sec61 Komplex führt zu einer Konformationsänderung und Öffnung von Sec61 $\alpha$ , welches den Hauptweg für die Proteintranslokation über die Membran des ER darstellt. Durch die Ausbildung einer großen Pore zum Transport von Polypeptiden führt Sec61 $\alpha$  auch zu einer Ca<sup>2+</sup> Freisetzung aus dem ER. Die Rolle von Sec61 $\alpha$  an der Ca<sup>2+</sup> Homöostase während der Proteinbiosynthese ist bisher jedoch nicht bekannt. In der vorliegenden Arbeit habe ich die Sec61 $\alpha$ -abhängige Ca<sup>2+</sup> Freisetzung, ihre Modulation während der Proteinbiosynthese, sowie ihr Anteil an der totalen basalen Ca<sup>2+</sup> Freisetzung aus dem ER quantifiziert. Dazu wurden Ca<sup>2+</sup> Imaging Experimente mit Hilfe von FURA-2 zur Detektion des zytosolischen Ca<sup>2+</sup> und D1ER, einem genetisch kodierten Ca<sup>2+</sup> Indikator zur Messung des Ca<sup>2+</sup> im ER an Einzelzellen durchgeführt. Hierfür wurden neue HEK293 und HeLa Zelllinien mit D1ER im ER hergestellt. Messungen des ER Ca<sup>2+</sup> ergaben unter Ruhebedingungen eine mittlere basale Freisetzungsrates von  $2.34 \pm 0.15 \mu\text{M/s}$ . Durch die Behandlung der Zellen mit kleinen Molekülen (Inhibitoren der Proteinsynthese, Calmodulin-Inhibitoren und Inhibitoren der N-verknüpften Glykosylierung) wurde der Sec61 Komplex in Stadien versetzt, welche die natürlichen Schritte der Translokation nachahmen: besetzt mit einer Polypeptidkette, Freigabe von Polypeptidketten und ohne Translokationsaktivität. Zu all diesen extremen Stadien der kotranslationalen Translokation wurde die Ca<sup>2+</sup> Freisetzungsrates aus dem ER gemessen. Im Vergleich zum basalen Wert in Ruhe reduzierte sich die Ca<sup>2+</sup> Freisetzungsrates auf 42-59% wenn Sec61 $\alpha$  mit einer Polypeptidkette besetzt war oder wenn *SEC61A1*, das Sec61 $\alpha$ -kodierende Gen, stillgelegt wurde. Im Gegensatz dazu erhöhte sich die Ca<sup>2+</sup> Freisetzungsrates auf 172-185% wenn die Polypeptidkette von Sec61 $\alpha$  freigegeben wurde. Zudem wurden die neuen Substanzen Mycolactone und Eeyarestatin auf die Ca<sup>2+</sup> Veränderung im ER getestet. Mycolactone benötigte eine lange Inkubationszeit zur Reduktion der Ca<sup>2+</sup> Konzentration im ER, wohingegen die akute Applikation von Eeyarestatin unmittelbar die Ca<sup>2+</sup> Homöostase unterbrach. Die Abwesenheit des Effektes von Eeyarestatin nach Stilllegen des *SEC61A1* Genes weist darauf hin, dass Eeyarestatin Sec61 $\alpha$  direkt in ein Ca<sup>2+</sup> permeables Stadium versetzt. Schlussfolgernd lässt sich sagen,

dass i) Sec61 Komplexe eine  $\text{Ca}^{2+}$  Freisetzung begünstigen wenn Sie an ein Ribosom gebunden und frei von einer Polypeptidkette sind, ii) die Sec61 $\alpha$ -abhängige  $\text{Ca}^{2+}$  Freisetzung 40-60% der basalen  $\text{Ca}^{2+}$  Freisetzung aus dem ER ausmacht, und iii) eine pharmakologische Modulation des Sec61 Komplexes die  $\text{Ca}^{2+}$  Freisetzungsratesignifikant erhöhen kann. Zusammengefasst liefert die vorliegende Studie ein umfassendes semiquantitatives Modell der  $\text{Ca}^{2+}$  Freisetzung aus dem ER, die eng mit allen Schritten der Biosynthese sekretorischer Proteine verknüpft ist.

## 2 Introduction

### 2.1 $\text{Ca}^{2+}$ in the organism

Calcium ( $\text{Ca}^{2+}$ ) has been studied for decades and the relevance of its role in the physiological and pathological states is becoming more and more evident each year. The ions of  $\text{Ca}^{2+}$  can function as the first, the second and even the third intracellular messenger (Clapham 2007).  $\text{Ca}^{2+}$  is ideally suited for these roles due to its stereochemistry. Indeed, usually there are 6-8 oxygen atoms (4-12 in general) accommodated in the  $\text{Ca}^{2+}$  coordination sphere that makes its size around 2.5 Å. At the same time the closest ion to  $\text{Ca}^{2+}$ , the magnesium ion ( $\text{Mg}^{2+}$ ), can accommodate only up to 6 oxygen atoms in its coordination sphere, which results in the smaller size of about 2 Å. This seriously restricts the flexibility of ion-protein complexes and dramatically diminishes the binding abilities of  $\text{Mg}^{2+}$ . The “importance” of  $\text{Ca}^{2+}$  for physiological processes was first revealed with the discovery of its role in heart by Sydney Ringer in the 1880s (Miller 2004, Ringer 1883), and later it was found that calcium is essential for processes among almost all living systems inside the organism: from gene expression to complex brain functioning and memory (Brini and Carafoli 2009).

### 2.2 $\text{Ca}^{2+}$ homeostasis in the cell

The homeostasis of  $\text{Ca}^{2+}$  inside the cell can be generally understood as all processes, which happen with this ion. Calcium ions ( $\text{Ca}^{2+}$ ) show a distinct spatial distribution inside the cell with tightly controlled dynamics (Dupont et al. 2011).  $\text{Ca}^{2+}$  is involved in both endo- and exocytosis, protein transport and activation of kinases (Brini and Carafoli 2009, Cullen 2003). Various  $\text{Ca}^{2+}$  pumps and channels are widely distributed inside the cell and cellular compartments (Figure 2.1). Entering the cell through plasma membrane  $\text{Ca}^{2+}$  channels (Clapham 2007),  $\text{Ca}^{2+}$  can activate several signaling pathways as a second messenger and then can be bound by intracellular calcium buffers (Bers 2014). Both mitochondria and SERCA pumps transport  $\text{Ca}^{2+}$  from the cytosol into intracellular compartments and at the same time the excess of  $\text{Ca}^{2+}$  in the cytosol can be extruded to the extracellular space by PMCA (Lewis 2001). The presence of  $\text{Ca}^{2+}$  in mitochondria is

required for the correct functioning of the respiratory chain and ER-cytosol  $\text{Ca}^{2+}$  balance is important for intracellular function (Griffiths and Rutter 2009).

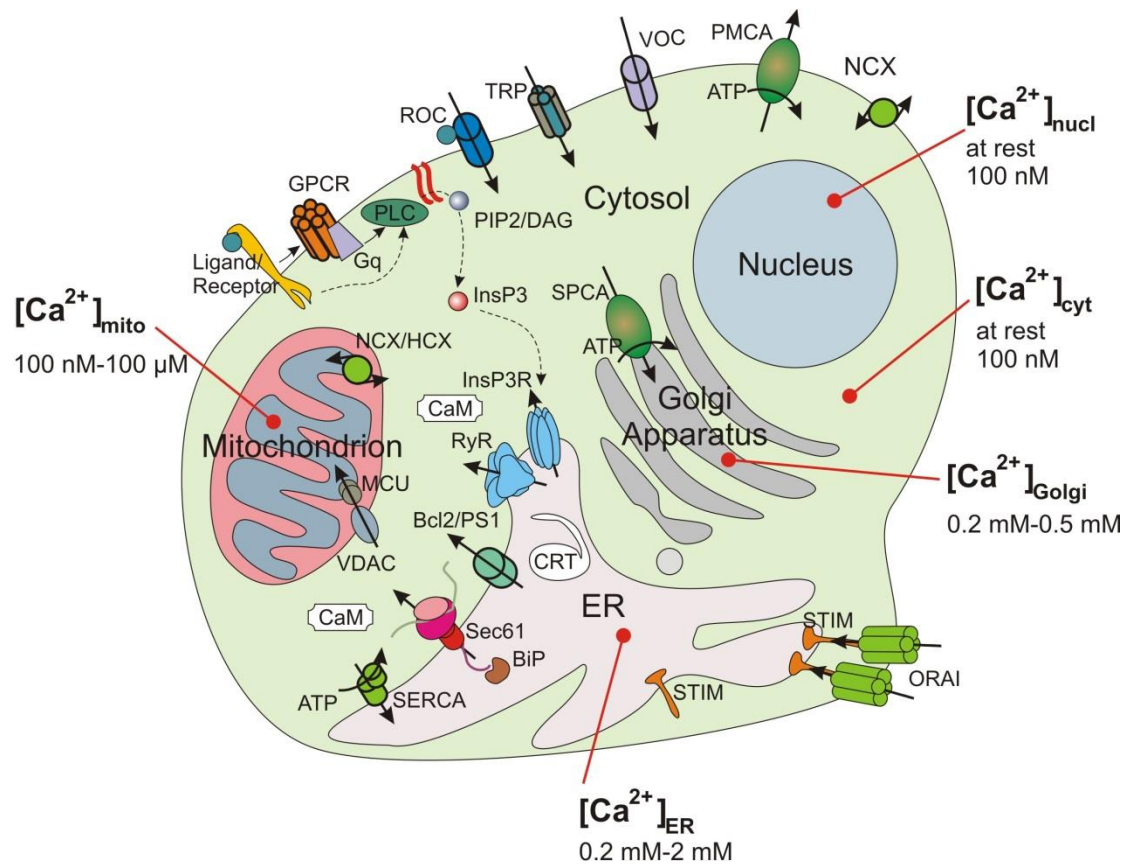


**Figure 2.1.** General scheme of  $\text{Ca}^{2+}$  signaling in the cell.  $\text{Ca}^{2+}$  entry to the cytosol through channels depicted as ROC (receptor operated channels), VOC (voltage operated channels), TRP (transient receptor potential), and ORAI channels activated via stromal interference molecule (STIM).  $\text{Ca}^{2+}$  flux from the endoplasmic reticulum (ER) through activation of the GPCR (G-protein coupled receptors) pathway with activation of phospholipase C (PLC), synthesis of (PIP2)/diacylglycerol (DAG) and inositol-3-phosphate (InsP3), which in turn activates inositol-3-phosphate receptors on the ER membrane for  $\text{Ca}^{2+}$  release from the ER. Ryanodine receptor (RyR) also releases ER  $\text{Ca}^{2+}$  after activation with ryanodine (not shown). The ER  $\text{Ca}^{2+}$  leakage into cytosol can be mediated by Bcl2 and presenilin1 (Bcl2/PS1) and also through a translocon (Sec61). This can be attenuated by calmodulin (CaM) which is also a cytosolic calcium buffer. Intraluminal buffering occurs by calreticulin (CRT). Cytosolic  $\text{Ca}^{2+}$  clearance mechanisms shown as sarcoplasmic-endoplasmic reticulum calcium ATPase (SERCA), plasma membrane calcium ATPase (PMCA) and secretory pathway calcium ATPase (SPCA) of Golgi Apparatus. In addition, sodium-calcium exchanger (NCX) of plasma membrane, sodium-calcium exchanger and proton-calcium exchanger (NCX/HCX) of mitochondrion together with voltage-dependent anion channel

(VDAC) and mitochondrial calcium uniporter (MCU) help to maintain low cytosolic  $\text{Ca}^{2+}$  level.

### 2.2.1 $\text{Ca}^{2+}$ channels in the plasma membrane

The entering of  $\text{Ca}^{2+}$  from the extracellular milieu into the cytosol happens through the plasma membrane  $\text{Ca}^{2+}$  channels. There are several types of  $\text{Ca}^{2+}$  channels on the plasma membrane: receptor activated (receptor operated) channels, which are activated via binding to the extracellular ligand; store operated channels, which open under store depletion conditions, and voltage gated channels that react to changes of the membrane potential.

Voltage-gated channels transduce electric stimulation of the cell into  $\text{Ca}^{2+}$  transients and are present in excitable, neuro- and endocrine cells (Catterall 2011). They were identified and divided into several groups based on their pore forming subunit and the particular current-voltage relationship: L, P/Q, N, R and T-type channels. Each group of the channels has distinct activation and inactivation kinetics. They are highly selective for  $\text{Ca}^{2+}$ , despite of the presence of smaller “biological” ions such as  $\text{N}^+$ ,  $\text{K}^+$  and  $\text{Cl}^-$  (Tang et al. 2014). All voltage-gated  $\text{Ca}^{2+}$  channels can also be grouped into three subfamilies: Cav1, Cav2, and Cav3 (Catterall 2011). The Cav1 subfamily mediates the L-type current that plays a role in muscle contraction, hormone secretion, regulation of gene expression, and integration of synaptic signals. The Cav2 subfamily channels initiate synaptic transmission at fast synapses, providing release of neurotransmitters and form N-type, P/Q and R currents. The Cav3 subfamily supports T-type  $\text{Ca}^{2+}$  current and are responsible for the repetitive firing of action potentials (Cain and Snutch 2013).

Receptor-activated channels, or ligand-activated channels, need a special molecule (ligand) for the activation. Glutamate receptor channels belong to receptor-activated channels that have been shown to have an important function in the mammalian brain. Glutamate plays a very important role in synaptic transmission via activation of two types of receptors: metabotropic (mGluR) and ionotropic (iGluR). iGluRs are activated by specific agonists: AMPA, NMDA and KA (kainate),. Metabotropic receptors function through binding to the G-proteins. In turn they activate PLC reaction cascades and can also inhibit or activate adenylyl cyclase. mGluRs are present in the nervous system and their malfunctioning leads to pathological states and diseases (Traynelis et al. 2010).

There are special sensors in cells, that react to ER  $\text{Ca}^{2+}$  depletion by activating store-operated channels (Parekh and Putney 2005). ER depletion can be evoked by disrupting the  $\text{Ca}^{2+}$  balance between the cytosol and the lumen (for instance by inhibiting SERCA pumps), or by the release of  $\text{Ca}^{2+}$  through the channels present on the ER membrane, such as those activated by inositol-3-phosphate (InsP3). The receptor that detects ER depletion, called STIM (stromal interaction molecule), is an ER membrane spanning protein, which is bound to  $\text{Ca}^{2+}$  from the luminal side (Stathopoulos and Ikura 2013). ER  $\text{Ca}^{2+}$  depletion causes the unfolding of STIM molecules. Then the unfolded STIM molecules bind to the ORAI proteins of the plasma membrane forming  $\text{Ca}^{2+}$  channels. This occurs in the regions where ER is close to the plasma membrane (ER-PM junctions) and the oligomerization of STIM-ORAI complexes is required (Feske et al. 2015, Prakriya 2013). This process, called store-operated  $\text{Ca}^{2+}$  entry, was, for instance, observed as a prolonged activation signal in cells such as mast cells or T-lymphocytes (Lewis 2001).

The most recently discovered class of plasma membrane channels, that are critical for  $\text{Ca}^{2+}$  homeostasis, is transient receptor potential (TRP) channels, which have been originally proposed as store-operated channels. They are comprised into several groups according to their activation properties: TRPC (canonical), TRPA (ankyrin), TRPV (vanilloid), TRPM (melastatin), TRPML (mucolipin) and TRPP (polycystin). They are usually activated by  $\text{PIP}_2$  following receptor activation, can be regulated by  $\text{Ca}^{2+}$  and also show non-specific conductance (Flockerzi 2007). The question of the assembling oligomers of different types of TRP channels to form new functional complexes has been a very recent topic in this field (Stewart et al. 2010).

### **2.2.2 Intracellular $\text{Ca}^{2+}$ channels**

The intracellular  $\text{Ca}^{2+}$  stores also have sites that are permeable for  $\text{Ca}^{2+}$  (Krause 1991). These include  $\text{Ca}^{2+}$  transporters and channels on the endoplasmic/sarcoplasmic reticulum (ER/SR) membrane,  $\text{Ca}^{2+}$  ATPase of the Golgi Apparatus and mitochondrial pumps and exchangers (Brini and Carafoli 2009). The most well studied of the receptor activated intracellular channels on the ER membrane are inositol 3-phosphate receptor (InsP3R) and ryanodine receptor (RyR) channels (Camello et al. 2002). InsP3R is a large protein (240 kDa) with six transmembrane helices, which form a  $\text{Ca}^{2+}$  channel on the ER

membrane (Hattori et al. 2004). This ubiquitous channel is activated through binding to inositol-3-phosphate (InsP3), which is produced by phospholipase C (PLC). InsP3 participates actively in intracellular  $\text{Ca}^{2+}$  signaling and  $\text{Ca}^{2+}$  oscillations and can be modulated by CaM or  $\beta$ 3-subunits of the Cav channels. InsP3R are also sensitive to  $\text{Ca}^{2+}$  both from the lumen and the cytosol, which are proposed to be the site of regulation and attenuation mechanism of InsP3R activity (Taylor and Laude 2002). RyRs are very important proteins. They are the largest discovered class of channels; as homo-tetramers with a mass of ~2 MDa (Zalk et al. 2007, Zalk et al. 2015). RyRs are widely present in muscles, where they participate in muscle contraction (RyR1 in skeletal and heart muscles), are also present in Purkinje neurons in the cerebellum and cerebral cortex (RyR2), and in almost every tissue (RyR3, low expression). RyRs are known to have spontaneous activation forming a  $\text{Ca}^{2+}$  spark in the cytosol, supporting  $\text{Ca}^{2+}$  leak from SR in muscle cells (Bers 2014).

The next group of proteins, the B cell lymphoma-2 (Bcl-2) family of proteins, was proposed to be a key player in apoptosis (Czabotar et al. 2014). One of the mechanisms by which Bcl-2 induces apoptosis is tightly regulated by  $\text{Ca}^{2+}$  signaling (Rong and Distelhorst 2008). Upon sustained  $\text{Ca}^{2+}$  elevation in the cytosol,  $\text{Ca}^{2+}$  leak from the ER is enhanced, mitochondria absorbs  $\text{Ca}^{2+}$  which can lead to the opening of the mitochondrial permeability transition pore (mPTP) and *cytochrome c* release, which, in turn leads to caspase cascade activation and cell death. Bcl-2 can be localized in the ER membrane (Krajewski et al. 1993) attenuating  $\text{Ca}^{2+}$  uptake by SERCA and enhancing or inhibiting leak from InsP3 channels (Bonneau et al. 2013, Distelhorst and Bootman 2011).

Another protein family associated with cell death (neuronal cells) are presenilins, which form the  $\gamma$ -secretase complex responsible for  $\beta$ -amyloid formation and causing familial Alzheimer disease (Zhang et al. 2010). This nine transmembrane structure complex of presenelin protein has been proposed (Laudon et al. 2005) to be also located on the ER membrane, forming a  $\text{Ca}^{2+}$  leak channel (Annaert et al. 1999, Supnet and Bezprozvanny 2011) and modulating the  $\text{Ca}^{2+}$  homeostasis (Honarnejad and Herms 2012). Presenilins are also essential in neuronal signaling (Zhang et al. 2009).

### **2.2.3 $\text{Ca}^{2+}$ pumps**

Unlike  $\text{Ca}^{2+}$  channels, the movement of  $\text{Ca}^{2+}$  ions across the membranes against the concentration gradient requires active ion transport. The transporters that require ATP

hydrolysis for carrying of ions through biological membranes are called pumps (ion ATPase).  $\text{Ca}^{2+}$  pumps are present in the plasma membrane, the ER/SR membrane, and in the membrane of Golgi apparatus (Brini and Carafoli 2009). All pumps have a higher affinity to  $\text{Ca}^{2+}$  at the side with lower  $\text{Ca}^{2+}$  concentration and lower affinity to  $\text{Ca}^{2+}$  at the side with higher  $\text{Ca}^{2+}$  concentration (Carafoli and Brini 2000); this explains the turnover mode of sarco-endoplasmic reticulum ATPases (SERCA pumps) under severe depletion of the ER (Shannon et al. 2000). SERCA pumps move two  $\text{Ca}^{2+}$  ions inside the ER lumen with the hydrolysis of one ATP molecule from the cytosolic side. This sets thermodynamic boundaries on the concentration of free  $\text{Ca}^{2+}$ , which can be pumped into the ER (Shannon and Bers 1997). Cloning experiments showed that three families of SERCA are expressed in different tissues: SERCA1a and SERCA1b are expressed in the skeletal muscles, SERCA2a in the heart, skeletal muscles, smooth muscles and SERCA2b is ubiquitously expressed. SERCA2 can be regulated by PKA via phosphorylating phospholamban, which when in an unphosphorylated state inhibits SERCA activity (Periasamy et al. 2008). SERCA3, due to its low affinity to  $\text{Ca}^{2+}$ , is supposed to be active only if cytosolic  $\text{Ca}^{2+}$  reaches extremely high levels. Secretory pathway  $\text{Ca}^{2+}$  ATPases (SPCAs) are located in the Golgi complex and are supposed to be active in cells with high secretory activity and are presented in two isoforms; SPCA1 and SPCA2 (for details see (Brini and Carafoli 2009)). Plasma membrane  $\text{Ca}^{2+}$  ATPases (PMCAs) are presented in four isoforms (PMCA1-4) and are widely distributed in the organism. They have affinity to calmodulin (PMCA2 and PMCA3 > PMCA1 and PMCA4), which inhibits the pump activity. PMCAs remove  $\text{Ca}^{2+}$  from the cytosol to the extracellular space, performing a very important clearance function, which prevents the cell from  $\text{Ca}^{2+}$  overload. PMCA can be inhibited by lanthanides such as  $\text{La}^{3+}$  or  $\text{Gd}^{3+}$ , which lead to the accumulation of  $\text{Ca}^{2+}$  in the cytosol (Chen et al. 2003). Alongside pumps, ion exchangers are also functioning in cells. Thus, the sodium-calcium exchanger (NCX) on the plasma membrane removes  $\text{Ca}^{2+}$  from the cytosol transporting  $\text{Na}^+$  inside the cell. This process is ATP-independent and driven by the electrochemical gradient across the plasma membrane: three  $\text{Na}^+$  ions are exchanged for one  $\text{Ca}^{2+}$  ion. The NCX activity can be reversed (because of the electrochemical nature of the mechanism) and transport  $\text{Ca}^{2+}$  into the cell. Exchangers were shown to have increased activity (up-regulation) as a compensatory effect for down-regulated SERCA pumps in diabetic beta-cells (Liang et al. 2014). The pumps and exchangers participate in the intracellular  $\text{Ca}^{2+}$  signaling, which also occurs with two  $\text{Ca}^{2+}$  buffering organelles: mitochondria and ER.

### 2.2.4 Mitochondria

The structure of mitochondria includes the outer mitochondrial membrane (OMM), which is permeable to ions and the inner mitochondrial membrane (IMM), where the respiratory chain and ATP synthesis occurs (Kuhlbrandt 2015). In general terms for  $\text{Ca}^{2+}$ , mitochondria is suggested to be a  $\text{Ca}^{2+}$ -buffering organelle due to its complex structure; the negative potential on the IMM allows very fast  $\text{Ca}^{2+}$  absorption through MCU (e.g. (Mallilankaraman et al. 2015)), however this occurs only when cytosolic  $\text{Ca}^{2+}$  reaches a threshold level. Electrochemical gradient around the IMM is maintained by three exchangers:  $\text{Ca}^{2+}/\text{H}^+$  (two protons inside vs. one  $\text{Ca}^{2+}$  outside),  $\text{Ca}^{2+}/\text{Na}^+$  (NCX, three  $\text{Na}^+$  inside vs. one  $\text{Ca}^{2+}$  outside) and  $\text{Na}^+/\text{H}^+$  (one sodium to one proton) exchanger. NCX was shown to play an important role in the heart (Torrente et al. 2015). Continuous increase of mitochondrial  $\text{Ca}^{2+}$  level can lead to the opening of mPTP, releasing cytochromes and causing apoptosis (Giorgi et al. 2012). Mitochondria were shown to be in  $\text{Ca}^{2+}$  communication with another  $\text{Ca}^{2+}$  buffering organelle – ER (Franzini-Armstrong 2007).

### 2.2.5 Endoplasmic reticulum

The distribution and  $\text{Ca}^{2+}$  dynamics inside the cell has an important impact on cellular processes. In the present study I was interested in the interaction between protein biosynthesis and  $\text{Ca}^{2+}$  signaling. The ER/SR is a major  $\text{Ca}^{2+}$  store and also a very important site for protein biosynthesis including co-translational and post-translational translocation, protein folding, and retrotranslocation (Rapoport 2007, Zimmermann et al. 2011). The ER is a system of intracellular connected tubes occupying up to 10% of the cell volume. Generally, the ER can be divided into three types. Rough ER, named due to the presence of ribosomes on its surface, is very active in protein biosynthesis (Zimmermann et al. 2011). Smooth ER has no ribosomes on the surface, but is a site for lipid, steroid synthesis, and also a main part of ER in muscle, where it functions as a dynamic  $\text{Ca}^{2+}$  store (Voeltz et al. 2002). And the third one is nuclear envelope (NE), which actively participates in the cell division (Goldberg and Allen 1995). The ER contains between  $100\mu\text{M}$ - $2\text{mM}$  of  $\text{Ca}^{2+}$  (Bygrave and Benedetti 1996). SERCA pumps transport  $\text{Ca}^{2+}$  into the ER lumen, where two states of  $\text{Ca}^{2+}$  are possible: free  $\text{Ca}^{2+}$  and buffered  $\text{Ca}^{2+}$ .  $\text{Ca}^{2+}$  can be buffered within the lumen by calreticulin, BiP/GRP78, PDI,

GRP94, and calsequestrin in SR (Prins and Michalak 2011). Calreticulin binds  $\text{Ca}^{2+}$  with its C-domain with low affinity ( $K_D$  2 mM) but high capacity (25 mol of  $\text{Ca}^{2+}$  per mol of protein), within the physiological intraluminal  $\text{Ca}^{2+}$  level of about 400 $\mu\text{M}$  (Nakamura et al. 2001, Villamil Giraldo et al. 2010). Changes in the intraluminal binding in calreticulin-deficient mice cause severe problems in cardiac functioning, such as myofibrillar development (Mesaeli et al. 1999). On the other hand, overexpression of calreticulin increases the storage capacitance of the ER and therefore inhibits store-operated  $\text{Ca}^{2+}$  entry due to the delayed store depletion (Fasolato et al. 1998, Mery et al. 1996). BiP/GRP78 is a widely expressed ER resident chaperone with a primary role in protein folding. It is a prerequisite for life as deletion of its gene is lethal (Luo et al. 2006). BiP buffers  $\text{Ca}^{2+}$  while sitting on the ER membrane with low affinity and  $\text{Ca}^{2+}$  is required for BiP activity, changing the energy consumption (ATP hydrolysis on BiP) (Lamb et al. 2006). An additional function of BiP is the sealing of Sec61a pore from the luminal side (Alder et al. 2005) that can restrict  $\text{Ca}^{2+}$  efflux from the ER (Schauble et al. 2012, Simon and Blobel 1991). PDI (protein disulfide isomerase) is also known for its  $\text{Ca}^{2+}$  buffering abilities (19 mol of protein per mole of  $\text{Ca}^{2+}$ ), which is also needed for the PDI functioning. Also ER membrane resident proteins have buffering  $\text{Ca}^{2+}$  abilities: STIM1 is permanently bound to  $\text{Ca}^{2+}$  and its depletion results in store-operated calcium entry (Parekh and Putney 2005).

### 2.2.6 Theoretical modeling of $\text{Ca}^{2+}$ homeostasis

There has been number of studies done on theoretical modeling of  $\text{Ca}^{2+}$  homeostasis in the cell, e.g. (Atri et al. 1993, Hunding and Ipsen 2003). A general scheme of  $\text{Ca}^{2+}$  fluxes was proposed as system of equations describing movements of  $\text{Ca}^{2+}$  ions between intracellular compartments. The  $\text{Ca}^{2+}$  leak was described by the properties of the functioning agents. The general increase of cytosolic  $\text{Ca}^{2+}$  comes from  $\text{Ca}^{2+}$  conducting channels of the PM and from the intracellular  $\text{Ca}^{2+}$  stores. SERCA pumps remove  $\text{Ca}^{2+}$  to the ER, mitochondria that absorb  $\text{Ca}^{2+}$ , and PMCA pumps remove  $\text{Ca}^{2+}$  to the extracellular space, providing a  $\text{Ca}^{2+}$  clearance mechanism as schematically illustrated in Figure 2.2.

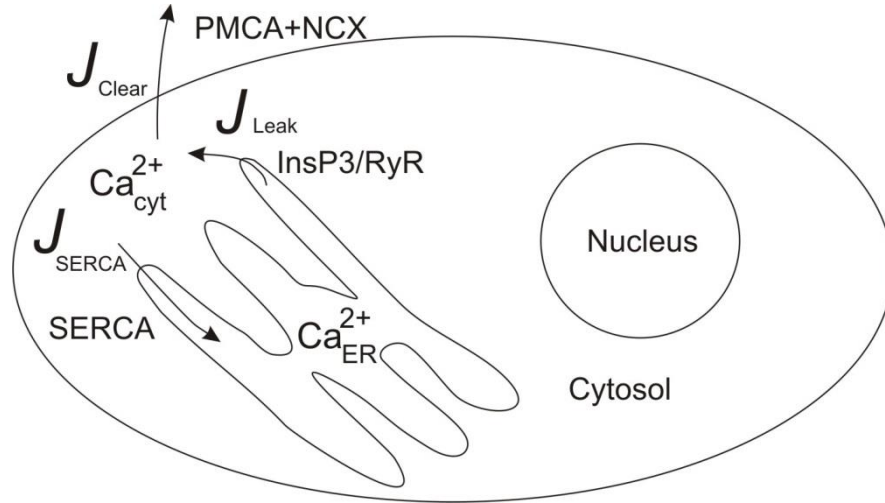


**Figure 2.2.** Simplified model of the cell shows main Ca<sup>2+</sup> fluxes.

Usually, general Ca<sup>2+</sup> signaling modeling is shown as a set of equations including the changing of Ca<sup>2+</sup> concentrations over time in different cellular compartments (Somogyi and Stucki 1991) (see Figure 2.2). Ca<sup>2+</sup> concentration changes are described mathematically by the following system of equations:

Eq. 1:

$$\frac{d[Ca^{2+}]_{cyt}}{dt} = J_{leak} + J_{InsP3R/RyR} - J_{SERCA} - J_{mito_{uptake}} + J_{mito_{leak}} - J_{PMCA+NCX};$$

Eq. 2:

$$\frac{d[Ca^{2+}]_{ER}}{dt} = \rho \cdot (-J_{leak} - J_{InsP3R/RyR} + J_{SERCA});$$

where  $J_{leak}$  is a passive leak through the ER membrane,  $J_{InsP3R/RyR}$  is Ca<sup>2+</sup> release through ER membrane channels such as InsP3R or RyR,  $J_{mito}$  represents mitochondrial uptake and  $J_{PMCA+NCX}$  represents the PM clearance mechanism of Ca<sup>2+</sup> from the cytosol. The coefficient  $\rho$  represents the actual ratio between compartment buffering capacitances and is included to be able to solve this system of equations.

At the steady state the Ca<sup>2+</sup> leak from the ER is mainly supported by not yet defined mechanisms, which are counterbalanced by the activity of SERCA pumps:

Eq. 3:

$$\frac{d[Ca^{2+}]_{ER}}{dt} = -J_{leak} + J_{SERCA};$$

In general, any type of  $Ca^{2+}$  leak from the ER was proposed to be a gradient driven process (Kiryushko et al. 2002).

Eq. 4:

$$J_{leak} = K_{leak}([Ca^{2+}]_{ER} - [Ca^{2+}]_{cyt});$$

where  $K_{leak}$  is the  $Ca^{2+}$  leak rate constant.

The theoretical approach allows modelling of basic  $Ca^{2+}$  fluxes and their complex cell responses that replicate the real data obtained from cells as was shown in some studies (Bergling et al. 1998).

### 2.3 Sec61 complex

Being the main site of secretory protein biosynthesis, the ER also represents highly regulated machinery. There are several mechanisms of protein biosynthesis on the ER: post-translational, co-translational translocations and “tailed-anchored” proteins targeting. They also can be dependent on the signal recognition particle (SRP) (Pool 2005), which binds to the signal sequence of the newly created peptide. Thus co-translational is SRP dependent and post-translational translocation is SPR independent; i.e. the transport of the peptide after the translation. Translation starts with the assembly of the small ribosomal subunits with mRNA with the help of initiation factor (Figure 2.3). After the connection to the large ribosome subunit the production of the new polypeptide chain occurs, with the help of elongation factors. In general proteins are folded with help of chaperones, but with different folding sites.

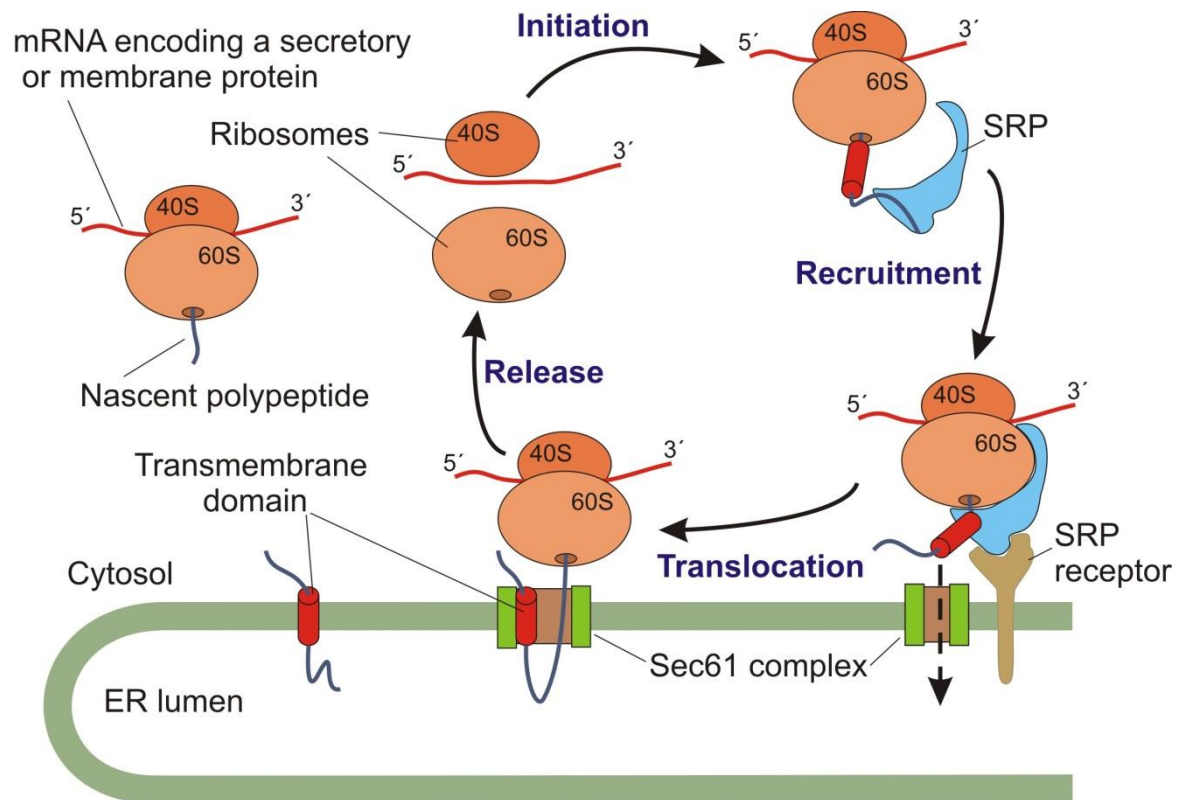


**Figure 2.3. Translocation process.** The illustration represents the translocation process starting with **Initiation**, **Recruitment** of ribosome-nascent chain complex to the Sec61, co-translational translocation into the ER lumen or insertion of transmembrane domains, and then **disassembly** and **release** of the ribosomes from the translocon and further transport of the protein according to the secretory pathway. Modified from (Reid and Nicchitta 2015).

Thus for post-translational translocated and “tail-anchored” proteins, the cytosol is a folding site, and co-translational translocated proteins are folded after entering the ER lumen. The sequence of the first amino acids of the polypeptide represents the signal sequence to which SRP (signal recognition particle) binds. In the case of co-translational translocation, SRP carries the ribosome-nascent chain complex (RNC) associated with mRNA to the SR (signal receptor), which in turn associates with the translocon, Sec61 protein complex for protein translocation into the ER lumen (see Figure 2.4). In the case of post-translational translocation or “tail-anchored” protein targeting, SRP as well as other carrying proteins are involved (see Table 2.1 and references therein).

**Table 2.1. Major agents of protein translocation:**

Agent	Type of the nascent polypeptide transport		
	Co-translational translocation	Post-translational translocation	"Tail-anchored" protein targeting
Carriers of the polypeptide	RNC (ribosome nascent chain complex) associated with SRP, through special component SRP54 (Pool 2005); requires GTP for transporting (Kurzchalia et al. 1986) (Connolly and Gilmore 1989)	Cytosolic chaperone Hsp70 (Ngosuwan et al. 2003) (Zimmermann et al. 1990); Calmodulin (Shao and Hegde 2011); carrying through binding to the N-terminal sequence of the protein (Muller and Zimmermann 1987); TRC40 (Johnson et al. 2012)	Chaperones Hsp40/Hsp70 ATP dependent (Abell et al. 2007) binding of subset of TA proteins (Rabu et al. 2008); BAG6-TRC40 complex (Stefanovic and Hegde 2007) (Favaloro et al. 2008); SRP binding to the C-terminus (tail-anchor region) (Abell et al. 2004);
ER membrane receptors	SR (SRP receptor), to which RNC-SRP complex binds via interaction of GTPase domains of SR $\alpha$ and SRP54 (Rapiejko and Gilmore 1997)	Direct targeting to Sec61 by protein carriers (Erdmann et al. 2009); TRC40 pathway: Tryptophan-rich basic protein (WRB) (Vilardi et al. 2011) associated with calcium-modulating cyclophilin ligand (CAML) (Yamamoto and Sakisaka 2012)	Tryptophan-rich basic protein (WRB) (Vilardi et al. 2011) associated with calcium-modulating cyclophilin ligand (CAML) (Yamamoto and Sakisaka 2012); SRP/SR GTP-dependent binding
Entrance into the ER lumen/ER membrane	Through Sec61 complex that forms the protein conduction pore on the ER membrane. (Mothes et al. 1994) and interact with ribosome during translation (Becker et al. 2009)	Through Sec61 complex, facilitated by Sec62/63 (Lang et al. 2012, Reithinger et al. 2013)	Unassisted incorporation into the ER membrane of highly hydrophobic TA after Hsp40/Hsp70 carrying (Rabu et al. 2009), SR-Sec61 interaction lateral gate opening and with the assistance of WRB-CAML receptors (Mariappan et al. 2010)

In the current study I studied the Sec61 machinery as major channel for protein translocation inside the ER. The Sec61 complex generally consists of three subunits Sec61 $\alpha$ , Sec61 $\beta$ , and Sec61 $\gamma$  and also SP (signal peptidase, which cleaves the signal sequence off the nascent polypeptide chain after it passes to the lumen (Weihofen et al. 2002)), TRAM (translocation associated membrane protein, not shown), and OST (oligo-saccharyl transferase, adding N-glycans to the nascent polypeptide chain) are present (Figure 2.4).

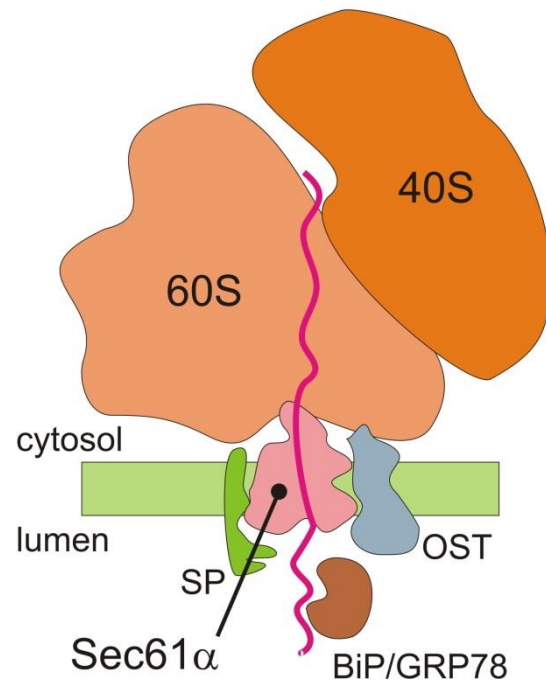


**Figure 2.4. Ribosome-translocon interaction.** Modified from (Voorhees et al. 2014) structure of the ribosome 60S and 40S (orange and light brown, as indicated) subunits interacting with Sec61 complex (light red) on the ER membrane (light green, indicating cytosol and lumen). Additional subunits SP (signal peptidase, green) and OST (oligo-saccharyl transferase, gray) are indicated. Nascent polypeptide chain (magenta) is coming through the ribosome-translocon complex and picked up by BiP/GRP78 (brown) for the folding in the lumen.

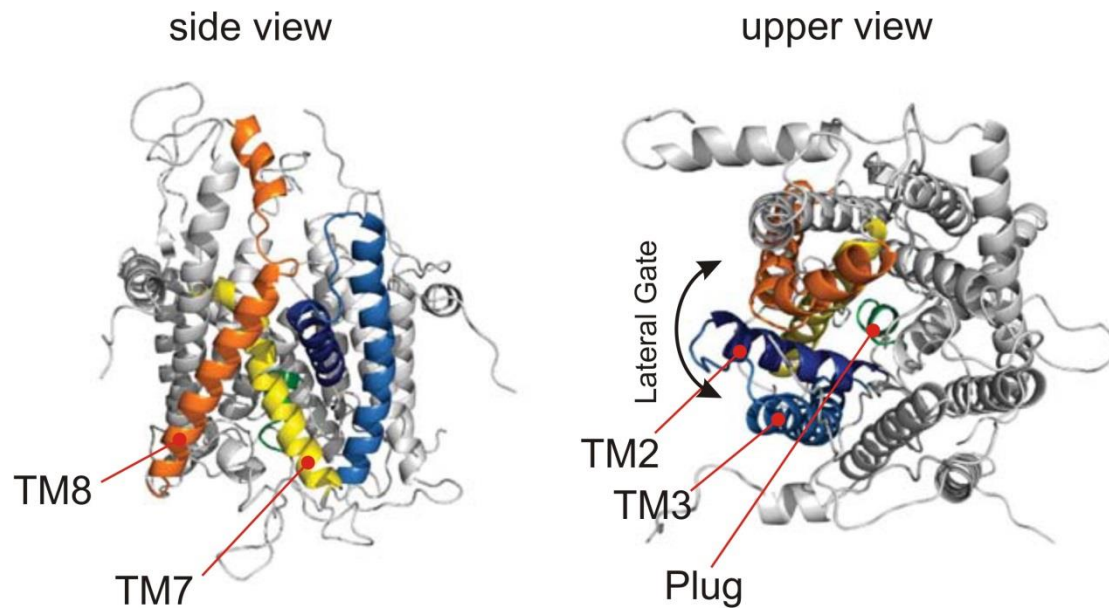


**Figure 2.5. Lateral gate opening of Sec61.** Transmembrane domains TM2, TM3 and TM7, TM8 form lateral gates. The plug (green) is removed during lateral gate opening. Modified from (Zimmermann et al. 2011).

The structure of the translocon complex was resolved (Figure 2.5) and ribosome binding results in conformational changes of Sec61 leading to the opening (Figure 2.6) (Voorhees et al. 2014). In the closed state, Sec61 has an hourglass shape and has been proposed to be sealed with the plug in order to prevent ion and small molecule flux from the ER. The size of the “closed” pore was estimated to be ~15 Å and the opened state ~60 Å (Johnson and van Waes 1999). The process of opening of Sec61 $\alpha$  is suggested to be through the lateral gate opening between TM2, TM3 and TM7, TM8 (has been demonstrated on SecYE $\beta$  complexes which have homology to human/mammalian Sec61) for the insertion of the transmembrane subunit of a new protein (Zimmermann et al. 2011). The opening require the mobilization of the BiP from the luminal site which is supposed to facilitate the movement of the polypeptide inside the lumen (Jensen and Johnson 1999).

Two putative agents can restrict Ca<sup>2+</sup> from the endoplasmic reticulum through Sec61; it was shown that BiP/GRP78 seals the pore from the luminal side and calmodulin has affinity to the Sec61 complex from the cytosolic side (Schauble et al. 2012) (Figure 2.6).

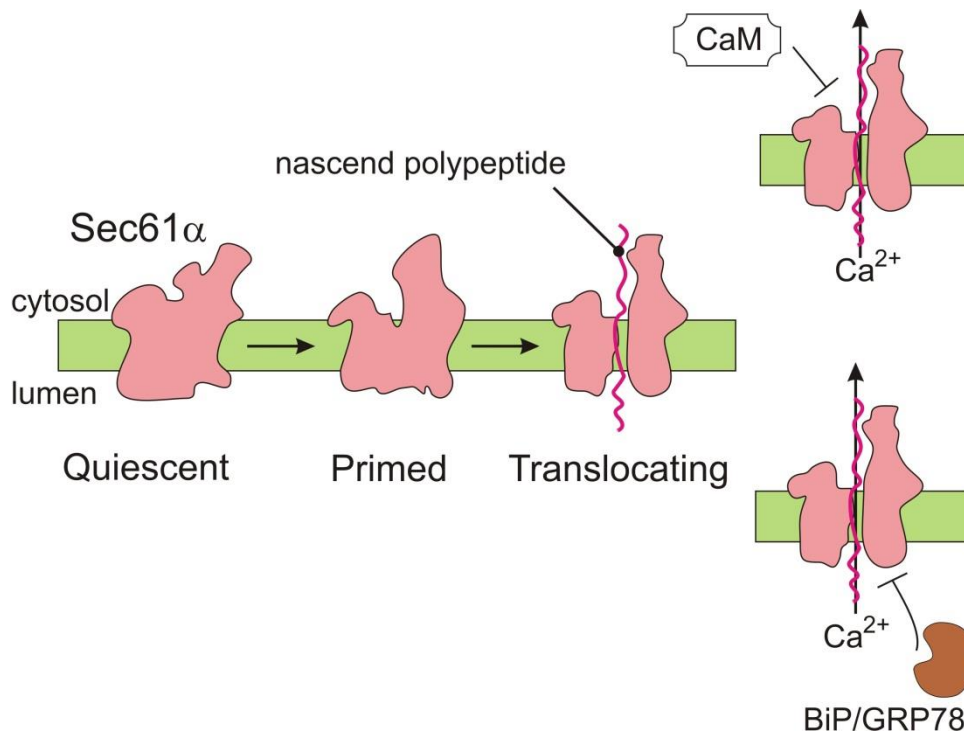


**Figure 2.6. Putative Ca<sup>2+</sup> leakage through Sec61.** Ca<sup>2+</sup> leakage is driven by the concentration gradient through Sec61α (modified from (Voorhees et al. 2014) and can be attenuated by CaM (empty rectangle like form) and BiP/GRP78 (brown) (Erdmann et al. 2011, Schauble et al. 2012). The conformational changing of the ribosome-translocon complex (states of the Sec61 indicated by arrows from left to right) can lead to the modification of Ca<sup>2+</sup> leakage.

## 2.4 Human diseases related to the endoplasmic reticulum

The ER has a dual function as both for protein synthesis machinery and Ca<sup>2+</sup> store. Disruption of each of these main functions of the ER leads to pathologies. There are some states bound to the ER protein production and control. Pathologies disrupt ER Ca<sup>2+</sup> homeostasis and vice versa the changes in Ca<sup>2+</sup> signaling are tightly bound to pathologies (Mekahli et al. 2011). Under normal physiological condition, the malfunctioning of protein biosynthesis should activate pathways known as the UPR (unfolded protein response). UPR includes three main pathways: inositol requiring enzyme 1 (Ire1), activation transcription factor 6 (ATF6) and protein kinase-like ER kinase (PERK) (for review (Wang and Kaufman 2014)). It was also demonstrated that UPR disruptions are related to the diabetic pathologies such as hyperglycemia, hyperlipidemia, and insulin

anabolic responses (Kaufman 2002). The disruption in UPR results in continuous ER stress, which can result in cell death and therefore cause neurodegenerative diseases, metabolic diseases, inflammation and cancer (Wang and Kaufman 2012). ER stress can lead to metabolic syndromes causing obesity, fatty liver, dyslipidemia (Fu et al. 2012), changes in hepatic gluconeogenesis (Zhou et al. 2011), and adipogenesis (Basseri et al. 2009). During inflammation caused by infections, high amounts of immunoglobulin are produced, to which the correct functioning of UPR in B cells is required (Reimold et al. 2001). Cancer cells show mutations in the PERK domain allowing them to survive in a hypoxic state (Fels and Koumenis 2006) and also to promote proliferation and growth (Bobrovnikova-Marjon et al. 2010).

The UPR is also linked to Endoplasmic Reticulum Associated Degradation (ERAD) (for review (Ruggiano et al. 2014)). In the case of misfolded proteins, they have to be retrotranslocated from the ER to the cytosol where they are degraded by proteasomes. The degradation starts with binding of ubiquitin molecules to the retrotranslocated polypeptide, then after polyubiquitination the degradation by the 26S proteasome occurs. It has been estimated that up to 30% of newly synthesized proteins have some defects and need to be degraded (Ruggiano et al. 2014). If there any mutation in the signal sequence, it can cause the mislocalization of the protein, can lead to hypoparathyroidism, familial central diabetes insipidus etc. (Rutishauser and Spiess 2002). Inhibition of proteasomes was used as treatment for myeloma (Dimopoulos et al. 2011) and pancreatic cancer (Nawrocki et al. 2005).

Increase  $\text{Ca}^{2+}$  levels were observed in metabolic diseases with hyperglycemia, supposed to the elevated ER  $\text{Ca}^{2+}$  leakage (Levy 1999, Verkhatsky and Fernyhough 2008). Continuous decrease in ER  $\text{Ca}^{2+}$  cause diabetic like phenotype impairing the production and the secretion of insulin (Oyadomari and Mori 2004) or evoke apoptosis of  $\beta$ -cells (Araki et al. 2003). Wolfram syndrome shows lowered ER  $\text{Ca}^{2+}$ , which triggers apoptosis of  $\beta$ -cells (Yamada et al. 2006). It was proposed that it forms  $\text{Ca}^{2+}$  channel on the ER membrane (Osman et al. 2003). ER stress induced by palmitic acid promotes insulin secretion, but causes UPR and can damage  $\beta$ -cells (Gwiazda et al. 2009).

It was shown that SERCA pumps are impacted under pathological conditions of ER stress. (Cunha et al. 2008, Evans-Molina et al. 2009). The SERCA can be inhibited by phospholamban, which is upregulated in cardiac myopathy (Kim et al. 2001). Both changes in  $\text{Ca}^{2+}$  and induced UPR are observed in the early stages of nephropathy (Chen et al. 2008). The most sensitive cells are neurons, where the ER stress can lead to

neuropathies (Verkhatsky and Fernyhough 2008). Induced ischemia causes both elevation of cytosolic  $\text{Ca}^{2+}$  and decrease of ER  $\text{Ca}^{2+}$  and causes neuronal cell death (Verkhatsky 2005). Here, the malfunctioning of the protein biosynthesis machinery causes severe problems with neurons and can result in incurable pathological conditions such as Parkinson (Ryu et al. 2002) and Alzheimer diseases (Berridge 2010).

The protein synthesis machinery and especially Sec61 was also proposed to be involved in  $\text{Ca}^{2+}$  signaling. The mutation in Sec61 caused diabetes in mice (Lloyd et al. 2010). ER stress can be caused by deficiency of ERdj4, the luminal co-chaperone of BiP (Fritz et al. 2014).

## 2.5 Aims of the work

The present study is focused on the ER  $\text{Ca}^{2+}$  homeostasis and the cytosolic-ER  $\text{Ca}^{2+}$  relationship, while the simultaneous measurements of cytosolic and ER  $\text{Ca}^{2+}$  provide the basis of the study. The analysis of ER  $\text{Ca}^{2+}$  dynamics gives insight in the important cell functioning processes, like it was shown on cardiac cells (Bers 2014). Similarly studies have not been performed with non-excitabile cells, such as those which produce secretory proteins. The main interest of the present study is on Sec61 complex, which is a main gate through the ER membrane for proteins destined for the secretory pathway. According to previous observations, Sec61 $\alpha$  can support  $\text{Ca}^{2+}$  leak from the ER (Ong et al. 2007, Schauble et al. 2012). The modulation of the protein biosynthesis via small molecules is a proper tool to study various states of Sec61 complexes in terms of  $\text{Ca}^{2+}$  signaling. As well as studying the possibility of direct activation of  $\text{Ca}^{2+}$  leak through Sec61 complexes with new compounds, the present study intends to explain both the previously unknown mechanisms of their action and to establish a new family of Sec61 complexes modulators. The quantification of Sec61-mediated  $\text{Ca}^{2+}$  leak from the ER and also the estimation of its part in the total ER  $\text{Ca}^{2+}$  leak would substantiate the importance of this protein-conducting channel in the intracellular  $\text{Ca}^{2+}$  homeostasis.

In detail, the aims of the present work are as follows:

- A1) Establish a reliable tool for measurements of ER  $\text{Ca}^{2+}$ , namely a cell line with stably expressed D1ER, an ER targeted genetically encoded  $\text{Ca}^{2+}$  sensor.
- A2) Provide a mathematical analysis of the imaging data to quantify the  $\text{Ca}^{2+}$  leak from the ER.
- A3) Mimic protein translocation steps through Sec61 $\alpha$  using small molecules (protein synthesis inhibitors, calmodulin inhibitor, N-linked glycosylation inhibitor) and quantify the Sec61-mediated  $\text{Ca}^{2+}$  leak.
- A4) Propose a model which explains every step of the protein translocation through Sec61 in terms of  $\text{Ca}^{2+}$  leak.
- A5) Investigate the role of two new compounds: mycolactone and eeyarestatin in disrupting cellular  $\text{Ca}^{2+}$  homeostasis. Check whether the observed effects are specific to Sec61 $\alpha$ .

### 3 Materials and methods

#### 3.1 Chemicals

Chemical substances for preparing extracellular- and intracellular-like solution as well as inorganic inhibitors of cytosolic  $\text{Ca}^{2+}$  clearance, cell membrane permeabilization chemicals and mediums required for cell culturing used in this study were purchased by Saarland University. Common name and Supplier of the chemicals are listed in Table 3.1.

**Table 3.1 Chemical substances.**

NaCl	MERCK
KCl	SIGMA Aldrich
CaCl <sub>2</sub>	SIGMA Aldrich
MgCl <sub>2</sub>	Fluka,SIGMA Aldrich
GdCl <sub>3</sub>	MERCK
NaOH	MERCK
KOH	SIGMA Aldrich
HCl	MERCK
HEPES	SIGMA Aldrich
Glucose	MERCK
Sucrose	MERCK
EGTA	SIGMA Aldrich
BAPTA	SIGMA Aldrich
Na <sub>3</sub> -HEDTA	SIGMA Aldrich
NTA	SIGMA Aldrich
Saponin	SIGMA Aldrich
Digitonin	SIGMA Aldrich
MEM	Gibco
PBS	Gibco
FCS	Gibco
FKS	Gibco
LB medium	
G418	SIGMA Aldrich
Trypsin	SIGMA Aldrich

## 3.2 Cell lines

### 3.2.1 HEK and HeLa cell lines

The current study focused on intracellular  $\text{Ca}^{2+}$  signaling and the changes which it undergoes during protein biosynthesis. HEK and HeLa cell lines were used for fluorescent  $\text{Ca}^{2+}$  imaging in cytosol and ER. Human embryonic kidney (HEK) cells are originally from embryonic epithelial-like kidney cells by modifying their genome with inserted adenoviral sequences, resulting in immortal cells and suitable for stable transfections (Graham et al. 1977). HeLa cells are cervical cancer cells named after Henriette Lacks, the patient from where they were taken in 1951 (Scherer et al. 1953). HeLa cells show extremely durable proliferation and near immortality. HEK293 and HeLa were acquired from ATCC (American Type Culture Collection) and purchased by Saarland University. Both cell lines were used for generating new cell lines stably expressing the  $\text{Ca}^{2+}$  sensitive indicator D1ER designed for ER  $\text{Ca}^{2+}$  measurements.

### 3.2.2 Cell culture

HEK and HeLa cells were cultured in a humidified incubator with 5%  $\text{CO}_2$  at 37°C. Basic culture medium contained MEM (31095-029 Gibco, Invitrogen) + 10% FCS (10270106 South America, Gibco, Invitrogen). Cells underwent splitting via trypsinisation (Trypsin EDTA solution, Sigma Aldrich, T4174, solved 1:10 in PBS, Sigma Aldrich, D8537) every 48-72 hours after reaching ~ 80% confluence. All culture media were kept in a refrigerator at 2-8°C and heated to 37°C in a water bath immediately prior to use.

### 3.2.3 Preparation of cells for $\text{Ca}^{2+}$ imaging

For  $\text{Ca}^{2+}$  imaging experiments cells, were cultured in 3.5 cm plastic Petri dishes (Greiner®) with 2.5 cm poly-L-lysine coated glass coverslips (special cut: 0.170 mm thickness Assistant®, Germany) on the bottom. The dishes were filled with 1.5 mL of MEM + 10% FCS medium. After 48-72 hours, cells adherent to coverslip were confluent enough to be taken for imaging experiments.

### 3.3 Plasmids

#### 3.3.1 D1ER

Measurements of ER  $\text{Ca}^{2+}$  were done via stably expressing the genetically encoded calcium indicator D1ER (Palmer and Tsien 2006). For introducing D1ER sequence into cellular genomes, the pcDNA3 D1ER plasmid was used. The central part of 7.4-kilo base-pairs pcDNA3 sequence includes coding sequences for ER-targeting of the sensor: calreticulin-coding sequence and KDEL-coding sequence and D1ER cassette is in between (Figure 3.1). D1ER cassette of 1984 base pairs consists of eCFP, D1  $\text{Ca}^{2+}$  sensor (mCaM and mM13), and citrine coding sequences (Palmer et al. 2004). D1ER pcDNA3 plasmid was a gift Prof. Dr. Roger Y. Tsien, University of California, San Diego ([www.tsienlab.ucsd.edu](http://www.tsienlab.ucsd.edu)). pcDNA3 D1ER has ampicillin and neomycin resistance for amplification and selection.

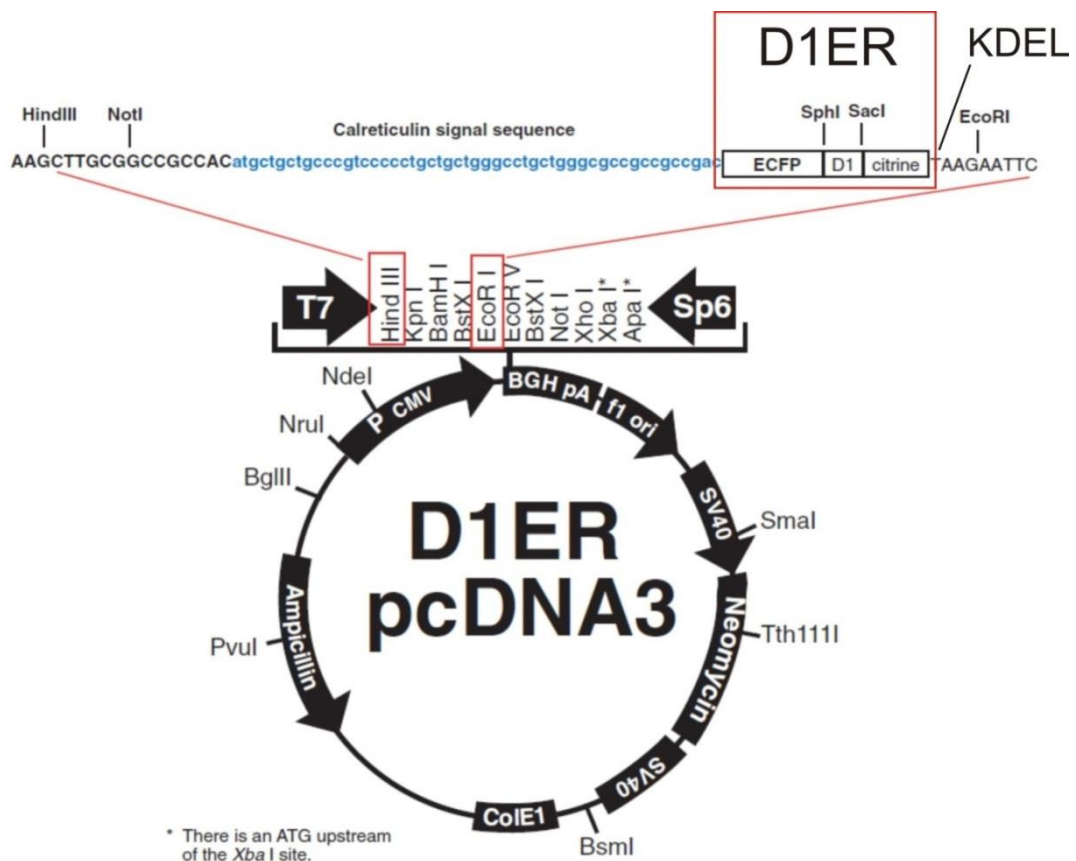


**Figure 3.1. pcDNA3 plasmid map of Ca<sup>2+</sup> sensitive D1ER chameleon. Calreticulin (blue) and KDEL sequences are for ER retention of the D1ER. ECFP and citrine are linked with the Ca<sup>2+</sup> sensor D1 (red box). Full sequence of the D1ER sensor: <https://www.addgene.org/36325/>.**

### 3.3.2 GFP analogue markers

ER targeted GFP analogue markers eCFP-ER and eYFP-ER were used for comparison with D1ER transfection. The proper targeting of D1ER proteins expressed in HEK 293 cells was measured by its fluorescence and compared to the pictures of HEK 293 cells expressing eCFP and eYFP fluorescent proteins. The plasmids pcDNA3 encoding eCFP and eYFP were kindly provided by Prof. Dr. Richard Zimmermann, Medical Biochemistry, Saarland University.

### 3.3.3 Plasmid amplification

Competent XL1-blue *E.coli* bacteria (Stratagene, Oregon, USA) were used for pcDNA3 D1ER plasmid amplification. Competent cells were kept at -80°C and thawed as needed. Using Eppendorf tubes (1.5 ml tube from Eppendorf Tubes™, Fischer Scientific), 300 µL of the competent cells were given 1 µg/µl of pcDNA3 D1ER and left for 30 minutes on ice. After this, the competent cells underwent heat shock at 42°C for one minute and were put again for 2 minutes on ice. 1000 µL Lysogeny broth (LB) medium were added and the competent cells were left shaking at 37°C for 1 hour. For the selection and growing of the bacterial colonies that expressed pcDNA3 D1ER plasmid, competent cells were plated on two LB-Amp. Plates (Ampicillin pretreated agar plates in 10cm plastic Petri dishes): on the first 100 µl of the solution, the remaining bacteria were centrifuged, resuspended and plated on the second LB-Amp. plate. Both plates were closed with lids and kept upside down in the incubator at 37°C overnight. Single colonies were taken with wooden stick and put into 100 ml LB medium with 50 µg/ml Ampicillin. The medium was left shaking at 37°C overnight. The Further Maxi Prep (with PureLink™ HiPure Plasmid DNA Purification Kit, Invitrogen™) took place according to the recommended protocol. The amount of final product was measured using a NanoDrop 1000 Spectrometer (Thermo Scientific™) and then diluted to 1 µg/µl and kept frozen at -20°C.

### 3.4 Analysis of protein expression levels

#### 3.4.1 Rough microsomes

Rough microsomes (RM) used as a positive control for all proteins that permanently exist in the ER membrane were extracted from canine pancreas. RMs were kindly provided by Prof. Dr. Richard Zimmermann, Medical Biochemistry Department, Saarland University. Protocols for RM preparations were similar to established ones (Walter and Blobel 1983, Watts et al. 1983). In my study it was used as a positive control of Sec61a protein in the silencing experiments.

#### 3.4.2 Primary and secondary antibodies

The Antibodies that we used for stripping of immunoblots and quantifying of the protein levels were as indicated in the Table 3.2. Primary antibodies were mainly custom made at Saarland University; Medical Biochemistry Department. Anti-Sec61 $\alpha$  from University of Göttingen was used during silencing of *SEC61A1* gene experiments, similarly to the established procedure in (Lang et al. 2012).

**Table 3.2 Primary and Secondary Antibodies**

Primary Antibodies		
target	Description	dilution
BiP	Polyclonal, N-terminus of ER chaperone BiP; Rabbit; UdS	1:500
GRP170	Polyclonal, N-terminus of ER chaperone GrRP170; Rabbit UdS	1:1000
$\beta$ -actin	Monoclonal, $\beta$ -actin, Mouse; Sigma	1:10000
ERj3	Polyclonal, ER co-chaperoneERj3; Rabbit; UdS	1:250
ERj6	Monoclonal, ER co-chaperoneERj6; Rabbit; Cell Signalling	1:1000
Sec61 $\alpha$	Polyclonal, C-terminus of Sec61 $\alpha$ subunit. Rabbit, Uni Göttingen	1:250

Secondary Antibodies		
name	description	dilution
$\alpha$ -Rabbit	Anti-Rabbit, Horsereadish Peroxidase. Goat , Sigma	1:1000
$\alpha$ -Mouse	Anti-Mouse, Horsereadish Peroxidase. Goat , Sigma	1:20000
$\alpha$ -Rabbit	Cy5, ECL <sup>TM</sup> Plex	1:1000
$\alpha$ -Mouse	Cy3, ECL <sup>TM</sup> Plex	1:2500

### 3.4.3 Western blot analysis

To check that HEK D1ER cells do not experience continuous ER stress after the cell line creation and also for manipulations with protein levels via silencing we needed to make an analysis of protein content of the cells. For the identification of protein levels HEK D1ER cells and HeLa cells were collected for immunoblot analysis. For every  $10^4$  cells was used 1  $\mu$ L of lysing buffer containing 0.1 mM PMSF, PLAC (1:1000), 10 mM NaCl, 10 mM Tris pH 8.0, 3 mM MgCl<sub>2</sub>, 0.5% NP40, and 1 mg/ml DNA-se. Lysing was performed at 37°C during 20 minutes with following incubation in SDS Laemmli buffer (60 mM Tris/HCL, pH 6.8, 10% (v/v) Glycerin, 2% (v/v) SDS, 5% (v/v)  $\beta$ -Mercaptoetanol, 0.01% (w/v) Bromphenol blue) during 10 minutes at 56°C.

SDS gel was casted between two glass slides with 14 x 11 (width x height) with about 0.5 cm distance between them and were sealed with agarose gel on the bottom. Running gel mixture was added after agarose gel had sealed the bottom with following isopropanol cover for keeping the running gel moisture during polymerization. The polymerization of the running gel usually took up to 2 hours, and after removal of isopropanol stacking gel mixture was added. Plastic gel-pocket former was installed immediately after stacking gel mixture and further 30 minutes were needed for staking gel polymerization Table 3.3. After complete polymerization SDS gel was installed in an electrophoresis chamber. The chamber was filled with electrophoresis buffer which was touching upper and bottom sides of the SDS gel. Electrophoresis buffer contained 50 mM TRIS/HCl, 384 mM Glycine, 0.1% (w/v) SDS in bi-distilled H<sub>2</sub>O. Gel pockets were loaded with 30  $\mu$ l of the sample cell lysate, 10  $\mu$ l of RM sample (see Rough Microsomes) for exact position of ER proteins of interest, and 5  $\mu$ l of blot marker (Page Ruler™ Prestained Protein Ladder) for apparent protein size identification. Then the electrophoresis chamber was covered with an electric safe lid and voltage corresponding to 5 mA current was applied in the direction of positive charges movements through the SDS gel. The electrophoresis for the described SDS gel takes of about 15 hours. Blotting was performed from the SDS gel to PVDF (polyvinylidene difluoride) membrane. PVDF membranes were activated with 100% methanol and put between Whatman paper from one side and the SDS gel from the other. Blotting buffer contained 96 mM Glycine, 12.4 mM Tris/HCl. Blotting chambers were cooled continuously by water flow cooling system down to 14°C. Voltage for blotting that was applied was enough to keep current of 400 mA, and the whole blotting took usually 2-2.5 hours. After blotting every PVDF membrane was blocked by 5% (w/v)

milk powder solution in TBS-T (10mM Tris/HCl pH 7.4, 150 mM NaCl, 0.05% (v/v) Triton X-100).

**Table 3.3 Casting gels for Immunoblot analysis.**

Running gel	
stock	"one gel" volume(ml)
Acrylamid 40%	4.7
Bisacrylamid 2%	1.25
H <sub>2</sub> O	2.9
1.875M Tris ph8.8	6
10% SDS	0.15
20% AMPS	0.045
TEMED	0.005
total volume	15

Stacking gel	
stock	"one gel" volume(ml)
Acrylamid 40%	0.9
Bisacrylamid 2%	0.2
H <sub>2</sub> O	5
1M Tris ph6.8	0.9
10% SDS	0.072
20% AMPS	0.0675
TEMED	0.0105
total volume	4

Then the membrane was washed twice with TBS-T during 5 min each. Primary antibody were resolved in 5% (w/v) milk powder in TBS-T as indicated (see Table 3.2) and applied upon the membrane overnight at 4°C in cold room. After this the primary antibody was washed away with TBS-T three times 15 min each and secondary antibody resolved in 5% (w/v) milk powder in TBS-T was applied. For the secondary antibody incubation time was 90 minutes with following washing steps with TBS-T (three times, 15 minutes). The membranes were covered with the luminescence mixture of luminescence agent and oxidizing agent (1:1, v/v) and put between two transparent plastic sheets for the equal distribution of the luminescent mixture. Images of the luminescent signals of the PVDF membrane were taken through CCD camera of Lumi-F1

imager, LAS3000, or LAS4000. Analysis of densitometry of the obtained bands was done with Fiji (ImageJ) Software.

### **3.5 Generation of cell lines stably expressing D1ER**

#### **3.5.1 General principles of transfection**

The electroporation is a method of cell transfection employing electrical impulse through cell suspension to polarize the hydrophobic membranes of the cells improving the permeation of polar molecules from the extracellular environment. For electroporation we used AMAXA Nucleofector II with disposable AMAXA electroporation cuvettes or cuvettes from Cell Projects. OptiMEM (Gibco, Invitrogen) and Amaxa NHDF Nucleofector Kit were routinely used. Cells were collected by trypsinisation and counted using Neubauer® counting chamber.  $1 \times 10^6$  of cells were put in a 1.5 ml Eppendorf tube and then centrifuged for 5 minutes at  $200 \times g$  for cell precipitation. It usually resulted in a pellet of cells precipitated on the tube bottom. After the precipitation the medium was removed from the tube and the mixture of plasmid and electroporation medium was added. The cell pellet was resuspended via pipetting and transferred to the electroporation cuvette. The cuvette was installed in AMAXA Nucleofector II. We used preinstalled programs for AMAXA Nucleofector II HEK (Q-001) and HeLa (O-005) cells. After electroporation was done the cuvette was removed from the Nucleofector. Then the cell suspension was diluted inside the cuvette with 500  $\mu\text{L}$  of culture medium, removed from the cuvette and transferred to culture dishes for further culturing.

#### **3.5.2 Transfection of D1ER pcDNA3**

For the creation of D1ER cell lines based on HEK293 and HeLa cells for more accurate measurement of ER  $\text{Ca}^{2+}$ , we used plasmid D1ER pcDNA3. 5  $\mu\text{g}$  D1ER pcDNA3 plasmid were resuspended in 100  $\mu\text{L}$  electroporation medium (AMAXA) for every  $10^6$  cells. We used transfection by electroporation with AMAXA Nucleofector II as described before.

## **3.6 Selection of cell clones stably expressing D1ER**

### **3.6.1 Analysis of D1ER fluorescence levels**

Transfected cells with D1ER chameleon require about 48 hours before reaching the D1ER protein expression level enough for fluorescent detection. Fluorescence of D1ER initially was observed as GFP fluorescence using Zeiss Axiovert 200M microscope with GFP filter and HXP 120C Illuminator light source.

### **3.6.2 FACS**

For the further selection of D1ER expressed cells Fluorescent Activated Cell Sorting (FACS) was performed. From HEK293 and HeLa cells transfected with D1ER chameleon two 96-well plates were filled with one cell per well.

### **3.6.3 Sub-cloning and clonal expansion**

The selection of individual cells with FACS and following culturing gave us individual cell colonies with the identical genome. These colonies were generally named after the name of the well where they had grown (for instance, the HEK colony from A7 was called HEK D1ER A7). Time to grow colonies from individual cells was about 3 month. Finally I have obtained 34 clones for HEK D1ER cells and 15 clones for HeLa D1ER cells. The clones were put on 2.5 cm “FRET glass” coverslips (special cut: 0.170 mm thickness Assistant®, Germany) to undergo morphological selection first. In this case the cells stably transfecting D1ER should show nice ER structure .We checked D1ER expression level, correct targeting to the ER, and the homogeneity of D1ER expression throughout the cell colony (Figure 3.2).

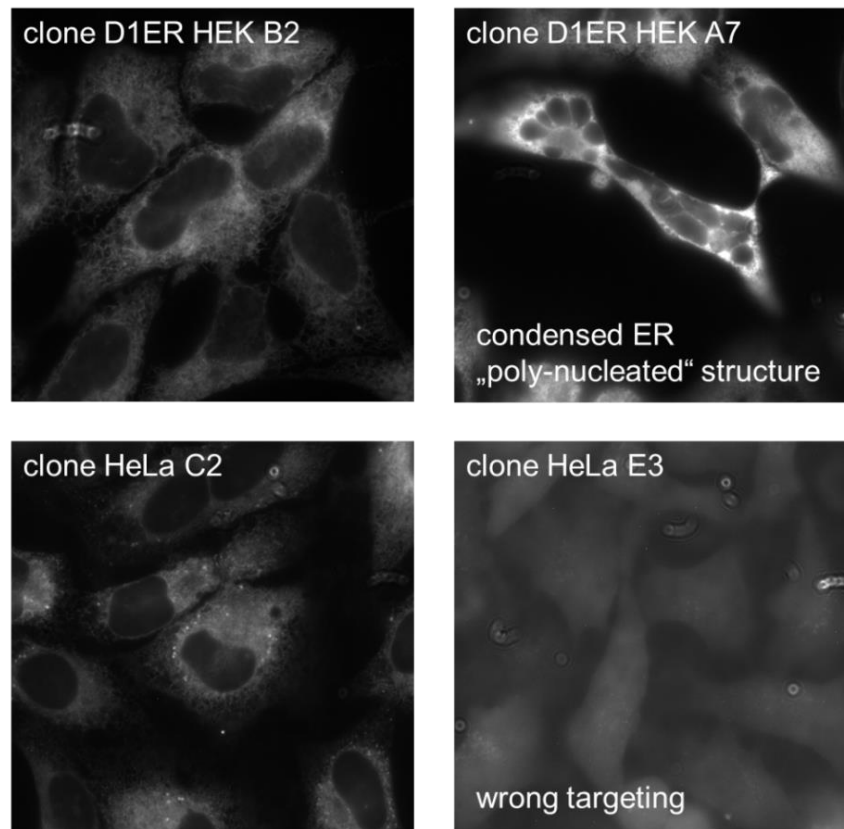


**Figure 3.2.** Morphological diversity of D1ER clones during cell line creation. *Left part:* “Good-looking” clones of HEK D1ER and HeLa D1ER with proper targeting and relative homogeneous D1ER expression. *Right part:* examples of stressed ER, influences and poly-nucleated structure (upper), morphological changes and wrong targeting (lower).

#### 3.6.4 Culture of D1ER cell lines

After selection of D1ER clones, cell colonies were frozen in liquid nitrogen with assistance of Heidi Löhler, Experimental and Clinical Pharmacology and Toxicology, Saarland University. Every time we needed cells were taken from liquid nitrogen, thawed and cultured for about one week before reaching useful confluence for  $\text{Ca}^{2+}$  imaging experiments. For HEK D1ER and HeLa D1ER stable cell lines 500  $\mu\text{g}/\text{ml}$  of selection marker geneticin (G418, Sigma Aldrich, G8168) was added to the culture medium.

#### 3.6.5 ER stress check in generated cell lines stably expressing D1ER

More exact check of ER stress levels after D1ER expression was done by detection of the levels of GRP170 and BiP, as ER stress markers on Western Blot (WB). The cells from “best looking” clones were collected and lysed for WB as described before. The relative

amount of BiP and GRP170 were compared to those of non-transfected HEK293 and HeLa cells. For the chosen clones of HEK D1ER cells no ER stress was detected (Figure 3.3), showing not elevated level of GRP170 and BiP. While the upregulation of BiP might indicate ER stress (Gulow et al. 2002).

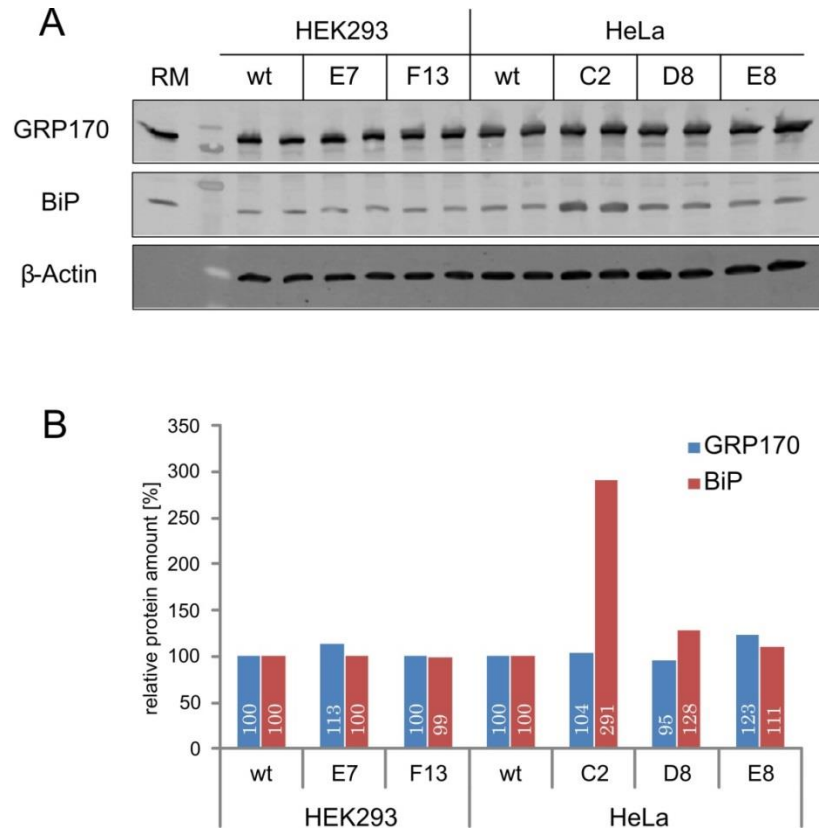


**Figure 3.3. D1ER stable cell lines check, whether expression of the chameleon causes ER stress. A. Western Blot for HEK D1ER clones (E7 and F13) and HeLa (C2, D8, and E8) clones stained versus GRP170 and BiP.  $\beta$ -actin was chosen as loading control. RM: rough microsomes. B. Relative protein content quantification to the corresponding clones versus HEK293 (wt) and HeLa (wt) untransfected cells respectively. Percentage indicated in columns shows the change in BiP (red columns) and GRP170 (blue columns) normalized to a.u. 100 each. (Courtesy of Stefan Schorr, Medical Biochemistry, Saarland University).**

### 3.7 Gene silencing

#### 3.7.1 General principles for gene silencing

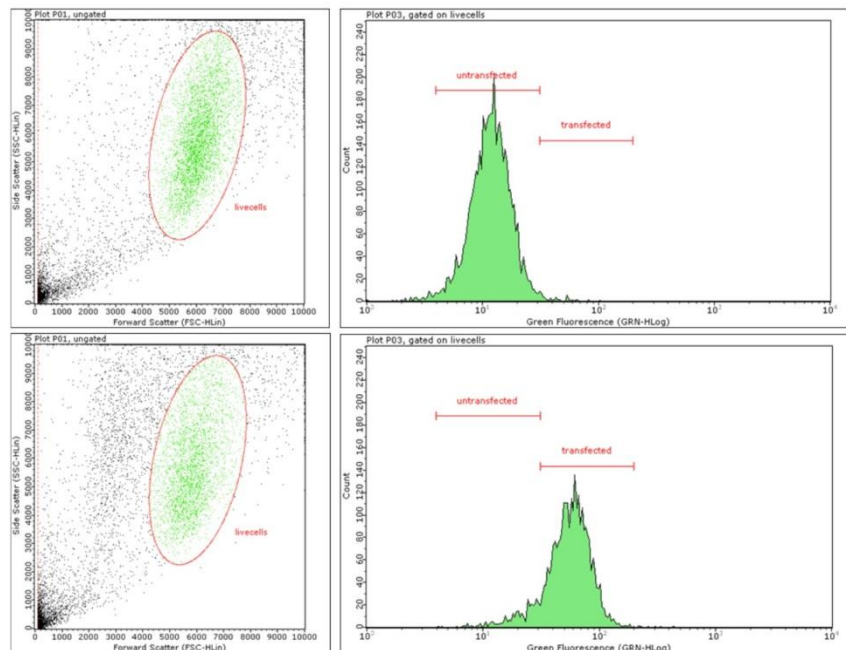
To study the contribution of translocon on  $\text{Ca}^{2+}$  signaling, we depleted Sec61 $\alpha$  proteins of HEK D1ER cells and HeLa cells by gene silencing. We silenced *SEC61A1* gene using

small interference RNA. In this case siRNA (20-25 base pairs) entering the cytosol via transfection, then cleaved by Dicer and forms RISC (RNA-induced silencing complex) which is binding to mRNA of interest and cleaving it. As a result no protein from the mRNA can be produced (Burnett and Rossi 2012). Due to protein turnover inside the cell the actual amount of the functional proteins of interest is reduced after inhibition of gene expression with siRNA.

HeLa cells and HEK D1ER cells were transfected with *SEC61A1* siRNA from Ambion (Table 3.4). I used AMAXA Nucleofector II to transfect HEK D1ER cells with siRNA (see 3.5.1).

To check the efficiency of the transfection with AMAXA Nucleofector II we transfected HEK293 with fluorescent labelled Alexa488-siRNA. After the transfection, cells were washed from the rest of fluorescent siRNAs: precipitated with 200xg and washed with fresh OptiMEM three times. Then cells were put on 96-well plate and compared the percentage of the transfected cells using Guava easyCyte 8HT cytometer (Figure 3.4).

A



B

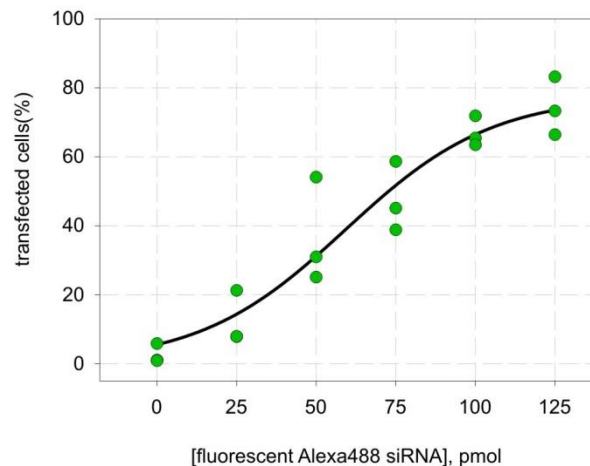


**Figure 3.4.** Transfection efficiency of siRNA in HEK cells. **A.** Guava EasyCyte 8HT pictures representing fluorescent changes of cells transfected with Alexa 488 fluorescent labelled siRNA. *Left part:* Dot-plotted graphs showing forward and side scatter; red ellipse and green points represent populations of living cells. *Right part:* Shift of the cell fluorescence of the transfected cells. **B.** Percentage of transfected cells obtained from Guava easyCyte 8HT analysis as a function the amount of transfected Alexa 488 siRNA per  $10^6$  cells. Points for each concentration are collected from three independent transfections. Black sigmoidal line shows fitting approach for binding curve.

For HeLa cells we were using chemical transfection. Chemical transfection implies creation of lipophilic complexes of transfection reagents with oligonucleotides to enhance plasma membrane permeability of cells. Usually transfection reagent is a suspension of liposomes inside which RNA molecules can enter, and then together enter the cytosol through the cell membrane. After entering the cytosol these complexes are degraded and oligonucleotides become free. Chemical transfection was done according to the suggested protocols for corresponding transfection reagents Lipofectamine2000, FuGene, HiPerfect. Usually cells were grown up to 80% confluence. The plasmids were incubated together with transfection reagent in Opti-MEM solution during 10-15 minutes. After this culture medium was changed to antibiotic free one and the mixture of transfection reagent with plasmids or nucleotides was added. According to manufacturer, transfection is completed after 1.5-2 hours. As needed transfection protocol with chemical reagent could be repeated according to established procedure (Lang et al. 2012).

### 3.7.2 “Small interference” RNA oligonucleotides

The gene *SEC61A1* coding the pore region of translocon Sec61 $\alpha$  was silenced via expression of siRNA in cells. As a side project, silencing of luminal co-chaperones ERj3 and ERj6 was studied in case of impact of these co-chaperones on intracellular Ca<sup>2+</sup> signaling. ERj3 and ERj6 silencing was done in Medical Biochemistry department, Saarland University by Stefan Schorr (Schorr et al. 2015). The list of siRNA sequences as indicated in Table 3.4.

**Table 3.4. siRNAs and their sense sequences.**

siRNA	sense sequence
<i>SEC61A1</i>	GGAAUUUGCCUGCUAAUCA <sub>tt</sub>
<i>SEC61A1 UTR</i>	CACUGAAAUGUCUACGUUU <sub>tt</sub>
<i>ERj3#1</i>	CGAAUGCCC <sub>UAAUGUCAAA</sub> <sub>tt</sub>
<i>ERj3#2</i>	GGACGAGAUUUCUAUAAG <sub>Att</sub>
<i>ERj6#1</i>	GGAGAACCUAGGAAAGCU <sub>Att</sub>
<i>ERj6#2</i>	GAAACGAGAUUAUUAUAA <sub>Att</sub>

All aliquotes of siRNA were solved to 20  $\mu\text{M}$  in RNase free  $\text{H}_2\text{O}$  were stored at  $-20^\circ\text{C}$ . Control siRNA was purchased from QIAGEN (scrRNA AllStars Neg.Control siRNA Cat.no.: 1027281) could have various sense sequences and was used as negative control in silencing experiments. Storing conditions were the same as for all oligonucleotides.

### 3.7.3 Silencing of *SEC61A1*

For  $\text{Ca}^{2+}$  imaging experiments, *SEC61A1* was silenced in HEK D1ER cells using AMAXA Nucleofector II transfection protocol like described before (see 3.5.1). Imaging experiments followed after 72hours transfection with 50 pmol *SEC61A1* UTR siRNA. At this point we currently obtained a reduction of Sec61 $\alpha$  to about 40% (Figure 3.5) having enough (8-10) cells to measure in a view field. Rest of the cells from the same dishes was collected by detaching from the dish bottom with trypsin and underwent further cell lysing procedure for Western Blot as described before.

For HeLa cells silencing of *SEC61A1* gene was done by using chemical reagent HiPerfect (Quiagen®). This reagent contains charged lipophilic granules to which either sitting on the surface or by going inside the granule RNA molecules can enter the cell. HeLa cells in amount of  $5.2 \times 10^5$  were seeded on 6cm Petri dish with 2.5 cm glass coverslip inside. Reagent mixture of 20  $\mu\text{M}$  of HiPerfect of 4  $\mu\text{M}$  of 20  $\mu\text{M}$  siRNA and 80  $\mu\text{L}$  Opti-MEM was added to every 6cm dish with 4ml of culture medium. After 24 hours, medium was changed to fresh and the similar reagent mixture was added again. After 48 hours medium was changed again and cells were cultured for total time for 96 hours from the first transfection.

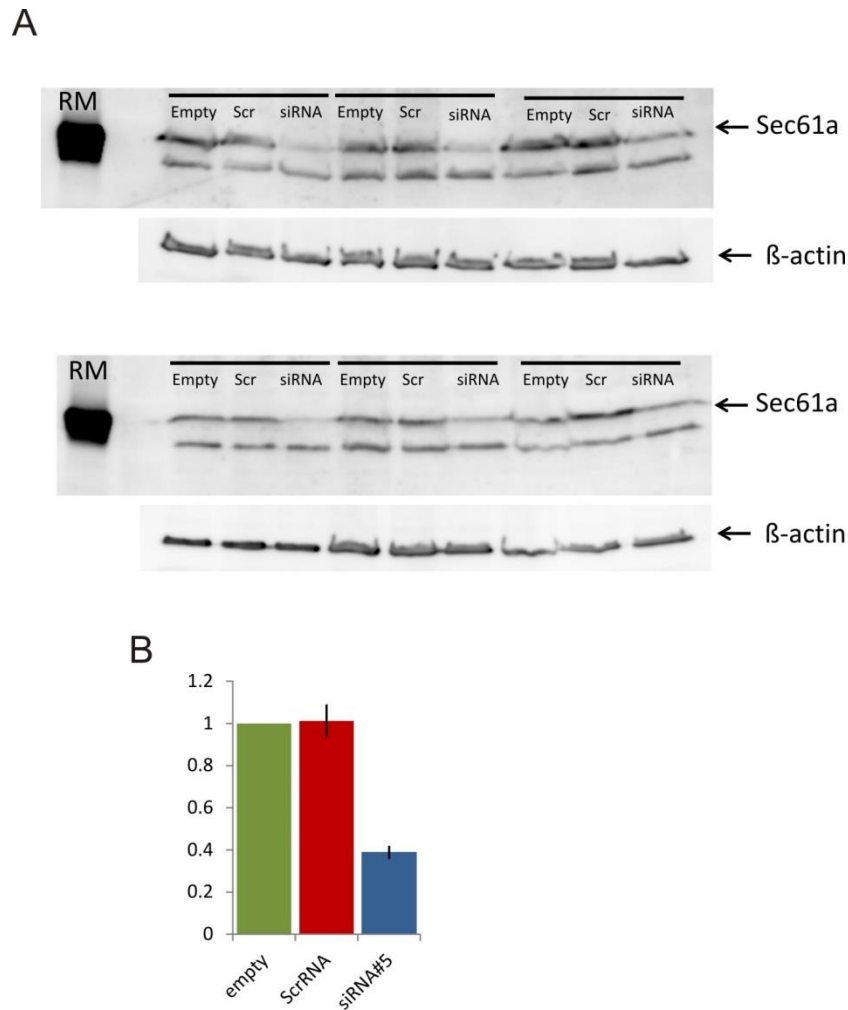


**Figure 3.5. Silencing efficiency with AMAXA. A.** Western blots of six independent *SEC61A1* silencing experiments with AMAXA Nucleofector II with 20nM *SEC61A1* UTR siRNA for 72 hours. **B.** Quantification of Sec61 protein levels in siRNA silencing experiments. Sec61 protein levels were normalized to  $\beta$ -actin levels and subsequently to the corresponding levels in non-transfected cells. (empty: non-transfected cells, scrRNA: cells transfected with control siRNA, siRNA#5: cells transfected with *SEC61A1* UTR siRNA; bars show mean  $\pm$  s.e.m., data collected from N=6 independent experiments).

### 3.7.4 Silencing of *ERj3* and *ERj6* co-chaperones

Silencing of ERj3 and ERj6 co-chaperones in HeLa cells was done as described in (Schorr et al. 2015).

### 3.8 Silencing efficiency

To check the efficiency of the transfection on the cells with siRNA performed with AMAXA Nucleofector II protocol we transfected HEK293 with fluorescent labelled Alexa488-siRNA. After the transfection cell were washed twice with fresh medium, precipitating with 200xg during 5 min, changing medium and resuspending. First, we compared the percentage of the transfected cells using Guava easyCyte 8HT cytometer (Figure 3.4). Subsequently, we compared the transfection efficiency with silencing efficiency of corresponding siRNA amounts after 96 and 120 hours by Western Blot (Figure 3.6).

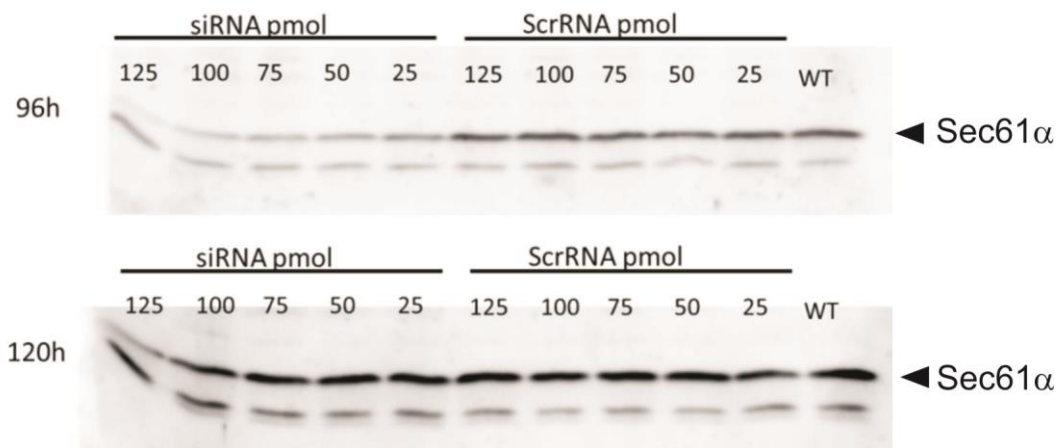


**Figure 3.6. Dose dependence of siRNA on silencing efficiency. Western Blots for 96 and 120 hours after transfection with 25, 50, 75, 100, 125 pmol of *SEC61A1* UTR siRNA with corresponding amounts of control siRNA. WT-non-transfected cells. level of Sec61α showed as black triangles obtained from the corresponding level of rough microsomes (not-shown on the blots). HEK293 were transfected with AMAXA Nucleofector II protocol as described before and collected after 96 and 120 hours after transfection.**

### 3.9 Recording solutions

HEK D1ER cells and HeLa cells during  $\text{Ca}^{2+}$  imaging experiments were treated in extracellular solutions presented in Table 3.5 for all experiments except calibration.

**Table 3.5 Experimental solutions:**

2mM $\text{Ca}^{2+}$ extracellular:		Nominal $\text{Ca}^{2+}$ free:		EGTA- $\text{Ca}^{2+}$ free:	
HEPES	25 mM	HEPES	25 mM	HEPES	25 mM
glucose	10 mM	glucose	10 mM	glucose	10 mM
NaCl	140 mM	NaCl	140 mM	NaCl	140 mM
KCl	4 mM	KCl	4 mM	KCl	4 mM
MgCl <sub>2</sub>	1 mM	MgCl <sub>2</sub>	1 mM	MgCl <sub>2</sub>	1 mM
CaCl <sub>2</sub>	2 mM	CaCl <sub>2</sub>	----	CaCl <sub>2</sub>	----
				EGTA	0.5 mM
pH	7.2 (NaOH)	pH	7.2 (NaOH)	pH	7.2 (NaOH)

The calibration of D1ER sensor in HEK D1ER cells was done in two steps. Firstly the maximal and minimal FRET ratio values were estimated. Secondly, defined steps of  $\text{Ca}^{2+}$  concentration were applied to D1ER sensor in vivo to estimate the  $K_D$  of the sensor in HEK D1ER cells. For the estimation maximal (DR<sub>max</sub>) and minimal (DR<sub>min</sub>) signal ratios  $\text{Ca}^{2+}$ -saturation solution (Table 3.6) and  $\text{Ca}^{2+}$ -depletion solution (Table 3.7) was applied on HEK D1ER cells.

**Table 3.6.  $\text{Ca}^{2+}$  -saturation extracellular.**

HEPES	25 mM
glucose	10 mM
NaCl	140 mM
KCl	4 mM
MgCl <sub>2</sub>	1 mM
CaCl <sub>2</sub>	50 mM
pH	7.2 (NaOH)
Nigericin	20 $\mu\text{M}$ (5 mM stock in DMSO)
Ionomycin	20 $\mu\text{M}$ (10 mM stock in DMSO)

**Table 3.7. Ca<sup>2+</sup>-depletion solution.**

HEPES	25mM
glucose	10 mM
NaCl	140 mM
KCl	4 mM
MgCl <sub>2</sub>	1 mM
CaCl <sub>2</sub>	---
EGTA	5 mM
pH	7.2 (NaOH)
Nigericin	20 μM (5 mM stock in DMSO)
Ionomycin	20 μM (10 mM stock in DMSO)

The calibration of D1ER signals was done on permeabilized HEK D1ER cells in intracellular-like solution (Table 3.8). This solution was applied on HEK D1ER cells together with saponin 0.003% (w/v) for 3 min, and then saponin was accurately removed by changing the solution to pure intracellular-like “0” solution.

**Table 3.8. Intracellular-like “0” solution.**

HEPES	25 mM
glucose	5 mM
NaCl	10 mM
KCl	135 mM
MgCl <sub>2</sub>	1 mM
sucrose	15 mM
pH	7.2 (KOH)

Calcium solutions with precise Ca<sup>2+</sup> concentrations (concentration steps) were applied on permeabilized HEK D1ER cells. Every concentration step was a result of a mixture of Ca<sup>2+</sup> containing solution (25 mM Ca<sup>2+</sup> in intracellular like “0” solution) and a solution containing Ca<sup>2+</sup>-buffer (25 mM of Ca<sup>2+</sup>-buffer prepared in intracellular like “0” solution). As Ca<sup>2+</sup> buffers EGTA, HEDTA, NTA (all Sigma Aldrich) were used. K<sub>DS</sub> of Ca<sup>2+</sup>-buffers and combination of Ca<sup>2+</sup> and Ca<sup>2+</sup>-buffer were calculated using Max Chelator Software (<http://maxchelator.stanford.edu/>). Combination between of Ca<sup>2+</sup>-buffer and Ca<sup>2+</sup> solution with adding pure intracellular-like “0” solution to obtain of 50 mL of calibration step solutions with precise concentrations of free Ca<sup>2+</sup> are in Table 3.9.

**Table 3.9. Ca<sup>2+</sup> calibration steps.**

Stock solutions		volume in mL for 50mL solution			
[Ca <sup>2+</sup> ] free	Buffer 25 mM	Buffer (mL)	Ca <sup>2+</sup> (mL)	Intra (mL)	pH
0	Ca-EGTA	2	0	48	<b>7.2</b>
30 nM	Ca-EGTA	2	0.296	47.704	<b>7.2</b>
100 nM	Ca-EGTA	2	0.734	47.266	<b>7.2</b>
300 nM	Ca-EGTA	2	1.268	46.732	<b>7.2</b>
1 μM	Ca-EGTA	2	1.31	46.69	<b>6.95</b>
1 μM	Ca-HEDTA	2	0.106	47.894	<b>7.5</b>
3 μM	Ca-HEDTA	2	0.2	47.8	<b>7.2</b>
10 μM	Ca-HEDTA	2	0.482	47.518	<b>7.2</b>
30 μM	Ca-HEDTA	2	0.892	47.108	<b>7.2</b>
100 μM	Ca-NTA	2	0.744	47.256	<b>7.2</b>
300 μM	Ca-NTA	2	1.644	46.356	<b>7.2</b>
1 mM	Ca-NTA	2	3.438	44.562	<b>7</b>
1 mM	Ca <sup>2+</sup>	0	2	48	<b>7.2</b>
3 mM	Ca <sup>2+</sup>	0	6	44	<b>7.2</b>
10 mM	Ca <sup>2+</sup>	0	20	30	<b>7.2</b>
25 mM	Ca <sup>2+</sup>	0	50	0	<b>7.2</b>

### 3.10 Chemical compounds and cell treatment

#### 3.10.1 Compounds

Various chemical compounds were used to study the role of the protein conducting channel Sec61 $\alpha$  in intracellular Ca<sup>2+</sup> homeostasis. The unmasking of passive Ca<sup>2+</sup> leak from the ER was done by inhibiting of SERCA functioning with thapsigargin. Cytosolic Ca<sup>2+</sup> clearance by mitochondria was impaired with CCCP (Montero et al. 2001). Ca<sup>2+</sup> fluxes through the plasma membrane were blocked by Gd<sup>3+</sup> (Amoroso et al. 1997, Blankenship et al. 2001). Protein synthesis inhibitors were used to identify the passive Ca<sup>2+</sup> leak from the Sec61 $\alpha$ . Puromycin and pactamycin were used to render the Sec 61 channel leaky by disassembling or preventing the assembly of the ribosome-translocon complex, respectively. Cycloheximide is supposed to stall the movement of the nascent

polypeptide chain inside the channel pore sealing the translocon for  $\text{Ca}^{2+}$  flux (Schneider-Poetsch et al. 2010, Van Coppenolle et al. 2004). Emetine is supposed to show similar results (Gupta and Siminovitch 1977). Trifluoperazine (TFP) is a calmodulin inhibitor working in the cytosol should prevent sealing of Sec61 $\alpha$  by CaM increasing the  $\text{Ca}^{2+}$  efflux from the ER. Tunicamycin is an inhibitor of N-glycosylation supposed to lead to UPR with following retrotranslocation through the Sec61 $\alpha$  and additional  $\text{Ca}^{2+}$  leak through the pore (Schauble et al. 2012). Eeyarestatin 1 and some of its analogues inhibit protein translocation through Sec61 complexes (Cross et al. 2009).

Name	Commercial supplier
Carbachol	SIGMA Aldrich
Thapsigargin	Molecular probes
Puromycin	SIGMA Aldrich
Pactamycin	SIGMA Aldrich
Cycloheximide	SIGMA Aldrich
CCCP	SIGMA Aldrich
Emetine	SIGMA Aldrich
Tunicamycin	SIGMA Aldrich
TFP	SIGMA Aldrich
Eeyarestatin 1	SIGMA Aldrich

### 3.10.2 “Online” treatment protocol

The cells were treated with substances during imaging experiments by bath application method. The experimental chamber consists of two round parts (upper and lower) with a sealing rubber ring on the bottom of the upper part. Assembly of the experimental chamber starts with placing of 2.5 cm glass coverslip on the lower part experimental chamber. Then, the upper part is placed on top and screwed to the lower tight enough for sealing rubber ring to keep experimental solution without leakage. The desired experimental solution is added to the experimental chamber and further change of solutions in “bath application” mode is possible. Bath application implies removal and re-addition by manual pipetting of the solutions directly in the experimental chamber. Initial volume of experimental solution in the experimental chamber was 300  $\mu\text{L}$  and addition of a substance meant application of another 300  $\mu\text{L}$  of the solution with 2 fold higher concentration of the substance. For next applications concentration of the substances in solutions were proportionally changed (for instance 3:1, for adding 300  $\mu\text{L}$  to existing 600  $\mu\text{L}$  etc.) to reach desired concentration of the substance in the whole experimental chamber.

### 3.10.3 “Offline” treatment protocol

Cell pretreatment with protein synthesis inhibitors (see 3.10.1) was done in experiments when we were studying rather effect of the effect of long time application than acute effects. Cells were cultured as described above and were put in 3.5 cm dishes with 2.5 cm glass coverslip inside each dish (see 3.2.3). Corresponding amount of antibiotic was dissolved in the same culture medium where cells were kept. The solution of antibiotic was added back to the dishes and cells were incubated for 10 minutes and up to 24 hours before imaging.

## 3.11 Single cell calcium imaging

Fluorescence microscopy is widely used in biology: small fluorescent molecules can be located inside the cell, be bound to antibody, or targeted to the specific organelle etc. The excitation of the fluorescent molecule with light causes accumulation of energy by electrons, which is then released as photons with longer wavelength than the initial excitation wavelength. It requires manufactured light sources and filter set for wavelength separation for distinguishing between excitation and emission lights.

### 3.11.1 Ratiometric measurements of cytosolic $\text{Ca}^{2+}$ with FURA-2

We used one of the most popular in use  $\text{Ca}^{2+}$  sensitive dye FURA-2 for cytosolic  $\text{Ca}^{2+}$  measurements. Cells can be loaded with amino ester group AM-tagged FURA, FURA-2-AM. This ester make the whole molecular non-polar, allowing it to pass the lipid barrier of the plasma membrane. In the AM form FURA-2 is  $\text{Ca}^{2+}$  insensitive. In the cytosol esterase cleaves the AM group and released FURA-2 can bind calcium ions with  $K_D=224$  nM. The spectral properties as well as synthesis of FURA-2 were described previously (Grynkiewicz et al. 1985). In Figure 3.7  $\text{Ca}^{2+}$ -unbound form of FURA-2 molecule has excitation maximum at 380 nm. Upon binding of FURA-2 to calcium ions the excitation spectrum shifted to the shorter wavelength, and has its absorption maximum at 340 nm. Both  $\text{Ca}^{2+}$ -bound and  $\text{Ca}^{2+}$ -free forms have their emissions maximum at 512 nm (Figure 3.7). In our experiments we were loading cells with 4  $\mu\text{L}$  of FURA-2-AM (Invitrogen, Molecular Probes) stock solution (1 mM in DMSO) in 1 mL of culture medium during 20 minutes for HEK293 and HEK D1ER and for 30 minutes for

HeLa cells at RT. About another 10 minutes before start recording were usually taken to complete the desferification of the AM form inside the cells.

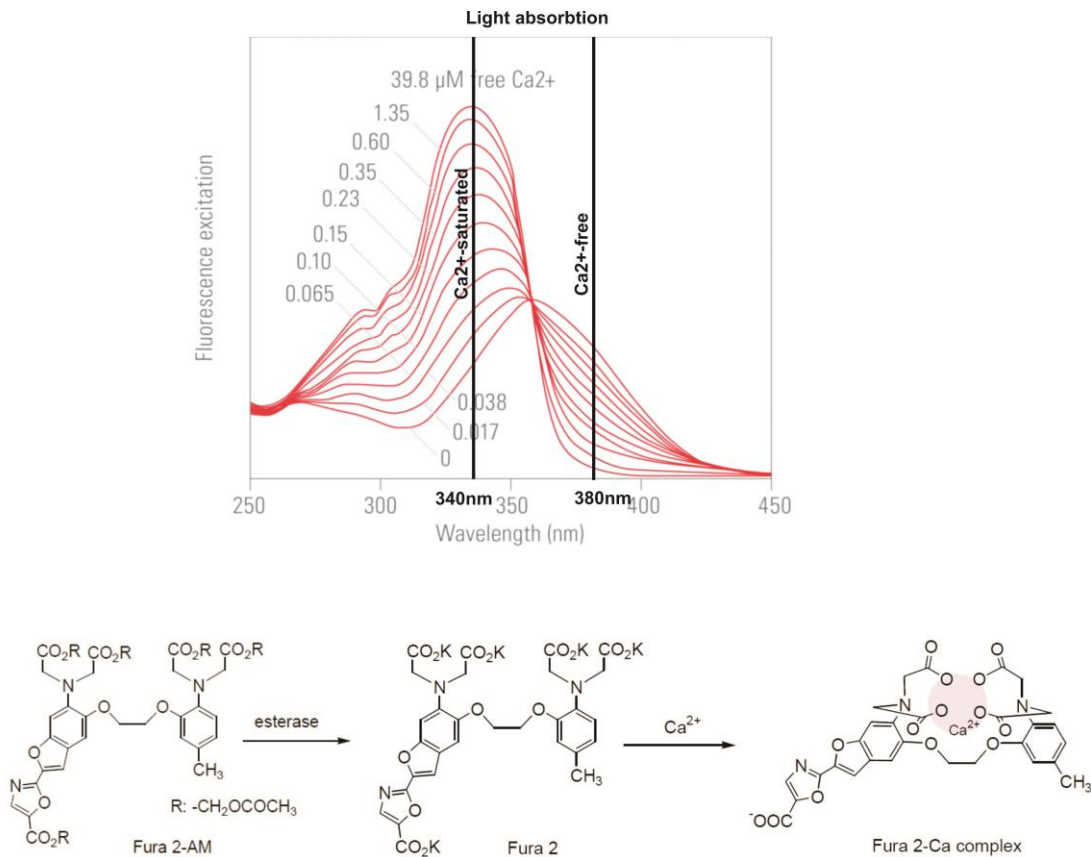


**Figure 3.7. FURA-2. Upper: FURA-2 dye excitation spectra with various concentration of  $\text{Ca}^{2+}$ . 340nm is used for  $\text{Ca}^{2+}$  saturated form, and 380nm for  $\text{Ca}^{2+}$ -free state. Lower: scheme of the deesterification of FURA2-AM in the cytosol and binding of  $\text{Ca}^{2+}$  to FURA-2. (Adapted from: Leica microsystems, Molecular Probes Handbook.)**

FURA-2 is used as a ratiometric  $\text{Ca}^{2+}$  sensitive dye. The ratio between emission intensities of  $\text{Ca}^{2+}$ -bound form i.e. with 340 nm excitation light, and  $\text{Ca}^{2+}$ -free form with the maximum of emission at 380 nm excitation light represent the amount of  $\text{Ca}^{2+}$ -free to FURA-2 in solution. The relation between fluorescent intensities obtained  $\text{Ca}^{2+}$ -bound form, excited with 340 nm, and  $\text{Ca}^{2+}$ -free form, excited with 380 nm can be represented as ratio FR:

Eq. 5:

$$FR = \frac{F340 - bg340}{F380 - bg380};$$

where bg340 and bg380 are background intensities for 340 nm and 380 nm excitations respectively.

### 3.11.2 Principles of FRET-based measurements of ER Ca<sup>2+</sup> with D1ER

Ca<sup>2+</sup> concentrations inside intracellular compartments can differ drastically from cytosolic. Thus, due to high Ca<sup>2+</sup> concentration inside the ER the last was referred to as an important store of releasable Ca<sup>2+</sup>. The release of Ca<sup>2+</sup> from the ER participates in and regulates a lot of intracellular functions. Ca<sup>2+</sup> indicators designed for the ER Ca<sup>2+</sup> measurements have either biological or chemical nature and in both cases should have suitable affinity to Ca<sup>2+</sup> for intraluminal measurements. Due to the importance of ER Ca<sup>2+</sup> measurements many indicators have been designed to the date. The chemical compounds like FLUO-5N, Mag-FLUO-2, Mag-FURA-2 can be delivered to the cell as AM-form and then trapped in the ER lumen (for the review (Gerasimenko and Tepikin 2005)). They are relatively stable to the wide range of pH changes; however, the question of drastically changes in pH inside the ER lumen at physiological conditions remains unclear. Other Ca<sup>2+</sup> indicators that are used nowadays are based on fluorescent proteins. The era of fluorescent proteins starts with jellyfish *Aequoria victoria* in which two major fluorescent proteins (FP) were found- Aequorin and GFP (for review (Whitaker 2010)). Ca<sup>2+</sup>-sensitive Aequorin has a bioluminescence, but not that bright as GFP. GFP and its recombinants are now widely used in cellular biology. Fluorescent markers based on GFP-like FPs, FRET sensors, and GCaMPs are routinely used. FPs for Ca<sup>2+</sup> measurements that can be used inside cells by including their sequence to cell genome called Genetically Encoded Calcium Indicators (GECI). GECIs are much more “natural” for the cell and can be expressed constantly; however their fluorescent properties (brightness and resistance to photobleaching) are not that good as for designed chemical dyes or nanodots. The GECI can be directly delivered to the chosen organelle by adding retention sequence providing much better targeting of the indicator then for chemical ones (Gerasimenko and Tepikin 2005). However building up a Ca<sup>2+</sup> sensitive system based on GECI needs to overcome several moments. The proper targeting of GECI to its destination is crucial for intraorganell measurements. As every protein GECI should be translocated, folded and delivered to its destination, which requires some time and that make acute transfection very versatile in expression level and retention of the FPs. Continuous excessive expression of the non-native protein can lead to the ER stress and apoptosis; therefore

using GECI requires a control of expression level, which in many cases interferes with the desirable brightness. FP-based sensors are also very sensitive to pH which leads to certain restrictions for measurements in lysosomes and lytic granules (Demaurex 2005).

The theory of Resonance Energy Transfer between two closely located fluorophores originated from ideas in quantum physics at the beginning of 1920's, however was fully proposed by Förster (Forster 1948). FRET (Förster Resonance Energy Transfer) principle is a non-radiative transfer of energy between two oscillating dipoles located on a short distance and, for the best energy transfer, parallel in spatial orientation. According to Stock's principle the energy stored in oscillations can only be transferred to the lower wavelengths, therefore the initial oscillator, called the "donor", always activates the following oscillator the "acceptor", which has its spectrum located on the right of donor spectrum. FRET requires also a spectral overlap, which represents how much the emission spectrum of the donor overlaps with the excitation spectrum of the acceptor. The overlap integral shows the transfer of the non-emitted photons from donor to the acceptor (Figure 3.8 A, B). Quantum yield of a fluorescent molecule is relation of the emitted photons to the absorbed photons. All together these factors can be presented as FRET efficiency. The FRET efficiency is defined as fraction of the photons transferred to the acceptor to the amount of the photon absorbed by the donor (Figure 3.8 C). FRET is used for biological fluorescent imaging. GFP-like donor-acceptor pairs can be used as universal fluorescent markers that report the shortening distance between donor and acceptor via FRET. Either connected in one molecule and linked by a sensor, or linked to the separate molecules of the interacting proteins of interest, FRET based sensors allow wide range of measurements like caspase activation, enzymatic cleavage, assembly of the oligomers,  $\text{Ca}^{2+}$  imaging etc.

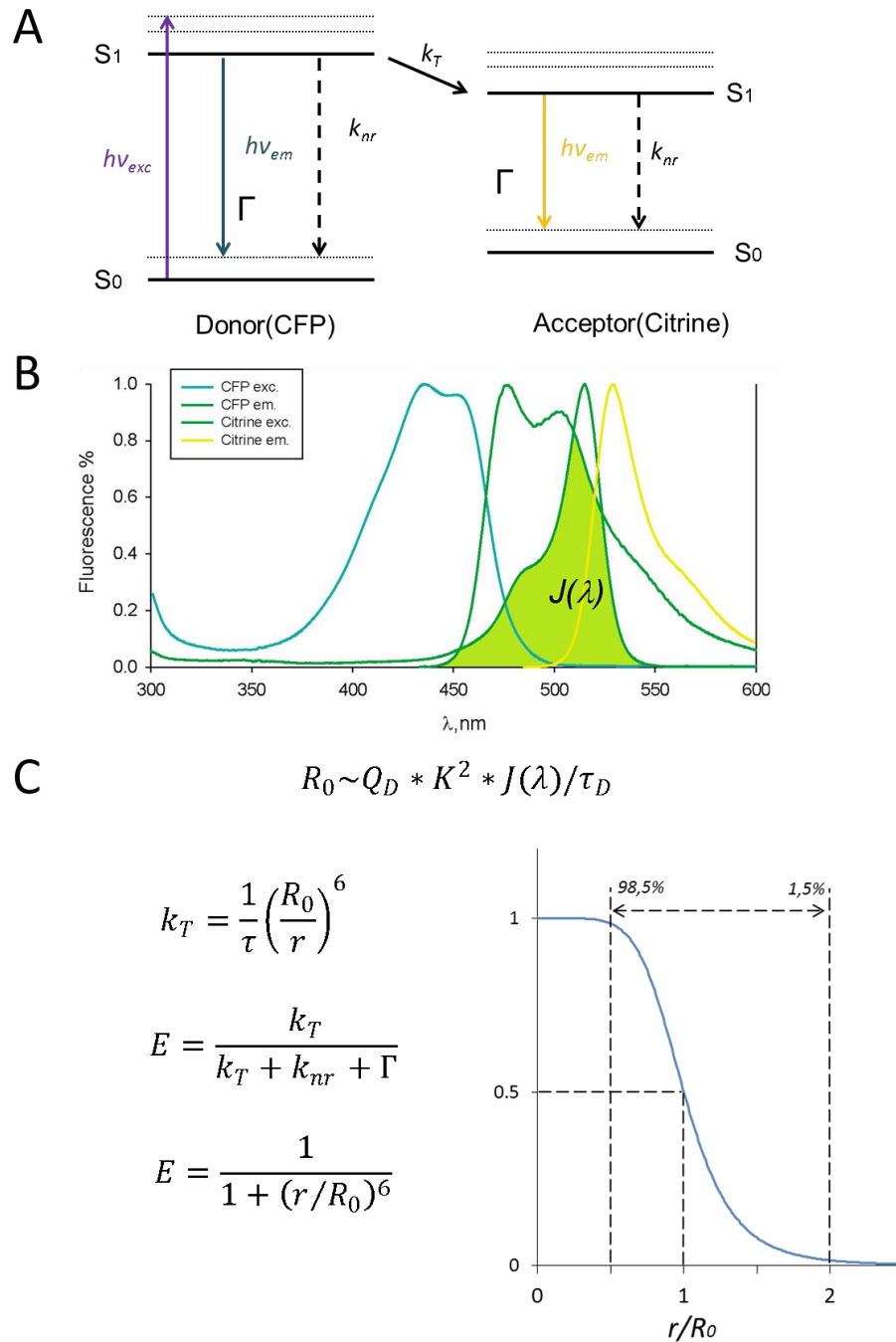


**Figure 3.8. Principles of Förster Resonance Energy Transfer (FRET).** **A:** Jablonski diagram between two excited states of donor (CFP) and acceptor (Citrine),  $k_T$  –non-radiative transfer of energy (FRET) rate from excited energetic level of donor  $h\nu_{exc}$  (from  $S_0$  non-excited energetic level to  $S_1$  excitatory energetic level of the donor) to the excited state of acceptor with following radiative emission with energy  $h\nu_{em}$  (from  $S_1$  excited energetic level to  $S_0$  non-excited energetic level of the acceptor, the  $\Gamma$  function) Dashed lines: energetic

sublevels showing changes of the energy states by non-radiative dissipation inside each of the molecules. B. Spectral diagram: Overlap integral  $J(\lambda)$  on the spectral diagram between CFP and Citrine shows the amount of fluorescence energy that can be transferred (normalized spectra taken from R.Tsien Lab database for FPs, [www.tsienlab.ucsd.edu/Documents/REF%20-%20Fluorophore%20Spectra.xls](http://www.tsienlab.ucsd.edu/Documents/REF%20-%20Fluorophore%20Spectra.xls)). C.  $R_0$ -characteristic distance (Förster radius) is proportional to donor quantum yield  $Q_D$ , orientation factor  $K$ , and overlap integral  $J(\lambda)$ .  $\tau$  is oscillation lifetime of the excited molecule. Transfer rate  $k_T$  and FRET Efficiency  $E$  are proportional to the distance  $r$  between donor and acceptor. (Adapted from: (Periasamy and Day 2005))

In the present study we used FRET-based  $\text{Ca}^{2+}$ -sensitive chameleon D1ER. D1ER was designed for intraluminal  $\text{Ca}^{2+}$  imaging by Roger Tsien's group and described in (Palmer et al. 2004) D1ER is a Genetically Encoded Calcium Indicator, which has ECFP as donor and Citrine as acceptor (see Figure 3.1). It has also calreticulin signal sequence and KDEL retention sequence which accurate targeting of the indicator to ER.

As illustrated in Figure 3.9  $\text{Ca}^{2+}$  sensor of D1ER is an amino acid sequence containing CaM and myosin light chain kinase (MLCK, M13). Upon binding to four  $\text{Ca}^{2+}$  ions it changes its conformation and decreases the distance between CFP and Citrine allowing FRET to occur.

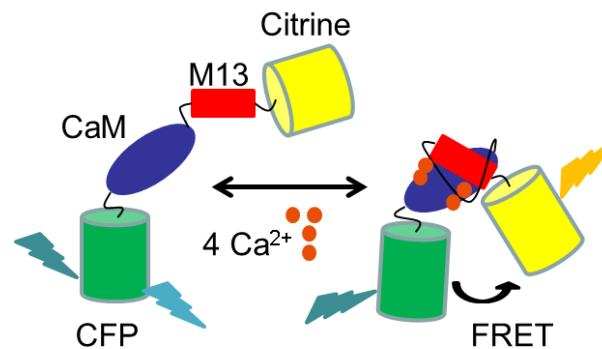


**Figure 3.9. Schematic structural conformation changes of the D1ER molecule upon  $\text{Ca}^{2+}$  binding.**

D1ER is a ratiometric  $\text{Ca}^{2+}$  indicator, its FRET efficiency changes to maximum upon binding to  $\text{Ca}^{2+}$  ions. In a  $\text{Ca}^{2+}$  free environment, FRET between ECFP and Citrine does not occur and, therefore, upon excitation with 433 nm, the fluorescence emitted by D1ER is the cyan fluorescence of about 488 nm. Conversely, there is a strong FRET between

ECFP and Citrine in the  $\text{Ca}^{2+}$ -bound form of D1ER and the excitation of ECFP with 433 nm produces mainly the Citrine fluorescence of about 536 nm. The background corrected ratio between Citrine and CFP emission light intensities represents the concentration of the free  $\text{Ca}^{2+}$ .

Eq. 6:

$$FRET\ Ratio = \frac{F_{CITRINE} - bg_{CITRINE}}{F_{ECFP} - bg_{ECFP}},$$

For the more accurate ER  $\text{Ca}^{2+}$  measurements we have cell lines with stably expressing D1ER in the ER based on HEK and HeLa cells.

### 3.12 Imaging setup

#### 3.12.1 iMIC microscope and illumination system.

The possibility of simultaneous measurements of cytosolic and luminal  $\text{Ca}^{2+}$  using FURA-2 and D1ER has been previously shown in MCF-7 and HeLa cells (Palmer et al. 2004). To perform simultaneous measurements of cytosolic and ER  $\text{Ca}^{2+}$  in HEK D1ER cell line we used iMIC digital microscope (Till Photonics) and Polychrome V light source (Till Photonics). The computerized system of iMIC microscope with Live Acquisition software (v.2.0101 Till Photonics.) allowed changes of filter sets with minimal delay of 0.503 s. The imaging system is schematically illustrated in Figure 3.10. The exposure time with required wave lengths from Polychrome V light source was chosen empirically to prevent photobleaching of D1ER. The exposure time of 25 ms was enough to see major amount of HEK D1ER cells with the intensity at least 100 a.u. above the background intensity for both CFP and Citrine fluorescences. The time between two frames was chosen as 10-12 s showing linear bleaching of 0.75 % per minute. Considering this decrease of the fluorescent negligible with comparison to fast changes in ER  $\text{Ca}^{2+}$ , no photobleaching correction was applied for the chosen exposure time and period.

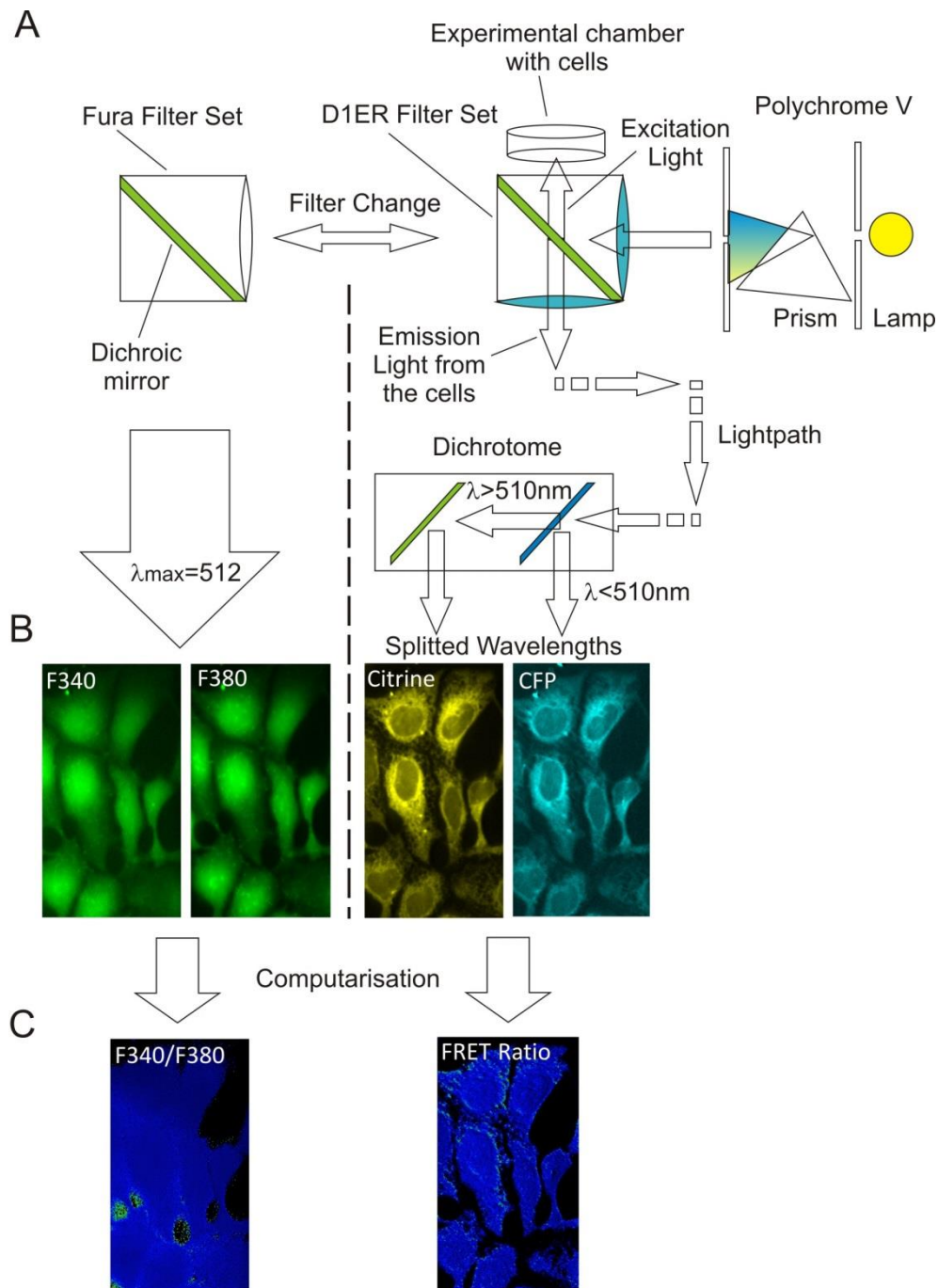


**Figure 3.10.** System used for simultaneous imaging of cytosolic and ER  $\text{Ca}^{2+}$ . **A.** Principal scheme of iMIC digital microscope with Polychrome V light source. *Right:* Sample is illuminated through D1ER filter set with 433 nm excitation light. Emitted light comes through lightpath to the Dichrotome which splits Cyan (469 nm) and Citrine (536 nm) emitted wavelengths. *Left:* FURA-2 filter set has the similar principle with excitation wavelength of 340 nm and 380 nm and with emission of 512 nm which is obtained for both excitations from only one part of the dichrotome output. **B** Raw images of the cells obtained in gray scale with ANDOR camera and represented as colored images with corresponding

emission colors. C. Calculated Ratio images of the FURA-2 ratio (F340/F380) and FRET ratio signals.

### 3.12.2 Optical filters

The automatic microscope iMIC from TILL Photonics together with iMIC Control Unit and Live Acquisition Software were used for  $\text{Ca}^{2+}$  imaging. The construction of iMIC microscope allowed us making imaging from cells illuminated through different filter sets with the light from Polychrome V light source (for the principle scheme see Figure 3.10). Light filter sets were as required for imaging GFP, FURA-2, and D1ER (AHF F56-017, from AHF, Germany). For parameters see Table 3.10.

**Table 3.10. Excitation and emission of D1ER and FURA-2 during experiments.\*LP- long path filter.**

	$\lambda_{\text{excitation}}$ max / bandwidth	$\lambda_{\text{emission}}$ max / bandwidth	Filter set
D1ER $\text{Ca}^{2+}$ -bound	433 / 15 nm	536 / 27 nm	AHF F56-017
D1ER $\text{Ca}^{2+}$ -free	433 / 15 nm	469 / 23 nm	AHF F56-017
FURA-2 $\text{Ca}^{2+}$ -bound	340 / 15 nm	512 nm / LP*	FURA-2
FURA-2 $\text{Ca}^{2+}$ -free	380 / 15 nm	512 nm / LP	FURA-2

### 3.12.3 Software control

Live Acquisition Software v 2.0101 allowed automatic control of iMIC microscope via iMIC control unit. All D1ER FRET Ratio signals from cells were taken as individual image frames of Citrine and CFP pictures via ANDOR camera through iMIC microscope, taken with 25 ms of exposure time for every wavelength and transferred to Live Acquisition Software where underwent 2x2 digital binning. Corresponding ROI from

“left” (FRET) and “right” (CFP) side (due to dichrotome split wavelengths) on the camera chip were overlapped and correct position of images adjusted. Ratio from background corrected intensities as average value of non-zero “pixel to pixel” ratios between FRET ROI and CFP ROI was taken as FRET Ratio. Time dependent stack of FRET Ratios from single ROI represents full FRET trace and was saved as Microsoft Excel file for further analysis. The original videos are also saved as TIFF files.

### **3.13 Simultaneous measurement of FURA-2 and D1ER signals.**

For simultaneous measurements of cytosolic and ER  $\text{Ca}^{2+}$  HEK D1ER and HeLa cells were cultured and put into 3.5 cm dishes with glass coverslips as described before. HEK D1ER cells were loaded with FURA-2 via incubating in culture medium with  $4\mu\text{M}$  of FURA-2-AM at RT. After 20 minutes the medium was removed and cells were washed twice with  $2\text{mM}$   $\text{Ca}^{2+}$  extracellular solution and let for about 10 minutes to complete de-esterification of AM tails inside cells before the imaging of cells starts. Shifts between FURA-2 and D1ER filter sets required 0.503 second. Exposure time for FRET and FURA-2 images was the same and adjusted to 25 ms. Time between two frames was set up to 12 s to avoid photobleaching of the D1ER. However for the short periods of recordings (up to 10 minutes) time between taking images could be reduced to 3 seconds without having a crucial effect of D1ER photobleaching on FRET Ratio signals.

#### **3.13.1 Spectral overlap of FURA-2 and D1ER fluorescence**

Fluorescent properties of D1ER and FURA-2 show fluorescence spectral overlap (Figure 3.11). FURA-2 (Figure 3.11 A) has a maximum of absorbance in  $\text{Ca}^{2+}$ -bound form at 340 nm and in  $\text{Ca}^{2+}$ -free form at 367 nm. The emission of both  $\text{Ca}^{2+}$  bound and  $\text{Ca}^{2+}$  free forms have a maximum at 512 nm (Figure 3.11 A) with the difference in amplitudes of emission spectra representing the relative amount of  $\text{Ca}^{2+}$  bound to the FURA-2. Spectra of D1ER sensor (Figure 3.11 B) consists of eCFP excitation spectrum (maximal absorption at 433 nm), Citrine excitation spectrum (maximal absorption at 488 nm) eCFP emission spectrum (maximal emission at 469 nm) and Citrine emission spectrum (maximal emission at 536 nm). The spectral overlap between FURA-2 and D1ER occurs both on the excitation and emission parts of the spectra (Figure 3.11). During the measurement of cytosolic  $\text{Ca}^{2+}$  the excitation of  $\text{Ca}^{2+}$ -free form of FURA-2 (blue line crossing FURA-2 excitation spectrum, Figure 3.11 A) has an excitatory effect on D1ER

excitation spectra (blue line crossing eCFP, Figure 3.11 B). The emission of the excited D1ER bound to  $\text{Ca}^{2+}$  (yellow line crossing Citrine emission spectrum, Figure 3.11 B) is seen as light with the wavelength close to the FURA-2 emission maximum (yellow line crossing FURA-2 emission spectrum, Figure 3.11 A). Therefore the bleed-through, while using the FURA-2 and D1ER fluorescent filter sets, was accounted for.

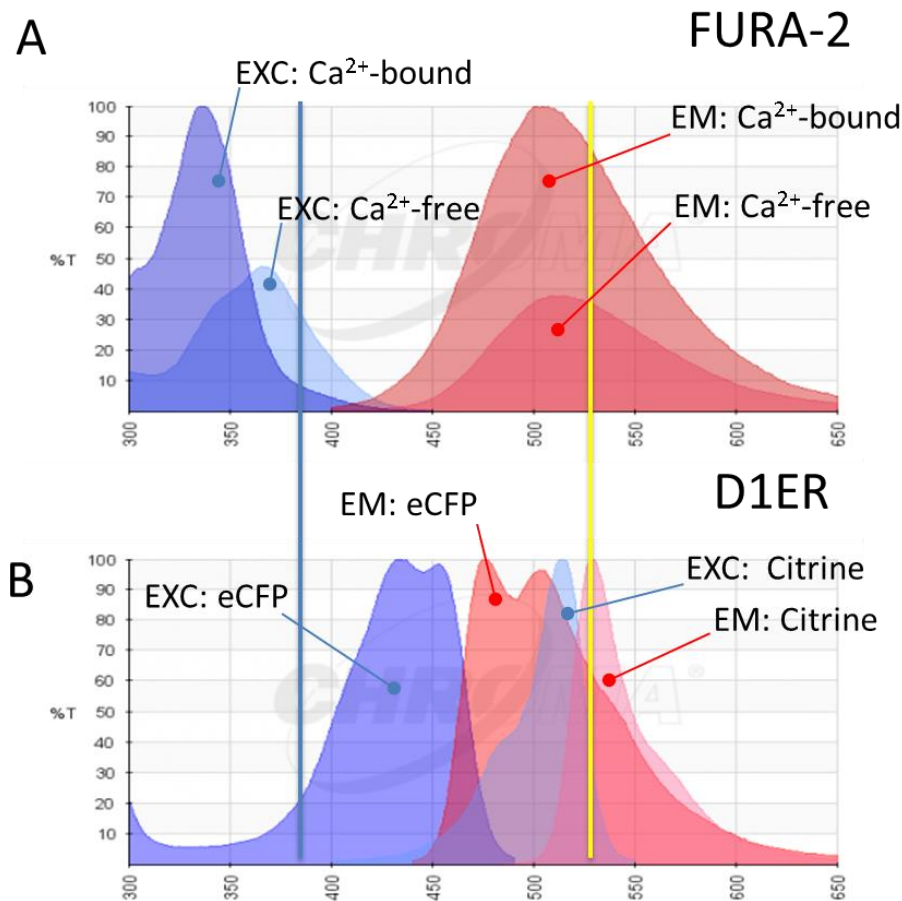


**Figure 3.11.** Comparison of excitation and emission spectra of FURA-2 and fluorophores of D1ER. A. Excitation (blue) and emission (red) spectra of FURA-2 in the  $\text{Ca}^{2+}$ -free (EXC:  $\text{Ca}^{2+}$ -free) and  $\text{Ca}^{2+}$ -bound (EXC:  $\text{Ca}^{2+}$ -bound) form. B. D1ER spectra of the fluorescent proteins eCFP as donor and Citrine as acceptor for FRET. Shown are the excitation (blue, “EXC: eCFP” and “EXC: Citrine”) and emission (red, “EM: eCFP” and “EM: Citrine”) spectra of eCFP and Citrine. Excitation with 380 nm (vertical blue line) would excite FURA-2 and eCFP. The emission of Citrine partially overlaps with the emission of FURA-2 (yellow vertical line). Spectra were created with CHROMA application ([www.chroma.com](http://www.chroma.com))

### 3.13.2 Bleed through

The bleed through of D1ER fluorescence to FURA-2 fluorescence and *vice versa* was observed using D1ER and FURA-2 filter sets (Table 3.10).

For the estimation of bleed through of FURA-2 to D1ER fluorescence, HEK293 (expressing no D1ER) were loaded with FURA-2 (see 3.11.1). Using FURA-2 filter set the fluorescence of  $\text{Ca}^{2+}$ -free form (excitation at 380 nm, and emission at 512 nm) and  $\text{Ca}^{2+}$ -bound form (excitation at 340 nm, and emission at 512 nm) was measured. Then the FURA-2 fluorescence filter was changed to D1ER fluorescence filter set and the fluorescence from the same cells of FURA-2  $\text{Ca}^{2+}$ -free form (excitation at 380 nm, and fluorescence seen through Citrine and eCFP emission filters) and FURA-2  $\text{Ca}^{2+}$ -bound form (excitation at 340 nm, and fluorescence seen through Citrine and eCFP emission filters) was measured. For each individual cell the FURA-2 fluorescence in  $\text{Ca}^{2+}$ -free form (excitation with 340 nm) was plotted as blue squares with y-axis value of the fluorescence measured through FURA-2 filter set (Figure 3.12 A, Emission F340) and x-axis value of the fluorescence seen through D1ER filter set (the measured fluorescence through Citrine emission filter plus the fluorescence measured through eCFP emission filter, Figure 3.12 A, Emission F536 + F469). In the same way the fluorescence values from the same cells were plotted as blue circles after the excitation with 380 nm (y-axis, Emission F380; x-axis: Emission F536 + F469, Figure 3.12 A).

For the estimation of D1ER bleed through to FURA-2 fluorescence, HEK D1ER cells, not loaded with FURA-2, were used. The fluorescence of D1ER was measured through D1ER filter set after excitation with 433 nm (eCFP excitation) as fluorescence seen through Citrine emission filter plus the fluorescence through eCFP filter. Then the same cells were observed through FURA-2 filter set. The fluorescence was measured after excitation with 340 nm and 380 nm of the same D1ER cells. The fluorescence values after excitation with 340 nm were plotted as green squares on y-axis (Figure 3.12 A, Emission F340) and x-axis values of D1ER corresponding fluorescence (Figure 3.12 A, Emission F536 + F469). The fluorescence values after excitation with 380 nm of the same D1ER cells were plotted as green circles (y-axis, Emission F380; x-axis: Emission F536 + F469, Figure 3.12 A).

The HEK293 cells, not expressing D1ER and not loaded with FURA-2, were used to estimate an auto fluorescent background. The way of observation was analogous to that

described above and the fluorescent values, measured through FURA-2 filter set, were plotted as gray squares (after excitation with 340 nm) and gray circles (after excitation with 380 nm) versus the corresponding fluorescence values observed through D1ER filter set (Emission F536 + F469, after excitation with 433 nm, Figure 3.12 A). Fluorescent values of these cells were taken as auto fluorescent background for the expected fluorescence signals seen through FURA-2 filter set (horizontal red dashed line, Figure 3.12 A) and D1ER filter set (vertical red dashed line, Figure 3.12 A). The cells loaded with FURA-2 (blue circles and squares) and cells expressing D1ER (green circles and squares) showed linear relationships in D1ER and FURA-2 bleed through (black dashed lines, Figure 3.12 A). For the cells loaded with FURA-2 (blue circles and squares) the bleed through of FURA-2 to D1ER was negligible: black dashed lines made through blue circles and squares are almost overlapping with vertical red dashed line, which represents D1ER auto fluorescent background (Figure 3.12 A). The D1ER bleed through to FURA-2 fluorescence, however, has a significant value. Both excitations with 340 nm (green squares) and 380 nm (green circles) showed linear relationships depending on D1ER fluorescent: black dashed lines are tilted from the auto fluorescent background (horizontal red dashed line, Figure 3.12 A).

Therefore, for the used illumination system (D1ER, FURA-2 filter sets and Polychrome V light source, see 3.12.1) the bleed through of D1ER to FURA-2 fluorescent was estimated at 0.10 of measurable D1ER fluorescence after excitation with 340 nm and 0.32 of measurable D1ER fluorescence after excitation with 380 nm:

Eq. 7:

$$F_{D1ER\_to\_F340} = 0.10 * (F536 + F469);$$

and:

Eq. 8:

$$F_{D1ER\_to\_F380} = 0.32 * (F536 + F469);$$

The  $Ca^{2+}$  dependence of the bleed through of D1ER to FURA-2 fluorescence (and vice versa) was tested on HEK D1ER cells (not loaded with FURA-2) and HEK293 cells (loaded with FURA-2, but not expressing D1ER). Thapsigargin, the irreversible inhibitor of SERCA pumps, was applied to destroy intracellular  $Ca^{2+}$  homeostasis by inducing the

$\text{Ca}^{2+}$  depletion of endoplasmic reticulum. However, the cells loaded with FURA-2 showed no change in observed D1ER Ratio (F536/F469) after the application of thapsigargin (arrow indicated, left graph on Figure 3.12 B). Neither that HEK D1ER cells (not loaded with FURA-2) showed any change in observed FURA-2 ratio (F340/F380) application of thapsigargin (arrow indicated, right graph on Figure 3.12 B). Therefore, the bleed through was considered to be  $[\text{Ca}^{2+}]$  independent, and the proposed coefficients (of D1ER bleed through to FURA-2) were valid for the correction of the observed FURA-2 fluorescence in HEK D1ER cells loaded with FURA-2 at any moment of the fluorescent measurement.

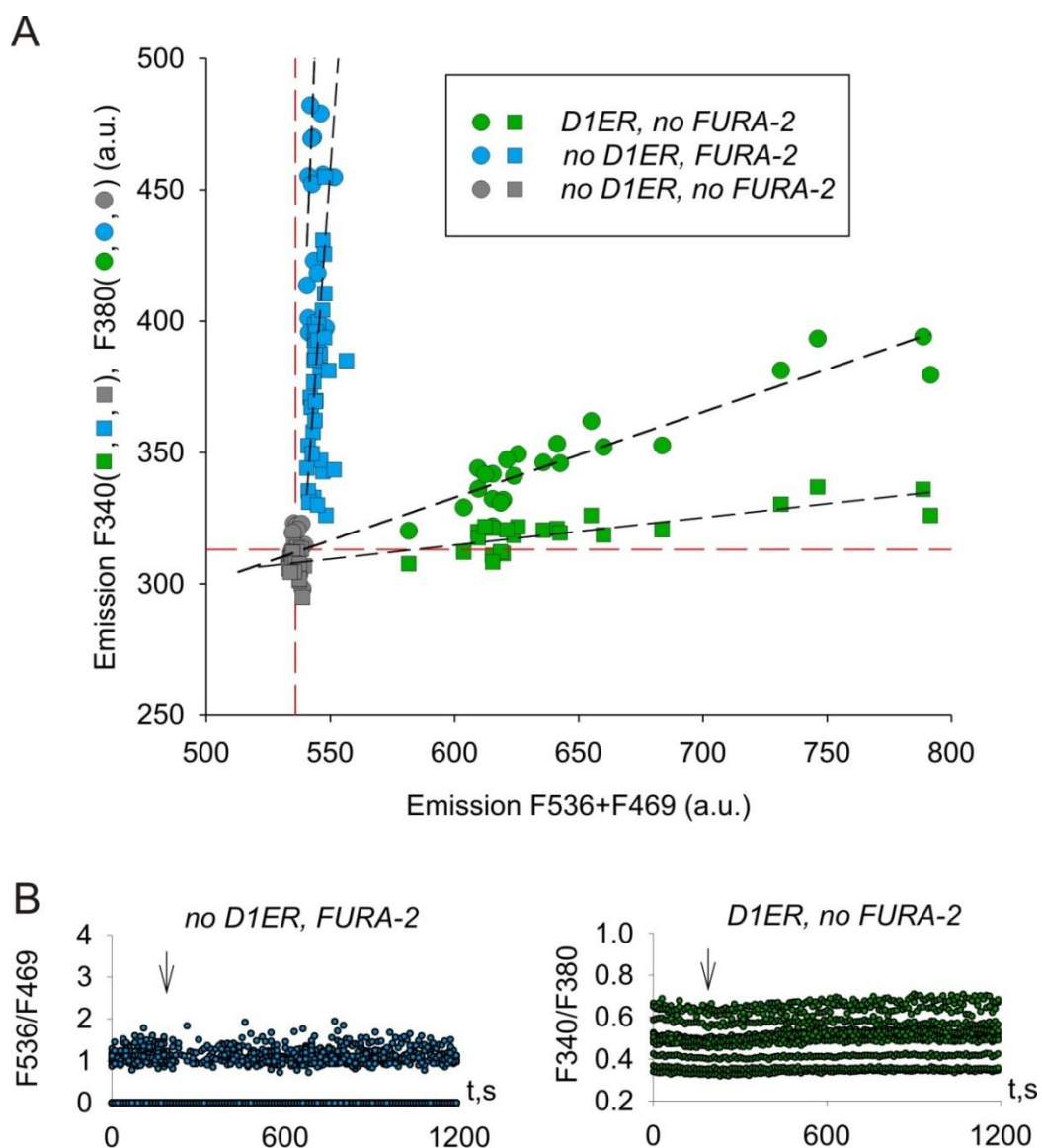


**Figure 3.12.** Bleed-through in simultaneous measurements of cytosolic and ER  $\text{Ca}^{2+}$  with FURA-2 and D1ER respectively. A Actual bleed through from D1ER and FURA-2 through

iMIC Filter sets. For HEK D1ER cells not loaded with FURA-2, represented as green: total D1ER emission (through D1ER filter set ,F536 + F469) intensities plotted as x-values after 433 nm excitation, and as y-values for emission (512 nm) intensities detected through FURA-2 Filter Set after 340 nm excitation (F340,squares), and 380 nm excitation (F380,circles). For HEK293 cells loaded with FURA-2 and not expressing D1ER represented as blue: total FURA-2 emission (through D1ER filter set, F536 + F469) intensities plotted as x-values after 433nm excitation, and as y-values for emission (512 nm) intensities seen from FURA-2 Filter Set after 340nm excitation (F340, squares), and 380nm excitation (F380, circles); non-loaded HEK293 as non-fluorescent controls are grey circles and squares. Red dashed lines: average backgrounds. Black dashed lines: linear regressions of bleed through signals between FURA-2 and D1ER fluorescence according to equations (page 57). B. Time course of FURA-2 bleed through seen from D1ER filter set after application of TG (arrow) on HEK293 loaded with FURA-2 (left), and time course of D1ER bleed through seen from FURA-2 filter set after application of TG (arrow) on HEK D1ER cells (right). C. Example of corrections in FURA-2 signals. TG response in HEK D1ER loaded with FURA-2 green: uncorrected vs. black: corrected; red: TG response in HEK293 loaded with FURA-2;

### 3.13.3 Calibration of FURA-2 signals

Calibration of the FURA-2 was done on HEK293 cells loaded with FURA-2 as described (3.11.1). Maximal (FR<sub>max</sub>) and minimal (FR<sub>min</sub>) ratio values of FURA-2 was measured by adding of 25 mM Ca<sup>2+</sup> and 0.5 mM EGTA to nominal Ca<sup>2+</sup> free solution (see 3.9; Table 3.5). Obtained values were used routinely in the calibration of FURA-2 signal, and the procedure of FR<sub>max</sub> and FR<sub>min</sub> measurement was repeated every time when Polychrome V lamp was changed.

To determine the experimental dissociation constant ( $\beta K_D$ ) of FURA-2 standard calibration FURA-2 kit (Invitrogen™, Molecular Probes®, F6774) was used. Steps of the Ca<sup>2+</sup> concentration seen as dot-plot (Figure 3.13), where the relation between FURA-2 ratio (FR) and Ca<sup>2+</sup> concentration was calculated following the formula from (Grynkiewicz et al. 1985):

Eq. 9:

$$[Ca^{2+}]_{cyt} = \beta K_D \frac{FR - FR_{min}}{FR_{max} - FR};$$

$\beta K_D$  was estimated as 5.26  $\mu\text{M}$  after fitting of the dot-plot with linear function and the extrapolation of this function to the x-axis interception (red line, black solid reference line showing  $\beta K_D$  on Log (free  $\text{Ca}^{2+}$ ) axis, Figure 3.13)

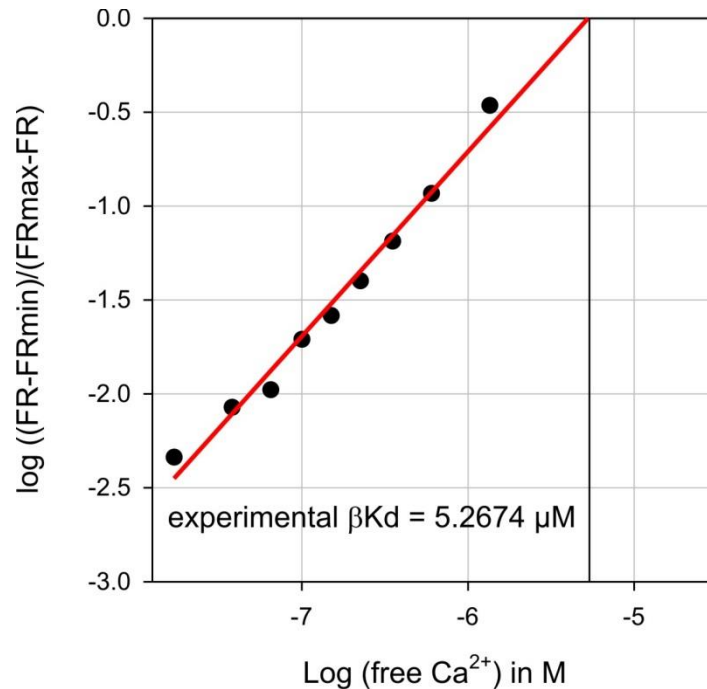


**Figure 3.13. Experimental calibration of FURA-2 on iMIC System. Points obtained from background corrected ratio of FURA-2 standard solutions (Invitrogen™, Molecular Probes®, F6774) plotted versus corresponding free  $\text{Ca}^{2+}$  concentrations. Red line: linear function, fitting of the dot-plot, which leads to the x-axis interception showing the experimental  $K_D$  of 5.2674  $\mu\text{M}$**

#### 3.13.4 Calibration of D1ER signals

The proposed model of D1ER binding to  $\text{Ca}^{2+}$  has double hill-shape and predicts  $K_{DS}$  of 0.8  $\mu\text{M}$  and 56  $\mu\text{M}$  *in vitro*,  $k_{on}$  and  $k_{off}$  were  $3.6 \cdot 10^6 \text{ M}^{-1} \text{ s}^{-1}$  and  $250 \text{ s}^{-1}$  respectively (Palmer and Tsien 2006) .

Calibration of D1ER sensor was done *in vivo*. During experiments I analyzed more than 500 cells from which D1ER signal (FRET Ratio, DR) was measured. To collect  $DR_{max}$  I performed saturation of the intraluminal sensor D1ER by exposing the cells to 25 mM  $\text{Ca}^{2+}$  with 10  $\mu\text{M}$  *Ionomycin*.  $DR_{min}$  was measured with 10  $\mu\text{M}$  *Ionomycin* in  $\text{Ca}^{2+}$ -free solution contained 0.5 EGTA. DR values were collected from several dishes after time

enough to stabilize the  $\text{Ca}^{2+}$  level in the ER. The dynamic range of D1ER sensor in HEK D1ER cells ( $\text{DR}_{\text{max}} / \text{DR}_{\text{min}}$ ) was estimated at about 1.67 (Figure 3.14).

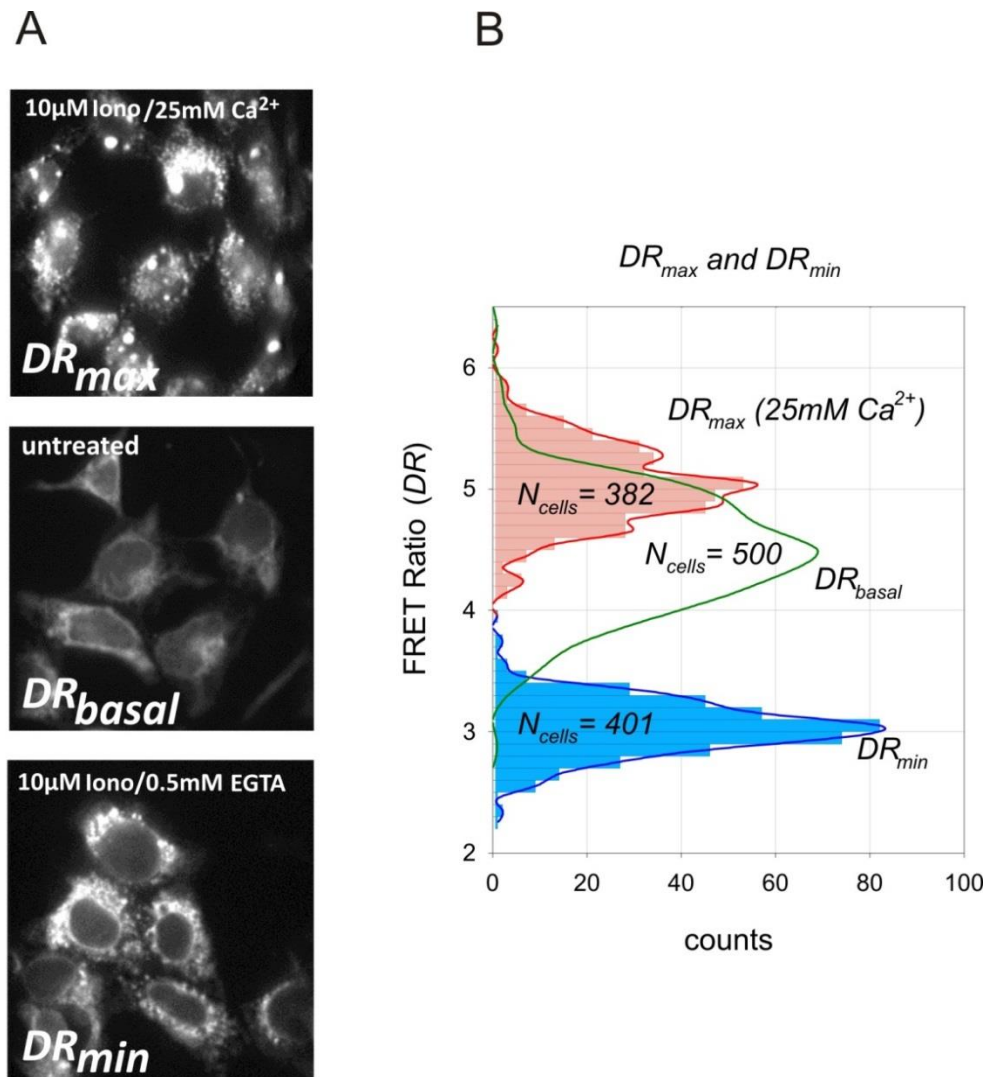


**Figure 3.14. Determining the dynamic range of D1ER in HEK D1ER cells. A.** HEK D1ER cells after permeabilisation (*upper* with 25 mM  $\text{Ca}^{2+}$  and *lower* with 0.5 mM EGTA) using *Saponin* and untreated cells (in the *middle*). **B.** D1ER fluorescence ratios were measured as DR (F536/F469). Distribution of ratios obtained from the permeabilized cells in intracellular like solution with 25 mM  $\text{Ca}^{2+}$  ( $\text{DR}_{\text{max}}$ ) and with 0.5 mM EGTA ( $\text{DR}_{\text{min}}$ ), or D1ER basal ratio distribution of untreated cell ( $\text{DR}_{\text{basal}}$ ).

Firstly, I found that  $\text{DR}_{\text{max}}$  and  $\text{DR}_{\text{min}}$  are proportional. For this purpose HEK D1ER cells were permeabilized with 10  $\mu\text{M}$  ionomycin and 10  $\mu\text{M}$  nigericin and 25 mM  $\text{Ca}^{2+}$  was added to detect  $\text{DR}_{\text{max}}$ , after washing step experimental bath solution was changed to 0.5 mM EGTA to detect  $\text{DR}_{\text{min}}$  (Figure 3.15 B). Plotting corresponding  $\text{DR}_{\text{max}}$  vs  $\text{DR}_{\text{min}}$

for each cell I found a linear relationship with a slope coefficient of 1.689 (Figure 3.15 B).

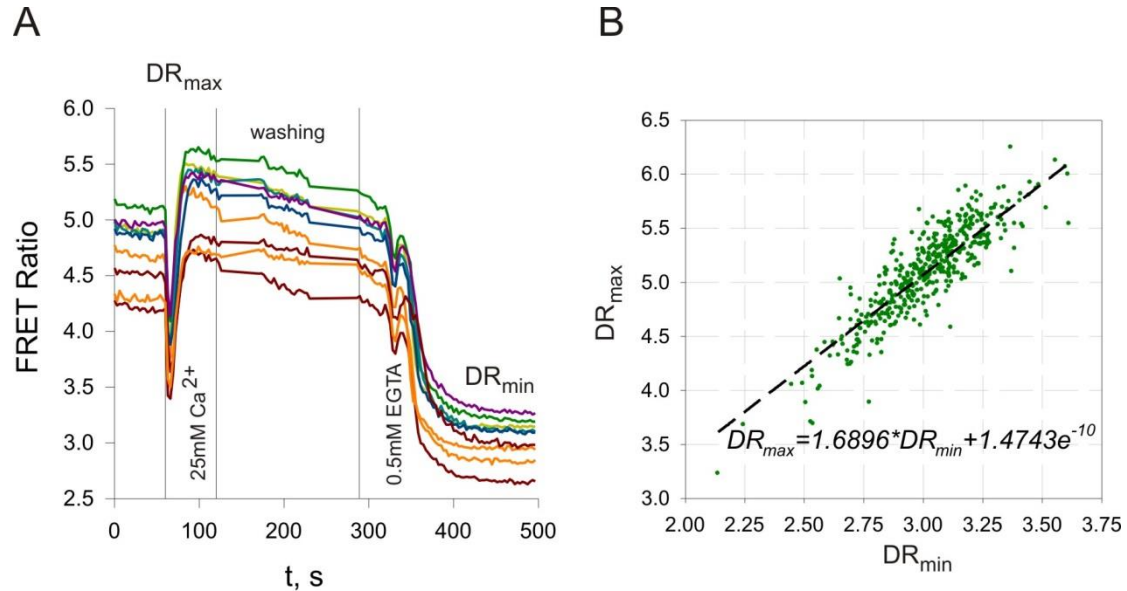


**Figure 3.15. Analysis of extreme D1ER signal (FRET Ratio) values in HEK D1ER cells. A. Experimental measurements of D1ER signals (FRET Ratio) extreme values *in vivo*:  $DR_{max}$  (saturation with 25 mM  $Ca^{2+}$ ) and  $DR_{min}$  (depletion with 0.5 mM EGTA). B. Relationship between  $DR_{max}$  and  $DR_{min}$  shows linear relationship (fitting, black dashed line).**

This leads to the useful approach when the individual  $DR_{max}$  for every cell can be estimated from the  $DR_{min}$  obtained after depletion of  $Ca^{2+}$  with ionomycin at the end of every experiment. The relation between  $DR_{max}$  and  $DR_{min}$ , which is:

Eq. 10:

$$DR_{max} = 1.6896 * DR_{min};$$

was used for calibration of D1ER signals.

To obtain  $K_D$  single step calibration was done *in vivo*. Cells were permeabilized with saponin (0.003%; 3mg/100ml) in the intracellular like solution (see 3.9, Table 3.8, Table 3.9). Corresponding changes of the solutions were following several overlapping ranges of concentrations (30 nM-1  $\mu$ M, 1  $\mu$ M-1 mM, 1 mM-25 mM), and the average of FRET ratio signal was taken for every point. The experimental  $K_D$  of 165  $\mu$ M was obtained using FURA-2-like calibration formula (see 3.1.13) with presumed Hill coefficient of 1,

which was seen from the fitting, despite the fact that D1ER *in vitro* might bind four  $\text{Ca}^{2+}$  ions (Palmer and Tsien, 2006). FRET Ratio signals diversity has Log-Normal distribution and can be explained due to various ER  $\text{Ca}^{2+}$  concentrations.

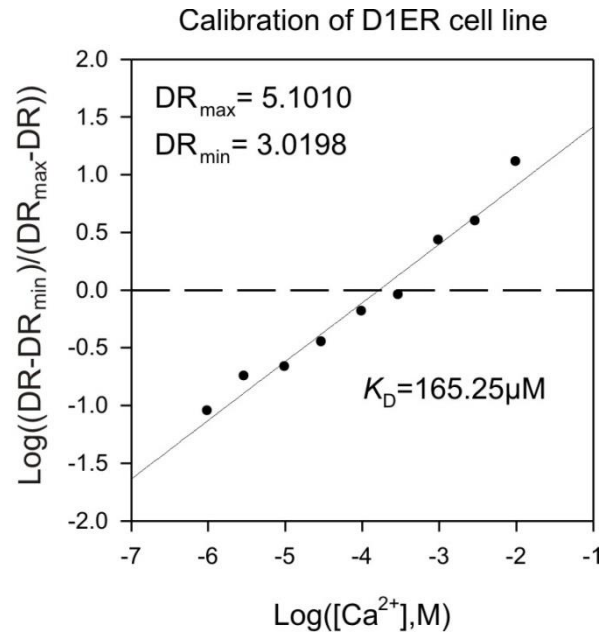


**Figure 3.16. Obtaining D1ER  $K_D$  *in vivo*.** On permeabilized HEK D1ER cells were applied  $\text{Ca}^{2+}$  concentration steps (black dots,  $\text{Log}([\text{Ca}^{2+}],\text{M})$ ). Corresponding DR were measured and plotted using calibration formula, DR<sub>max</sub> (5.1010) and DR<sub>min</sub> (3.0198). Obtained relationship was fitted with linear function (thin black line) which showed the x-axis (black dashed line) interception in point corresponding to  $K_D$  of 165.25  $\mu\text{M}$ .

Based on  $K_D$ ,  $\text{DR}_{\text{max}}$  and  $\text{DR}_{\text{min}}$  the calibration of D1ER signals (FRET Ratio, DR) was done. Every trace which is proportionally shifted from the mean trace obtains a correction factor  $\alpha$ , which is a proportion of FRET ratio basal of a given cell to the average FRET ratio basal of a group of cells (Figure 3.17 A). Accepting the homogeneity of FRET ratio distribution throughout D1ER cell culture without any treatment between different groups of cells, taken as individual experiments (dishes), the  $\text{DR}_{\text{max}}$  and  $\text{DR}_{\text{min}}$  for each individual cell can be recalculated based on average  $\text{DR}_{\text{max}}$  and average  $\text{DR}_{\text{min}}$  obtained for the large number of cells. This approach provide more accurate ER  $\text{Ca}^{2+}$  estimation than with fixed  $\text{DR}_{\text{max}}$  and  $\text{DR}_{\text{min}}$  for cells which can even show abnormal  $\text{Ca}^{2+}$  after calibration. Factor  $\alpha$  can be calculated from moment of  $t=t_{\text{end}}$  (last moment of the recording), to estimate the  $\text{DR}_{\text{min}}$  in the experiments when at the end stores are depleted,

because in this case the signal diversity is independent from the differences of basal  $\text{Ca}^{2+}$  levels (Figure 3.17 B).

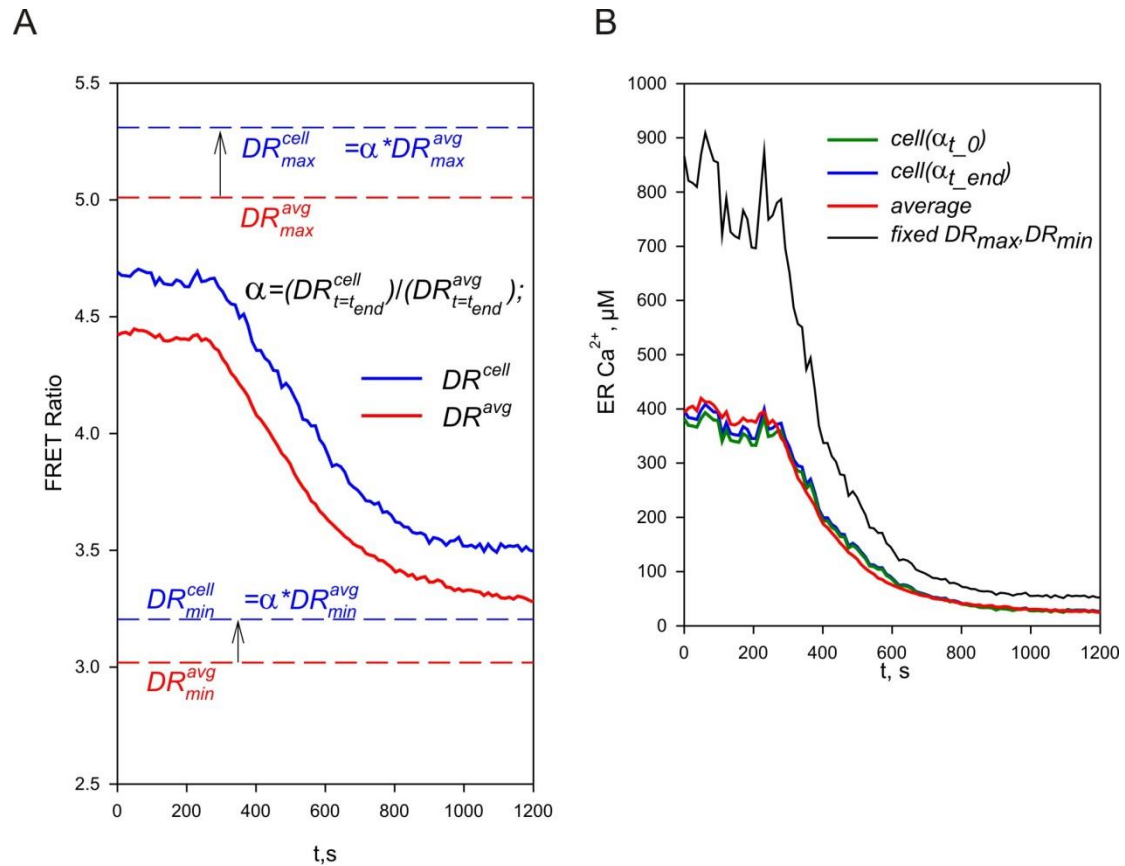


**Figure 3.17. Correction of a FRET Ratio signal. A. Individual cell  $DR_{max}$  and  $DR_{min}$  corrections based on average  $DR_{max}$  and average  $DR_{min}$ , factor  $\alpha$  is a proportion of individual cell FRET Ratio (blue solid line) at  $t=t_{end}$  to the average FRET Ratio of a group of cells (red solid line), change in FRET Ratio is due to store depletions evoked by thapsigargin application at  $t=180$  s. B. time courses of calibrated traces: black-no correction, blue- $\alpha$  factor as a proportion to last recording point ( $t_{end}$ ), green-  $\alpha$  factor as a proportion to first recording point ( $t_0$ ), red-calibrated average FRET Ratio from group of cells.**

Based on this ways of FRET Ratio signals calibration I have analysed the ER  $\text{Ca}^{2+}$  content of HEK D1ER cells at resting conditions. Taking fixed  $DR_{max}$  of 5.1010 and  $DR_{min}$  of 3.0198 basal ER  $\text{Ca}^{2+}$  of HEK D1ER has its maximum at 2.5 mM which is not exceeding the thermodynamic limit due to the energy of one ATP molecule hydrolysis required for transporting of two  $\text{Ca}^{2+}$  ions across the concentration gradient between ER and Cytosol (Figure 3.18 A, left). Introducing the correction for the calibration, i.e.

recalculating  $DR_{\max}$  value on  $DR_{\min}$  value due to the found equation  $DR_{\max}=1.689*DR_{\min}$  (see 3.13.4, Eq. 10), the distribution of ER  $Ca^{2+}$  was similar to those without correction (Figure 3.18 A). Overlapping the both distributions has shown the same mode for Log-Normal ER  $Ca^{2+}$  distribution with about 450  $\mu M$  basal intraluminal  $Ca^{2+}$  for HEK D1ER cells (Figure 3.18 B).

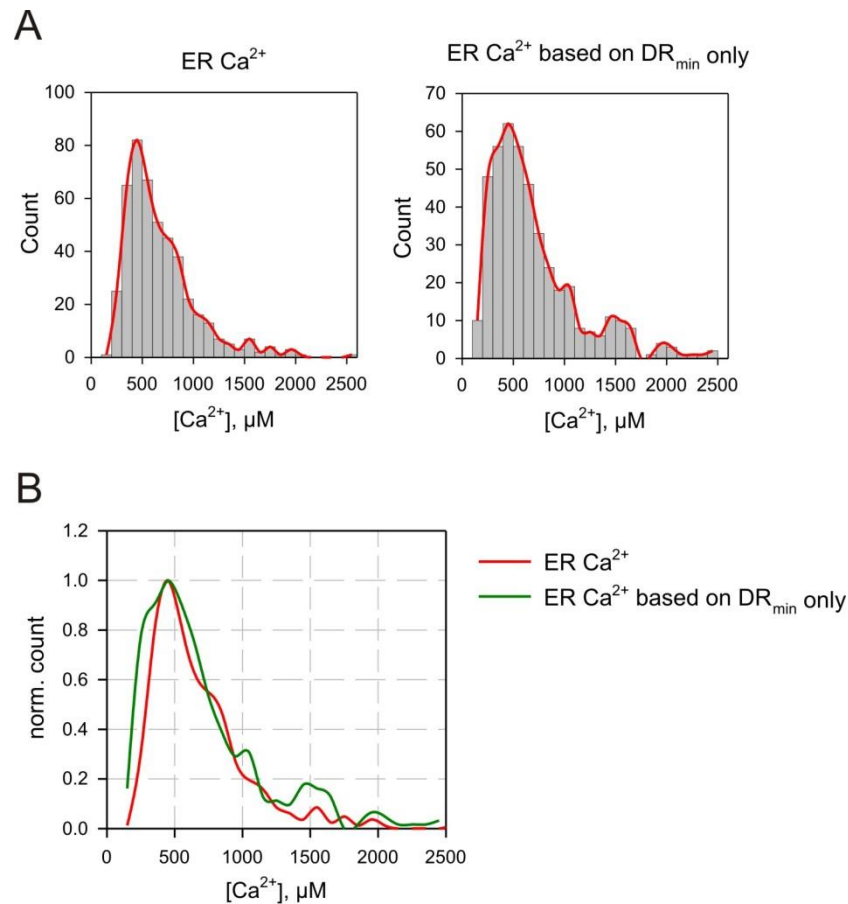


**Figure 3.18. ER  $Ca^{2+}$  distribution. A. Distributions of ER  $Ca^{2+}$  depending of calibration ways left: with fixed average  $DR_{\max}$  and  $DR_{\min}$ , and right: with  $DR_{\max}$  calculated from  $DR_{\min}$  B. Both methods show the same mode of Log-normal ER  $Ca^{2+}$ -distribution.**

HEK D1ER cells loaded with Fura2 for cytosolic  $Ca^{2+}$  measurements underwent the same calibration procedure as for HEK293, but traces included corrections due to fluorescence overlap between D1ER and FURA-2. (see 3.13). In this case the corrected signal of thapsigargin-evoked cytosolic  $Ca^{2+}$  response (seen as FURA-2 ratio signal, Figure 3.19) was corrected for HEK D1ER cells and compared to HEK293 cells (both cell lines were loaded with FURA-2 in the same way, see 3.11.1)

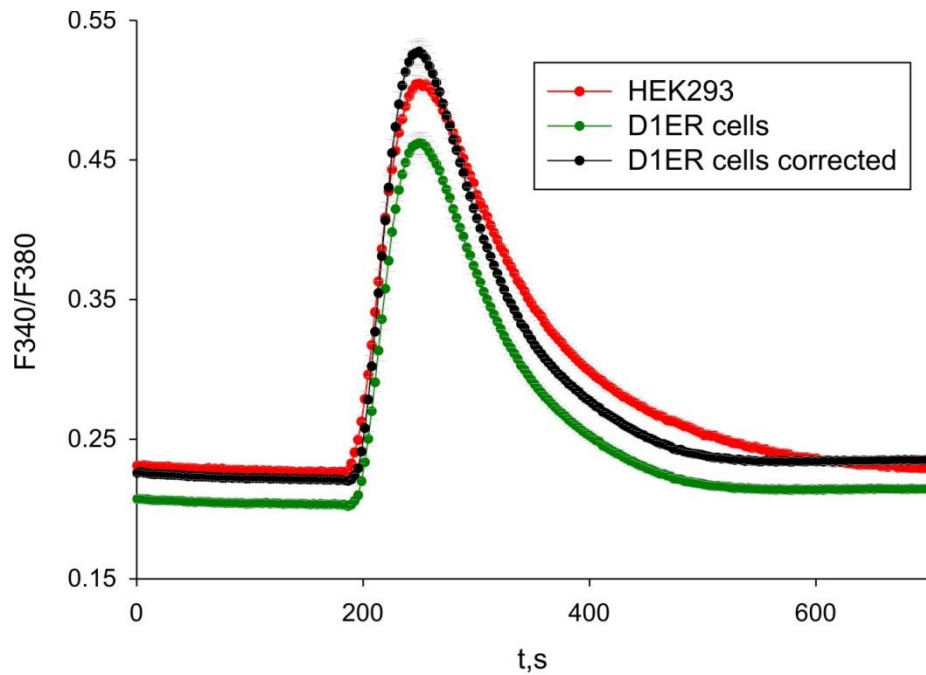


**Figure 3.19. Correction of FURA-2 ratio signal.** HEK D1ER and HEK293 cells were loaded with FURA-2 for cytosolic  $\text{Ca}^{2+}$  measurements (see 3.11.1). HEK D1ER cells (green) and HEK293 (red) were treated with  $1 \mu\text{M}$  thapsigargin at 180 s. Black trace show corrected FURA-2 ratio signal of HEK D1ER cells (green trace) according to method described in section 3.13.

### 3.14 Analysis and $\text{Ca}^{2+}$ imaging data

During the analysis of raw FRET ratio signals, we have found that “signal to noise” relation has to be improved in order to obtain reliable calculation of first derivation. The noise didn’t have constant period i.e. significant changes due to “narrow” dynamic range could have been observed between two points independent from time period of taking frames. For smoothing data we have chosen Savitzky-Goley digital filter with MatLab (Mathworks®) Software for data processing (Figure 3.20). For every data point Savitzky-Goley filter builds a new data point with the least squares method fitting for a polynomial function with a given degree  $n$  using at least  $2n+1$  neighboring points including current data point. As a result a new trace is overlapping old one with significantly reduced noise without much distortion of a general time course. We used parameters for Savitzky-Goley digital filter 3 and 5 polynomial degree with 11 to 17 points in MatLab script automatically smoothing traces with preinstalled function *sgolayfilt* (*data, degree, points*). The MatLab script could be changed due to needs, for

instance to take first derivative of the traces or to fit with two exponential function. All data obtained in MatLab were transferred to Excel and Sigma Plot 10 for further processing and building figures.

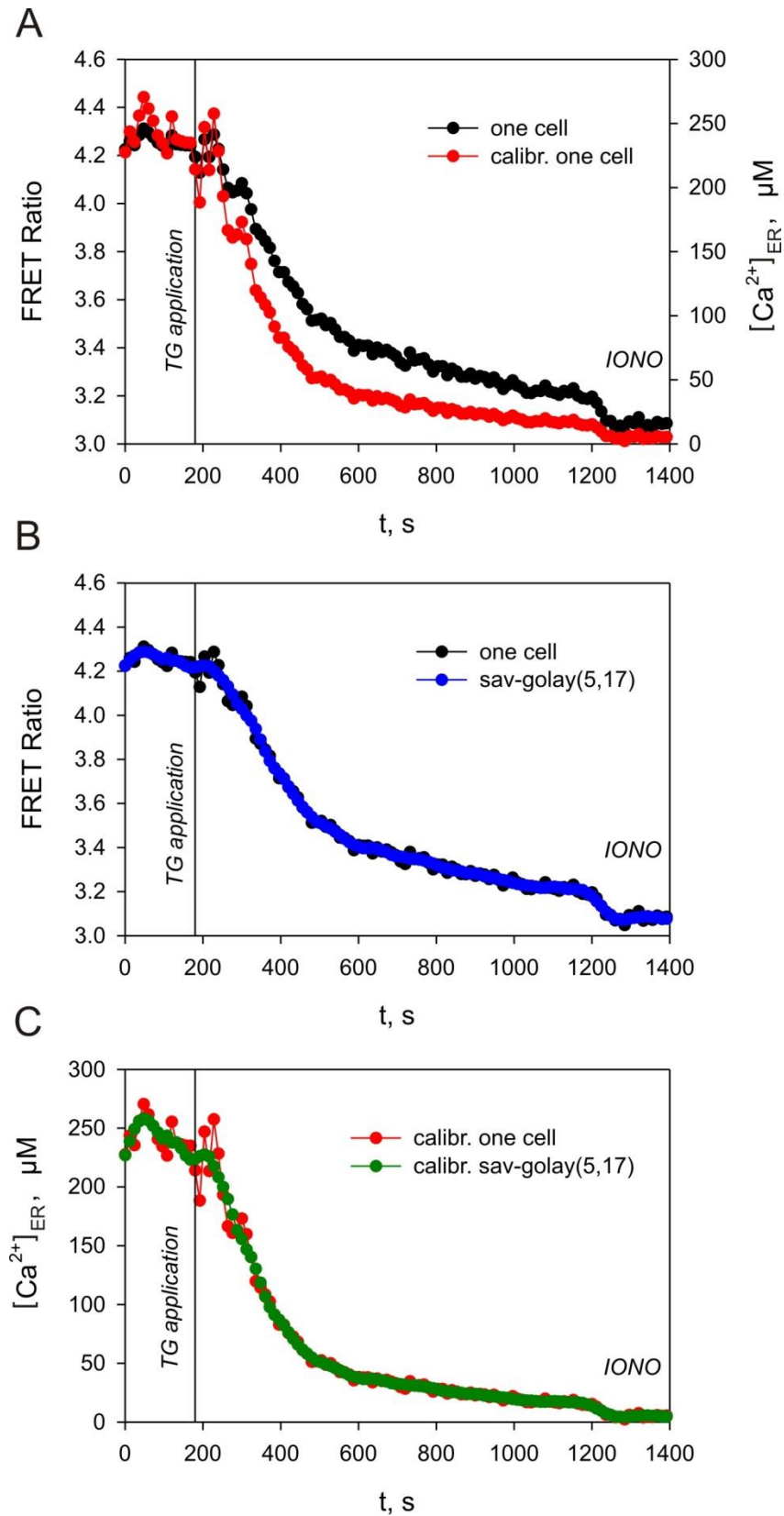


**Figure 3.20. FRET ratio traces smoothed by Savitzky-Goley digital filtering. A. TG response of one cell FRET trace (black, Left y-axis) plotted with corresponding calibration (red, right y- axis). B. Savitzky-Goley digital smoothing of FRET ratio trace (blue) applied with parameters: 5 degree polynomial and 17 data points to original trace (black). C. Calibration Savitzky-Goley digital filtering (green) overlaps with the main time course of calibrated FRET ratio trace (red). (TG-thapsigargin, IONO-ionomycin).**

### **3.15 Statistical analysis**

Statistical analysis was performed in SigmaPlot 10.0, Microsoft Excel 2010 (Microsoft Corp.), and MatLab R2015a (Mathworks®). Values for analysis were taken from at least 3 independent measurements (independent seeding of cells, i.e. different experimental days for each value). Analyzed values are represented as mean±s.e.m (standard error of the mean). Student's t-test and ANOVA statistical test were used in the sets of data with normal distribution. Due to Log-normal distribution statistical data underwent two-sample Kolmogorov-Smirnov test. Rejection of the “null” theory with p value less than 0.05 was considered as significant difference. Statistical differences in significance represented as asterisks based on p-values obtained from the statistical test, where \*  $p \leq 0.05$ , \*\*  $p < 0.01$ , and \*\*\*  $p < 0.001$ .

## 4 Results

### 4.1 Analysis of endoplasmic reticulum $\text{Ca}^{2+}$ efflux

$\text{Ca}^{2+}$  efflux from the endoplasmic reticulum under resting conditions was analysed in HEK D1ER cells, which were cultured and prepared for imaging according to the procedure described above (see 3.2.3). To evoke  $\text{Ca}^{2+}$  efflux from the ER, the selective inhibitor of SERCA pumps thapsigargin (TG) with concentration 1  $\mu\text{M}$  was applied at 3 minutes after the of start of the recording. The obtained ratio traces, were calibrated to get ER  $\text{Ca}^{2+}$  signals (see 3.13.4). The latter are plotted as for a representative cell in Figure 4.1 A for different moments of time. The traces were cleared from the noise via digital data smoothing with Savitzki-Golay filtering (see 3.14). This method involves polynomial fitting, therefore the smoothing has natural “boundary” deviation, which is clearly seen at the first ten seconds before TG application. Nevertheless, at the moment of TG application and thereafter, the smoothed trace reproduces the raw trace tendency perfectly. The smoothing reduces the noise and allows us to calculate the first derivative of the concentration. This derivative, taken with a negative sign

Eq. 11:

$$\frac{-d[\text{Ca}^{2+}]_{ER}}{dt};$$

is nothing but a speed of ER  $\text{Ca}^{2+}$  leakage, which hereafter is referred to as the “leak rate”. After TG application the leak rate has a peak shape. It rises rapidly from zero to the maximum value and then slowly decays. This decay coincides with the ER  $\text{Ca}^{2+}$  concentration after appropriate rescaling: black and orange line in Figure 4.1 A, respectively. This suggests that the decay has an exponential form and can be modeled as mono-

Eq. 12:

$$y = A_1 * e^{-K_1*t} + B;$$

or bi-exponential:

Eq. 13:

$$y = A_1 * e^{-K_1*t} + A_2 * e^{-K_2*t};$$

Here  $A_1$  and  $A_1+A_2$  represent ER  $\text{Ca}^{2+}$  level at resting state ( $t=0$ ) and constants  $K$  are the leak rate constants. The general course of the decay was started from the base-line ER  $\text{Ca}^{2+}$  at the moment of TG application and drops at the end usually to about  $30 \mu\text{M}$  (Figure 4.1 A). The delay between the TG application and the moment of maximal steepness is around 100 seconds. The part of the trace that begins with the decrease of ER  $\text{Ca}^{2+}$  starts and was taken for a fitting with two-exponential model using a script from MATLAB Software (Mathworks®) to estimate the constant parameters from the equation model. Originally parameters were set for  $A_1=300 \mu\text{M}$  and  $A_2=100 \mu\text{M}$ ;  $K_1=0.01 \text{ s}^{-1}$  and  $K_2=0.001 \text{ s}^{-1}$ . The script was saving automatically all fitting results of every cell for the further statistical analysis.

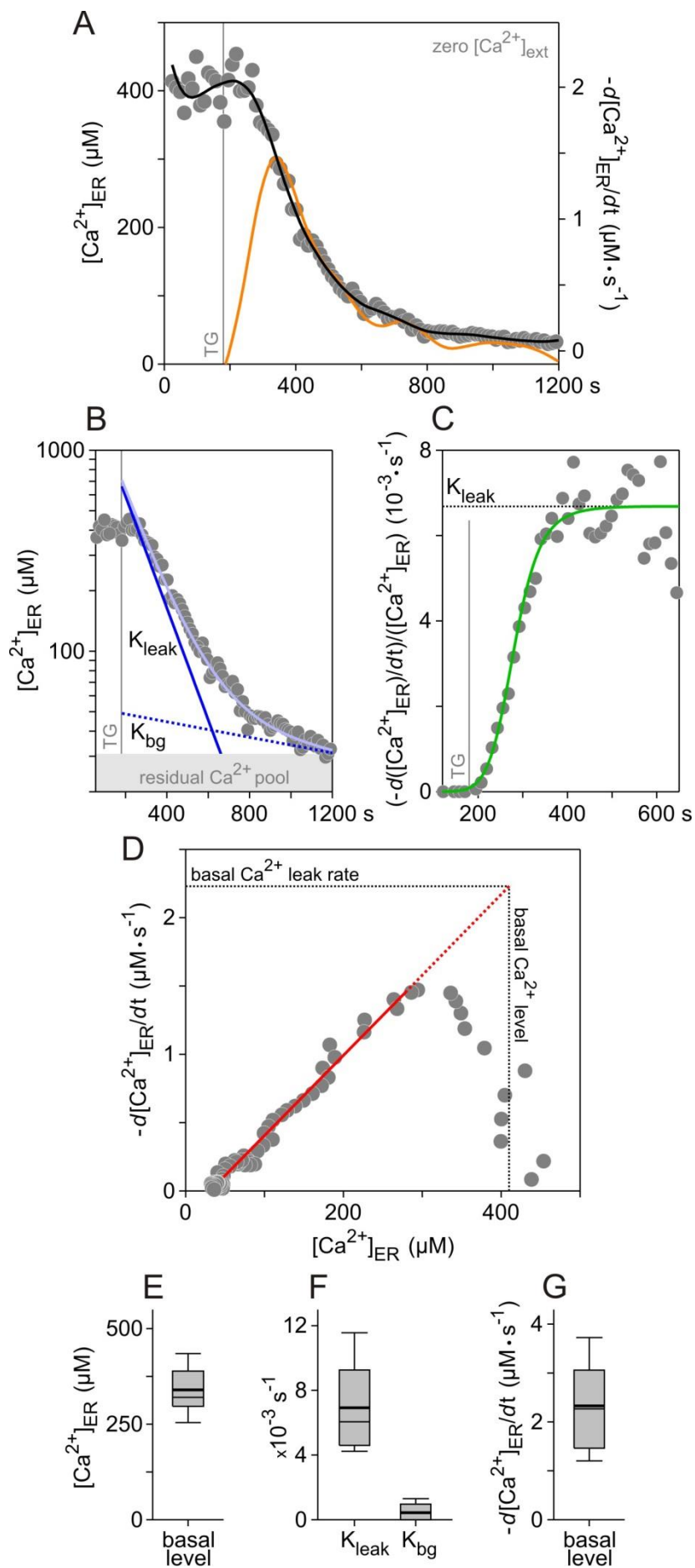


**Figure 4.1. Analysis of ER Ca<sup>2+</sup> efflux. A. Representative HEK D1ER cell showing ER Ca<sup>2+</sup> decay after application of 1μM thapsigargin at 3 minutes in Ca<sup>2+</sup>-free 0.5 EGTA extracellular solution. ER Ca<sup>2+</sup> was obtained as FRET Ratio and calibrated (as described in Methods) and plotted (gray circles) versus time. Smoothing of the trace is represented as black line. Corresponding first derivative (yellow line) of the smoothed trace was overlapped with the original and smoothed traces and showed with changed sign (right y-axis). B. Logarithmic plot of the same trace showing two exponential components of the thapsigargin-evoked decay (linear parts of the grey circle trace). Light blue line shows the fitting results of two-exponential model applied on the original data. Straight lines indicated as  $K_{leak}$  (solid blue line) and  $K_{bg}$  (dotted blue line) showing separate single-exponential decays taken from the parameters obtained from two-exponential fitting. It is seen, that the major part of ER Ca<sup>2+</sup> decay is following by first exponent ( $K_{leak}$ ). Grey zone shows residual ER Ca<sup>2+</sup> that is reached by thapsigargin depletion. C. Estimation of the ER Ca<sup>2+</sup> leak rate constant,  $K_{leak}$ , based on one-exponential model of ER Ca<sup>2+</sup> decay, which was taken as first derivative divided by ER Ca<sup>2+</sup>(gray circles). Sigmoidal shape of the graph and can be fitted with Hill function (green line). At times longer than 400 s, the curve reaches a value that equals  $K_{leak}$ . D. Plotting of the first derivative of ER Ca<sup>2+</sup> versus ER Ca<sup>2+</sup> (grey circles) based on single-exponential model (solid red line). Further extrapolation of the same character of leak (dotted red line) until crossing with basal ER Ca<sup>2+</sup> level gives the basal ER Ca<sup>2+</sup> leak rate. E. Box-plot representing the distribution of basal ER Ca<sup>2+</sup> from the HEK D1ER cells in 0.5 mM EGTA extracellular. F.  $K_{leak}$  and  $K_{bg}$  distributions represented as box-plots. G. Estimated basal ER Ca<sup>2+</sup> leakage rate distribution. Box-plot (here and before) bars: 10% and 90% percentiles, main box: 25% and 75% percentiles, thin black line: median, thick black line: mean value.**

To clarify the physical meaning of the two different contributions to the decay process I plotted separately the exponential laws obtained from the fitting procedure (using Eq 13) in Figure 4.1B. I could clearly distinguish the “fast” or “main leak” that is given by the first exponential law and has bigger amplitude and the leak rate constant comparing to the second contribution that describes the “slow” or “background leak”:

Eq. 14:

$$y_{fast} = A_{main} * e^{-k_{leak}*t};$$

Eq. 15:

$$y_{slow} = A_{background} * e^{-k_{background}*t};$$

where:

$$A_{main} \gg A_{background}; \text{ or } k_{main} \gg k_{background};$$

The one-exponential or two exponential models, proposed for the fitting, should reach “zero” when time rises infinitely. However, our observations showed stable level of the ER  $\text{Ca}^{2+}$  at the end of the measurements, so this was accepted as residual pool of non-releasable free  $\text{Ca}^{2+}$ . Because of the negligent contribution of “slow”, “background leak”, the one-exponential decay (Eq.12) was used to model main leak seen in thapsigargin effect. Within this assumption the leak rate constant “ $K_{leak}$ ”, or  $\text{Ca}^{2+}$  release rate from the ER, can be obtained as a ratio of the first derivative of the concentration to the concentration itself:

Eq. 16:

$$\frac{dy}{dt} = -K_{leak} * A_{main} * e^{-K_{leak}*t};$$

Eq. 17:

$$K_{leak} = \frac{-\frac{dy}{dt}}{y};$$

This ratio (in Eq.17) as a function of time is plotted in Figure 4.1 C. This dependance can be fitted with the Hill function:

Eq. 18:

$$y = \frac{ax^b}{c^b + x^b};$$

with the Hill coefficient  $b$ , which was set to 1.

The rise of this ratio is shown in Figure 4.1 C and reflects that SERCA pumps are inhibited with the thapsigargin, so the cell can no longer retain  $\text{Ca}^{2+}$  in the ER. The maximum of the ratio corresponds to the maximal leak rate when the maximal number of SERCAs is inhibited by thapsigargin. It is seen that fitting with Hill function is a perfect before 500 s. At longer times there is a considerable scatter, which can be explained as the end of one-exponential phase due to the significant ER depletion. Another reason for this is that mathematical error of the first derivative calculation increases when the trace becomes more “flat”. The  $K_{leak}$  maximal values from the Hill fitting were taken as maximal speed constants of  $\text{Ca}^{2+}$  release rate for every cell. Plotting of ER  $\text{Ca}^{2+}$  vs. its release rate (i.e. first derivative with a negative sign) shows a linear character because of

their one-exponential nature (Figure 4.1 D). To estimate basal  $\text{Ca}^{2+}$  leak rate, i.e. the  $\text{Ca}^{2+}$  leak rate before application of thapsigargin, the approximation of a linear part of the ER  $\text{Ca}^{2+}$  leak vs.  $\text{Ca}^{2+}$  release rate was done. For a representative cell, as seen in Figure 4.1 D, the straight line is extrapolated to the level of basal  $\text{Ca}^{2+}$  (of about 410  $\mu\text{M}$ ) which allows us to obtain the corresponding value of basal  $\text{Ca}^{2+}$  release rate of 2.17  $\mu\text{M}/\text{s}$ . The data was collected from a group of 40 HEK D1ER cells, on which thapsigargin response was analyzed in 0.5 mM EGTA extracellular solution. The basal ER  $\text{Ca}^{2+}$  level showed (Figure 4.1 E) log-normal distribution with 10%-90% of the cells between 253  $\mu\text{M}$  and 434  $\mu\text{M}$ , 25%-75% of the cells between 294  $\mu\text{M}$  and 389  $\mu\text{M}$ , a median of 317  $\mu\text{M}$  and mean value of 338  $\mu\text{M}$ . The  $\text{Ca}^{2+}$  leak constant for the same group of cells showed (Figure 4.1 F) a negligible value of  $k_{\text{background}}$  which was approximately 15 fold lower than  $K_{\text{leak}}$ :  $4.6 \cdot 10^{-4} \text{ s}^{-1}$  for  $k_{\text{background}}$  and  $7 \cdot 10^{-3} \text{ s}^{-1}$ ; for  $K_{\text{leak}}$  10%-90% of the cells between  $4.2 \cdot 10^{-3} \text{ s}^{-1}$  and  $11.5 \cdot 10^{-3} \text{ s}^{-1}$ , 25%-75% of the cells between  $4.5 \cdot 10^{-3} \text{ s}^{-1}$  and  $9.3 \cdot 10^{-3} \text{ s}^{-1}$ , median at  $6 \cdot 10^{-3} \text{ s}^{-1}$  and mean value of  $6.8 \cdot 10^{-3} \text{ s}^{-1}$ . Basal  $\text{Ca}^{2+}$  release rate estimated for the same group of cells (Figure 4.1 G) was with 10%-90% of the cells between 1.2  $\mu\text{M} \cdot \text{s}^{-1}$  and 3.73  $\mu\text{M} \cdot \text{s}^{-1}$ , 25%-75% of the cells between 1.47  $\mu\text{M} \cdot \text{s}^{-1}$  and 3.04  $\mu\text{M} \cdot \text{s}^{-1}$ , median at 2.28  $\mu\text{M} \cdot \text{s}^{-1}$  and mean value of  $2.34 \pm 0.15 \mu\text{M} \cdot \text{s}^{-1}$ . Due to its distribution the statistical comparison between two groups of cells in the further experiments and analysis was done with two-sample Kolmogorov-Smirnov test. The differences in ER  $\text{Ca}^{2+}$  release evoked by thapsigargin and basal ER  $\text{Ca}^{2+}$  leak rate appeared similar for both 0.5 mM EGTA extracellular and 2 mM  $\text{Ca}^{2+}$  extracellular.

The main conclusions of these findings are that the  $\text{Ca}^{2+}$  leak from the ER follows the Fick's first law of diffusion and the ER  $\text{Ca}^{2+}$  depletion follows single-exponential decay, The  $\text{Ca}^{2+}$  leak constant for the chosen cell line D1ER was  $6.8 \cdot 10^{-3} \text{ s}^{-1}$ , and the basal  $\text{Ca}^{2+}$  efflux from the ER under physiological conditions is about 2.34  $\mu\text{M} \cdot \text{s}^{-1}$ .

## 4.2 Effects of protein synthesis inhibitors on $\text{Ca}^{2+}$ homeostasis

The analysis of ER  $\text{Ca}^{2+}$  release evoked by thapsigargin was used as a basic method to investigate the effects of protein synthesis inhibitors on  $\text{Ca}^{2+}$  homeostasis. Even though we have found that the kinetic parameters of such a release in HEK D1ER cells in  $\text{Ca}^{2+}$  free extracellular solution (0.5 mM EGTA) have no statistical difference compared to that

in 2 mM  $\text{Ca}^{2+}$  extracellular (Figure 4.2), the complete role of extracellular  $\text{Ca}^{2+}$  for protein synthesis in cells remains unclear.

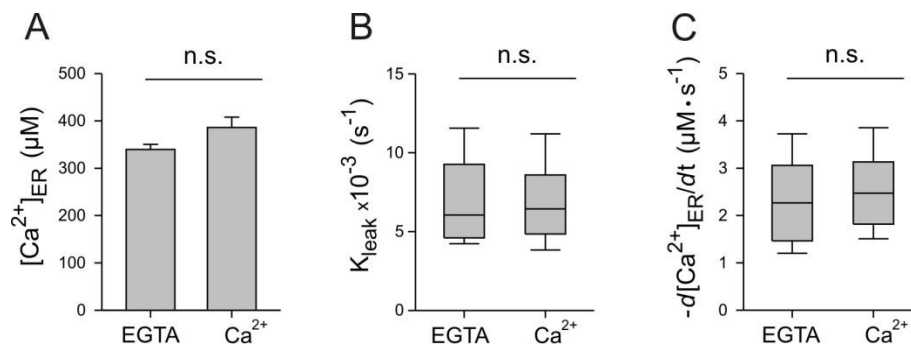


**Figure 4.2. Effect of extracellular  $\text{Ca}^{2+}$  on thapsigargin-evoked store depletion.** HEK D1ER cells were observed in 0.5 mM EGTA extracellular solution (EGTA) and 2 mM  $\text{Ca}^{2+}$  extracellular solution ( $\text{Ca}^{2+}$ ). A. basal ER  $\text{Ca}^{2+}$  at rest. B.  $\text{Ca}^{2+}$  leak constant. C. Basal  $\text{Ca}^{2+}$  leak rate. Two-Sample Kolmogorov-Smirnov test for 41 cells (EGTA) and 25 cells ( $\text{Ca}^{2+}$ ), n.s.  $p > 0.05$ .

Nevertheless, for the further investigation of the effects of protein synthesis inhibitors on  $\text{Ca}^{2+}$  homeostasis we used 2 mM  $\text{Ca}^{2+}$  extracellular solution, because it is similar to the natural physiological conditions. HEK D1ER cells were grown and prepared for the imaging experiments as described above (see 3.2.3). ER  $\text{Ca}^{2+}$  traces were obtained and calibrated according (see 3.13.4). In the “online” application protocol, we compare mock application with the application of the protein synthesis inhibitor applied at 3 minutes (Figure 4.3 A). To further unmask  $\text{Ca}^{2+}$  leakage from the ER we applied 1  $\mu\text{M}$  thapsigargin solution at 18 minutes. In this approach, we studied the effects of 5 mM cycloheximide, 1 mM emetine, 500  $\mu\text{M}$  puromycin and 25  $\mu\text{M}$  pactamycin on  $\text{Ca}^{2+}$  leakage from the ER. The mock application was used as described (see 3.10.2): the corresponding amount of a solvent was used to obtain a desired final concentration of the inhibitor. Along with the subsequent thapsigargin application it provides a control trace, which was analysed similar to (see 4.1). To estimate the maximal  $\text{Ca}^{2+}$  leak rate that can be detected with D1ER  $\text{Ca}^{2+}$  sensitive indicator we treated cells with 1  $\mu\text{M}$  solution of ionomycin (Figure 4.3 B). This ionophore depletes  $\text{Ca}^{2+}$  stores immediately and is usually used for the estimation of  $\text{Ca}^{2+}$  amount inside the cell. In my experiment, due to its fast action the time between frames was reduced to 1 s. The curve of ER  $\text{Ca}^{2+}$  depletion with

1  $\mu\text{M}$  ionomycin can be fitted nicely with one-exponential decay and goes lower than curve of 1  $\mu\text{M}$  thapsigargin–evoked ER  $\text{Ca}^{2+}$  depletion. This behavior proves the presence of non-releasable  $\text{Ca}^{2+}$  pool inside the ER. The  $K_{\text{leak}}$  of ionomycin–evoked release was  $204.9 \times 10^{-3} \pm 18.5 \times 10^{-3} \text{ s}^{-1}$  and basal  $\text{Ca}^{2+}$  leak rate at  $44.0 \pm 4.5 \mu\text{M} \cdot \text{s}^{-1}$ . (Table 4.1).

Cycloheximide belongs to glutarimide antibiotic group, and its main more is in blocking of the co-translational translocation. Namely, after the association of ribosome-translocon complex, cycloheximide inhibits the elongation step of translocation mediated by eEF-2 via binding to the 60S ribosome subunit at E-site. That was demonstrated as the increase of the 80S ribosomes fraction. (Schneider-Poetsch et al. 2010) This can be explained as the cessation of all ribosome-translocon complex machinery resulting in a stacking polypeptide chains within the pore region of Sec61 $\alpha$ . If the polypeptide chain remains for some period of time unmoving in the ribosome translocon complex, it initiates a protein degradation and leads to the disassembly of the ribosome-nascent chain complex and may result in the translocon opening. It was shown, that the incorporation of rough microsomes on lipid bilayers evokes additional conductance after releasing of the polypeptide chain and returning back from the disassembly of the ribosome translocon complex. That indicates no ion leak through the Sec61 $\alpha$  pore occupied with a polypeptide chain (Simon and Blobel 1991). Using FURA-2, it was shown that cycloheximide changes  $\text{Ca}^{2+}$  leak evoked by thapsigargin. The observation of cytosolic  $\text{Ca}^{2+}$  peak for LNCaP after the thapsigargin application in  $\text{Ca}^{2+}$  free extracellular solution showed that the thapsigargin-evoked peak was lower and wider than the control one, which indicates the reduction of the leak rate (Van Coppenolle et al. 2004). Therefore, for the direct observation of ER  $\text{Ca}^{2+}$  homeostasis, cycloheximide was used as an agent to seal all Sec61 complexes, involved in protein translocation, with polypeptide chains and to decrease the ion flux through the pore region of Sec61. The effect of cycloheximide presence was expected to be seen both in the increase of basal ER  $\text{Ca}^{2+}$  concentration and in the kinetic changes of  $\text{Ca}^{2+}$  efflux from ER evoked by the thapsigargin application. Cyclohexamide (5 mM) was applied at 3 minutes on HEK D1ER cells in 2 mM  $\text{Ca}^{2+}$  extracellular solution (Figure 4.3 A) with the subsequent 15 minutes incubation phase after which 1  $\mu\text{M}$  thapsigargin was applied. A rise of ER  $\text{Ca}^{2+}$  after the cyclohexamide application and before the thapsigargin application was estimated as insignificant comparing to the control mock application. However, after the application of 1  $\mu\text{M}$

thapsigargin the  $\text{Ca}^{2+}$  efflux from the ER was slower comparing to the case of the control mock application. The group of 16 HEK D1ER cells from 3 independent repeats was analyzed in the same manner as in (see 4.1). And it was found that  $K_{\text{leak}}$  constant for cells treated with 5 mM cycloheximide is almost 2.1 fold lower as for the mock treatment. The estimated basal  $\text{Ca}^{2+}$  leak had the same tendency: cycloheximide decreased leak 1.74 fold as for mock (Figure 4.3 B, C; Table 4.1). Statistical analysis was done between two groups of cells (16 for cycloheximide and 12 for control) with two-sample Kolmogorov-Smirnov test.

Emetine is an irreversible inhibitor of translational elongation. The mutation in CHO cells, which leads to the resistance to emetine, indicates the possible binding site at 40S ribosomal subunit (Gupta and Siminovitch 1977). The structural cryo-EM study of the 80S ribosome from the malaria-causing parasite *Plasmodium falciparum* pointed also on 40S subunit as a binding site of emetine (Wong et al. 2014). Emetine prevents  $\text{Ca}^{2+}$  efflux from the ER during UPR, induced on *Xenopus oocytes*, blocks eIF2 $\alpha$  phosphorylation and reduces BiP expression (Paredes et al. 2013). Emetine reduces both thapsigargin-induced peak and the following capacitative-calcium entry due to the  $\text{Ca}^{2+}$  readdition. (Ong et al. 2007). Due to its similarity of the  $\text{Ca}^{2+}$  effect to cycloheximide, emetine was used as a potent inhibitor of the ER  $\text{Ca}^{2+}$  leak. Emetine (1 mM) was applied on HEK D1ER cells, with 2 mM  $\text{Ca}^{2+}$  in the extracellular solution, at 3 minutes and no change in ER  $\text{Ca}^{2+}$  was observed during next 15 minutes before 1  $\mu\text{M}$  thapsigargin was applied to unmask the  $\text{Ca}^{2+}$  leakage (Figure 4.3 A). The ER  $\text{Ca}^{2+}$  efflux after the thapsigargin application was slower after the 1 mM emetine and resembles the effect of 5 mM cycloheximide. The ER  $\text{Ca}^{2+}$  leak constant ( $K_{\text{leak}}$ ) after the emetine treatment drops by the factor of 1.85 from that for the mock treatment. The ER  $\text{Ca}^{2+}$  leak rate after emetine was 1.73 fold less comparing to the control one (Figure 4.3 B, C; Table 4.1). Statistical analysis was done for two groups of cells (11 for emetine and 12 for control) with Two-Sample Kolmogorov-Smirnov test.

Pactamycin blocks protein translocation at the initiation step of ribosome complex assembly leading to the accumulation of the inactive ribosomal initiation complexes (Ong et al. 2007, Potter et al. 2001). It binds to the 40S small ribosomal subunit and blocks the release of the initiation factors and thus prevents its association with the 60S ribosomal subunit (Kappen et al. 1973). As a result no additional proteins can be produced, but the proteins, which have been already producing, can finish their

translocation successfully (Ong et al. 2007). If the large ribosomal subunit remains attached to the Sec61 complex on the ER membrane (Potter et al. 2001), that this might lead to the enhanced ER  $\text{Ca}^{2+}$  leak through the unengaged translocon.  $\text{Ca}^{2+}$  increase in the cytosol after Pactamycin treatment was detected using PMCA blocker  $\text{La}^{3+}$  and pointed as a result of store depletion due to activated capacitative-calcium entry (Ong et al. 2007). Furthermore,  $\text{Ca}^{2+}$  leak evoked by pactamycin was inhibited by emetine, which can be explained as a peculiarity of the initiation step inhibition and not as the result of the following translocation steps. In this study the expected enhance of ER  $\text{Ca}^{2+}$  leak was studied following pactamycin treatment on HEK D1ER cells through the Sec61 complexes. Cells were treated with 25  $\mu\text{M}$  pactamycin in 2 mM  $\text{Ca}^{2+}$  extracellular solution. The application of 25  $\mu\text{M}$  pactamycin showed insignificant tendency to decrease the ER  $\text{Ca}^{2+}$  concentration prior to 1  $\mu\text{M}$  thapsigargin application at 18 minutes (Figure 4.3 A). This indicated an enhanced  $\text{Ca}^{2+}$  leak from the ER. The kinetic of the 1  $\mu\text{M}$  thapsigargin response was faster after pactamycin application. The value of  $K_{\text{leak}}$  increased about by a factor 1.7 after pactamycin treatment. The similar increase by a factor 1.75 was found in basal ER  $\text{Ca}^{2+}$  leak after pactamycin treatment compared to the mock (Figure 4.3 B,C; Table 4.1). Statistical analysis of 3 independent repeats comprising two groups of cells (12 for pactamycin and 12 for control) was done with Two-Sample Kolmogorov-Smirnov test.

Puromycin is an adenosine-based (t-RNA-like) molecule that inhibits protein synthesis by binding to the nascent polypeptide chain and further blocking the next amino acid binding, this way cleaving the polypeptide chain and evoking its premature release (Pestka 1971). The working ribosome-translocon machinery moves the polypeptide chain inside the ER and it is assumed that the whole ribosome translocon complex is disassembled after translocation and the translocon might be sealed. Puromycin application should lead to the number of breakages upon current translocations of polypeptide chains leading to a number of ribosome-translocon complexes in an open state before they got disassembled. The free from chain translocons conduct ions through the ER membrane. Which was shown by puromycin application on the lipid bilayers studded with rough microsomes; and in the contrary, the application of concentrated KCl removes ribosomes from the translocons and decreases ion flux (Simon and Blobel 1991). The fact that puromycin starts to work at the moment of application was clearly demonstrated by the absence of fluorescence protein production (no fluorescence was detected) targeted to the ER on the cells simultaneously transfected and treated with

puromycin (Ong et al. 2007). Thapsigargin response measured by FURA-2 showed a peak which was smaller after puromycin treatment than the control. The measurement of ER  $\text{Ca}^{2+}$  leak was seen by mag-fluo-4 in the ER on LNCaP cells. This effect was prevented by simultaneous application of anisomycin, the antibiotic with the similar mechanism of action to cycloheximide. Puromycin-induced leak was also shown to be independent from ryanodine and  $\text{IP}_3$  release. (Van Coppenolle et al. 2004). However, the ER  $\text{Ca}^{2+}$  decrease was not quantified. The similar effect of puromycin on thapsigargin induced peak was observed in HeLa cells. After 3 minutes of incubation with 500  $\mu\text{M}$  puromycin the TG-evoked cytosolic  $\text{Ca}^{2+}$  peak was reduced comparing to the control treatment, which was not the case for the cells after silencing of the *SEC61A1* (Lang et al. 2012). But the direct observation of the ER  $\text{Ca}^{2+}$  after the puromycin was not performed. Thus, for the current study it was presumed that the puromycin treatment leads to a number of ion conducting chain-free open translocons, which can close but after some time. So a sustained  $\text{Ca}^{2+}$  leak from the ER was expected. 500  $\mu\text{M}$  puromycin was added at 3 minutes on HEK D1ER cells in 2 mM  $\text{Ca}^{2+}$  extracellular solution (Figure 4.3 A). The presence of puromycin showed significant decreasing ER  $\text{Ca}^{2+}$  before 1  $\mu\text{M}$  thapsigargin was applied at 18 minutes. The kinetics of the 1  $\mu\text{M}$  thapsigargin response was faster after puromycin application.  $K_{\text{leak}}$  increased about 2 after puromycin treatment from the mock treatment. The effect of puromycin on basal  $\text{Ca}^{2+}$  leak compared to the mock treatment was similar to those of pactamycin: 1.82 fold increase for puromycin compared to mock. (Figure 4.3 B, C; Table 4.1). Statistical analysis of 3 independent repeats comprising two groups of cells (11 for puromycin and 12 for control) was done with Two-Sample Kolmogorov-Smirnov test.

**Table 4.1 Effect of protein synthesis inhibitors on  $\text{Ca}^{2+}$  leak.**

treatment	$K_{\text{leak}}$ ( $\text{s}^{-1}$ )	basal $-\text{d}[\text{Ca}^{2+}]_{\text{ER}}/\text{dt}$ ( $\mu\text{M}\cdot\text{s}^{-1}$ )
mock	$8.38\cdot 10^{-3}\pm 1.07\cdot 10^{-3}$	$2.46\pm 0.505$
PUR	$16.9\cdot 10^{-3}\pm 0.97\cdot 10^{-3}$	$4.49\pm 0.54$
PAC	$14.6\cdot 10^{-3}\pm 0.52\cdot 10^{-3}$	$4.24\pm 0.59$
CHX	$4.02\cdot 10^{-3}\pm 0.54\cdot 10^{-3}$	$1.02\pm 0.16$
EME	$3.27\cdot 10^{-3}\pm 0.37\cdot 10^{-3}$	$1.42\pm 0.28$
IONO	$204.9\cdot 10^{-3}\pm 18.5\cdot 10^{-3}$	$44.03\pm 4.51$

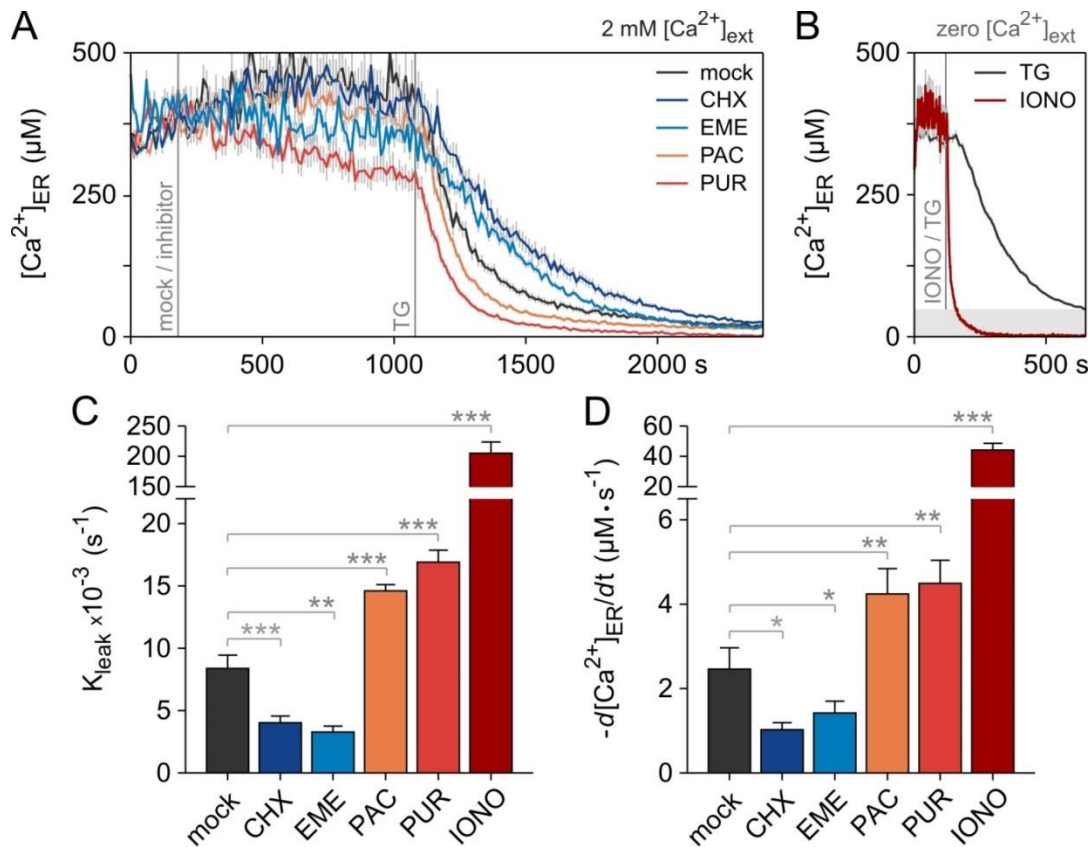


**Figure 4.3** Effect of protein synthesis inhibitors on  $\text{Ca}^{2+}$  leak. **A.** HEK D1ER cells were treated with protein synthesis inhibitors (cycloheximide-CHX, blue; emetine-EME, light blue; pactamycin-PAC, orange; puromycin-PUR, light red) at 3 minutes in 2mM  $\text{Ca}^{2+}$  extracellular with mock buffer application as a control. 1  $\mu\text{M}$  of thapsigargin was applied at 18 minutes (after 15 minutes from the first application). ER  $\text{Ca}^{2+}$  efflux showed continuous one-exponential decay. **B.** Comparison of maximal leak rate achieved by application of 1  $\mu\text{M}$  ionomycin (IONO, red line) to the release of ER  $\text{Ca}^{2+}$  by thapsigargin (TG, black line). **C.**  $\text{Ca}^{2+}$  release speed constant after protein synthesis inhibitors treatment:  $K_{\text{leak}}$ , calculated from fitting with single-exponential model and represented as mean  $\pm$  s.e.m. **D.** Estimated basal  $\text{Ca}^{2+}$  leak rate after protein synthesis inhibitors treatment; represented as mean  $\pm$  s.e.m. Two sample Kolmogorov-Smirnov test was used to calculate the statistical significance between experiments: for each inhibitor 3 independent experiments were taken with the corresponding numbers of cell: 12, mock; 16, CHX; 11, EME; 12, PAC; 11, PUR) Significance represented as asterisks (\*\*\*)  $p < 0.001$ , \*\*  $p < 0.01$ , \*  $p < 0.05$ )

### 4.3 Effect of Sec61 $\alpha$ silencing on endoplasmic reticulum Ca<sup>2+</sup> leak

The very important method to understand the way of how ion leak channels work is to reduce channel protein levels in the cells. Complete removal of the channel protein does not require an additional inhibition of the channel function with chemical compounds; therefore it gives the insight to the “pure” role of the channel. However, the long term silencing of a life-important protein can interfere with the cellular homeostasis and even cause cell death. Therefore the silencing of Sec61 $\alpha$ , the main pore for protein translocation, can hardly reach 100% protein depletion. For the HeLa cells the cell growth stopped achieving 70% of the Sec61 $\alpha$  depletion (Lang et al. 2012). This observation was made already after 72 hours, and the maximal silencing efficiency was after 96 hours. After that silencing efficiency was decreasing with time presumably due to the death of the transfected cells and growing number of the cells, which were not transfected. The level of BiP and GRP170 was not changed in silenced cells, indicating that no induction of UPR (Lang 2012). Indirectly the effect of Sec61 $\alpha$  silencing on ER Ca<sup>2+</sup> homeostasis was shown on HeLa cells (Lang et al. 2012). The depletion of the Sec61a reached about 80% and was enough to see the differences in cytosolic Ca<sup>2+</sup>. Namely, the silencing of *SEC61A1* led to the smaller thapsigargin-evoked peak with no effect of the translocon opener puromycin (500  $\mu$ M during 3 minutes). The roles of BiP and CaM attenuating Ca<sup>2+</sup> release to the cytosol through Sec61 $\alpha$  was also investigated on HeLa cells by silencing of *SEC61A1* gene (Erdmann et al. 2011, Schauble et al. 2012). Up to now no direct observation and analysis of ER Ca<sup>2+</sup> under Sec61 $\alpha$  silencing conditions was done. Therefore, I used the silencing of *SEC61A1* procedure on HEK D1ER cells to estimate the effect of Sec61 $\alpha$  on ER Ca<sup>2+</sup> leak. HEK D1ER cells were silenced as follows: 10<sup>6</sup> cells were transfected using Amaxa Nucleofector II (see 3.7) with 50 pmol of *SEC61A1* siRNA. Then control cells were separated in to two groups. The first 10<sup>6</sup> cells underwent the same transfection procedure but without any of nucleotides in the solution (mock transfection), the second 10<sup>6</sup> cells were transfected with the same amount of scrRNA as for the silencing transfection (siRNA). The cells were taken to the imaging experiments after 72 hours. Imaging experiments were conducted in the extracellular Ca<sup>2+</sup> free solution containing 0.5mM EGTA. For the simultaneous control of the protein content by immunoblot (see 3.4), cells were collected from the

same dishes where the coverslips for the imaging were taken. Cells didn't show any change in the basal ER  $\text{Ca}^{2+}$  due to silencing procedure.

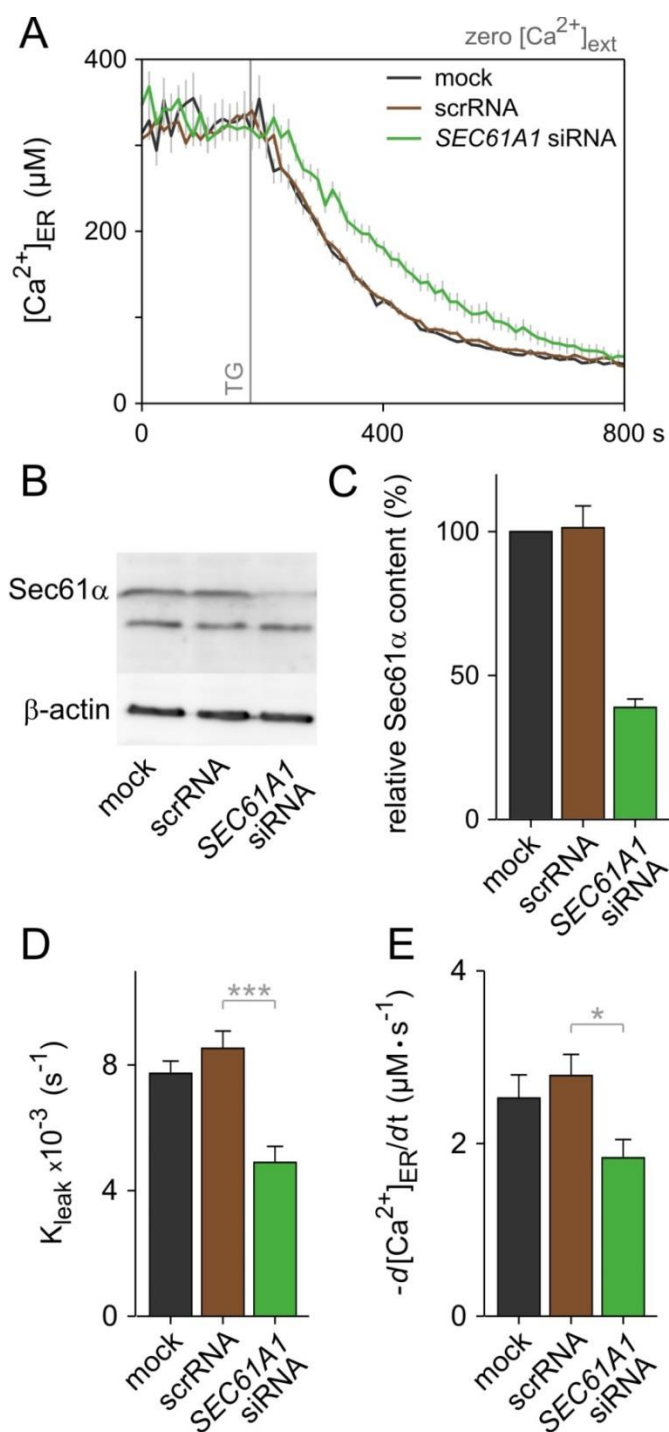


**Figure 4.4** Effect of Sec61a silencing on ER  $\text{Ca}^{2+}$  efflux. **A.** Imaging of thapsigargin responses on HEK D1ER cells after silencing of SEC61A1 gene. Silenced and control cells were treated with 1  $\mu\text{M}$  thapsigargin at 3 minutes in  $\text{Ca}^{2+}$  free extracellular solution (0.5 mM EGTA extracellular). **B.** Corresponding protein content of Sec61 $\alpha$  after silencing

with *SEC61A1* siRNA comparing to the mock transfection and scrRNA transfection (as indicated). Normalized to the amount of  $\beta$ -actin used as loading control. C. Quantification of Western Blot shows the rest of Sec61 $\alpha$  on the silenced cells. The silencing efficiency for the performed protocol was about 60%. D. Analysis of ER Ca<sup>2+</sup> speed depletion shows significant decrease between scrRNA transfected cells and *SEC61A1* siRNA transfected cells. E. Estimated basal ER Ca<sup>2+</sup> leak showed reduction for silenced cells; experimental data was analyzed from 3 independent repeats for each group of cells (mock transfection:18 cells, scrRNA transfection:33 cells, *SEC61A1* siRNA 18cells. Statistical analysis between groups of cells was done with Two-sample Kolmogorov-Smirnov test. Significance represented as asterisks (\*\*\*)  $p < 0.001$ , \*\*  $p < 0.01$ , \*  $p < 0.05$ ).

Then, to investigate the difference in the ER Ca<sup>2+</sup> leak kinetics, the cells were treated with 1  $\mu$ M thapsigargin at 3 minutes. Both mock transfection and scrRNA showed complete depletion of ER Ca<sup>2+</sup> already after 7 minutes. The analysis of the protein content via the densitometry bands showed that the amount of Sec61a was the same in the mock transfected and scrRNA transfected cells, while for the *SEC61A1* siRNA transfected cells this amount had a lower value. All proteins levels were normalized to the corresponding amount of  $\beta$ -actin as a loading control. Quantification showed that the proposed protocol of Sec61 $\alpha$  silencing on HEK D1ER cells allowed us to achieve up to 60% reduction of the protein amount. This was enough to see differences in the main ER Ca<sup>2+</sup> leakage evoked by 1  $\mu$ M thapsigargin. The analysis of the ER Ca<sup>2+</sup> decay was done (see 4.1) and showed that  $K_{\text{leak}}$  was 1.75 fold less for the cells transfected with *SEC61A1* siRNA than for the cells transfected with scrRNA. Basal ER Ca<sup>2+</sup> leak rate showed the same tendency in reduction: a decrease by a factor of about 1.35 for the cells transfected with *SEC61A1* siRNA comparing with the cells transfected with scrRNA. Statistic was done from 3 independent repeats with amount of cells: mock transfection: 18 cells, scrRNA transfection: 33 cells, *SEC61A1* siRNA: 18 cells.

#### 4.4 Effect of Calmodulin and UPR on ER Ca<sup>2+</sup> leak

Sec61 is a complex machinery for protein translocation. As it was proposed, translocons are always in various assembly states with ribosomes and other subunits and are unlikely to be completely disassembled (Potter et al. 2001). It was also shown that a luminal chaperon BiP seals the translocon pore from the luminal side inhibiting the ion leakage through Sec61 $\alpha$ . This was demonstrated as an enhancement of Ca<sup>2+</sup> leak into the cytosol from the ER leak in BiP silenced HeLa cells (Schauble et al. 2012). The increase of thapsigargin-evoked peak after BiP silencing was explained due to additional ER Ca<sup>2+</sup> leak from the unsealed translocons. The direct measurement of ER Ca<sup>2+</sup> using Fluo5N showed the faster time of luminal Ca<sup>2+</sup> depletion evoked by thapsigargin. BiP is an important agent for correct protein folding. It is upregulated during long UPR as a result of an accumulation of unfolded or misfolded proteins in the ER. BiPs are mobilized from their places to cover the unfolded protein. It was shown that at rest, BiP is bound to IRE-1, one of the UPR receptor, and the disassembly of BiP would cause the receptor activation. Tunicamycin blocks the N-glycosylation and provides an increase in amount of non-glycosylated proteins in the ER lumen. This leads to the two possible scenarios: a) mobilization of BiP, and further induction of UPR, and b) retrotranslocation of misfolded proteins for their degradation in the cytosol, the process called ERAD. Tunicamycin was shown to induce Ca<sup>2+</sup> leak by measuring cytosolic peak after the thapsigargin application. This effect was however absent upon BiP silencing, which indicates that tunicamycin induces BiP mobilization and unseals translocons (Schauble et al. 2012). Still, no data was available on ER Ca<sup>2+</sup> leak after the tunicamycin application. Therefore, I performed the measurement of ER Ca<sup>2+</sup> on HEK D1ER and estimated the changes in Ca<sup>2+</sup> signalization. HEK D1ER cells were cultured and prepared for imaging as described before (see 3.2.3). Experiments were completed in 0.5 mM EGTA extracellular Ca<sup>2+</sup>-free solution. Tunicamycin (10  $\mu$ M) was applied for 3 minutes before the application of 1  $\mu$ M thapsigargin. The cells treated with tunicamycin didn't show the decrease of ER Ca<sup>2+</sup> before thapsigargin compared to the control mock application. The time course of the thapsigargin-evoked ER Ca<sup>2+</sup> efflux showed the increase of Ca<sup>2+</sup> leak for tunicamycin-treated cells, but rather with statistical significance of  $p < 0.05$  calculated by two-sample Kolmogorov-Smirnov test. The Ca<sup>2+</sup> leak rate was 1.2 fold higher for 25 cells treated with tunicamycin comparing with 41 cells of control mock treatment (both groups of cells

collected from 3 independent repeats). The basal ER  $\text{Ca}^{2+}$  leak rate was also about 1.23 fold higher after the tunicamycin treatment compared to the control mock-treated cells.

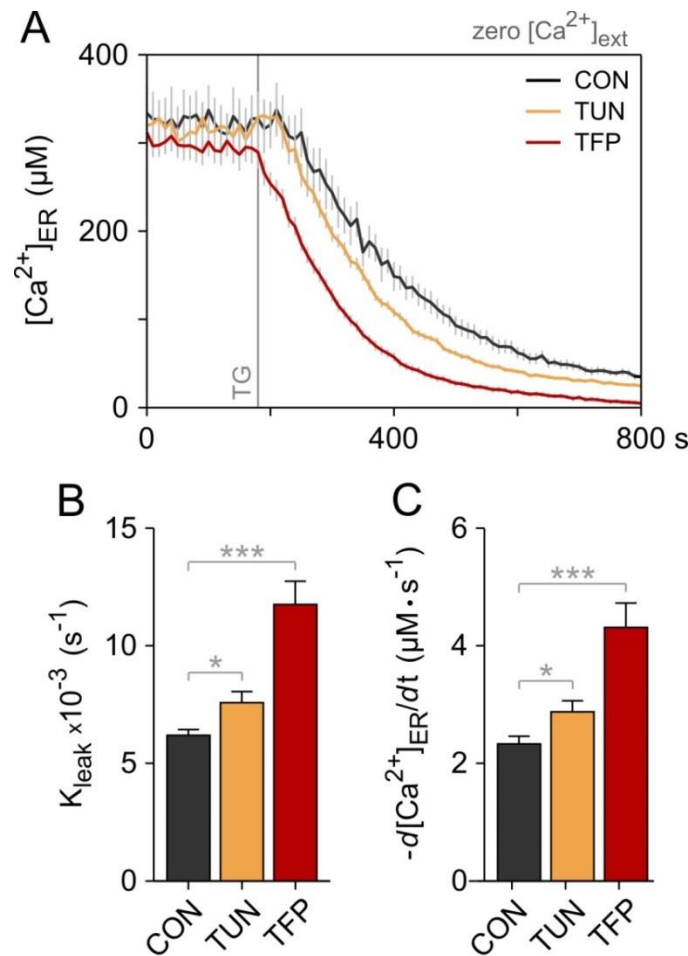


**Figure 4.5. Effect of Calmodulin and UPR on ER  $\text{Ca}^{2+}$  leak. A.** Overlapping of the ER  $\text{Ca}^{2+}$  traces of control, tunicamycin treated (3 minutes before thapsigargin, TG) and TFP treated (5 minutes before thapsigargin, TG) HEK D1ER cells. Application of Thapsigargin showed the decrease in ER  $\text{Ca}^{2+}$ . **B.** Statistics for  $K_{\text{leak}}$  analyzed as one-exponential fitting of thapsigargin evoked decay on ER  $\text{Ca}^{2+}$  on the cells treated with tunicamycin and TFP compared to the control treated cells. **C.** Basal ER  $\text{Ca}^{2+}$  leak from the cells treated with tunicamycin and TFP compared to the control treated cells. Experimental data was analyzed from 3 independent repeats for each group of cells (control treatment: 41 cells, tunicamycin-treated: 18 cells, TFP treated: 18 cells). Statistical analysis between groups of cells was done with Two-sample Kolmogorov-Smirnov test. Significance represented as asterisks (\*\*\*)  $p < 0.001$ , \*\*  $p < 0.01$ , \*  $p < 0.05$ ).

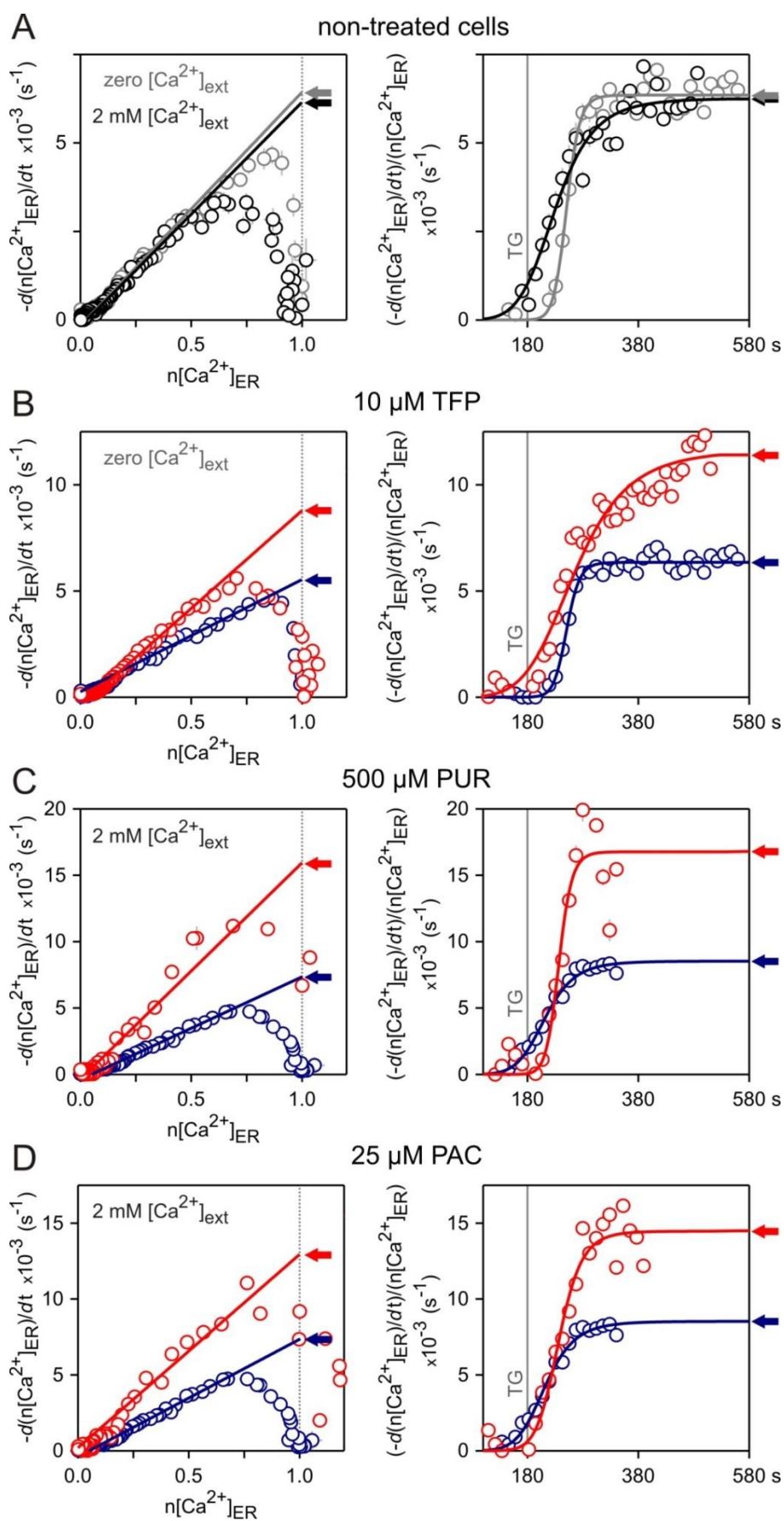
Then I studied the effect of calmodulin inhibition on the ER  $\text{Ca}^{2+}$  leak. Calmodulin is an important cytosolic  $\text{Ca}^{2+}$ -binding protein that plays an enormous role in the intracellular calcium signaling. It was shown that calmodulin also participates in  $\text{Ca}^{2+}$  leak from the

ER. Cytosolic increase of  $\text{Ca}^{2+}$  was detected by applying calmodulin inhibitors ophiobolin A and trifluoperazine (TFP), with the following increase of thapsigargin-induced peak compared to the control experiments (Schauble et al. 2012). The *SEC61A1* silencing on HeLa cells significantly reduced this leak, and in addition a potential binding site for CaM on the cytosolic site of Sec61 $\alpha$  was found (Erdmann et al. 2011). So far it was no direct observation of ER  $\text{Ca}^{2+}$  upon inhibiting of calmodulin binding to the Sec61 complex. Therefore, I have used HEK D1ER cells for direct observation of ER  $\text{Ca}^{2+}$  signaling upon calmodulin inhibition. The cells were cultured and prepared for the imaging experiments as before (see 3.2.3). The measurements were done in 0.5 mM EGTA extracellular  $\text{Ca}^{2+}$  free solution. The cells showed a slight decrease of ER  $\text{Ca}^{2+}$  after 5 minutes application of 10  $\mu\text{M}$  TFP prior to the thapsigargin (1  $\mu\text{M}$ ) application. The kinetics of the thapsigargin-evoked ER  $\text{Ca}^{2+}$  depletion was faster after TFP treatment.  $K_{\text{leak}}$  was 1.9 fold higher than the control mock treatment. Basal ER  $\text{Ca}^{2+}$  leakage was 1.86 fold higher for TFP-treated cells (3 independent repeats for each group of cells with 41 control cells and 16 TFP-treated cells).

## 4.5 Summarizing analysis of endoplasmic reticulum $\text{Ca}^{2+}$ leak through Sec61 complexes

In previous experiments, I have analyzed how ER  $\text{Ca}^{2+}$  leak changes after the application of various protein synthesis inhibitors, also after the deletion of Sec61a protein, calmodulin inhibition, and the induction of the UPR. We concluded that the reduction of  $\text{Ca}^{2+}$  leak obtained by silencing of *SEC61A1* suggests that the Sec61 complexes form dynamic  $\text{Ca}^{2+}$  leak channels in the ER. Therefore, the detailed analysis of ER  $\text{Ca}^{2+}$  leakage is required. In this chapter we perform mathematical analysis to identify the part of ER  $\text{Ca}^{2+}$  leak through the Sec61 complex. Data obtained from the previous experiments collected as single cell traces were calibrated and smoothed as described above (see 3.14). For the correct estimation of ER  $\text{Ca}^{2+}$  changes in each experiment, the normalization to basal ER  $\text{Ca}^{2+}$  was done. The normalized traces were analyzed like in 4.1. Two major parameters were estimated: the leak rate constant ( $K_{\text{leak}}$ ) and the basal ER  $\text{Ca}^{2+}$  rate ( $-d[\text{Ca}^{2+}]_{\text{ER}}/dt$ ). The thapsigargin-evoked decay was the same for both 2 mM  $\text{Ca}^{2+}$  and 0.5 mM EGTA extracellular solutions (black and grey circles in Figure 4.6, respectively). The analysis of the effect of compounds used to modulate  $\text{Ca}^{2+}$  leak was done simultaneously with the analysis of the corresponding control treatment. The control treatments are presented as blue circles in Figure 4.6 B-H, while the substance treatments are indicated there as red circles. The normalized and non-normalized traced showed the same tendencies. Namely, 10  $\mu\text{M}$  TFP, 500  $\mu\text{M}$  puromycin, 25  $\mu\text{M}$  pactamycin, and 10  $\mu\text{g/ml}$  tunicamycin showed both proportional increase in  $K_{\text{leak}}$  and in basal ER  $\text{Ca}^{2+}$  efflux (Figure 4.6 B-E). Silencing of *SEC61A1* gene, 5 mM cycloheximide and 100 $\mu\text{M}$  emetine treatment lowered the basal ER  $\text{Ca}^{2+}$  leak and the leak rate constant  $K_{\text{leak}}$  (Figure 4.6 F-H). I have noticed that  $K_{\text{leak}}$  found from the linear extrapolation of the first derivative of the ER  $\text{Ca}^{2+}$  (left side on Figure 4.6) equals to the  $K_{\text{leak}}$  that is found after the fitting with Hill-function (right side on Figure 4.6). This fact is in favor for the single-exponential model of the ER  $\text{Ca}^{2+}$  decay. This model indicates that changes of the ER  $\text{Ca}^{2+}$  leak are mainly due to the changes in ER membrane permeabilisation for  $\text{Ca}^{2+}$  ions, considering previous findings of the influence of the used compounds on the Sec61 complexes. This proves that translocon is an active participant in the ER  $\text{Ca}^{2+}$  leak. Performing normalization to the control treatment cell traces allows us to obtain the fraction of ER  $\text{Ca}^{2+}$  leak mediated by Sec61 $\alpha$  (Figure 4.7). The treatment of puromycin, pactamycin and TFP showed the increase of the ER  $\text{Ca}^{2+}$  leakage and  $K_{\text{leak}}$  to 172%–

186% comparing to the control mock treated cells. Silencing of the *SEC61A1* gene, which on the HEK D1ER cells were leaving about 40% Sec61 active, inhibited the leak rate to 39%. Emetine and cycloheximide showed an inhibition of 45%–59% of the basal ER  $\text{Ca}^{2+}$  leak and also the same tendency to  $K_{\text{leak}}$  comparing to the mock control treatment. The main conclusion is that ER  $\text{Ca}^{2+}$  leak in the cells can change approximately from 45% to 185% due to the Sec61 $\alpha$ -mediated  $\text{Ca}^{2+}$  leak, under various translocation steps.



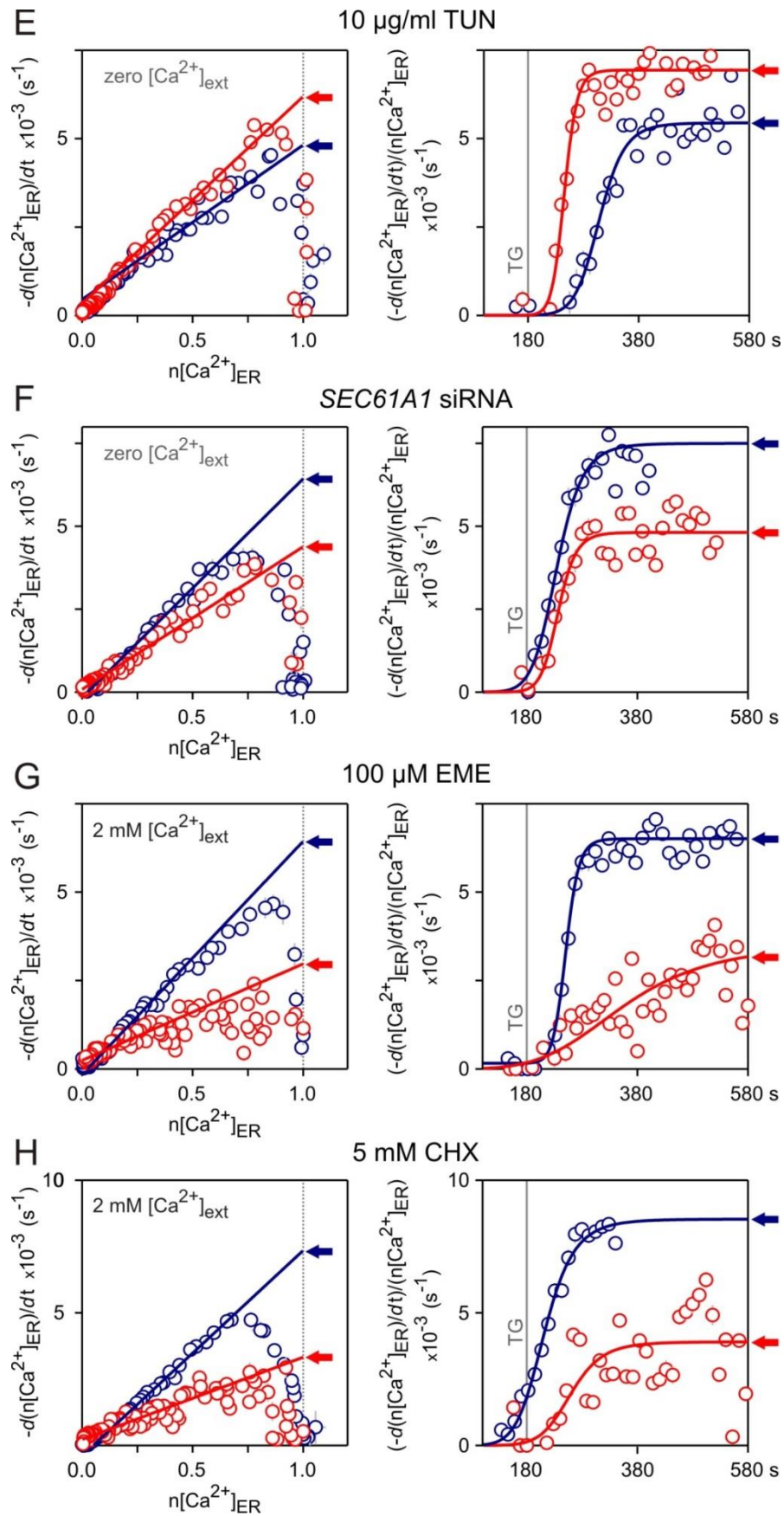


**Figure 4.6. Numerical approach on the normalized traces. HEK D1ER cells were treated with 1  $\mu$ M thapsigargin at moment of  $t=180$  s. Calibrated and normalized responses of ER  $\text{Ca}^{2+}$  were smoothed (see 3.14) and the first derivative was taken (see 4.1). Estimation of basal  $\text{Ca}^{2+}$  leak rate (every section of figure on the left) was done like in 4.1 for normilised responses on the graph of first derivative versus normalized ER  $\text{Ca}^{2+}$  via linear fitting and extrapolating of the linear part of the graph, which is indicated as arrows after crossing the “1”.  $\text{Ca}^{2+}$  leak rate constant (every section on the right) was estimated like in 4.1 for normalized responses and indicated as arrows for fitting with Hill-function after reaching a maximum. Corresponding treatment of HEK D1ER cells are color indicated for circles, lines, and arrows. A. Non-treated HEK D1ER cells showed responses to 1  $\mu$ M thapsigargin in 2 mM  $\text{Ca}^{2+}$  extracellular (black) and 0.5 mM EGTA extracellular (gray). B. Analysis of the 1  $\mu$ M thapsigargin response after treatment for 5 minutes with 10  $\mu$ M TFP (red symbols) comparing to the control (blue symbols) in 0.5 mM EGTA extracellular. C. Analysis of the 1  $\mu$ M thapsigargin response after treatment for 15 minutes with 500  $\mu$ M puromycin (red symbols) comparing to the control (blue symbols) in 2 mM  $\text{Ca}^{2+}$  extracellular. D. Analysis of the 1  $\mu$ M thapsigargin response after treatment for 15 minutes with 25  $\mu$ M pactamycin (red symbols) comparing to the control (blue symbols) in 2 mM  $\text{Ca}^{2+}$  extracellular. E. Analysis of the 1  $\mu$ M thapsigargin response after treatment for 5 minutes with 10  $\mu$ g/ml tunicamycin (red symbols) comparing to the control (blue symbols) in 0.5 mM EGTA extracellular. F. Analysis of the 1  $\mu$ M thapsigargin response after silencing of *SEC61A1* gene (red symbols) comparing to the control (blue symbols) in 0.5 mM EGTA extracellular. G. Analysis of the 1  $\mu$ M thapsigargin response after treatment for 15 minutes with 100  $\mu$ M emetine (red symbols) comparing to the control (blue symbols) in 2 mM  $\text{Ca}^{2+}$  extracellular. H. Analysis of the 1  $\mu$ M thapsigargin response after treatment for 15 minutes with 5 mM cycloheximide (red symbols) comparing to the control (blue symbols) in 2 mM  $\text{Ca}^{2+}$  extracellular.**

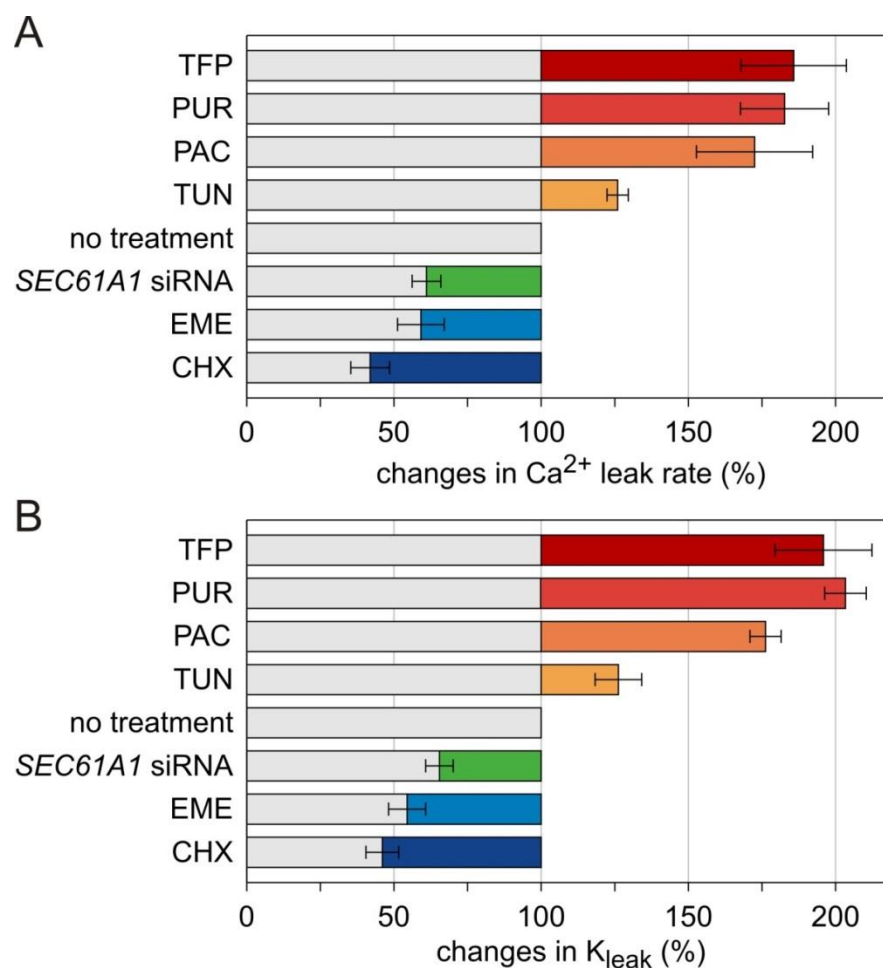


**Figure 4.7. Estimation of ER Ca<sup>2+</sup> leak through Sec61 complex. A. Relative changes in basal ER Ca<sup>2+</sup> leak rate due to the treatment with compounds as indicated. Bars representing mean of the group of cells in each experiment normalized to the corresponding control treatment. Error bars showing s.e.m. B. A. Relative changes in K<sub>leak</sub> due to the treatment with compounds as indicated (the same treatment protocols, color-coded bars). Bars representing mean of the group of cells in each experiment normalized to the corresponding control treatment. Error bars showing s.e.m.**

## 4.6 Cytosolic-endoplasmic reticulum $\text{Ca}^{2+}$ relationship of $\text{Ca}^{2+}$ leak through Sec61 complexes

Simultaneous monitoring of ER and cytosolic  $\text{Ca}^{2+}$  allows us to better understand of the relation between cytosolic  $\text{Ca}^{2+}$  clearance mechanisms and ER  $\text{Ca}^{2+}$  efflux. So far, the activation of  $\text{Ca}^{2+}$  leak through translocons has been investigated by studying changes in cytosolic  $\text{Ca}^{2+}$  (e.g. (Lang et al. 2012)) and little is known about the corresponding changes of ER  $\text{Ca}^{2+}$ . The cytosolic clearance mechanism involves a system of ion channels and pumps to keep the concentration of ions in cytosol constant. This system activates when the intracellular ion concentration is disturbed, and it stops working when the resting conditions are restored. In this way, the whole  $\text{Ca}^{2+}$  homeostasis is kept in balance, and here I study the effects on cytosolic  $\text{Ca}^{2+}$  resulted from the ER  $\text{Ca}^{2+}$  leak through Sec61 via inducing  $\text{Ca}^{2+}$  release from the ER. SERCA pumps use ATP energy to pump  $\text{Ca}^{2+}$  inside the ER lumen against the concentration gradient. Their activity can be changed according to the amount of ER  $\text{Ca}^{2+}$  leakage, but the maximal amount of pumped  $\text{Ca}^{2+}$  cannot overcome certain value that follows from the thermodynamic principles (Shannon et al. 2000). SERCAs are the only known ER  $\text{Ca}^{2+}$  pump therefore we used a selective blocker of SERCA thapsigargin to unmask the whole  $\text{Ca}^{2+}$  efflux from the ER. After reaching the cytosol,  $\text{Ca}^{2+}$  from the ER can follow different scenarios. One is to be pumped out by sodium-calcium exchanger (NCX) located on the plasma membrane and plasma membrane  $\text{Ca}^{2+}$  ATPases (PMCA). The physiological concentration of extracellular  $\text{Ca}^{2+}$  is 1-2.5 mM therefore pumping  $\text{Ca}^{2+}$  outside the cell to keep cytosolic  $\text{Ca}^{2+}$  at 100 nM also requires hydrolysis of ATP. The  $\text{Ca}^{2+}$  fluxes through the plasma membrane can be inhibited by lanthanides ( $\text{La}^{3+}$ ,  $\text{Gd}^{3+}$ ). To check if  $\text{Ca}^{2+}$  fluxes through Sec61 are maintained by plasma membrane clearance mechanisms, we used 1 mM  $\text{Gd}^{3+}$  extracellular and observed changes in cytosolic  $\text{Ca}^{2+}$  comparing to the control treatment (Figure 4.8). Another way to keep cytosolic  $\text{Ca}^{2+}$  at its physiological level during long lasting enhancement of ER  $\text{Ca}^{2+}$  leakage is to be absorbed by mitochondria. Located closely to the ER and building ER associated membranes, mitochondria are organelles that are very likely to catch  $\text{Ca}^{2+}$  directly from the ER proximity. Absorption of  $\text{Ca}^{2+}$  ions inside mitochondria is driven by the electric gradient of the IMM and works through Mitochondrial Calcium Uniporter (MCU). Therefore, we wanted to identify the ways where  $\text{Ca}^{2+}$  goes after leaking out from ER through Sec61 $\alpha$ . To enhance the  $\text{Ca}^{2+}$  removal mechanism, HEK293 cells prepared as in (see 3.2.3) were

treated in 0.5 mM EGTA extracellular  $\text{Ca}^{2+}$  free solution to avoid capacitative calcium entry. As an agent to enhance the  $\text{Ca}^{2+}$  leak from the translocon I used 500  $\mu\text{M}$  puromycin and compared with the corresponding control mock treatment (Figure 4.8).

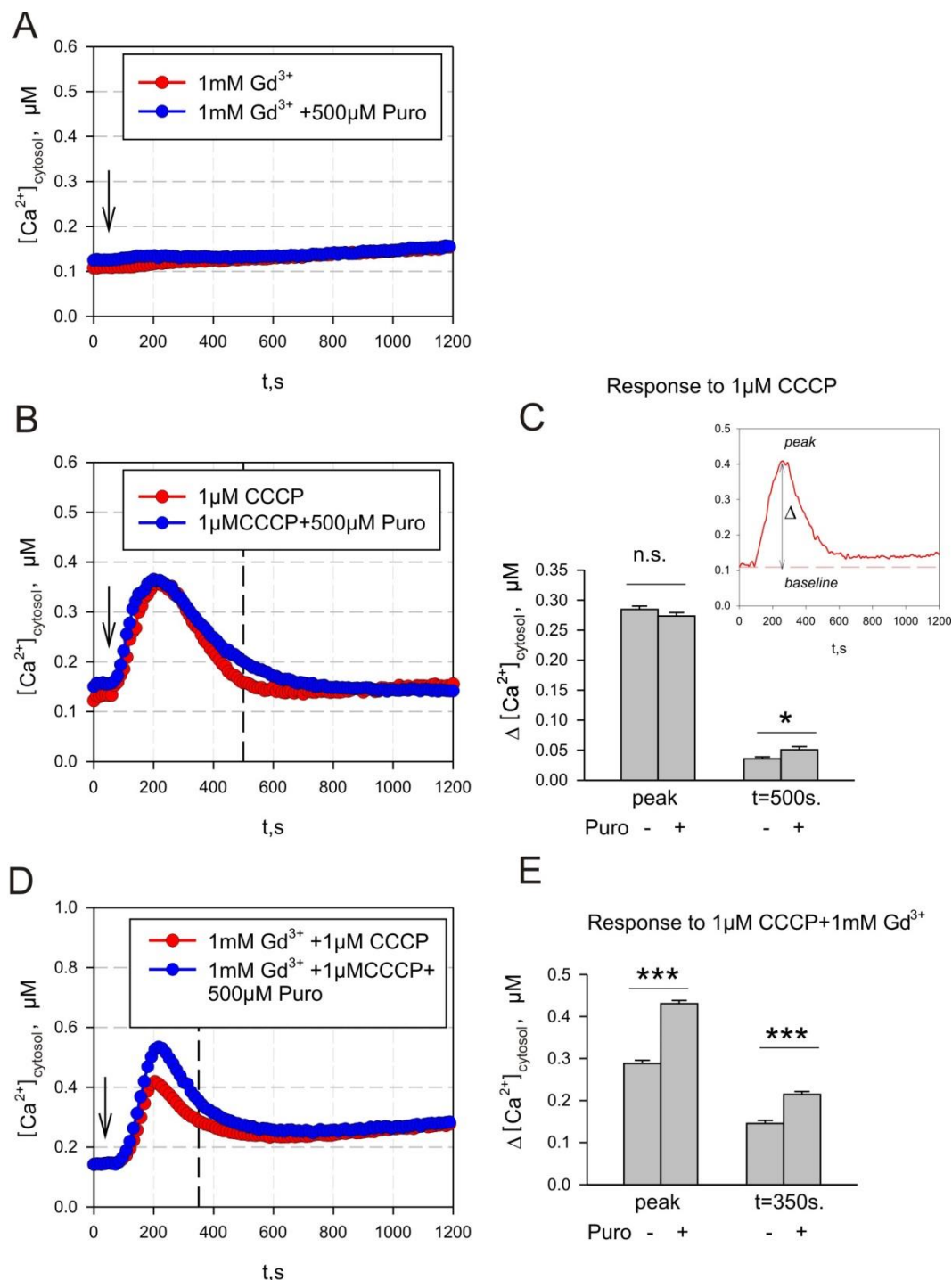


**Figure 4.8. Clearance mechanisms of  $\text{Ca}^{2+}$  leak through Sec61 complexes.** A. Cell plasmam membrane clearance mechanisms were blocked with 1 mM  $\text{Gd}^{3+}$  in order to unmask cytosolic  $\text{Ca}^{2+}$  increase evoked application (arrow indicated) 500  $\mu\text{M}$  puromycin (blue)

comparing to the control mock application (red). **B. Mitochondrial uptake blocker CCCP** (application of 1  $\mu\text{M}$ , arrow indicated) evoked peak both with simultaneous puromycin treatment (blue) and control (red). **C. Statistics from traces of evoked  $\text{Ca}^{2+}$  peaks.** Peak amplitude was calculated as in inlet left from A., and level of cytosolic  $\text{Ca}^{2+}$  at a given time point (500 s). one-way Student's t-test. n.s.-non significant. \*  $p < 0.05$ . **D. Simultaneous blocking of plasma membrane clearance mechanisms by  $\text{Gd}^{3+}$  and uncoupling mitochondria membrane with CCCP: puromycin application (blue trace), and control (red trace) are arrow indicated.** The statistics for this treatment is shown on E for the peak amplitude and the level of signal at 350 s; Significance was tested with one way Student's t-test, \*\*\*  $p < 0.001$ .

The inhibition of plasma membrane clearance mechanisms by 1 mM  $\text{Gd}^{3+}$  evoked slow continuous increase in basal  $\text{Ca}^{2+}$  level and the corresponding cytosolic  $\text{Ca}^{2+}$  after 500  $\mu\text{M}$  puromycin treatment was not significantly different from the mock treatment level (Figure 4.8 A). Therefore, the first conclusion was that  $\text{Ca}^{2+}$  leak through the translocon has different clearance mechanism. The depolarisation of IMM with 1  $\mu\text{M}$  protonophore CCCP applied on cells led to the release of  $\text{Ca}^{2+}$  kept in mitochondria by a negative electric gradient. This was seen as a cytosolic  $\text{Ca}^{2+}$  peak immediately after 1  $\mu\text{M}$  CCCP application which returns to basal  $\text{Ca}^{2+}$  level after about 5 minutes (Figure 4.8 B). Simultaneous application of 500  $\mu\text{M}$  puromycin and 1  $\mu\text{M}$  CCCP evoked the peak with the same amplitude but the decay after reaching maximum had been prolonged. This indicates that  $\text{Ca}^{2+}$  coming from the ER through the Sec61 can no longer be absorbed by mitochondria. Simultaneous blocking of PM clearance mechanisms by 1 mM  $\text{Cd}^{3+}$  and the destruction of IMM potential by 1  $\mu\text{M}$  CCCP evoked higher  $\text{Ca}^{2+}$  peak in cytosol comparing to that without  $\text{Gd}^{3+}$ . Additional simultaneous treatment with 500  $\mu\text{M}$  puromycin (Figure 4.8 D) led to the significant amplitude increase of the peak evoked by CCCP and to the longer decay after reaching maximum. This indicates that the plasma membrane clearance mechanism removes the rest of  $\text{Ca}^{2+}$  coming from the ER through Sec61, which was not absorbed by the mitochondria. Thus, the conclusion is that both plasma membrane clearance mechanisms and mitochondria are involved in regulating of cytosolic  $\text{Ca}^{2+}$  influx from the ER through Sec61 $\alpha$ . Simultaneous observation of cytosolic and ER  $\text{Ca}^{2+}$  after puromycin incubation gives the insight to the relation of cytosolic and ER  $\text{Ca}^{2+}$  responses due to the enhanced  $\text{Ca}^{2+}$  leak through Sec61 $\alpha$ . I also performed experiments with HEK D1ER cells that were cultured and prepared for imaging as

described in sec. 3.2.3. Effect of puromycin incubation during 10 minutes prior to imaging in cultured medium was observed in  $\text{Ca}^{2+}$  free extracellular solution to avoid capacitative calcium entry. Without  $\text{Ca}^{2+}$  in the extracellular bath solution (0.5 mM EGTA extracellular) the cells were treated with 1  $\mu\text{M}$  TG to unmask the ER  $\text{Ca}^{2+}$  leak. Changes in the thapsigargin-evoked peak were noticeable due to incubation with puromycin for concentrations above 200  $\mu\text{M}$ . The cytosolic  $\text{Ca}^{2+}$  peak was lower and narrower, which can be explained by  $\text{Ca}^{2+}$  loss from the ER during the incubation (Figure 4.9 A). However, the difference in ER  $\text{Ca}^{2+}$  decay between control mock incubation and 200  $\mu\text{M}$  puromycin incubation was not seen, as well as in basal cytosolic  $\text{Ca}^{2+}$  level before thapsigargin application (Figure 4.9 B). This can be explained by an insignificant enhancement of  $\text{Ca}^{2+}$  leakage from the ER: the cells keep the cytosolic and the ER  $\text{Ca}^{2+}$  balance despite the leak evoked by puromycin. Nevertheless, a small portion of  $\text{Ca}^{2+}$  was released from the ER leading to narrowing of the cytosolic  $\text{Ca}^{2+}$  peak after thapsigargin. To increase  $\text{Ca}^{2+}$  leakage through Sec61 incubation with 1000  $\mu\text{M}$  puromycin for 10 minutes was performed. Basal  $\text{Ca}^{2+}$  cytosolic level after the incubation was higher for the cytosol and lower for the ER (Figure 4.9 A). This can be explained by the continuous  $\text{Ca}^{2+}$  release from the ER resulting in the decrease of ER  $\text{Ca}^{2+}$ . This decrease was stronger for 1000  $\mu\text{M}$  puromycin than for 200  $\mu\text{M}$  puromycin incubation, which resulted in the significant drop of the thapsigargin-evoked cytosolic  $\text{Ca}^{2+}$  peak after 1000  $\mu\text{M}$  puromycin incubation. Observation of the ER  $\text{Ca}^{2+}$  also showed faster ER depletion after 1000  $\mu\text{M}$  puromycin incubation (Figure 4.9 B).

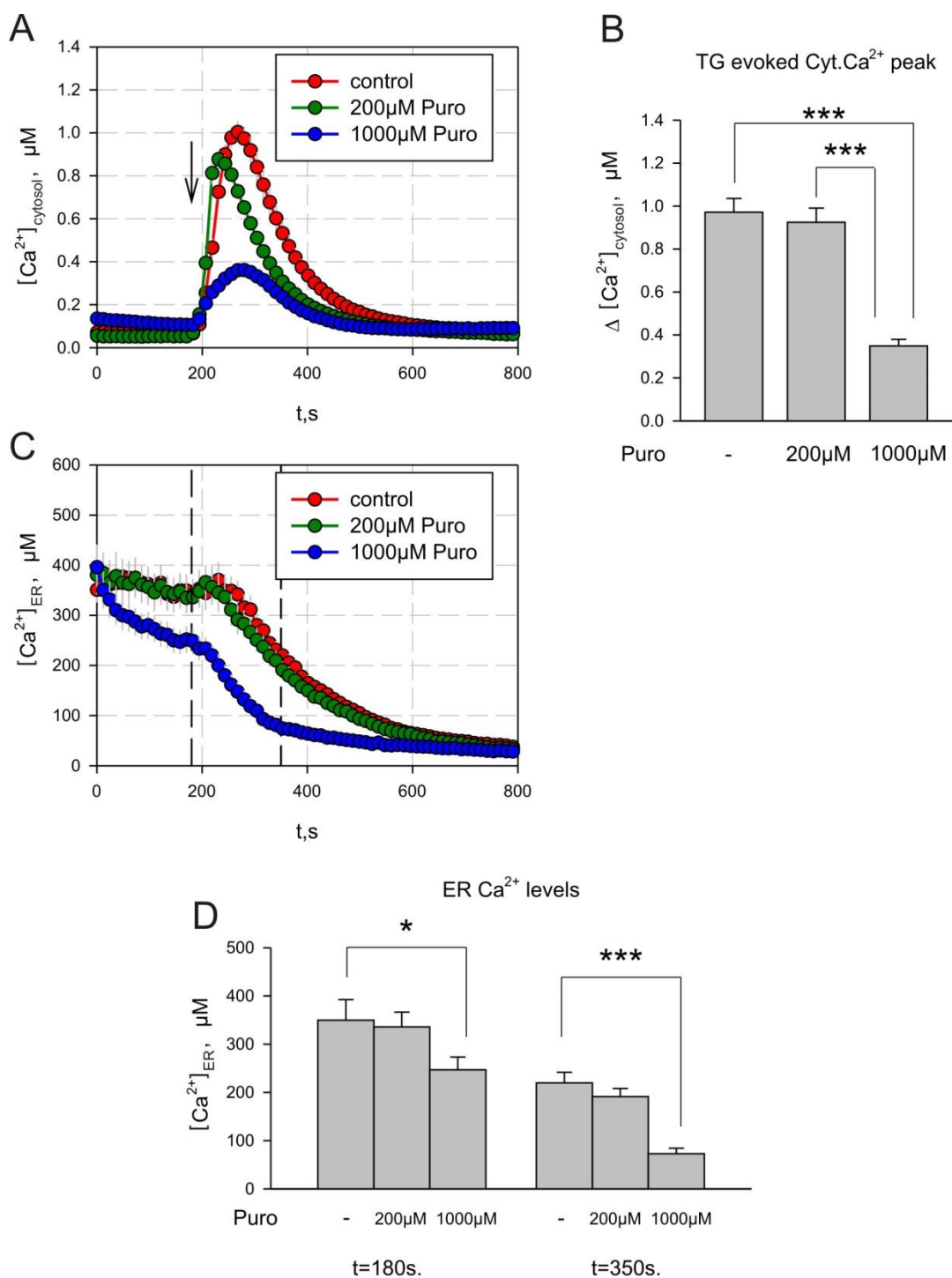


**Figure 4.9. Dose-dependent effects to puromycin on  $Ca^{2+}$  leak from ER.** HEK D1ER were incubated for 10 minutes culture medium with puromycin (concentrations as indicated) and taken for simultaneous imaging of cytosolic and ER  $Ca^{2+}$  in 0.5 mM EGTA extracellular. **A** Application of 1  $\mu\text{M}$  thapsigargin (arrow indicated) evoked peaks of cytosolic  $Ca^{2+}$  on HEK D1ER cells incubated with puromycin (Puro, concentrations as indicated). **B** Statistics for peak amplitude: one way students-t-test. \*\*\*  $p < 0.001$ . **C**. Corresponding responses of ER  $Ca^{2+}$  to thapsigargin measured simultaneously. **D**. Statistic

**of ER Ca<sup>2+</sup> levels at application time (t = 180 s) and given time point (t = 350 s). one way students t-test. \*\*\* p<0.001, \* p<0.05.**

Pactamycin was used as another opener of Sec61 for ion flux. As it was shown previously, pactamycin application in the presence of Ca<sup>2+</sup> accelerates the kinetic of ER Ca<sup>2+</sup> release evoked by thapsigargin (see 4.2). To investigate the effect of pactamycin on cytosolic-ER Ca<sup>2+</sup> relationship, HEK D1ER cells were cultured and prepared for imaging experiments as described before (see 3.2.3), and the experiments were conducted in 0.5 mM EGTA extracellular solution to avoid capacitative calcium entry. The cells were treated with pactamycin at 3 minutes after recording start with following thapsigargin application at 20 minutes (Figure 4.10). Pactamycin (5 μM) did not evoke any changes in cytosolic Ca<sup>2+</sup> and ER Ca<sup>2+</sup> before thapsigargin. The thapsigargin-evoked peak of cytosolic Ca<sup>2+</sup> after 5 μM pactamycin had the same amplitude as after control mock treatment. The peak was insignificantly narrower and ER Ca<sup>2+</sup> decay didn't show any difference in the kinetics (Figure 4.10 A). Increasing the concentration of pactamycin to 25 μM, however, had a significant effect on Ca<sup>2+</sup> signalization. The direct increase of cytosolic Ca<sup>2+</sup> with the corresponding continuous decrease of ER Ca<sup>2+</sup> were observed after the application of 25 μM pactamycin even before thapsigargin application. This decrease of ER Ca<sup>2+</sup> was also observed in 2 mM Ca<sup>2+</sup> extracellular (see 4.2), however it was not significant. Pactamycin (25 μM) also evoked faster release from ER after 1 μM thapsigargin application comparing to the control mock treatment (Figure 4.10 A). The cytosolic Ca<sup>2+</sup>-thapsigargin peak was higher and narrower than for mock treated cells, indicating both increase in ER Ca<sup>2+</sup> leak rate and ER Ca<sup>2+</sup> depletion due to 25 μM pactamycin application. More detailed observation of “pure” pactamycin effect on cytosolic and ER Ca<sup>2+</sup> was done with two higher concentration of pactamycin: 50 μM and 100 μM. However, I had presumed a high toxicity of this amount of the protein synthesis inhibitor; therefore the observations were done only for short time without thapsigargin application (Figure 4.11). As was already noticed before, 5 μM pactamycin application was not different from to mock treatment and 25 μM pactamycin application evokes both increase of cytosolic Ca<sup>2+</sup> and decrease of ER Ca<sup>2+</sup> in 0.5 mM EGTA extracellular solution.

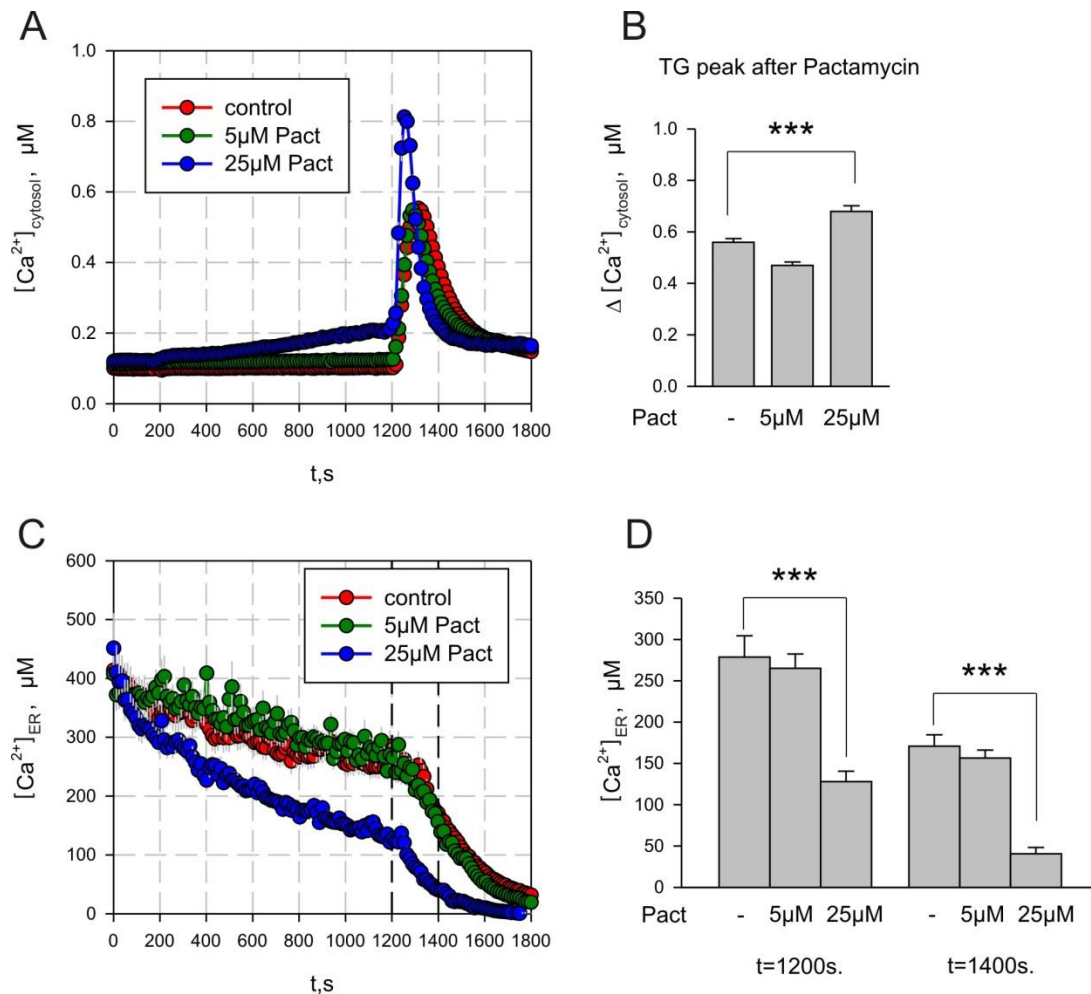


**Figure 4.10.** Dose dependent effect of pactamycin. HEK D1ER cells were taken for simultaneous imaging of cytosolic and ER  $Ca^{2+}$  in 0.5 mM EGTA extracellular solution. A. Pactamycin (Pact) or control mock application (color-coded) were applied at 180 s with following 1  $\mu M$  thapsigargin application at 20 minutes; traces of cytosolic  $Ca^{2+}$  increase were analyzed in B. Statistics for thapsigargin-evoked peak amplitude. One way Student's-t-test. \*\*\*  $p < 0.001$ . C. Corresponding responses of ER  $Ca^{2+}$  to pactamycin or control mock application as indicated (application at 3 minutes). Following application of thapsigargin (1  $\mu M$ ) at 20 minutes was analyzed. D: Statistics for thapsigargin-evoked  $Ca^{2+}$  decay. ER  $Ca^{2+}$  levels at the moment of application (t=1200 s) and at a given time point (t=1400s). One way Students t-test, \*\*\*  $p < 0.001$

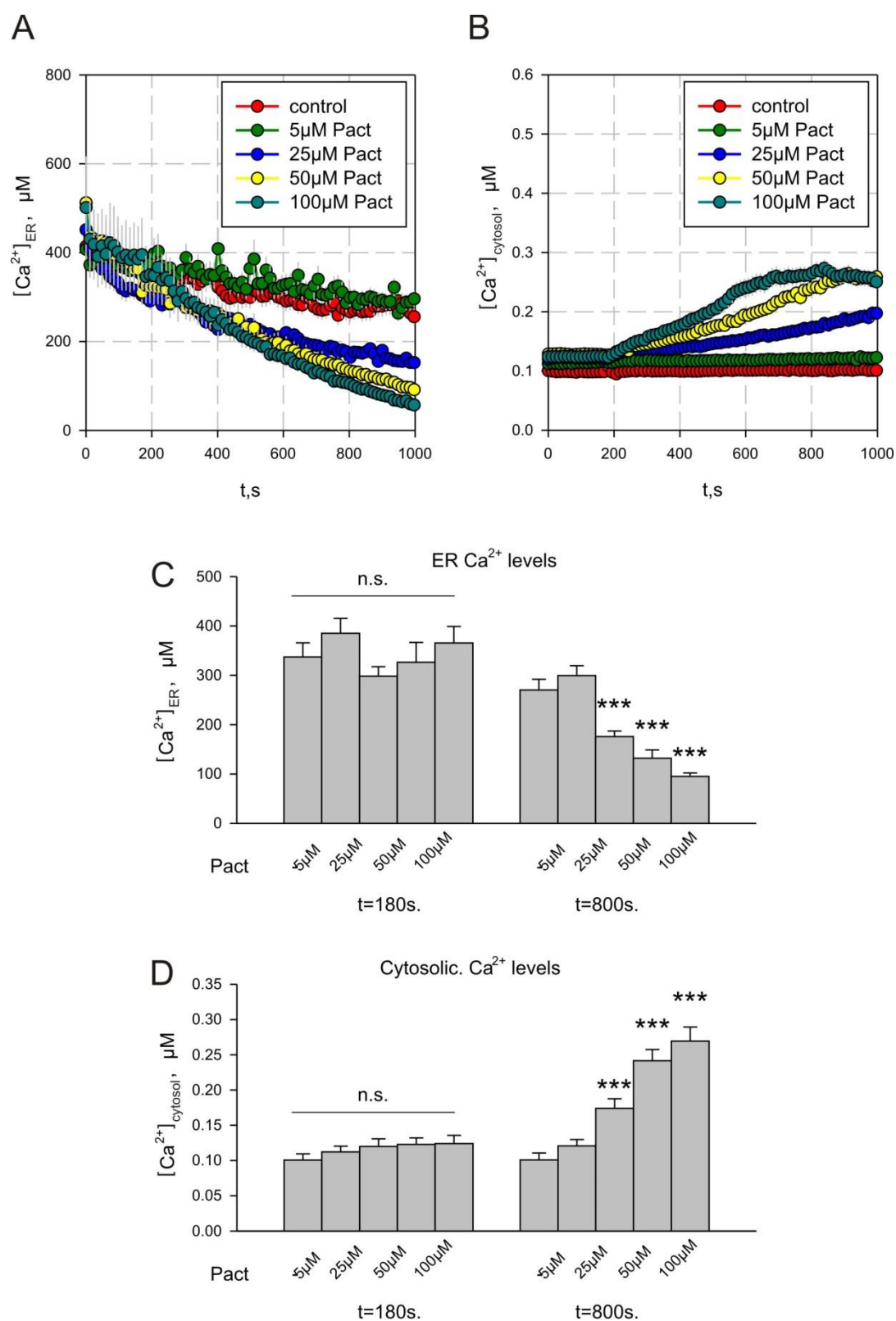


**Figure 4.11. Online effect of pactamycin.** HEK D1ER cells were maintained in 0.5 mM EGTA extracellular solution for simultaneous cytosolic and ER  $Ca^{2+}$  imaging. **A.** ER  $Ca^{2+}$  responses to pactamycin and control mock (color coded traces, application at 3 minutes). **B** Corresponding cytosolic  $Ca^{2+}$  responses evoked by pactamycin (concentrations are color

---

coded) applied at 3 minutes. **C. Analysis of ER Ca<sup>2+</sup> levels at application point. ANOVA, n.s. p>0.05, and at a given time point t=800 s. comparing with the control, unpaired Students t-test, \*\*\* p<0.001. D. Analysis of corresponding cytosolic Ca<sup>2+</sup> levels at application point. ANOVA, n.s. p>0.05, and at a given time point t=800 s. comparing with the control, unpaired Students t-test, \*\*\* p<0.001.**

The applications of 50  $\mu\text{M}$  and 100  $\mu\text{M}$  pactamycin evoke stronger responses on cytosolic and ER Ca<sup>2+</sup> (Figure 4.11).

Statistical analysis of all concentrations of pactamycin showed dose-dependent effects on Ca<sup>2+</sup> leak from the ER to the cytosol (Figure 4.11 C, D). As it seen, the apparent K<sub>D</sub> for pactamycin on HEK D1ER cells is between 5  $\mu\text{M}$  and 25  $\mu\text{M}$ . Taken together, the analysis of simultaneous responses of cytosolic and ER Ca<sup>2+</sup> lead to the conclusion that the ER Ca<sup>2+</sup> leak enhanced through Sec61 $\alpha$  can be maintained by intracellular activity until it reaches certain values where the depletion of ER Ca<sup>2+</sup> become significant.

## 4.7 Endoplasmic reticulum Ca<sup>2+</sup> leak mediated by luminal co-chaperones

Translocation machinery is a complex mechanism that consists of a large number of subunits. It was demonstrated that a luminal chaperon BiP seals the translocon from the luminal side for Ca<sup>2+</sup> efflux (Schauble et al. 2012). This explains the Ca<sup>2+</sup> leak from the ER through Sec61 upon UPR. However, the function of BiP also depends on co-chaperones. In particular, ERj3 and ERj6 luminal co-chaperones were proposed to facilitate BiP activity and play a role in Ca<sup>2+</sup> homeostasis (Weitzmann et al. 2007). As a side project, we have analyzed cytosolic and ER Ca<sup>2+</sup> to identify the changes in the intracellular Ca<sup>2+</sup> signaling resulting from ERj3 and ERj6 activities. To prove the role of these co-chaperones as potent attenuating agents of Sec61a-mediated Ca<sup>2+</sup>-leak, we used HeLa D1ER cells (see 3.5, 3.6). The silencing procedure was performed as described in (Lang et al. 2012). HeLa D1ER cells were prepared for the imaging and the rest collected for WB to identify the silencing efficiency of ERj3 and ERj6 (Schorr et al. 2015). Simultaneous silencing reached about 90% for each of the co-chaperones. The silenced and control HeLa D1ER cells were put in 0.5 mM EGTA extracellular solution and 1  $\mu$ M thapsigargin was applied at 3 minutes (Figure 4.12). Cytosolic response to 1  $\mu$ M thapsigargin application was in a form of peak with the amplitude 37% higher (normalized FURA-2 ratio signals) for silenced cells than for the cells after the control transfection (Figure 4.12 A, inset). The cells transfected with combination of *ERj3* siRNA and *ERj6* siRNA showed also faster depletion of ER Ca<sup>2+</sup> upon thapsigargin application. The ER Ca<sup>2+</sup> depletion rate was estimated as  $\tau_{1/2}$  (time of reaching 50% of the total ER Ca<sup>2+</sup> depletion) of the normalized FRET Ratio traces of each cell: silenced cells had  $\tau_{1/2}$  about 23% less than cell transfected with corresponding amount of scrRNA (Figure 4.12 A, inset). Taken together that proves that BiP co-chaperones ERj3 and ERj6 are also attenuating BiP in sealing of the Sec61 pore from the luminal side for Ca<sup>2+</sup> leak.

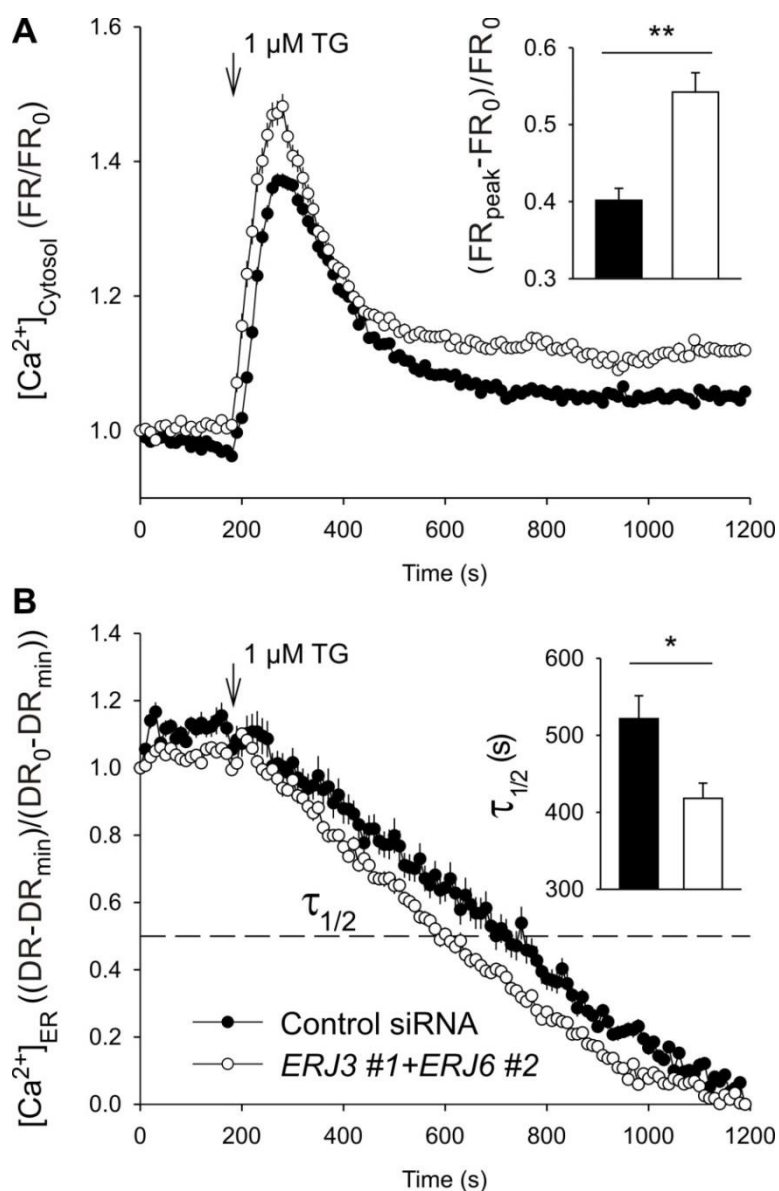


**Figure 4.12.** Effect of ERj3 and ERj6 on intracellular  $Ca^{2+}$  signaling. **A.** Normalized Fura2 traces of HeLa D1ER cells responding to 1  $\mu$ M Thapsigargin applied at 3 minutes. Empty circles: silenced cells with *ERj3* siRNA and *ERj6* siRNA simultaneously; black full circles: control mock transfection. Inset shows statistic for the amplitudes of thapsigargin-evoked peak (circles and bars shown as mean; whiskers and error bars: s.e.m.; black: control cells, empty silenced cells). **B.** Normalized FRET ratio traces measured simultaneously with FURA-2 traces from A. Thapsigargin applied at 3 minutes, dashed line shows the level of 50% of the response for calculating  $\tau_{1/2}$ . Statistics for  $\tau_{1/2}$  is in inset. Full black circles and inset bar: control scrRNA transfected cells; empty circles and inset bar: cells silenced with *ERj3* siRNA and *ERj6* siRNA simultaneously; (circles and bars shown as mean; whiskers and error bars: s.e.m.). Modified from (Schorr et al. 2015).

## 4.8 Mycolactone and endoplasmic reticulum $\text{Ca}^{2+}$ homeostasis

Mycolactone is a toxin derived from *Mycobacterium ulcerans* that causes *Buruli ulcer* (Walsh et al. 2008), a malignant painless ulcer lesions. HEK D1ER cells were used for simultaneous measurement of cytosolic and ER  $\text{Ca}^{2+}$ . As for the initial experiments, we used 500 ng/ml of mycolactone, which was supplied from Dr. Rachel Simmonds, University of Surrey. Mycolactone (500 ng/ml) was added to the culture medium of HEK D1ER (see 3.2.2) 1.5 hours prior to the measurements. Loading of the cells with FURA-2 (see 3.11.1) was done in the same solution during last 20 minutes of incubation. The cells were washed twice and the imaging measurements were conducted in 0.5 mM EGTA extracellular solution (see 3.13). To unmask  $\text{Ca}^{2+}$  efflux from the ER a selective inhibitor of SERCA pumps thapsigargin (1  $\mu\text{M}$ ) was used. The application of thapsigargin at 3 minutes after recording start evoked both a peak of cytosolic  $\text{Ca}^{2+}$  (Figure 4.13 A) and an exponent like depletion of the ER  $\text{Ca}^{2+}$  (Figure 4.13 B). The basal ER  $\text{Ca}^{2+}$  level decreased after mycolactone treatment (Figure 4.13 B), the cytosolic  $\text{Ca}^{2+}$  peak was not significantly different in the height but narrower comparing to the mock control incubation (Figure 4.13 A). Thus, mycolactone has likely induced a  $\text{Ca}^{2+}$  leak from the ER.

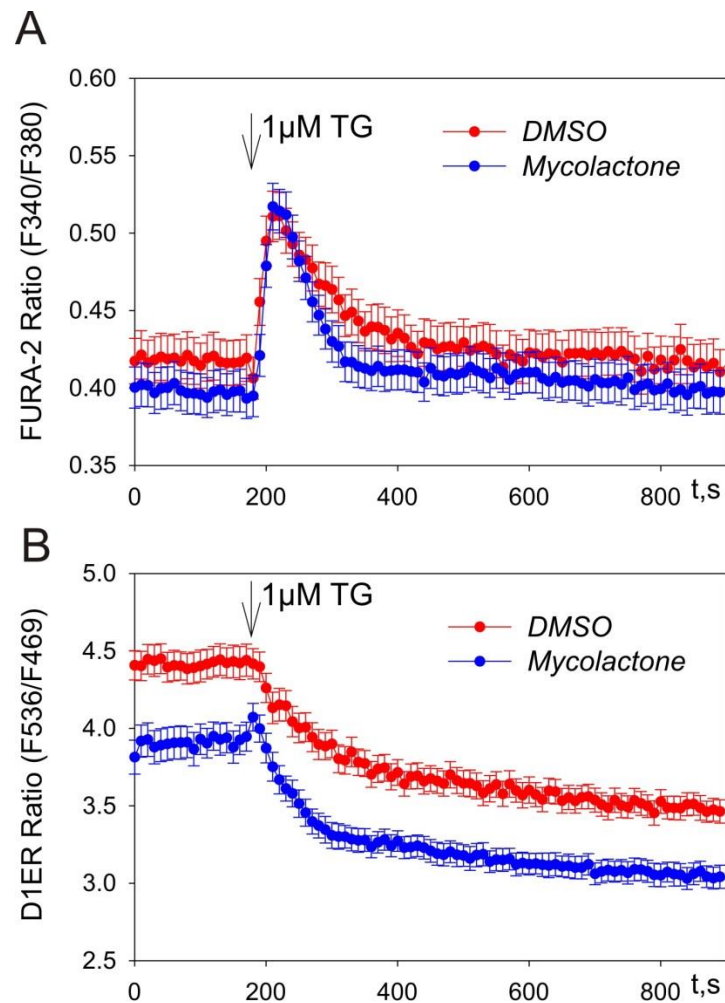


**Figure 4.13. Mycolactone 1.5 hours on HEK D1ER cells.** Mycolactone (500 ng/ml) was added to D1ER cells and incubated 1.5 hours before imaging. Thapsigargin (1  $\mu$ M) was applied at 3 minutes (arrow indicated) during simultaneous imaging of cytosolic and ER  $\text{Ca}^{2+}$ . **A.** Cytosolic  $\text{Ca}^{2+}$  responses measured as FURA-2 Ratios. **B.** Corresponding ER  $\text{Ca}^{2+}$  decay due to thapsigargin application (arrow). DMSO (0.1%) control mock incubation (red), mycolactone (500 ng/ml) incubation (blue). Number of cells: 8, mycolactone-treated; 11, control DMSO (0.1%) treated.

The next experiments were conducted as “online” effect (acute application) of mycolactone on HEK D1ER cells in 0.5 mM EGTA extracellular solution. For this series of experiments I used lower concentration of mycolactone than in previous experiments. DMSO (0.025%) as mock control or 125 ng/ml of mycolactone were added at 3 minutes after recording start with following 1  $\mu$ M thapsigargin application at 20 minutes. Mycolactone evoked small increase of cytosolic  $\text{Ca}^{2+}$  and the corresponding decrease of ER  $\text{Ca}^{2+}$  (Figure 4.14). This effect however was not significantly different from the

control. The application of 1  $\mu\text{M}$  thapsigargin evoked a cytosolic  $\text{Ca}^{2+}$  peak and the corresponding depletion of the ER  $\text{Ca}^{2+}$ . Mycolactone-treated cells showed faster kinetics of the ER  $\text{Ca}^{2+}$  depletion. However the cytosolic  $\text{Ca}^{2+}$  peak evoked by thapsigargin was smaller to those of DMSO (0.025%, v/v) control treatment. This can be explained as continuously enhanced  $\text{Ca}^{2+}$  leak from the ER due to the mycolactone action, resulting in faster kinetics of the ER  $\text{Ca}^{2+}$  depletion and activation of cytosolic the  $\text{Ca}^{2+}$  clearance mechanisms, which are removing  $\text{Ca}^{2+}$  faster and therefore decreasing the cytosolic  $\text{Ca}^{2+}$  peak evoked by thapsigargin.

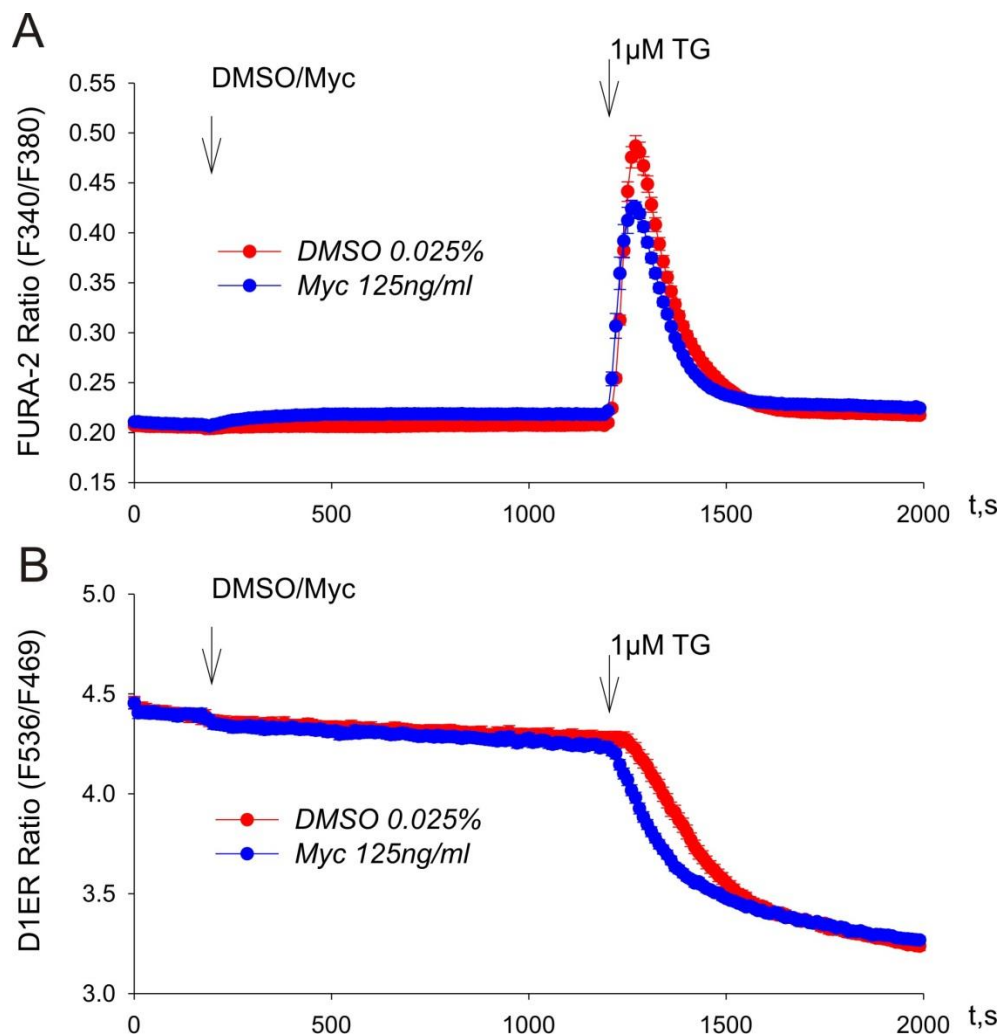


**Figure 4.14.** Mycolactone “online” on HEK D1ER cells. Mycolactone (125 ng/ml) or control DMSO (0.025%) was added to D1ER cells at 3 minutes (arrow) and 1  $\mu\text{M}$  thapsigargin was applied at 20 minutes (arrow indicated) during simultaneous imaging of cytosolic and ER  $\text{Ca}^{2+}$ . A. Cytosolic  $\text{Ca}^{2+}$  responses measured as FURA-2. B. Corresponding ER  $\text{Ca}^{2+}$  decay due to thapsigargin application (arrow). DMSO (0.025%) control mock incubation (red),

---

**125 ng/ml mycolactone incubation (blue). Number of cells: 56, mycolactone-treated, 57, control DMSO (0.1%) treated.**

In the next step the incubation time with 125 ng/ml of mycolactone was prolonged to overnight (18+ hours). The HEK D1ER cells were prepared for imaging experiments as described (see 3.11). Mycolactone was added to the cultured solution in the dishes cells and left in the incubator overnight (18+ hours). Next day the cells were taken to the imaging experiments. The cells were loaded with FURA-2 as before (see 3.11.1, 3.13), washed twice and put into 0.5 mM EGTA extracellular solution. The incubation with mycolactone showed a slight increase of cytosolic  $\text{Ca}^{2+}$  and a severe decrease of ER  $\text{Ca}^{2+}$  concentration (Figure 4.15). This favors the idea that mycolactone enhances  $\text{Ca}^{2+}$  leakage from the ER. Thapsigargin (1  $\mu\text{M}$ ) was added to unmask a ER  $\text{Ca}^{2+}$  efflux at 3 minutes after recording start. The cytosolic  $\text{Ca}^{2+}$  peak after mycolactone incubation was smaller than the control, which can be explained by significant ER  $\text{Ca}^{2+}$  depletion. The kinetic of the ER  $\text{Ca}^{2+}$  depletion after 1  $\mu\text{M}$  thapsigargin application was faster for the cells after mycolactone treatment than for the control treated ones.

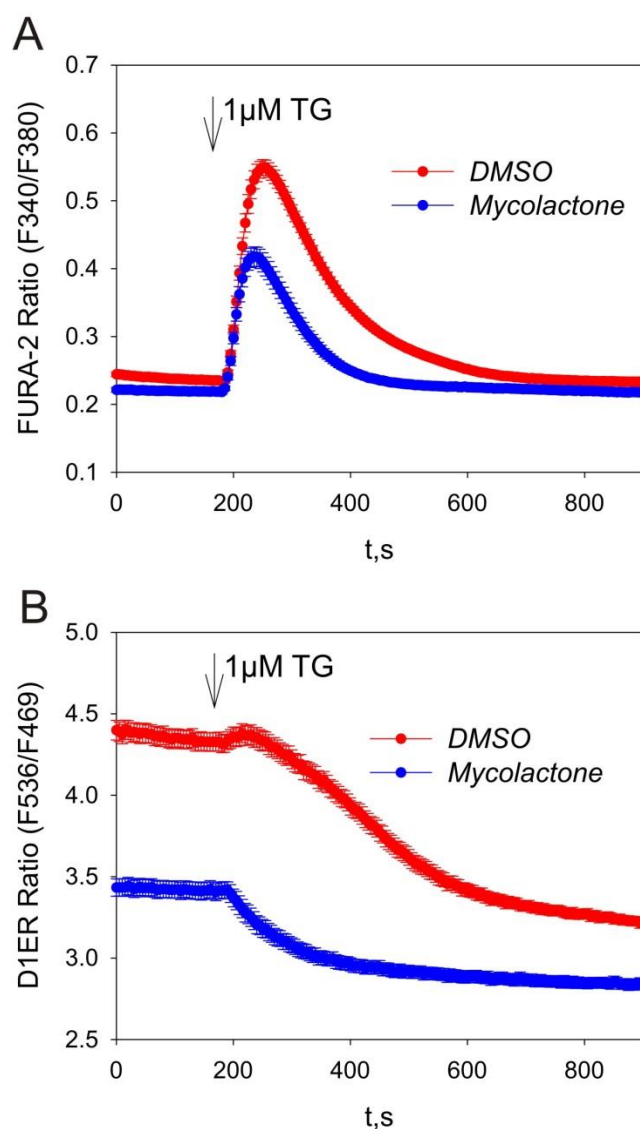


**Figure 4.15.** Mycolactone overnight on HEK D1ER cells. Mycolactone (125 ng/ml) was added to D1ER cells and incubated overnight at 37°C. thapsigargin (1 µM) was applied at 3 minutes (arrow) during simultaneous imaging of cytosolic and ER Ca<sup>2+</sup>. **A.** Cytosolic Ca<sup>2+</sup> responses measured as FURA-2. **B.** Corresponding ER Ca<sup>2+</sup> decay due to thapsigargin application (arrow). DMSO (0.025%) control mock incubation (red), 125 ng/ml mycolactone incubation (blue). Number of cells: 28, mycolactone-treated, 23, control DMSO (0.025%) treated.

The further decrease of mycolactone concentration was analyzed in the experiments with shorter incubation time. Mycolactone (100 ng/ml) was added to the culture medium of HEK D1ER cells after preparing them for imaging experiments (see 3.2.3, 3.11.1). The incubation time with 100 ng/ml of mycolactone was set up to 6 hours prior to imaging. After the incubation the cells were loaded with FURA-2 as before, washed twice and put

in 0.5 mM EGTA extracellular solution. The application of 1  $\mu\text{M}$  thapsigargin evoked both a cytosolic  $\text{Ca}^{2+}$  peak and an ER  $\text{Ca}^{2+}$  depletion signal. The cells treated with mycolactone showed higher basal cytosolic  $\text{Ca}^{2+}$  and bigger amplitude of the thapsigargin-evoked peak. The ER  $\text{Ca}^{2+}$  depletion kinetic after mycolactone treatment was faster comparing to those in the cells treated with DMSO (0.02%) control. The effect of increase of the cytosolic  $\text{Ca}^{2+}$  peak can be explained as the enhanced  $\text{Ca}^{2+}$  leak from the ER. However, such enhanced  $\text{Ca}^{2+}$  leak was not sufficient to decrease ER  $\text{Ca}^{2+}$  levels significantly.

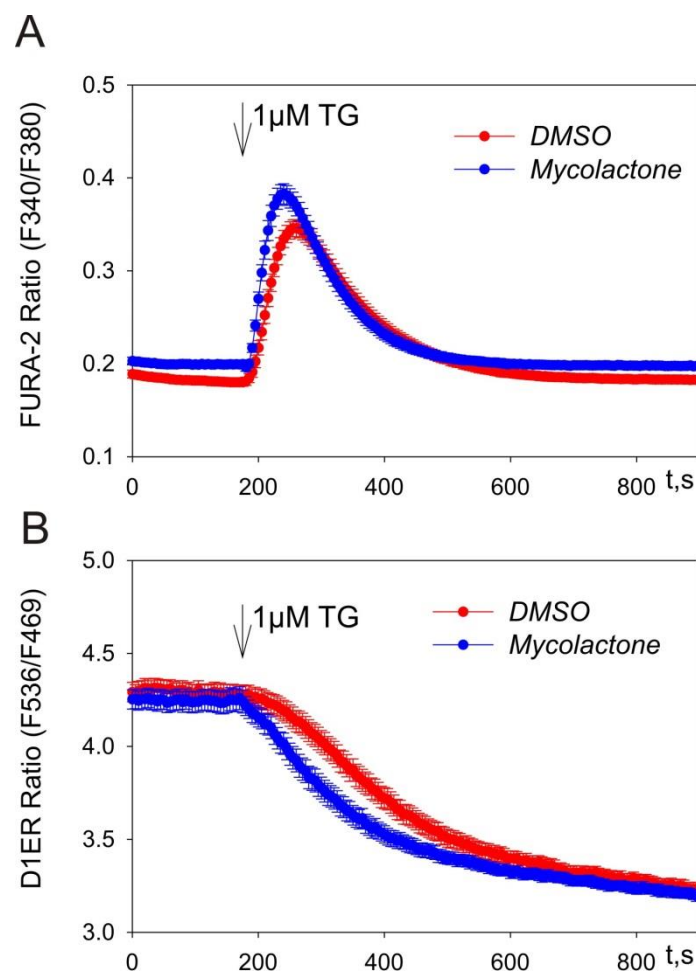


**Figure 4.16.** Mycolactone 6 hours on HEK D1ER cells. Mycolactone (100 ng/ml) was added to D1ER cells and incubated exactly 6 Hours before imaging. Thapsigargin (1  $\mu\text{M}$ ) was applied at 3 minutes (arrow) during simultaneous imaging of cytosolic and ER  $\text{Ca}^{2+}$ . A. Cytosolic  $\text{Ca}^{2+}$  responses measured as FURA-2. B. Corresponding ER  $\text{Ca}^{2+}$  decay due to thapsigargin application (arrow). DMSO (0.1%) control mock incubation (red), 500 ng/ml

**mycolactone incubation (blue). Number of cells: 18, mycolactone-treated; 20, control DMSO (0.02%) treated.**

The analysis of the kinetics as  $t_{1/2}$  of the thapsigargin-evoked ER  $\text{Ca}^{2+}$  depletion shows that mycolactone in all proposed experiments enhanced  $\text{Ca}^{2+}$  leakage (Figure 4.17). Thus  $t_{1/2}$  was reduced by  $60.2 \pm 4.6\%$  for online mycolactone (125 ng/ml) treatment comparing to the DMSO treatment, by  $67.9 \pm 10.8\%$  for 6 hours incubation with 100 ng/ml mycolactone, and by  $36.7 \pm 13.9\%$  for overnight incubation with 125 ng/ml of mycolactone incubation.

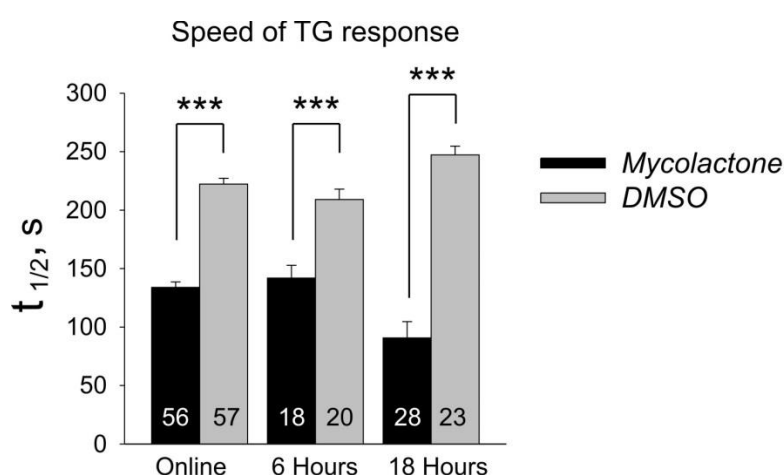


**Figure 4.17. Enhanced  $\text{Ca}^{2+}$  leak induced by mycolactone. Bar graph indicates the time to 50% of responses ( $t_{1/2}$ ) from cells pretreated with mycolactone and compared to the control DMSO treatment. Cells for analysis were taken from previously shown experiments. thus: “online”: mycolactone (125 ng/ml, black) or control DMSO (0.025%,gray) was added to D1ER cells at 3 minutes and  $1\mu\text{M}$  thapsigargin was applied at 20 minutes. “6 hours”: mycolactone (100 ng/ml) was added to D1ER cells and incubated in 6 hours before imaging. “18 hours”: mycolactone (125 ng/ml) was added to D1ER cells and incubated overnight at  $37^\circ\text{C}$ . Numbers of cells are corresponding to the experiments and are indicated on each bar.**

## 4.9 Effect of eeyarestatin 1 and its analogues on $\text{Ca}^{2+}$ homeostasis

Eeyarestatin1 (ES1) has been proposed for inhibiting translocation in eukaryotes (Cross et al. 2009). Its effect has been clearly demonstrated as an ERAD inhibition in cancer cells (Brem et al. 2013), but the full picture of ES1 activities is still missing. We have tested ES1 and its chemical analogues (Figure 4.18), which were kindly provided by Prof. Dr. Stephen High, University of Manchester. HEK D1ER cells were cultured and prepared for simultaneous imaging of cytosolic and ER  $\text{Ca}^{2+}$  as described above (see 3.2.3).

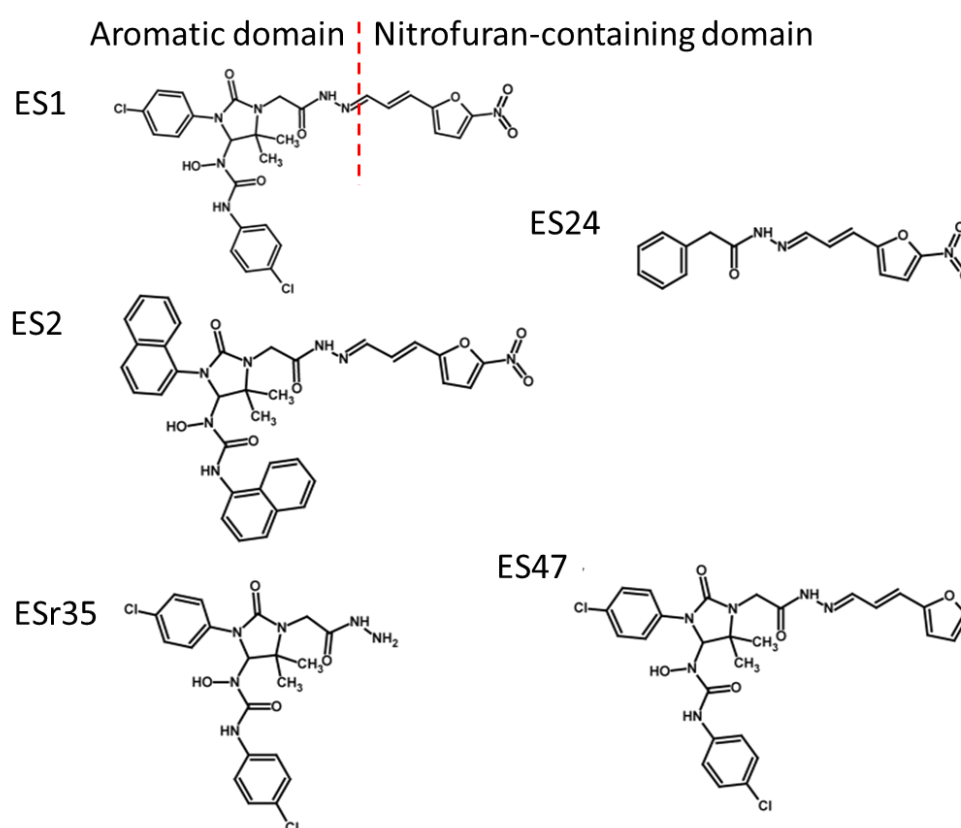


**Figure 4.18. Structure of eeyarestatins. Chemical structure of eeyarestatin 1 and analogs. Eeyarestatin1 (ES1) consists of aromatic and nitrofuran-containing (NFC) domains (parts separated by red dashed line). Analogs of ES1: ES2 has enlarged aromatic domain; ES24 has truncated aromatic domain; ESr35 has no NFC domain; ES47 has NFC domain with missing nitro group. Courtesy of Prof. Dr. Stephen High, University of Manchester.**

To avoid capacitative  $\text{Ca}^{2+}$  entry all experiments with eeyarestatin1 and its analogues were done in 0.5mM EGTA extracellular  $\text{Ca}^{2+}$  free solution. In the first series of experiments various concentrations of ES1 were tested: 0.1  $\mu\text{M}$ , 1  $\mu\text{M}$ , and 10  $\mu\text{M}$ . Eeyarestatin1 or control mock application were applied at 3 minutes with the following 1  $\mu\text{M}$  thapsigargin application. Removal of the extracellular  $\text{Ca}^{2+}$  didn't change much of the basal cytosolic  $\text{Ca}^{2+}$  level (Figure 4.19A), but caused a slow decrease of ER  $\text{Ca}^{2+}$  (Figure 4.19 B), which was about 0.75% per minute. As seen in Figure 4.19 application of ES1 causes changes both in cytosolic (A) and ER  $\text{Ca}^{2+}$  (B).

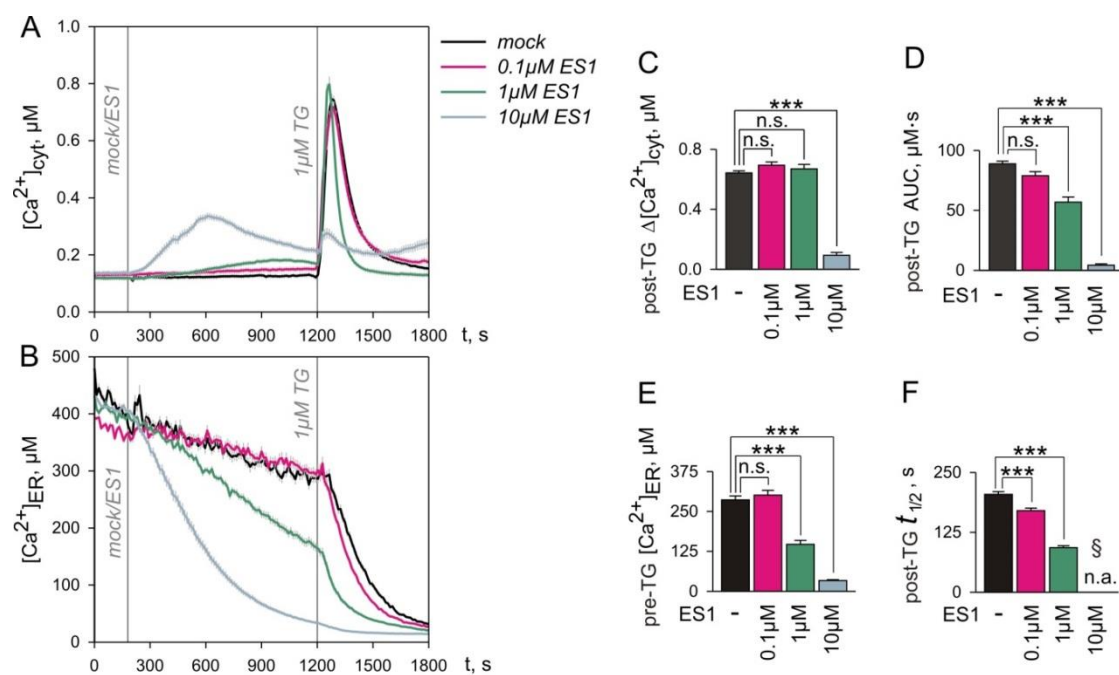


**Figure 4.19. Effect of ES1 on  $\text{Ca}^{2+}$  homeostasis.** HEK D1ER cells were treated with 0.1  $\mu\text{M}$ , 1  $\mu\text{M}$ , and 10  $\mu\text{M}$  of ES1 at 3 minutes with the following application of 1  $\mu\text{M}$  thapsigargin at 20 minutes. Simultaneous measurement of cytosolic  $\text{Ca}^{2+}$  (A) and ER  $\text{Ca}^{2+}$  (B) (Corresponding concentrations are color coded). Analysis of the amplitude thapsigargin-evoked peak (C) showed as mean $\pm$ s.e.m. D. Area under the curve after 1 $\mu\text{M}$  thapsigargin application (mean $\pm$ s.e.m). E. ER  $\text{Ca}^{2+}$  decay evoked by ES1 application analysis just before 1 $\mu\text{M}$  thapsigargin application (mean $\pm$ s.e.m, concentrations of ES1 are color coded). F. Analysis of the kinetic of ER  $\text{Ca}^{2+}$  efflux after 1 $\mu\text{M}$  thapsigargin application. (Two-Sample Kolmogorov-Smirnov test, for cells at least 3 independent repeats 37 cells (mock), 45 cells (0.1  $\mu\text{M}$  ES1), 47 cells (1  $\mu\text{M}$  ES1), 47 cells (10  $\mu\text{M}$  ES1);\*\*\*  $p < 0.001$ , n.s.-not significant  $p > 0.05$ ; n.a.,§- not analyzed value, see text)

The application of 10  $\mu\text{M}$  of ES1 caused increase of cytosolic calcium in form of a peak with a simultaneous decrease of ER  $\text{Ca}^{2+}$  (Figure 4.19). The observed effect was that strong that additional application of 1  $\mu\text{M}$  thapsigargin evoked only a small peak in the cytosol (Figure 4.19 C,D) and couldn't be detected in ER  $\text{Ca}^{2+}$  due to the total depletion (Figure 4.19 E). The effect of 1  $\mu\text{M}$  eeyarestatin1 was less pronounced; however, overall qualitative response was the same. Namely, there was an increase of cytosolic  $\text{Ca}^{2+}$  and decrease of ER  $\text{Ca}^{2+}$ . During 17 minutes of 1  $\mu\text{M}$  eeyarestatin1 presence ER  $\text{Ca}^{2+}$  dropped almost twice comparing to those after the control mock application. (Figure 4.19 E). However, the following application of 1  $\mu\text{M}$  thapsigargin showed the same amplitude of the peak (Figure 4.19 C) but with smaller area under the curve (Figure 4.19 D), which is the result of ER  $\text{Ca}^{2+}$  depletion. Analysis of the ER  $\text{Ca}^{2+}$  decay after thapsigargin application showed that  $t_{1/2}$  became about 50% shorter at 1  $\mu\text{M}$  ES1 comparing to the control mock application. Further decrease of added eeyarestatin1 concentration to 0.1  $\mu\text{M}$  didn't show any significant differences for the analyzed values to the control mock treatment for the chosen protocol.

Structural analogues of ES1— ES2 and ES24 have different potency on translocation inhibition (Cross et al. 2009). The potency of drugs can be estimated as the following comparison  $\text{ES2} < \text{ES1} \ll \text{ES24}$ . I have used the concentration of 10  $\mu\text{M}$  to check the effect on cytosolic and ER  $\text{Ca}^{2+}$ . All compounds were studied using the same protocol: 3 minutes eeyaresatin-like compound or control mock application and at 20 minutes 1  $\mu\text{M}$  thapsigargin. Applications of eeyrestatin-like compounds (ES2 and ES24) had effects on cytosolic on ER  $\text{Ca}^{2+}$  during application in 0.5 mM EGTA extracellular solution (Figure 4.20). Thus application of 10  $\mu\text{M}$  of ES2 resembled the previous observed application of 1  $\mu\text{M}$  of ES1 (Figure 4.19). It evoked continuous increase in cytosolic  $\text{Ca}^{2+}$  and narrowed the  $\text{Ca}^{2+}$  peak after the thapsigargin application; however, keeping the peak amplitude on the same level as for the control like it was for 1  $\mu\text{M}$  ES1. The exponential decay of ER  $\text{Ca}^{2+}$  was about 2 times faster as for control mock application. Application of 10  $\mu\text{M}$  ES24 evoked strong release of ER  $\text{Ca}^{2+}$  into the cytosol which could be characterized as a cytosolic  $\text{Ca}^{2+}$  peak. The total duration of the ES24 response in the cytosol was about 400 s, after which it is seen that ER  $\text{Ca}^{2+}$  was depleted. However, after this time the cytosolic  $\text{Ca}^{2+}$  continued to rise, indicating other processes occurring presumably due to toxicity of ES24. Thapsigargin application effect couldn't be detected after 17 minutes of 10  $\mu\text{M}$  ES24 presence. Analysis of  $t_{1/2}$  of the ER  $\text{Ca}^{2+}$  decay between eeyarestatins/mock

applications showed the potency for ES24 higher than for ES1:  $t_{1/2}$  is 2.5 times less. ES2 was on the other side—2.5 times slower than ES1.

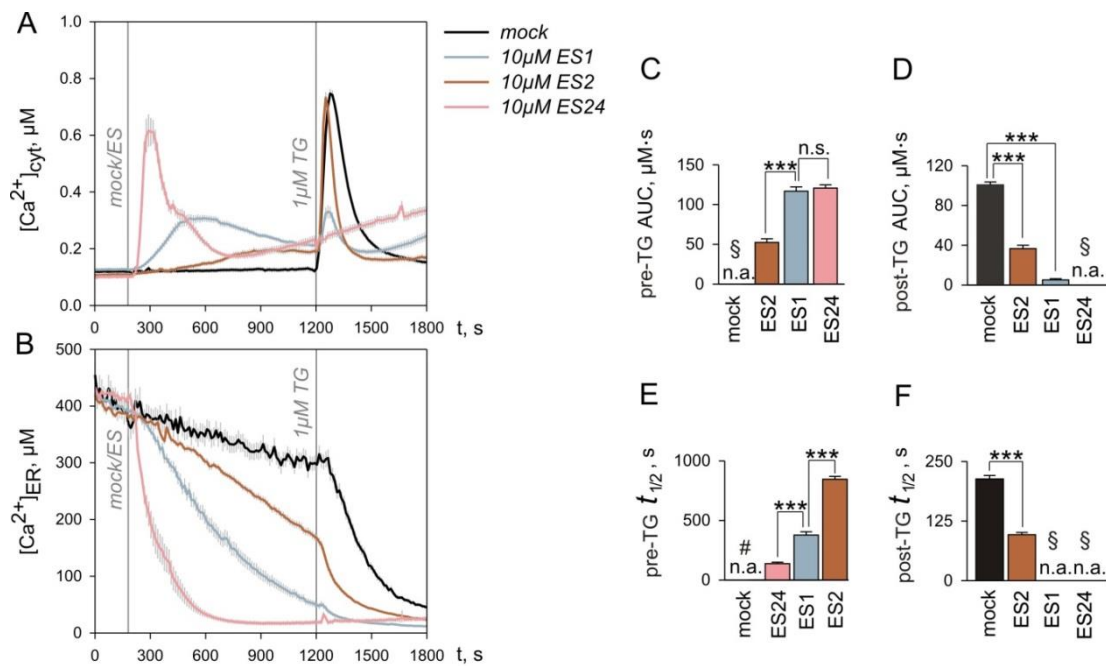


**Figure 4.20. Comparison of ES1, ES2 and ES24 on  $\text{Ca}^{2+}$  homeostasis.** HEK D1ER cells were treated with 10  $\mu\text{M}$  ES1, 10  $\mu\text{M}$  ES2, and 10  $\mu\text{M}$  ES24 at 3 minutes with the following application of 1  $\mu\text{M}$  thapsigargin at 20 minutes. Simultaneous measurement of cytosolic  $\text{Ca}^{2+}$  (A) and ER  $\text{Ca}^{2+}$  (B) (Corresponding compounds are color coded). Analysis of the area under the curve of ES-evoked peak (C) showed as mean $\pm$ s.e.m. D. Area under the curve after 1  $\mu\text{M}$  thapsigargin application (mean $\pm$ s.e.m). E. Kinetic of the ER  $\text{Ca}^{2+}$  decay evoked by ES1 application analysis just before 1  $\mu\text{M}$  thapsigargin application (mean $\pm$ s.e.m, compounds are color coded). F. Analysis of the kinetic of ER  $\text{Ca}^{2+}$  efflux after 1  $\mu\text{M}$  thapsigargin application. (Two-Sample Kolmogorov-Smirnov test, for cells from at least 3 independent repeats, 37 cells (mock), 44 cells (10  $\mu\text{M}$  ES2), 48 cells (10  $\mu\text{M}$  ES1), 40 cells (10  $\mu\text{M}$  ES24);\*\*\*  $p < 0.001$ , n.s-not significant  $p > 0.05$ ; n.a.,§, #- not analyzed value, see text)

Two ES1 analogues ESr35 and ES47 were indicated as those which have very small impact on protein translocation (Cross et al. 2009). Application on HEK D1ER cells of ESr35 and ES47 were done at 3 minutes with following application of 1  $\mu\text{M}$  thapsigargin at 20 minutes in 0.5 mM EGTA extracellular  $\text{Ca}^{2+}$  free solution (Figure 4.21). During the time between applications of eeyarestatin compounds and thapsigargin application none of them showed significant difference in  $\text{Ca}^{2+}$  signaling comparing to the control mock

application (Figure 4.21 A, B). Thapsigargin-evoked peak for ES47 was slightly less than the control one, the same tendency was observed for area under the curve. These results show no tendency to the eeyarestatin1 effect on the cytosolic  $\text{Ca}^{2+}$  signaling which was observed before. The simultaneous measurement of ER  $\text{Ca}^{2+}$  decay after thapsigargin application showed also slightly slowed kinetics of the response in case of 10  $\mu\text{M}$  ES47 application. Statistical significance, however was estimated only as  $p < 0.05$  using Two-Sample Kolmogorov-Smirnov test. No significant differences in the estimated parameters were detected after application for ESr35.

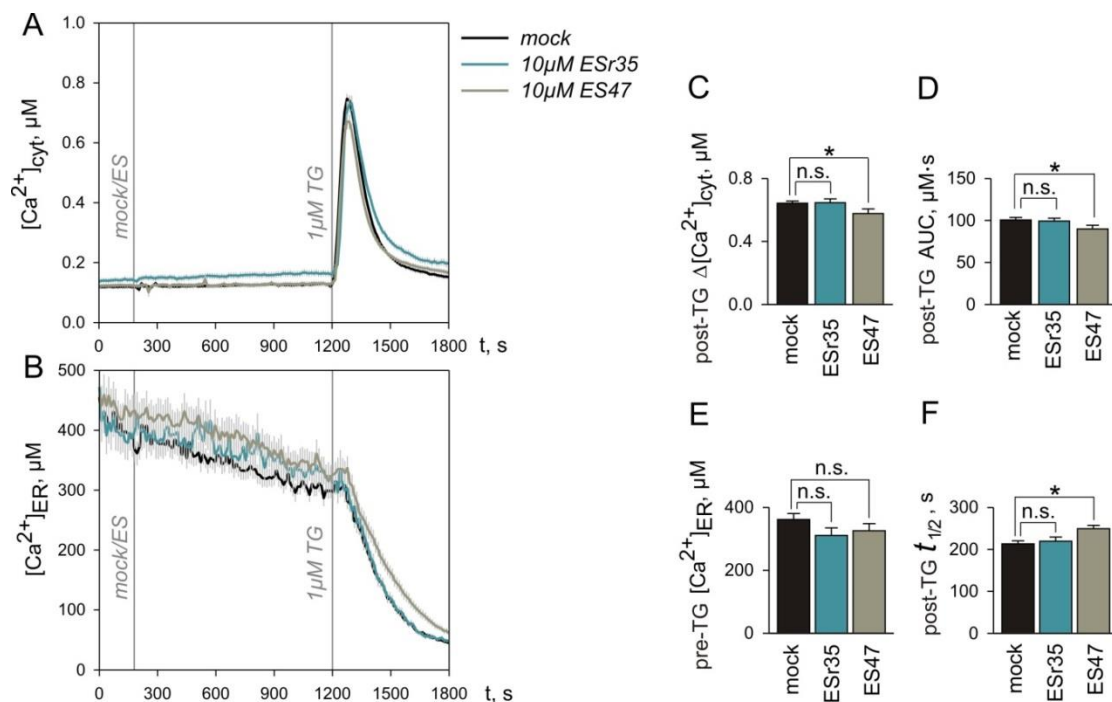


**Figure 4.21. Effect of ESr35 and ES47 on  $\text{Ca}^{2+}$  homeostasis.** HEK D1ER cells were treated with mock control application, 10  $\mu\text{M}$  ESr35, and 10  $\mu\text{M}$  of ES47 at 3 minutes with the following application of 1  $\mu\text{M}$  thapsigargin. Simultaneous measurement of cytosolic  $\text{Ca}^{2+}$  (A) and ER  $\text{Ca}^{2+}$  (B) (Corresponding concentrations are color coded). Analysis of the amplitude thapsigargin-evoked peak (C) showed as mean $\pm$ s.e.m. D. Area under the curve after 1  $\mu\text{M}$  thapsigargin application (mean $\pm$ s.e.m). E. ER  $\text{Ca}^{2+}$  decay evoked by ES1 analogues application analysis just before 1  $\mu\text{M}$  thapsigargin application (mean $\pm$ s.e.m, concentrations of ES1 are color coded). F. Analysis of the kinetic of ER  $\text{Ca}^{2+}$  efflux after 1  $\mu\text{M}$  thapsigargin application. (Two-Sample Kolmogorov-Smirnov test, for cells at least 3 independent repeats, 25 cells (mock), 36 cells (10 $\mu\text{M}$  ESr35), 29 cells (10 $\mu\text{M}$  ES47), \*  $p < 0.05$ , n.s-not significant  $p > 0.05$ )

The time between eeyarestatin/mock application and the application of thapsigargin was chosen empirically. As a result, the following relationships between ER  $\text{Ca}^{2+}$  and cytosolic  $\text{Ca}^{2+}$  were observed. From the first experiments with ES1 the application of 1  $\mu\text{M}$  ES1 didn't change the amplitude of Cytosolic  $\text{Ca}^{2+}$  peak evoked by thapsigargin, despite ER  $\text{Ca}^{2+}$  had decreased. Increasing the concentration to 10 $\mu\text{M}$  of ES1 depleted ER  $\text{Ca}^{2+}$  stronger and decreased cytosolic thapsigargin-evoked  $\text{Ca}^{2+}$  peak. In the following experiments I have tested the effect of shorter time incubation with ES1. HEK D1ER cells were cultured and prepared for simultaneous cytosolic and ER  $\text{Ca}^{2+}$  imaging as before (see 3.11). Application of ES1 or control mock application was done at 3 minutes in 0.5 mM EGTA extracellular solution with following 1  $\mu\text{M}$  thapsigargin application at 7 minutes. Thus, the time of ES1 effect was shortened from 17 minutes to 4 minutes. Comparing with the results of observed thapsigargin responses for 4 minutes and 17 minutes for 1  $\mu\text{M}$  ES1 shows that despite the decrease of ER  $\text{Ca}^{2+}$ , the amplitude of thapsigargin-evoked cytosolic  $\text{Ca}^{2+}$  peak remained unchanged (Figure 4.22 A). This leads to the conclusion that the increased  $\text{Ca}^{2+}$  leak rate due to the ES1 action is enough to overcome cytosolic  $\text{Ca}^{2+}$  clearance mechanisms.

To prevent ER  $\text{Ca}^{2+}$  decrease from depletion and to increase the ER  $\text{Ca}^{2+}$  leak rate 10  $\mu\text{M}$  ES1 was added at 3 minutes with following 1  $\mu\text{M}$  thapsigargin application at 7 minutes. ES1 (10  $\mu\text{M}$ ) evoked cytosolic  $\text{Ca}^{2+}$  increase and simultaneously decreased ER  $\text{Ca}^{2+}$  (Figure 4.22). Application of 1  $\mu\text{M}$  thapsigargin had fully unmasked ER  $\text{Ca}^{2+}$  efflux and showed the increase in cytosolic  $\text{Ca}^{2+}$  peak about 400 nM higher comparing to those of control mock application. Apparently the decrease of ER  $\text{Ca}^{2+}$  due to the action of 10  $\mu\text{M}$  ES1 for 4 minutes and 1  $\mu\text{M}$  ES1 for 17 minutes were similar, however the effects on cytosolic  $\text{Ca}^{2+}$  peaks were different. This indicates that not only the amount of ER  $\text{Ca}^{2+}$  defines the amplitude of cytosolic  $\text{Ca}^{2+}$  peak evoked by thapsigargin but also the ER  $\text{Ca}^{2+}$  leak rate.

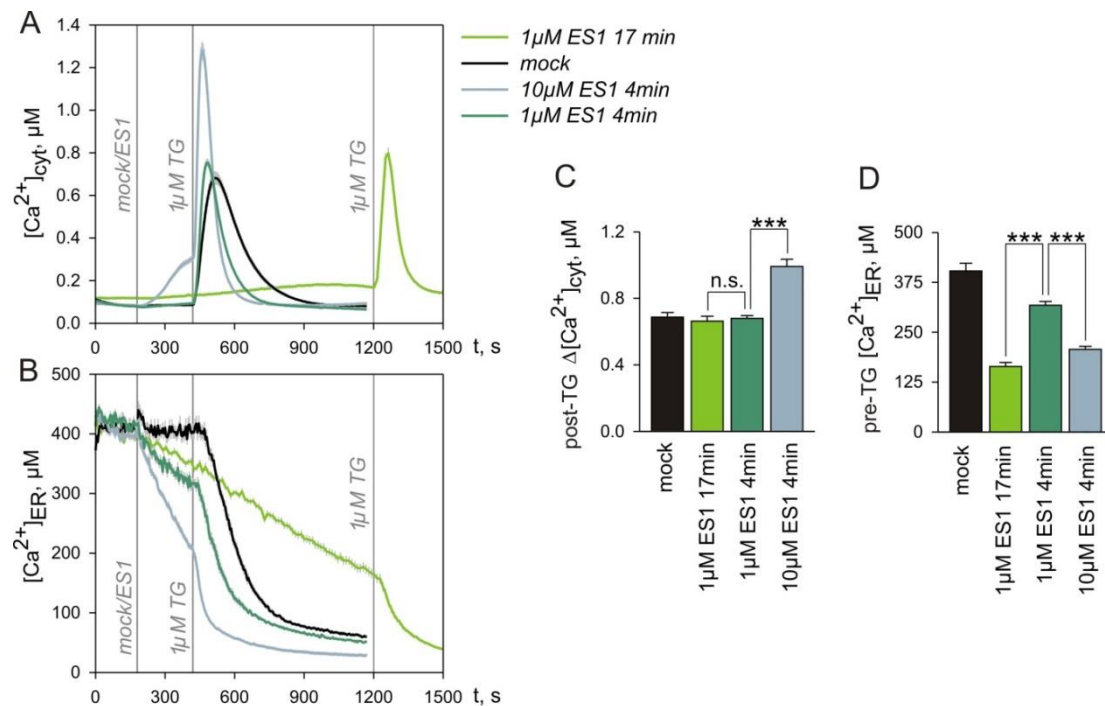


**Figure 4.22. Differential effects of ES1 at different incubation times. Comparison of application thapsigargin at 7 minutes and 20 minutes after application of 1  $\mu M$  ES1 and 10  $\mu M$  ES1 at 3 minutes. A. Cytosolic  $Ca^{2+}$  response (A) of HEK D1ER cells measured simultaneously with ER  $Ca^{2+}$  (B) (concentrations of applied ES1 and mock application are color coded). 1  $\mu M$  thapsigargin was applied at 7 minutes and 20 minutes as indicated by lines. C. Amplitudes of thapsigargin-evoked peak measured from the moment of application. D. Level of ER  $Ca^{2+}$  just before thapsigargin application indicates the effect of ES1 on ER  $Ca^{2+}$  depletion for chosen times. Statistic shown as mean $\pm$ s.e.m. Significance check was done with Two-Sample Kolmogorov-Smirnov test, for cells from at least 3 independent repeats, 31 cells (mock), 31 cells (1  $\mu M$  ES1 for 4 minutes), 47 cells (1  $\mu M$  ES1 for 17 minutes), 30 cells (10  $\mu M$  ES1 for 4 minutes); \*\*\*  $p < 0.001$ , n.s.-non-significant,  $p > 0.05$ . Minutes are indicated as “min” on this picture.**

The previous series of experiments were done to identify conditions at which the increased  $Ca^{2+}$  leak from the ER could be detected clearly by the cytosolic  $Ca^{2+}$  response. The short incubation time with ES1 should increase the thapsigargin evoked cytosolic  $Ca^{2+}$  peak. As the next, I have checked the hypothesis that the action site for ES1 is the Sec61 $\alpha$  complex. The specific to eeyarestatin effects were tested using silencing of *SEC61A1*, coding the pore-forming subunit of the translocon complex, through which the  $Ca^{2+}$  leak has been identified. The levels of Sec61 $\alpha$  complex silencing using siRNA (see 3.7) are about 60% for HEK D1ER cells, while for HeLa cells this level can be much higher 80-90%. (Lang et al. 2012) Therefore, I had chosen HeLa cells for silencing

experiments. Silencing of *SEC61A1* was done on HeLa cells with the silencing protocol designed both for the imaging and relative protein amount quantification (Lang et al. 2011a). The rest of HeLa cells were collected from each dish for the evaluation of the relative amount of Sec61 $\alpha$  after silencing comparing to the mock transfected cells. Both the silencing procedure and the Western Blot with the following analysis were kindly assisted by Marie-Christine Klein and Prof. Dr. Richard Zimmermann, Medical Biochemistry department, Faculty of Medicine, Saarland University. Silencing was done using two different siRNAs (see 3.7), called siRNA#4 and siRNA#5 both acting with *SEC61A1* gene. The cells were loaded with FURA-2 for cytosolic Ca<sup>2+</sup> imaging. The application protocol resembled those one of HEK D1ER cells: application of 10  $\mu$ M ES1 or control mock application at 3 minutes with following application of 1  $\mu$ M thapsigargin at 7 minutes (Figure 4.23). Calibration of obtained FURA-2 signals and conversion cytosolic Ca<sup>2+</sup> signals were similar to those of described in (3.13.3). As a control to the silencing procedure with actual siRNAs the transfection with scrRNA was done. The Effect of *SEC61A1* silencing on HeLa cells resulted in a decreased thapsigargin-evoked peak both for siRNA#4 and siRNA#5 comparing to the scrRNA transfection. The relative level of the rest Sec61 $\alpha$  was estimated by normalization to  $\beta$ -actin:  $20 \pm 3\%$  for siRNA#4 and  $18 \pm 2\%$  for siRNA#5. Thapsigargin-evoked peak after 10  $\mu$ M ES1 application for scrRNA transfected cells were higher of about 20% comparing to the control mock application. However, after silencing with siRNA#4 and siRNA#5 no significant changes in thapsigargin-evoked peak were observed. All traces were similar to those which represent the mock application with following thapsigargin application after silencing of Sec61 $\alpha$  (either with siRNA#4 or siRNA#5).

The similar effect of the Sec61 $\alpha$  removal via silencing of *SEC61A1* was observed on the ES24 action. The silencing of *SEC61A1* gene was done as before, kindly assisted by Marie-Christine Klein and Prof. Dr. Richard Zimmermann, Medical Biochemistry department, Faculty of Medicine, Saarland University. The relative amount of Sec61 $\alpha$  after silencing was  $22 \pm 2\%$  and  $21 \pm 2\%$  for siRNA#4 and siRNA#5 transfected cells respectively. The cells were loaded with FURA-2 and imaging experiments were done in 0.5 mM EGTA extracellular solution. ES24 (1  $\mu$ M) or mock application were at 3 minutes with the following 1  $\mu$ M thapsigargin application at 7 minutes (Figure 4.24).

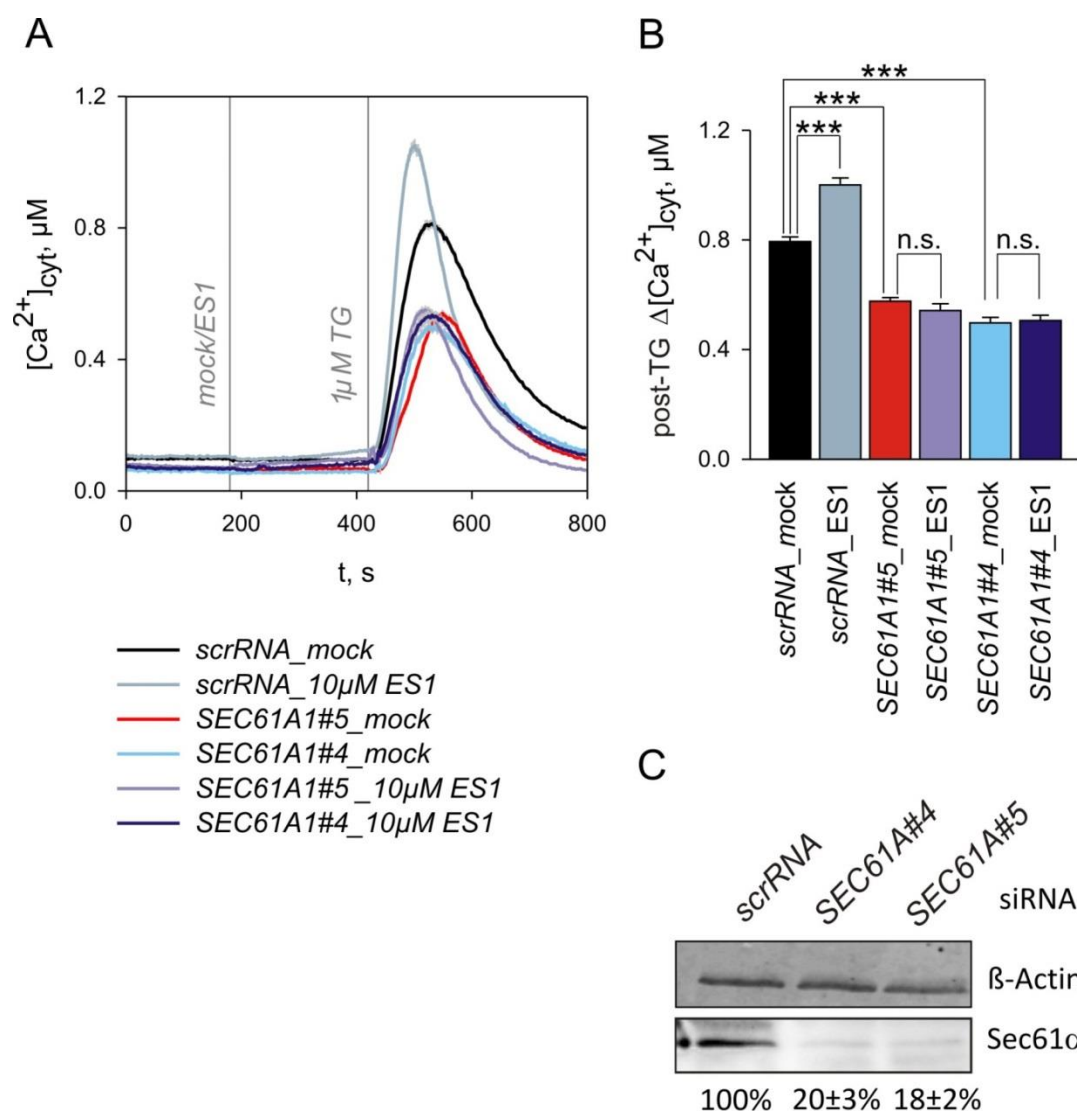


**Figure 4.23.** Effect of silencing of Sec61 on ES1-evoked ER  $Ca^{2+}$  leakage. **A.** HeLa cells treated with 10μM ES1 at 3 minutes with following 1μM Thapsigargin application (line-indicated) compared to the mock treatment with following 1μM Thapsigargin application (line-indicated). Every trace for pair-experiments: HeLa *scrRNA* transfection, silenced HeLa with *SEC61A1* siRNA#4, and silenced HeLa with *SEC61A1* siRNA#5 are color indicated. **B.** Amplitudes of thapsigargin-evoked peaks. Treatment and transfections as indicated. Represented as mean±s.e.m. Statistical significance done with Two-Sample Kolmogorov-Smirnov test, \*\*\*  $p < 0.001$ , n.s., non-significant,  $p > 0.05$ . **C.** Silencing efficiency of the transfection procedure. Relative amount of Sec61a protein from *SEC61A1* siRNA#4 and *SEC61A1* siRNA#5 transfections normalized to *scrRNA* transfection from the cells normalized to β-actin. Shown statistic is from 3 independent experiments, represented as mean±s.e.m. from the whole cell passage. Number of cells: 222 cells (*scrRNA\_mock*), 81 cells (*SEC61A1#4\_mock*), 163 cells (*SEC61A1#5\_mock*), 188 cells (*scrRNA\_10μM ES1*), 110 cells (*SEC61A1#4\_10μM ES1*), 94 cells (*SEC61A1#5\_10μM ES1*).

Thapsigargin-evoked peak after ES24 application was  $60.0 \pm 3.5\%$  higher for scrRNA transfected cells compared to those after the mock application. The effect of ES24 on thapsigargin peak was completely absent for the cells silenced with siRNA#4 and siRNA#5.

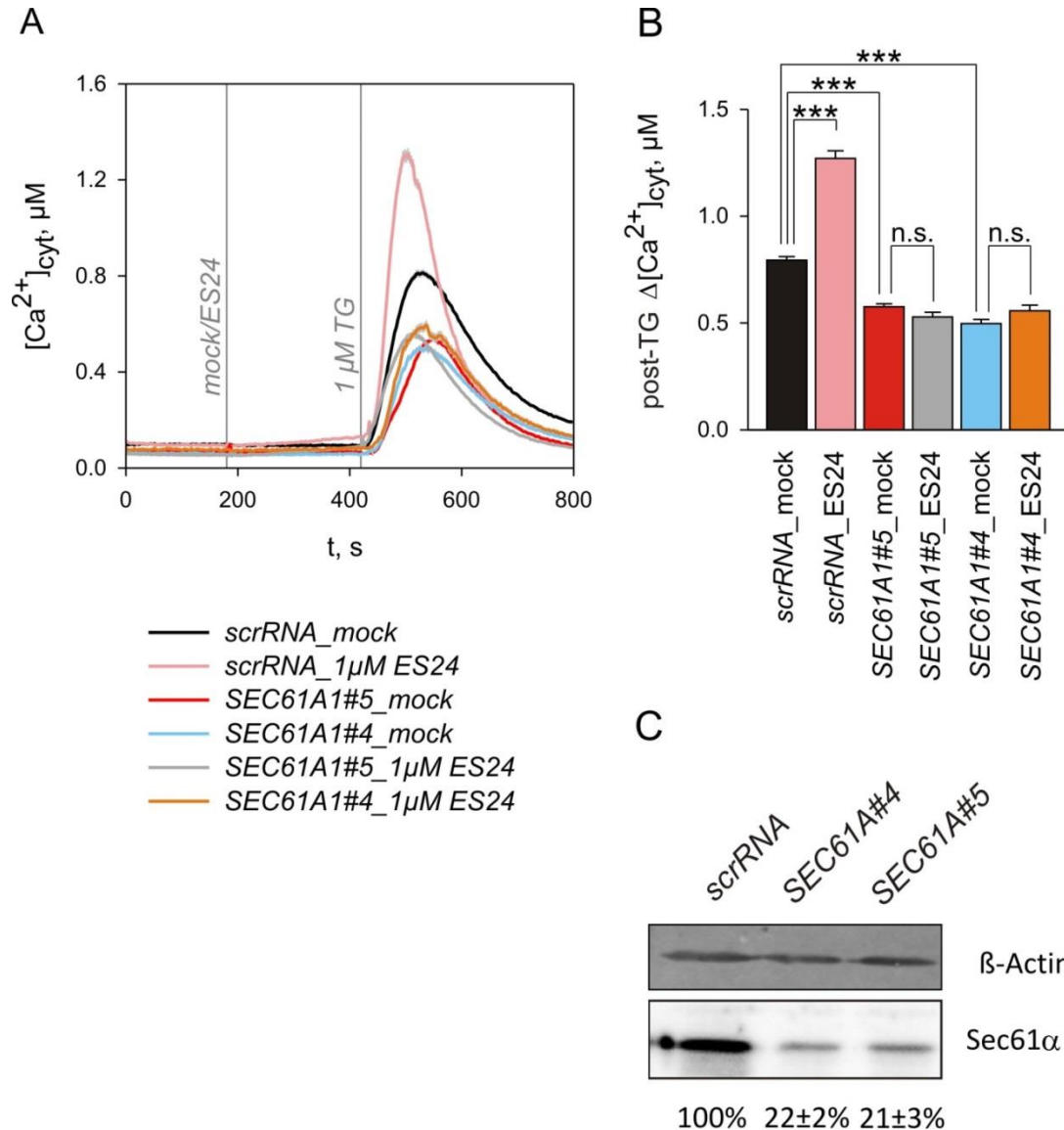


**Figure 4.24.** Effect of silencing of Sec61 on ES24-evoked ER  $\text{Ca}^{2+}$  leakage. **A.** HeLa cells treated with  $1 \mu\text{M}$  ES24 at 3 minutes with following  $1 \mu\text{M}$  Thapsigargin application (line-indicated) compared to the mock treatment with following  $1 \mu\text{M}$  Thapsigargin application (line-indicated). Every trace for pair-experiments: HeLa scr RNA transfection, silenced HeLa with *SEC61A1* siRNA#4, and silenced HeLa with *SEC61A1* siRNA#5 are color indicated. **B.** Amplitudes of thapsigargin-evoked peaks. Treatment and transfections as indicated. Represented as mean $\pm$ s.e.m. Statistical significance done with Two-Sample Kolmogorov-Smirnov test, \*\*\*  $p < 0.001$ , n.s.-non-significant,  $p > 0.05$ . **C.** Silencing efficiency of the transfection procedure. Relative amount of Sec61 $\alpha$  protein from *SEC61A1* siRNA#4

---

and *SEC61A1* siRNA#5 transfections normalized to scrRNA transfection from the cells normalized to  $\beta$ -actin. Shown statistic is from 3 independent experiments, represented as mean $\pm$ s.e.m. from the whole cell passage. Number of cells: 222 cells (*scrRNA\_mock*), 81 cells (*SEC61A1#4\_mock*), 163 cells (*SEC61A1#5\_mock*), 177 cells (*scrRNA\_1 $\mu$ M ES24*), 60 cells (*SEC61A1#4\_1 $\mu$ M ES24*), 128 cells (*SEC61A1#5\_1 $\mu$ M ES24*)

Statistical analysis showed no significant differences in the amplitudes between the thapsigargin-evoked peaks of all silenced cells: all peaks were similar to those of mock application demonstrating the decrease of the peak amplitude due to Sec61 $\alpha$  silencing. These experiments lead to the conclusion that ES1 and its more potent analogue ES24 act very likely through Sec61 $\alpha$  subunit of the translocon complex rendering the pore leaky for Ca<sup>2+</sup> ions.

## 5 Discussion

### 5.1 The direct measurement of the $\text{Ca}^{2+}$ concentration in the ER gives the better insight of the functioning of this organelle about the $\text{Ca}^{2+}$ homeostasis

The measurements with chemical probes like Mag-Fura have a major problem concerning correct targeting to the ER (Gerasimenko and Tepikin 2005). Much better it is to use genetically encoded  $\text{Ca}^{2+}$  indicators, because they can be specifically targeted to the desired intracellular compartment. In this study, I used a designed probe D1ER, which has KDEL sequence and calreticulin signal sequence for retaining it in the ER (Palmer and Tsien 2006). The expression of D1ER in HEK and HeLa cells revealed a nice ER structure (Figure 3.2). D1ER signal can be observed as a ratio between the FRET signal and donor signal, which has an advantage in front of single wavelength measurements like GCaMPs (Chen et al. 2013), because the normalization to the amount of the expressed proteins is not required for D1ER. D1ER was suggested to have a relative narrow dynamic range (Palmer et al. 2004). This means that in proportion between saturated state ( $\text{DR}_{\text{max}}$ ) and depleted state ( $\text{DR}_{\text{min}}$ ) should be not more than 2. For comparison, newest single wavelength sensors like GCaMPs have theoretical dynamic range, i.e. the proportion between maximal  $I_{\text{max}}$ , and minimal  $I_{\text{min}}$ , fluorescent intensities about 40-60 (Chen et al. 2013). In my experiments (Figure 3.14)  $\text{DR}_{\text{max}}$  was 5.101 and  $\text{DR}_{\text{min}}$  3.098 which gives the dynamic range similar to those previously observed in other studies (e.g.(Erickson et al. 2001, Greotti et al. 2016, Luciani et al. 2009, Palmer et al. 2004, Shambharkar et al. 2015)). That confirms the correct functional folding of the  $\text{Ca}^{2+}$  sensor protein. For obtaining a D1ER ratio (FRET ratio) I used the automatized iMIC light microscope with the AHF FRET filter system (see 3.12) for splitting the wavelengths as suggested (Palmer and Tsien 2006). With the chosen optical magnification it was enough to see clearly the ER structure and neither the movements of the ER nor the slight change in the cell shape were compromising the FRET Ratio signal during measurements. The excitation light intensity was chosen empirically based on the observed photobleaching of this fluorescent protein in iMIC filter sets. The bleaching of the D1ER signals was analyzed as individual wavelengths through CFP and YFP filter sets (Table 3.10). The exposure time of 25 ms for one imaging frame with various time

periods between frames was chosen. The slow constant bleaching was observed at 3 s time increment between imaging shots and had nice exponential decrease at 200 ms increment with a noise of 0.05 units in terms of FRET Ratio (see 3.12.1). The bleaching of the sensor can be treated via photobleaching correction. However, routinely images were taken with 10-12 s increment and therefore no bleaching of D1ER signals was detected. The measurement of ratiometric signal should be independent from the amount of the D1ER in every cell. However, the stable expression of D1ER and the correct targeting of the sensor are required. The solution of this problem was the creation of stable cell lines (see 3.5). The creation of the stable cell line allowed the use of standardized correction procedure of the FRET ratio signals (see 3.13.4, 3.14), and this was used later to calibrate D1ER signals. The FRET ratio signal diversity can be explained by every cell deviations of the intraluminal  $\text{Ca}^{2+}$ . But in addition, the level of D1ER expression and the intraluminal pH play important roles. The mechanism of pH changing in the ER lumen is not comprehensively studied. However, the sensitivity of the D1ER sensor to pH changes is much less than of the single wavelength probes like GCaMPs (Chen et al. 2013). The overexpression of D1ER could cause the ER stress, which in turn could impact  $\text{Ca}^{2+}$  homeostasis but in the chosen clones of HEK D1ER cells no upregulation of BiP, as an ER stress marker, was noticed. The calibration of the FRET ratio signals for obtaining corresponding  $\text{Ca}^{2+}$  signals was performed for every cell as suggested by (Palmer and Tsien 2006), using the formalism reported by (Grynkiewicz et al. 1985). The experimental  $K_D$  of D1ER was based on experiments with permeabilized cells and was estimated as 165.25  $\mu\text{M}$ . The proposed theoretical  $K_D$  for D1ER measured in vitro were 3  $\mu\text{M}$  and 56  $\mu\text{M}$  (Palmer and Tsien 2006). I used my experimental  $K_D$  for calibration because it includes all the features of the imaging system, where the experiments were conducted. The shifting of the FRET ratio signal can be explained as variations of ER  $\text{Ca}^{2+}$  at basal level. However, due relatively low dynamic range of D1ER it can still distort the calibration of D1ER signal and the correct estimation of  $[\text{Ca}^{2+}]_{\text{ER}}$ . The calibration of D1ER in HEK D1ER cells showed the distribution of basal level of ER  $\text{Ca}^{2+}$  not exceeding 2.5 mM (Figure 3.18). From the thermodynamic properties of the functioning of SERCA, the ER  $\text{Ca}^{2+}$  pump, the gradient made of free  $\text{Ca}^{2+}$  concentration of 2.5 mM cannot be exceeded. This was calculated as a movement of two  $\text{Ca}^{2+}$  ions with an energy obtained after hydrolysis of one ATP molecule by SERCA against the concentration gradient (Shannon et al. 2000). This leads to the conclusion that free  $\text{Ca}^{2+}$  at rest measured with D1ER sensor are in thermodynamic range, despite relative close

$DR_{\text{basal}}$  to  $DR_{\text{max}}$ . The cell line showed a stable signal and therefore is able to be used in the knock down experiments. Simultaneous imaging of cytosolic and ER luminal  $\text{Ca}^{2+}$  gives the comprehensive insight in the intracellular  $\text{Ca}^{2+}$  homeostasis. In HEK D1ER cells, I used cytosolic  $\text{Ca}^{2+}$  dye FURA-2 to monitor the changes of the cytosolic  $\text{Ca}^{2+}$  simultaneously with the measurements of  $\text{Ca}^{2+}$  in the ER. This however requires an advanced light filter system. I used the system of two changing filter sets one of which is for FURA-2 measurement and another one is for D1ER measurement (Table 3.10). The spectra of D1ER and FURA-2 are partially overlapped, thus the correction was needed to get proper  $\text{Ca}^{2+}$  signals out of ratio signals (Figure 3.11). The observation of HEK293 cells with FURA-2 excited with D1ER excitation light (433 nm) through D1ER filter set showed minimal implication of FURA-2 presence on  $\text{Ca}^{2+}$  signal. However, the HEK D1ER cells excited with FURA-2 excitatory light and seen through the FURA-2 filter showed greater implication: about 30% of D1ER intensity excited with 380 nm and up to 10% of D1ER intensity excited with 340 nm can pass through the FURA-2 filter (Figure 3.12). The character of this implication was noticed as a linear regression, thus depending on the D1ER amount as similar to those described (Mori et al. 2011). This allowed making a general correction for the FURA-2 signals for every time point (Figure 3.19).

## **5.2 The correct estimation of the ER $\text{Ca}^{2+}$ content and dynamics remains to be a challenge for every cell line**

The level of basal ER  $\text{Ca}^{2+}$  in HEK D1ER cells for the total cell pool was between 280  $\mu\text{M}$  and 800  $\mu\text{M}$  with the mean of 350  $\mu\text{M}$ , while the reported value of basal ER  $\text{Ca}^{2+}$  estimated with CEPIA (one wavelength  $\text{Ca}^{2+}$  indicator for the ER, (Suzuki et al. 2014)) on HEK cells was higher up to 600 $\mu\text{M}$  in mean value, but also had a log-normal distribution of the  $\text{Ca}^{2+}$  concentration like in my experiments. The activity and also amount of SERCA pumps in various cell types may differ and  $\text{Ca}^{2+}$  can be absorbed by intraluminal buffers, therefore increasing the total ER  $\text{Ca}^{2+}$ . Analogous to the theory that  $\text{Ca}^{2+}$  in the ER is in “bound” and “free” states (Prins and Michalak 2011), the maximal ER  $\text{Ca}^{2+}$  depletion was checked using thapsigargin and ionomycin. Indeed, the total depletion of the  $\text{Ca}^{2+}$  stores evoked by ionomycin was faster and deeper than the same for thapsigargin. The ionomycin depletion was set as “0” for calibration purposes, and then the  $\text{Ca}^{2+}$  content after thapsigargin depletion was about 20-30  $\mu\text{M}$ , relatively to the total depletion with ionomycin (Figure 4.1, Figure 4.3). The log-normal distribution of the

basal ER  $\text{Ca}^{2+}$  level (Figure 3.18, also see Figure 5.1) can be based on some extreme states. One is the maximal limit of ER  $\text{Ca}^{2+}$  that can be absorbed by SERCAs, this is due to the thermodynamic limit of the energy spent on the  $\text{Ca}^{2+}$  ion movement versus the concentration gradient. Another one can be explained as a minimal threshold after which cells induce cell death, according to the theory that continuous depletion of the  $\text{Ca}^{2+}$  stores evokes apoptosis (Nakamura et al. 2000).

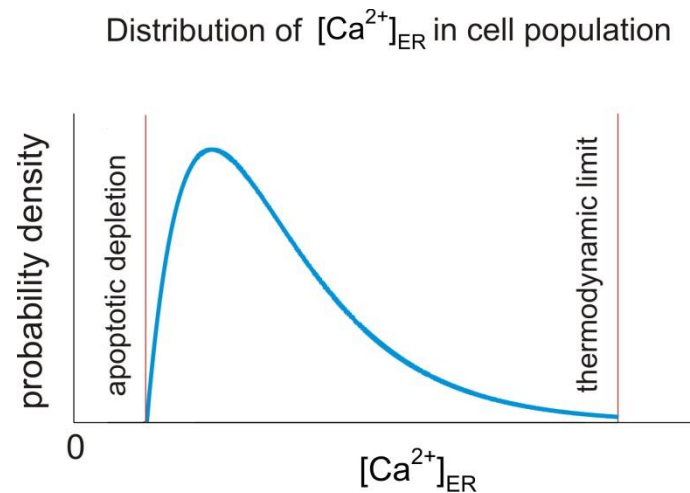


**Figure 5.1.** ER  $\text{Ca}^{2+}$  distribution in non-excitable cells.

### 5.3 The analysis of the ER $\text{Ca}^{2+}$ leak kinetics gives important numbers

The ER  $\text{Ca}^{2+}$  leak occurs through the release sites and channels in the ER membrane. In the current study the ER  $\text{Ca}^{2+}$  leak was analyzed by blocking the SERCA pumps with thapsigargin and therefore unmasking the  $\text{Ca}^{2+}$  leak through the ER membrane (see 4.1). Basal  $\text{Ca}^{2+}$  leak through all “present open” channels was observed and estimated. The observed shape of the ER  $\text{Ca}^{2+}$  response was seen as an exponential decrease. This corresponds to the very popular two-compartment model, which shows the mono exponential decrease of ER  $\text{Ca}^{2+}$  for passive leak (e.g. (Shannon et al. 2012)). This I used to determine the parameters of ER  $\text{Ca}^{2+}$  leak rate (see 2.2.6, 4.1). The maximal ER  $\text{Ca}^{2+}$  leak rate was observed after some time after thapsigargin application. This can be explained as a putative delay in allosteric inhibition of SERCA pumps by thapsigargin (see 4.1). However, this first phase of the TG response (Figure 4.1) on D1ER cells can also be explained by the presence of intraluminal  $\text{Ca}^{2+}$  buffers which replenish the

luminal  $\text{Ca}^{2+}$  during short time depletion (Chopra et al. 2007, Shannon 2007). That also can be concluded from the observation that during simultaneous measurements of luminal and cytosolic  $\text{Ca}^{2+}$ , the cytosolic response starts earlier than the corresponding luminal response. However, this was observed not only after SERCA pumps inhibition in my experiments, but also in the case of the fast responses evoked by histamine on HeLa or CCH on neurons (Guerrero-Hernandez et al. 2010, Solovyova et al. 2002). On the other hand, this should also include the inequality between the ER inner volume and the cytosolic volume of the cell. Therefore the relative decrease in ER  $\text{Ca}^{2+}$  is not always corresponding to the absolute increase in cytosolic  $\text{Ca}^{2+}$  which was also observed in my experiments. This can be corrected by including a correlation coefficient between ER and cytosolic buffering capacitances, and this is widely used in the modelling of  $\text{Ca}^{2+}$  homeostasis and intracellular  $\text{Ca}^{2+}$  signaling (Appleby et al. 2013). The analysis of thapsigargin response of HEK D1ER cells at rest gave two characteristic values (see 4.1). First, the mono-exponential fitting of the response gave the  $\text{Ca}^{2+}$  leak rate constant of  $6.8 \cdot 10^{-3} \text{ s}^{-1}$ . Second, the extrapolation of the signal shows a basal ER  $\text{Ca}^{2+}$  leak rate value, which was  $2.34 \mu\text{M/s}$ . These values are characteristic for HEK D1ER cell line, which can differ from other cell lines. For instance, in myocytes basal ER  $\text{Ca}^{2+}$  leak rate was estimated after using a selective blocker of ryanodine receptors, which supposed to be the main  $\text{Ca}^{2+}$  release channels in the ER membrane of myocytes (Bers 2014). There was estimated that  $\text{Ca}^{2+}$  release rate for myocytes is  $12 \mu\text{M/s}$ , which can be changed during the contraction. The reason for that is the functioning of SERCAs, which depend on ER  $\text{Ca}^{2+}$  loading (Koivumaki et al. 2009, Shannon et al. 2002). With the elevation of cytosolic  $\text{Ca}^{2+}$  in addition to SERCAs, which are pumping  $\text{Ca}^{2+}$  inside the lumen, other cellular mechanism perform  $\text{Ca}^{2+}$  clearance, returning cytosolic  $\text{Ca}^{2+}$  to the basal level. The removal of  $\text{Ca}^{2+}$  from the cytosol to the extracellular milieu is mainly provided by NCX exchangers and PMCA on the plasma membrane, while the functioning of mitochondria in  $\text{Ca}^{2+}$  signaling of muscle cells and myocytes were estimated as minor one (Shannon and Bers 2004). On the other hand, in adrenal chromaffin cells mitochondria are the major  $\text{Ca}^{2+}$  buffering organelles (Herrington et al. 1996). The continuous increase of cytosolic  $\text{Ca}^{2+}$  results in uptake by mitochondria (Szabadkai et al. 2003), which in turn can activate apoptosis (Hajnóczky et al. 2006).

## 5.4 The main point of my study was to determine the leak through Sec61 $\alpha$ complex in the ER membrane

The ER Ca<sup>2+</sup> leak through the Sec61 $\alpha$  complex, also named translocon, was determined on HEK D1ER cells, after treatment with various protein synthesis inhibitors as a change to the basal ER Ca<sup>2+</sup> leak (see 4.2). The ER Ca<sup>2+</sup> leak was unmasked by thapsigargin and analyzed as in 4.1. The idea that translocon can be both the protein and ion conducting channel was tested on the rough microsomes incorporated in the lipid bilayer (Simon and Blobel 1991, Wonderlin 2009). In this case the additional conductance was recorded after channel opening with puromycin. Several other indirect measurements of the puromycin effect of Ca<sup>2+</sup> efflux from the ER were done as changes in cytosolic Ca<sup>2+</sup> in pancreatic cells (Van Coppenolle et al. 2004) or in HeLa cells (Lang et al. 2012), observed as changed shape of the cytosolic Ca<sup>2+</sup> response to thapsigargin. The removal of the Sec61 $\alpha$  channel via silencing of *SEC61A1* gene on HeLa cells showed the decrease of the cytosolic TG-evoked Ca<sup>2+</sup> peak (Lang et al. 2011b). This was explained as the changed dynamics of Ca<sup>2+</sup> inside the cell, thus suggested as the decrease in ER Ca<sup>2+</sup> leak rate, as a result of Sec61 $\alpha$  removal. However, there has been no data of the direct observation of the Sec61 $\alpha$ -mediated Ca<sup>2+</sup> leak through the ER membrane. Creation of the HEK D1ER cell line (see 3.5, 3.6) allowed making silencing experiments and direct measurements of ER Ca<sup>2+</sup> with genetically encoded sensor D1ER (see 4.3). Despite the silencing of *SEC61A1* gene on HEK D1ER cells reached only 60% efficiency, my experiments show more than 40% reduction of the total basal ER Ca<sup>2+</sup> leakage rate (Figure 4.4). This can be explained as that the silencing of the life-important protein Sec61 $\alpha$  cannot be done completely, thus the many active translocons are still present on the ER membrane. Also for the chosen silencing protocol (see 3.7.3, and Figure 3.5) no significant change in basal ER Ca<sup>2+</sup> level was observed with only changed kinetics of thapsigargin response (Figure 4.4). Modulation of ER Ca<sup>2+</sup> leakage through the Sec61 $\alpha$  with direct observations of ER Ca<sup>2+</sup> allowed estimating its general impact in the Ca<sup>2+</sup> homeostasis (see 4.2, Figure 4.7). I tested the inhibition of the co-translational translocation with cycloheximide and emetine. Due to the previously proposed mechanisms of cycloheximide action, it arrests the elongation of the nascent polypeptide chain movement inside the lumen (Schneider-Poetsch et al. 2010). This was seen as an accumulation of the polyribosomes after the cycloheximide treatment. Effect on the cytosolic Ca<sup>2+</sup> was done on LNCaP cells and was

seen as the narrowed TG evoked cytosolic  $\text{Ca}^{2+}$  transient (Van Coppenolle et al. 2004). This indirectly led to the conclusion of inhibited  $\text{Ca}^{2+}$  leakage from the ER through the translocon. In my experiments (see 4.2, Figure 4.3, Figure 4.7) the incubation with cycloheximide resulted in the slowed kinetics of the TG-evoked depletion of ER  $\text{Ca}^{2+}$  in HEK D1ER cells. Emetine was also used as “closer” of Sec61 $\alpha$  (Lang et al. 2012), where the incubation with emetine has inhibitory effect on ER  $\text{Ca}^{2+}$  leakage. The mechanism of its action includes the inhibition of eIF2 $\alpha$  phosphorylation (Paredes et al. 2013) and therefore it is technically similar to the action of cycloheximide, leaving the polypeptide chain in the Sec61 $\alpha$  pore. Emetine was shown to reduce TG evoked increase of cytosolic  $\text{Ca}^{2+}$  and therefore inhibit the SOCE as a result of decreased store depletion rate (Ong et al. 2007). In my experiments both emetine and cycloheximide showed similar rate of the inhibition of ER basal rate. Cycloheximide and emetine showed each the inhibition of the ER  $\text{Ca}^{2+}$  leak rate of about 41-59% (see 4.2, Figure 4.7). This supports the theory that the polypeptide chain should seal the translocon (Wonderlin 2009). The complete cycle of the ribosome-translocon complex association-dissociation is not clear. According to the different theories the ribosome-nascent chain complex (RNC) is assembled in the cytosol and then brought by carriers to the translocon, where it associates with it and opens the translocon for polypeptide chain translocation (Zimmermann et al. 2011). However, (Potter et al. 2001) proposed that the large ribosomal subunit can be constantly associated with the translocon. I tested the effect of pactamycin, which supposed to prevent the assembly of the ribosomal nascent chain complex (RNC), therefore leaving the large ribosomal subunit free of polypeptide chain (Potter et al. 2001). I observed the increased  $\text{Ca}^{2+}$  efflux from the ER with the corresponding increase of cytosolic  $\text{Ca}^{2+}$ . The action of pactamycin was seen “online” directly after the application. It also enhances the kinetic of the thapsigargin response. Several evidences of the pactamycin effect have been already described (Ong et al. 2007). It was shown that pactamycin increases cytosolic  $\text{Ca}^{2+}$  level but only after PMCA was inhibited with lanthanides. Also pactamycin evoked a store-operated  $\text{Ca}^{2+}$  entry, which is the sign of ER depletion. The experiments with pactamycin showed that at some states of ribosomal association with the translocon the enhancement of ER  $\text{Ca}^{2+}$  leak exists and increases the total ER  $\text{Ca}^{2+}$  leak up to 175% (Figure 4.7). The direct observation of the puromycin effect on ER  $\text{Ca}^{2+}$  efflux was done in very few studies. For instance, it was shown that puromycin can evoke the ER depletion on LNCaP cells (Flourakis et al. 2006), which could be blocked by anisomycin.

In my experiments the incubation with puromycin evokes decrease of basal ER  $\text{Ca}^{2+}$ , which is in agreement with previous experiments (Lang et al. 2011b), also in direct luminal  $\text{Ca}^{2+}$  measurement puromycin enhances the leakage and therefore makes the kinetic of TG response faster (Figure 4.3, Figure 4.7). From another studies *in vitro* also known that the effect of puromycin on rough microsomes was terminal, representing that detaching microsomes inhibit the leakage through the translocon (Simon and Blobel 1991). But in cells, like it was also shown (Potter et al. 2001), the large ribosome subunit can remain attached to the translocon, therefore not breaking the additional leak evoked by puromycin. This resulted in the observed increased speed of thapsigargin response in my experiments (Figure 4.3, Figure 4.7). Luminal chaperone BiP is one of the key player in protein translocation (Preissler et al. 2015, Zimmermann et al. 2011). BiP seals the Sec61 $\alpha$  pore from the luminal side restricting the  $\text{Ca}^{2+}$  efflux. This was observed on HeLa cells using DTT and tunicamycin, which evoke UPR, and also after deletion of BiP (Schauble et al. 2012). I mobilized BiP by evoking amount of misfolded proteins with tunicamycin, which blocks the N-glycosylation of the newly synthesized polypeptides (Driscu et al. 1997). The effect was observed as slight conditional increase of the ER  $\text{Ca}^{2+}$  leak rate (see 4.4, Figure 4.5), presumably because tunicamycin doesn't work on the Sec61 $\alpha$  channel directly and also that other mechanisms of the inhibition of the translocon-mediated leak are still present. The co-chaperones of BiP were also tested to attenuate ER  $\text{Ca}^{2+}$  leakage. Here I tested the effect of silencing of luminal co-chaperones ERdj3 and ERdj6 on  $\text{Ca}^{2+}$  homeostasis. The silencing of both co-chaperones led to the increased leak of  $\text{Ca}^{2+}$  from the lumen, which I observed both in cytosolic and ER  $\text{Ca}^{2+}$  (Figure 4.12, (Schorr et al. 2015)). Therefore, the conclusion is that the disruption of folding machinery can impact  $\text{Ca}^{2+}$  homeostasis. The one explanation of the BiP effect on  $\text{Ca}^{2+}$ , is that BiP can be bound to the UPR receptor IRE-1 on  $\text{Ca}^{2+}$  dependent manner, which could facilitate the disassociation of these two proteins upon  $\text{Ca}^{2+}$  depletion and activation of IRE-1 receptor. Despite the  $\text{Ca}^{2+}$  concentration should drop severe, still the drop of local concentration nearby the opened translocon has been never studied. On the other hand, I tested the effect of CaM inhibition of ER  $\text{Ca}^{2+}$  leakage through the translocon from the cytosolic side. Previous data, with cytosolic  $\text{Ca}^{2+}$  measurements, proposed that inhibition of CaM should enhance ER  $\text{Ca}^{2+}$  leak (Erdmann et al. 2011). Trifluoperazine, the CaM inhibitor, enhanced the  $\text{Ca}^{2+}$  leakage from the ER about 2 fold (Figure 4.5). The total analysis of the all components described before showed that the

general role of Sec61a in steady state ER  $\text{Ca}^{2+}$  leakage is large: the inhibition of the leakage reduces the total basal leak up to 41% and openings of translocons could increase the total basal leak up to 185%. The similarity to which cycloheximide and emetine reduced ER  $\text{Ca}^{2+}$  leak and also the similarity between effects of pactamycin, puromycin and TFP, increasing the leak up to 175-185%, can speak from a certain “leaky” state of Sec61 $\alpha$  channel.

## 5.5 The cells should deal with Sec61 $\alpha$ -mediated $\text{Ca}^{2+}$ leak

As was mentioned before, the ER  $\text{Ca}^{2+}$  leak is counterbalanced by the SERCA and the cytosolic clearance mechanisms such as plasma membranes pumps and exchangers, and also mitochondria. In HEK293 cell line I have tested the action of puromycin on cytosolic  $\text{Ca}^{2+}$  (Figure 4.8) to identify the mechanisms, which counterbalance the Sec61 $\alpha$ -mediated  $\text{Ca}^{2+}$  leak. The increase of cytosolic  $\text{Ca}^{2+}$  was not observed after the inhibition of plasma membrane ion fluxes with  $\text{Gd}^{3+}$ . The destroying of mitochondrial IMM potential with CCCP, however, showed prolonged thapsigargin response after puromycin treatment. Combination of CCCP and  $\text{Gd}^{3+}$  resulted in higher thapsigargin peak of puromycin treated cells comparing to mock treated (Figure 4.8 D). These data favors the idea that mitochondria can actively absorb  $\text{Ca}^{2+}$  from the Sec61 $\alpha$ , however, the direct translocon-mitochondria connection is not known. On the other hand, mitochondrial position are various inside the cell (Park et al. 2001) therefore explaining the possibility of direct  $\text{Ca}^{2+}$  uptake from the “leaky” translocons. This may be a  $\text{Ca}^{2+}$  signal needed for stimulating ATP production, which is required for the further movement of polypeptide chains into the ER lumen (Zimmermann et al. 2011). And also during the pathological sustained leak,  $\text{Ca}^{2+}$  leak can be a signal for apoptosis (Hajnoczky et al. 2006). This data put the questions for the next research: how strong and how long the ER  $\text{Ca}^{2+}$  leakage from the Sec61 $\alpha$  can be in pathological conditions, and whether this leak is enough to disturb the whole cell  $\text{Ca}^{2+}$  homeostasis and induce apoptosis.

## 5.6 Two compounds mycolactone and eeyarestatin with previously unknown action on Sec61 $\alpha$ were tested in the present study

Mycolactone is a pathogenic toxin from *Mycobacterium ulcerans* (Sarfo et al. 2016, Walsh et al. 2008). It was shown that mycolactone inhibits translocation of the proteins with certain signal peptides through the ER membrane (Hall et al. 2014, McKenna et al. 2016). The proper incorporation of the RNC into the translocon seems to be impaired by mycolactone. However, I didn't see strong changes in Ca<sup>2+</sup> leakage from the ER immediately after mycolactone treatment, the effect was seen after some time, possibly due to the limited family of proteins, the synthesis of which mycolactone affects. However, the long-time incubation (from 6 hours up to overnight) led to the severe ER depletion. This leads to the conclusion that the intermediate state of RNC incorporation into the Sec61 $\alpha$  is also Ca<sup>2+</sup> leaky. Thapsigargin was also applied to estimate the changes in ER Ca<sup>2+</sup> leak after mycolactone treatment (Figures 4.13-4.16). The statistics of the mycolactone action presented on the Figure 4.17 show about 2 fold increase of the speed of thapsigargin responses, also favoring the idea of certain "leaky" state of Sec61 $\alpha$ . It leads to the preliminary conclusion that mycolactone can work directly on Sec61 $\alpha$ , thus affecting incorporation of the signal peptides into the Sec61 $\alpha$ . Additionally I tested Eeyarestatin1 and its several chemical analogues (Figure 4.18) whether they change Ca<sup>2+</sup> signalization (see 4.9). In my experiments short time treatment of HEK D1ER cells with ES1, ES2, and ES24 evoked Ca<sup>2+</sup> store depletion, while for ESr35 and ES47 the corresponding effect on Ca<sup>2+</sup> signalization was absent.

However, the full mechanism of Eeyarestatin1 action is unclear. It has been firstly proposed to inhibit ERAD via association with p97 (Wang et al. 2008). This was shown as an accumulation of poly-ubiquitinated substrates in the cytosol as a result of the inhibition of several deubiquitination pathways after 14 hours treatment with ES1. The deeper study of ES1 action on p97 inhibition was done due to separating putative functional compounds of ES1 molecule: nitrofuranyl moiety and aromatic domain. The nitrofuranyl moiety showed high cell toxicity while the aromatic domain was harmless in the proposed experiments. The closest analogue of ES1 to nitrofuranyl moiety, that I have tested, was ES24, which in my experiments evoked a much severe and faster Ca<sup>2+</sup> store depletion than ES1. This correlates fine with the before mentioned effects of the nitrofuranyl moiety of ES1. The aromatic domain was mentioned to lead ES1 to the ER

membrane, which was supposed just to “facilitate” the effect of ES1 (Wang et al. 2010). However, other studies showed the inhibition of protein transport into the ER lumen by ES1. The main target of ES1 was proposed Sec61 $\alpha$  complex (Cross et al. 2009). In that experiments ES1 did not block completely the protein synthesis rather led to the cytosolic accumulation of polypeptides, i.e. inhibited co-translational translocation. The model of action was proposed in the ES1 interaction between RNC and Sec61a complex during assembly of the RNC-translocon complex. Possibly, ES1 interacts with Sec61 $\alpha$  pore region stabilizing it in some intermediate state between completely closed state and normal functioning of the translocon. This can explain the fast Ca<sup>2+</sup> store depletion evoked by ES1. Another analogue of ES1, ES2 showed less potent effect on protein translocation and this correlates with my observation of a mild increase of the Ca<sup>2+</sup> leak from the ER. The molecule of ES2 is bigger than of ES1 in its aromatic region probably changing the binding affinity to Sec61 $\alpha$ . ESr35 is an ES1 analogue, which had no effect on protein translocation, also didn't change intracellular Ca<sup>2+</sup> signalization in my experiments. ESr35 lacks the nitrofuranyl moiety, and as the similar analog ES47 evoke no cytotoxicity. The analog ES47 of ES1 is similar to ESr35 but should provide better understanding; unlike ESr35 it lacks only NO<sub>2</sub> nitro part of nitrofuranyl moiety. But this is enough to impair its functioning both in the protein translocation and Ca<sup>2+</sup> signaling. Which part of the ES1 molecule interacts with Sec61a is an open question. It was suggested that nitrofuranyl moiety should work on p97 was proposed after long-time incubation with the ES1 (Wang et al. 2010). Unlike that, my experimental protocol suggests that ER Ca<sup>2+</sup> store depletion occurs already after first minutes of ES1 presence. The specificity of this action on Sec61 $\alpha$  was seen on HeLa cells experiments where the effects of ES1 and ES24 were lacking after silencing of *SEC61A1* gene. These data characterizes eeyarestatins and its analogues as novel tools for studying ER Ca<sup>2+</sup> leak associated with protein translocation.

## **5.7 The conclusions of this study can be presented as a model of Ca<sup>2+</sup> leak during secretory and membrane protein biosynthesis**

The Figure 5.2 shows that the protein transport through Sec61 $\alpha$  is a several step process, during each a Sec61 $\alpha$ -mediated Ca<sup>2+</sup> leak contributes to the steady state Ca<sup>2+</sup> leak.

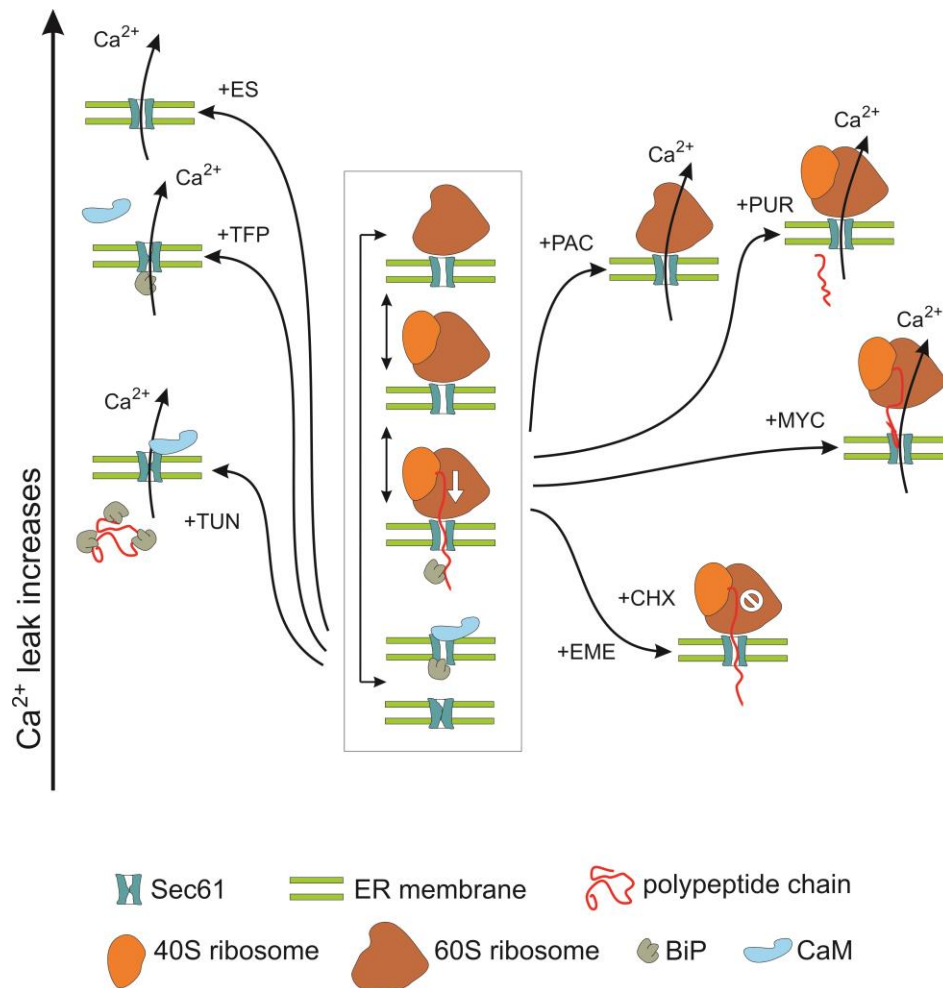


**Figure 5.2. Ca<sup>2+</sup> fluxes during secretory and membrane protein biosynthesis.** The protein translocation into the ER lumen (rectangle inlet in the middle) can be led to certain states (black arrows) with the corresponding relative increase of the ER Ca<sup>2+</sup> leak (y-axis). These states were achieved with eeyrestatin (ES), triflouperazine(TFP), tunicamycin (TUN), pactamycin (PAC), puromycin (PUR), mycilactone (MYC), cycloheximide (CHX) and emetine (EME).

The pathological states, like the UPR, at which BiP oligomerizes, or preceding the UPR an increased rate of protein production both lead to the increase of ER Ca<sup>2+</sup> leak rate. The action of toxins and chemicals like mycolactone and eeyrestatin also result in an enhancement of the ER Ca<sup>2+</sup> leak rate, making an important point that Sec61a can be treated directly turning into Ca<sup>2+</sup> leaky state. This might be an additional point on studying cell death and survival.

## 6 References

- Abell BM, Pool MR, Schlenker O, Sinning I, High S.** (2004). Signal recognition particle mediates post-translational targeting in eukaryotes. *EMBO J* 23: 2755-2764.
- Abell BM, Rabu C, Leznicki P, Young JC, High S.** (2007). Post-translational integration of tail-anchored proteins is facilitated by defined molecular chaperones. *J Cell Sci* 120: 1743-1751.
- Alder NN, Shen Y, Brodsky JL, Hendershot LM, Johnson AE.** (2005). The molecular mechanisms underlying BiP-mediated gating of the Sec61 translocon of the endoplasmic reticulum. *J Cell Biol* 168: 389-399.
- Amoroso S, De Maio M, Russo GM, Catalano A, Bassi A, Montagnani S, Renzo GD, Annunziato L.** (1997). Pharmacological evidence that the activation of the Na(+)-Ca<sup>2+</sup> exchanger protects C6 glioma cells during chemical hypoxia. *Br J Pharmacol* 121: 303-309.
- Annaert WG, Levesque L, Craessaerts K, Dierinck I, Snellings G, Westaway D, George-Hyslop PS, Cordell B, Fraser P, De Strooper B.** (1999). Presenilin 1 controls gamma-secretase processing of amyloid precursor protein in pre-golgi compartments of hippocampal neurons. *J Cell Biol* 147: 277-294.
- Appleby PA, Shabir S, Southgate J, Walker D.** (2013). Cell-type-specific modelling of intracellular calcium signalling: a urothelial cell model. *Journal of the Royal Society Interface* 10.
- Araki E, Oyadomari S, Mori M.** (2003). Impact of endoplasmic reticulum stress pathway on pancreatic beta-cells and diabetes mellitus. *Exp Biol Med (Maywood)* 228: 1213-1217.
- Atri A, Amundson J, Clapham D, Sneyd J.** (1993). A single-pool model for intracellular calcium oscillations and waves in the *Xenopus laevis* oocyte. *Biophys J* 65: 1727-1739.
- Basseri S, Lhotak S, Sharma AM, Austin RC.** (2009). The chemical chaperone 4-phenylbutyrate inhibits adipogenesis by modulating the unfolded protein response. *J Lipid Res* 50: 2486-2501.
- Becker T, Bhushan S, Jarasch A, Armache JP, Funes S, Jossinet F, Gumbart J, Mielke T, Berninghausen O, Schulten K, Westhof E, Gilmore R, Mandon EC, Beckmann R.** (2009). Structure of monomeric yeast and mammalian Sec61 complexes interacting with the translating ribosome. *Science* 326: 1369-1373.
- Bergling S, Dolmetsch R, Lewis RS, Keizer J.** (1998). A fluorometric method for estimating the calcium content of internal stores. *Cell Calcium* 23: 251-259.
- Berridge MJ.** (2010). Calcium hypothesis of Alzheimer's disease. *Pflugers Arch* 459: 441-449.
- Bers DM.** (2014). Cardiac Sarcoplasmic Reticulum Calcium Leak: Basis and Roles in Cardiac Dysfunction. *Annual Review of Physiology*, Vol 76 76: 107-127.
- Blankenship KA, Williams JJ, Lawrence MS, McLeish KR, Dean WL, Arthur JM.** (2001). The calcium-sensing receptor regulates calcium absorption in MDCK cells by inhibition of PMCA. *Am J Physiol Renal Physiol* 280: F815-822.
- Bobrovnikova-Marjon E, Grigoriadou C, Pytel D, Zhang F, Ye J, Koumenis C, Cavener D, Diehl JA.** (2010). PERK promotes cancer cell proliferation and tumor growth by limiting oxidative DNA damage. *Oncogene* 29: 3881-3895.
- Bonneau B, Prudent J, Popgeorgiev N, Gillet G.** (2013). Non-apoptotic roles of Bcl-2 family: the calcium connection. *Biochim Biophys Acta* 1833: 1755-1765.
- Brem GJ, Mylonas I, Bruning A.** (2013). Eeyarestatin causes cervical cancer cell sensitization to bortezomib treatment by augmenting ER stress and CHOP expression. *Gynecol Oncol* 128: 383-390.
- Brini M, Carafoli E.** (2009). Calcium Pumps in Health and Disease. *Physiological Reviews* 89: 1341-1378.
- Burnett JC, Rossi JJ.** (2012). RNA-based therapeutics: current progress and future prospects. *Chem Biol* 19: 60-71.
- Bygrave FL, Benedetti A.** (1996). What is the concentration of calcium ions in the endoplasmic reticulum? *Cell Calcium* 19: 547-551.
- Cain SM, Snutch TP.** (2013). T-type calcium channels in burst-firing, network synchrony, and epilepsy. *Biochim Biophys Acta* 1828: 1572-1578.

- Camello C, Lomax R, Petersen OH, Tepikin AV.** (2002). Calcium leak from intracellular stores--the enigma of calcium signalling. *Cell Calcium* 32: 355-361.
- Carafoli E, Brini M.** (2000). Calcium pumps: structural basis for and mechanism of calcium transmembrane transport. *Curr Opin Chem Biol* 4: 152-161.
- Catterall WA.** (2011). Voltage-Gated Calcium Channels. *Cold Spring Harbor Perspectives in Biology* 3.
- Chen L, Koh DS, Hille B.** (2003). Dynamics of calcium clearance in mouse pancreatic beta-cells. *Diabetes* 52: 1723-1731.
- Chen TW, Wardill TJ, Sun Y, Pulver SR, Renninger SL, Baohan A, Schreiter ER, Kerr RA, Orger MB, Jayaraman V, Looger LL, Svoboda K, Kim DS.** (2013). Ultrasensitive fluorescent proteins for imaging neuronal activity. *Nature* 499: 295-300.
- Chen Y, Liu CP, Xu KF, Mao XD, Lu YB, Fang L, Yang JW, Liu C.** (2008). Effect of taurine-conjugated ursodeoxycholic acid on endoplasmic reticulum stress and apoptosis induced by advanced glycation end products in cultured mouse podocytes. *Am J Nephrol* 28: 1014-1022.
- Chopra N, Kannankeril PJ, Yang T, Hlaing T, Holinstat I, Etensohn K, Pfeifer K, Akin B, Jones LR, Franzini-Armstrong C, Knollmann BC.** (2007). Modest reductions of cardiac calsequestrin increase sarcoplasmic reticulum Ca<sup>2+</sup> leak independent of lu510a1 Ca<sup>2+</sup> and trigger ventricular arrhythmias in mice. *Circulation Research* 101: 617-626.
- Clapham DE.** (2007). Calcium signaling. *Cell* 131: 1047-1058.
- Connolly T, Gilmore R.** (1989). The Signal Recognition Particle Receptor Mediates the Gtp-Dependent Displacement of Srp from the Signal Sequence of the Nascent Polypeptide. *Cell* 57: 599-610.
- Cross BC, McKibbin C, Callan AC, Roboti P, Piacenti M, Rabu C, Wilson CM, Whitehead R, Flitsch SL, Pool MR, High S, Swanton E.** (2009). Eeyarestatin I inhibits Sec61-mediated protein translocation at the endoplasmic reticulum. *J Cell Sci* 122: 4393-4400.
- Cullen PJ.** (2003). Calcium signalling: the ups and downs of protein kinase C. *Curr Biol* 13: R699-701.
- Cunha DA, Hekerman P, Ladriere L, Bazarra-Castro A, Ortis F, Wakeham MC, Moore F, Rasschaert J, Cardozo AK, Bellomo E, Overbergh L, Mathieu C, Lupi R, Hai T, Herchuelz A, Marchetti P, Rutter GA, Eizirik DL, Cnop M.** (2008). Initiation and execution of lipotoxic ER stress in pancreatic beta-cells. *J Cell Sci* 121: 2308-2318.
- Czabotar PE, Lessene G, Strasser A, Adams JM.** (2014). Control of apoptosis by the BCL-2 protein family: implications for physiology and therapy. *Nat Rev Mol Cell Biol* 15: 49-63.
- Demaurex N.** (2005). Calcium measurements in organelles with Ca<sup>2+</sup>-sensitive fluorescent proteins. *Cell Calcium* 38: 213-222.
- Dimopoulos MA, San-Miguel JF, Anderson KC.** (2011). Emerging therapies for the treatment of relapsed or refractory multiple myeloma. *European Journal of Haematology* 86: 1-15.
- Distelhorst CW, Bootman MD.** (2011). Bcl-2 interaction with the inositol 1,4,5-trisphosphate receptor: role in Ca(2+) signaling and disease. *Cell Calcium* 50: 234-241.
- Dricu A, Carlberg M, Wang M, Larsson O.** (1997). Inhibition of N-linked glycosylation using tunicamycin causes cell death in malignant cells: role of down-regulation of the insulin-like growth factor 1 receptor in induction of apoptosis. *Cancer Res* 57: 543-548.
- Dupont G, Combettes L, Bird GS, Putney JW.** (2011). Calcium oscillations. *Cold Spring Harb Perspect Biol* 3.
- Erdmann F, Jung M, Eyrisch S, Lang S, Helms V, Wagner R, Zimmermann R.** (2009). Lanthanum ions inhibit the mammalian Sec61 complex in its channel dynamics and protein transport activity. *FEBS Lett* 583: 2359-2364.
- Erdmann F, Schauble N, Lang S, Jung M, Honigmann A, Ahmad M, Dudek J, Benedix J, Harsman A, Kopp A, Helms V, Cavalie A, Wagner R, Zimmermann R.** (2011). Interaction of calmodulin with Sec61alpha limits Ca<sup>2+</sup> leakage from the endoplasmic reticulum. *EMBO J* 30: 17-31.
- Erickson MG, Alseikhan BA, Peterson BZ, Yue DT.** (2001). Preassociation of calmodulin with voltage-gated Ca(2+) channels revealed by FRET in single living cells. *Neuron* 31: 973-985.
- Evans-Molina C, Robbins RD, Kono T, Tersey SA, Vestermark GL, Nunemaker CS, Garmey JC, Deering TG, Keller SR, Maier B, Mirmira RG.** (2009). Peroxisome proliferator-

activated receptor gamma activation restores islet function in diabetic mice through reduction of endoplasmic reticulum stress and maintenance of euchromatin structure. *Mol Cell Biol* 29: 2053-2067.

**Fasolato C, Pizzo P, Pozzan T.** (1998). Delayed activation of the store-operated calcium current induced by calreticulin overexpression in RBL-1 cells. *Mol Biol Cell* 9: 1513-1522.

**Favaloro V, Spasic M, Schwappach B, Dobberstein B.** (2008). Distinct targeting pathways for the membrane insertion of tail-anchored (TA) proteins. *J Cell Sci* 121: 1832-1840.

**Fels DR, Koumenis C.** (2006). The PERK/eIF2alpha/ATF4 module of the UPR in hypoxia resistance and tumor growth. *Cancer Biol Ther* 5: 723-728.

**Feske S, Wulff H, Skolnik EY.** (2015). Ion Channels in Innate and Adaptive Immunity. *Annual Review of Immunology Vol 33* 33: 291-353.

**Flockerzi V.** (2007). An introduction on TRP channels. *Handb Exp Pharmacol*: 1-19.

**Flourakis M, Van Coppenolle F, Lehen'kyi V, Beck B, Skryma R, Prevarskaya N.** (2006). Passive calcium leak via translocon is a first step for iPLA2-pathway regulated store operated channels activation. *FASEB J* 20: 1215-1217.

**Forster T.** (1948). \*Zwischenmolekulare Energiewanderung Und Fluoreszenz. *Annalen Der Physik* 2: 55-75.

**Franzini-Armstrong C.** (2007). ER-mitochondria communication. How privileged? *Physiology (Bethesda)* 22: 261-268.

**Fritz JM, Dong M, Apsley KS, Martin EP, Na CL, Sitaraman S, Weaver TE.** (2014). Deficiency of the BiP cochaperone ERdj4 causes constitutive endoplasmic reticulum stress and metabolic defects. *Molecular Biology of the Cell* 25: 431-440.

**Fu S, Watkins SM, Hotamisligil GS.** (2012). The role of endoplasmic reticulum in hepatic lipid homeostasis and stress signaling. *Cell Metab* 15: 623-634.

**Gerasimenko O, Tepikin A.** (2005). How to measure Ca<sup>2+</sup> in cellular organelles? *Cell Calcium* 38: 201-211.

**Giorgi C, Baldassari F, Bononi A, Bonora M, De Marchi E, Marchi S, Missiroli S, Patergnani S, Rimessi A, Suski JM, Wieckowski MR, Pinton P.** (2012). Mitochondrial Ca(2+) and apoptosis. *Cell Calcium* 52: 36-43.

**Goldberg MW, Allen TD.** (1995). Structural and functional organization of the nuclear envelope. *Curr Opin Cell Biol* 7: 301-309.

**Graham FL, Smiley J, Russell WC, Nairn R.** (1977). Characteristics of a human cell line transformed by DNA from human adenovirus type 5. *J Gen Virol* 36: 59-74.

**Greotti E, Wong A, Pozzan T, Penden D, Pizzo P.** (2016). Characterization of the ER-Targeted Low Affinity Ca(2+) Probe D4ER. *Sensors (Basel)* 16.

**Griffiths EJ, Rutter GA.** (2009). Mitochondrial calcium as a key regulator of mitochondrial ATP production in mammalian cells. *Biochim Biophys Acta* 1787: 1324-1333.

**Grynkiewicz G, Poenie M, Tsien RY.** (1985). A new generation of Ca<sup>2+</sup> indicators with greatly improved fluorescence properties. *J Biol Chem* 260: 3440-3450.

**Guerrero-Hernandez A, Dagnino-Acosta A, Verkhratsky A.** (2010). An intelligent sarco-endoplasmic reticulum Ca<sup>2+</sup> store: release and leak channels have differential access to a concealed Ca<sup>2+</sup> pool. *Cell Calcium* 48: 143-149.

**Gulow K, Bienert D, Haas IG.** (2002). BiP is feed-back regulated by control of protein translation efficiency. *J Cell Sci* 115: 2443-2452.

**Gupta RS, Siminovitch L.** (1977). The molecular basis of emetine resistance in Chinese hamster ovary cells: alteration in the 40S ribosomal subunit. *Cell* 10: 61-66.

**Gwiazda KS, Yang TLB, Lin YL, Johnson JD.** (2009). Effects of palmitate on ER and cytosolic Ca<sup>2+</sup> homeostasis in beta-cells. *American Journal of Physiology-Endocrinology and Metabolism* 296: E690-E701.

**Hajnóczky G, Csordas G, Das S, Garcia-Perez C, Saotome M, Sinha Roy S, Yi M.** (2006). Mitochondrial calcium signalling and cell death: approaches for assessing the role of mitochondrial Ca<sup>2+</sup> uptake in apoptosis. *Cell Calcium* 40: 553-560.

**Hall BS, Hill K, McKenna M, Ogbechi J, High S, Willis AE, Simmonds RE.** (2014). The pathogenic mechanism of the Mycobacterium ulcerans virulence factor, mycolactone, depends on blockade of protein translocation into the ER. *PLoS Pathog* 10: e1004061.

- Hattori M, Suzuki AZ, Higo T, Miyauchi H, Michikawa T, Nakamura T, Inoue T, Mikoshiba K.** (2004). Distinct roles of inositol 1,4,5-trisphosphate receptor types 1 and 3 in Ca<sup>2+</sup> signaling. *J Biol Chem* 279: 11967-11975.
- Herrington J, Park YB, Babcock DF, Hille B.** (1996). Dominant role of mitochondria in clearance of large Ca<sup>2+</sup> loads from rat adrenal chromaffin cells. *Neuron* 16: 219-228.
- Honarnejad K, Herms J.** (2012). Presenilins: role in calcium homeostasis. *Int J Biochem Cell Biol* 44: 1983-1986.
- Hunding A, Ipsen M.** (2003). Simulation of waves in calcium models with 3D spherical geometry. *Math Biosci* 182: 45-66.
- Jensen RE, Johnson AE.** (1999). Protein translocation: Is Hsp70 pulling my chain? *Current Biology* 9: R779-R782.
- Johnson AE, van Waes MA.** (1999). The translocon: A dynamic gateway at the ER membrane. *Annual Review of Cell and Developmental Biology* 15: 799-842.
- Johnson N, Vilardi F, Lang S, Leznicki P, Zimmermann R, High S.** (2012). TRC40 can deliver short secretory proteins to the Sec61 translocon. *J Cell Sci* 125: 3612-3620.
- Kappen LS, Suzuki H, Goldberg IH.** (1973). Inhibition of reticulocyte peptide-chain initiation by pactamycin: accumulation of inactive ribosomal initiation complexes. *Proc Natl Acad Sci U S A* 70: 22-26.
- Kaufman RJ.** (2002). Orchestrating the unfolded protein response in health and disease. *J Clin Invest* 110: 1389-1398.
- Kim HW, Ch YS, Lee HR, Park SY, Kim YH.** (2001). Diabetic alterations in cardiac sarcoplasmic reticulum Ca<sup>2+</sup>-ATPase and phospholamban protein expression. *Life Sci* 70: 367-379.
- Kiryushko DV, Savtchenko LP, Verkhatsky AN, Korogod SM.** (2002). Theoretical estimation of the capacity of intracellular calcium stores in the Bergmann glial cell. *Pflugers Arch* 443: 643-651.
- Koivumaki JT, Takalo J, Korhonen T, Tavi P, Weckstrom M.** (2009). Modelling sarcoplasmic reticulum calcium ATPase and its regulation in cardiac myocytes. *Philosophical Transactions of the Royal Society a-Mathematical Physical and Engineering Sciences* 367: 2181-2202.
- Krajewski S, Tanaka S, Takayama S, Schibler MJ, Fenton W, Reed JC.** (1993). Investigation of the subcellular distribution of the bcl-2 oncoprotein: residence in the nuclear envelope, endoplasmic reticulum, and outer mitochondrial membranes. *Cancer Res* 53: 4701-4714.
- Krause KH.** (1991). Ca(2+)-storage organelles. *FEBS Lett* 285: 225-229.
- Kuhlbrandt W.** (2015). Structure and function of mitochondrial membrane protein complexes. *BMC Biol* 13: 89.
- Kurzchalia TV, Wiedmann M, Girshovich AS, Bochkareva ES, Bielka H, Rapoport TA.** (1986). The signal sequence of nascent preprolactin interacts with the 54K polypeptide of the signal recognition particle. *Nature* 320: 634-636.
- Lamb HK, Mee C, Xu W, Liu L, Blond S, Cooper A, Charles IG, Hawkins AR.** (2006). The affinity of a major Ca<sup>2+</sup> binding site on GRP78 is differentially enhanced by ADP and ATP. *J Biol Chem* 281: 8796-8805.
- Lang S.** (2012). Thesis: Charakterisierung der Funktionen und Regulationsmechanismen des humanen Sec61 Komplexes auf zellulärer Ebene; Saarland University, [http://scidok.sulb.uni-saarland.de/volltexte/2013/5308/pdf/PhD\\_Thesis\\_Sven\\_Lang\\_Version\\_Dekanat.pdf](http://scidok.sulb.uni-saarland.de/volltexte/2013/5308/pdf/PhD_Thesis_Sven_Lang_Version_Dekanat.pdf).
- Lang S, Schauble N, Cavalie A, Zimmermann R.** (2011a). Live cell calcium imaging combined with siRNA mediated gene silencing identifies Ca(2)(+) leak channels in the ER membrane and their regulatory mechanisms. *J Vis Exp*: e2730.
- Lang S, Erdmann F, Jung M, Wagner R, Cavalie A, Zimmermann R.** (2011b). Sec61 complexes form ubiquitous ER Ca<sup>2+</sup> leak channels. *Channels (Austin)* 5: 228-235.
- Lang S, Benedix J, Fedeles SV, Schorr S, Schirra C, Schauble N, Jalal C, Greiner M, Hassdenteufel S, Tatzelt J, Kreutzer B, Edelmann L, Krause E, Rettig J, Somlo S, Zimmermann R, Dudek J.** (2012). Different effects of Sec61 alpha, Sec62 and Sec63 depletion on transport of polypeptides into the endoplasmic reticulum of mammalian cells. *Journal of Cell Science* 125: 1958-1969.

- Laudon H, Hansson EM, Melen K, Bergman A, Farmery MR, Winblad B, Lendahl U, von Heijne G, Naslund J.** (2005). A nine-transmembrane domain topology for presenilin 1. *J Biol Chem* 280: 35352-35360.
- Levy J.** (1999). Abnormal cell calcium homeostasis in type 2 diabetes mellitus: a new look on old disease. *Endocrine* 10: 1-6.
- Lewis RS.** (2001). Calcium signaling mechanisms in T lymphocytes. *Annual Review of Immunology* 19: 497-521.
- Liang K, Du W, Lu J, Li F, Yang L, Xue Y, Hille B, Chen L.** (2014). Alterations of the Ca(2+)-signaling pathway in pancreatic beta-cells isolated from db/db mice. *Protein Cell* 5: 783-794.
- Lloyd DJ, Wheeler MC, Gekakis N.** (2010). A point mutation in Sec61alpha1 leads to diabetes and hepatosteatosis in mice. *Diabetes* 59: 460-470.
- Luciani DS, Gwiazda KS, Yang TL, Kalynyak TB, Bychkivska Y, Frey MH, Jeffrey KD, Sampaio AV, Underhill TM, Johnson JD.** (2009). Roles of IP3R and RyR Ca<sup>2+</sup> channels in endoplasmic reticulum stress and beta-cell death. *Diabetes* 58: 422-432.
- Luo SZ, Mao CH, Lee B, Lee AS.** (2006). GRP78/BiP is required for cell proliferation and protecting the inner cell mass from apoptosis during early mouse embryonic development. *Molecular and Cellular Biology* 26: 5688-5697.
- Mallilankaraman K, Cardenas C, Doonan PJ, Chandramoorthy HC, Irrinki KM, Golendar T, Csordas G, Madireddi P, Yang J, Muller M, Miller R, Kolesar JE, Molgo J, Kaufman B, Hajnoczky G, Foskett JK, Madesh M.** (2015). MCUR1 is an essential component of mitochondrial Ca(2+) uptake that regulates cellular metabolism. *Nat Cell Biol* 17: 953.
- Mariappan M, Li XZ, Stefanovic S, Sharma A, Mateja A, Keenan RJ, Hegde RS.** (2010). A ribosome-associating factor chaperones tail-anchored membrane proteins. *Nature* 466: 1120-U1138.
- McKenna M, Simmonds RE, High S.** (2016). Mechanistic insights into the inhibition of Sec61-dependent co- and post-translational translocation by mycolactone. *J Cell Sci* 129: 1404-1415.
- Mekahli D, Bultynck G, Parys JB, De Smedt H, Missiaen L.** (2011). Endoplasmic-reticulum calcium depletion and disease. *Cold Spring Harb Perspect Biol* 3.
- Mery L, Mesaeli N, Michalak M, Opas M, Lew DP, Krause KH.** (1996). Overexpression of calreticulin increases intracellular Ca<sup>2+</sup> storage and decreases store-operated Ca<sup>2+</sup> influx. *J Biol Chem* 271: 9332-9339.
- Mesaeli N, Nakamura K, Zvaritch E, Dickie P, Dziak E, Krause KH, Opas M, MacLennan DH, Michalak M.** (1999). Calreticulin is essential for cardiac development. *J Cell Biol* 144: 857-868.
- Miller DJ.** (2004). Sydney Ringer; physiological saline, calcium and the contraction of the heart. *Journal of Physiology-London* 555: 585-587.
- Montero M, Alonso MT, Albillos A, Garcia-Sancho J, Alvarez J.** (2001). Mitochondrial Ca(2+)-induced Ca(2+) release mediated by the Ca(2+) uniporter. *Mol Biol Cell* 12: 63-71.
- Mori MX, Imai Y, Itsuki K, Inoue R.** (2011). Quantitative Measurement of Ca<sup>2+</sup>-Dependent Calmodulin-Target Binding by Fura-2 and CFP and YFP FRET Imaging in Living Cells. *Biochemistry* 50: 4685-4696.
- Mothes W, Prehn S, Rapoport TA.** (1994). Systematic Probing of the Environment of a Translocating Secretory Protein during Translocation through the Er Membrane. *Embo Journal* 13: 3973-3982.
- Muller G, Zimmermann R.** (1987). Import of honeybee prepromelittin into the endoplasmic reticulum: structural basis for independence of SRP and docking protein. *EMBO J* 6: 2099-2107.
- Nakamura K, Bossy-Wetzell E, Burns K, Fadel MP, Lozyk M, Goping IS, Opas M, Bleackley RC, Green DR, Michalak M.** (2000). Changes in endoplasmic reticulum luminal environment affect cell sensitivity to apoptosis. *J Cell Biol* 150: 731-740.
- Nakamura K, Zuppin A, Arnaudeau S, Lynch J, Ahsan I, Krause R, Papp S, De Smedt H, Parys JB, Muller-Esterl W, Lew DP, Krause KH, Demaurex N, Opas M, Michalak M.** (2001). Functional specialization of calreticulin domains. *J Cell Biol* 154: 961-972.

- Nawrocki ST, Carew JS, Dunner K, Jr., Boise LH, Chiao PJ, Huang P, Abbruzzese JL, McConkey DJ.** (2005). Bortezomib inhibits PKR-like endoplasmic reticulum (ER) kinase and induces apoptosis via ER stress in human pancreatic cancer cells. *Cancer Res* 65: 11510-11519.
- Ngosuwan J, Wang NM, Fung KL, Chirico WJ.** (2003). Roles of cytosolic Hsp70 and Hsp40 molecular chaperones in post-translational translocation of presecretory proteins into the endoplasmic reticulum. *J Biol Chem* 278: 7034-7042.
- Ong HL, Liu X, Sharma A, Hegde RS, Ambudkar IS.** (2007). Intracellular Ca<sup>2+</sup> release via the ER translocon activates store-operated calcium entry. *Pflugers Arch* 453: 797-808.
- Osman AA, Saito M, Makepeace C, Permutt MA, Schlesinger P, Mueckler M.** (2003). Wolframin expression induces novel ion channel activity in endoplasmic reticulum membranes and increases intracellular calcium. *J Biol Chem* 278: 52755-52762.
- Oyadomari S, Mori M.** (2004). Roles of CHOP/GADD153 in endoplasmic reticulum stress. *Cell Death Differ* 11: 381-389.
- Palmer AE, Tsien RY.** (2006). Measuring calcium signaling using genetically targetable fluorescent indicators. *Nat Protoc* 1: 1057-1065.
- Palmer AE, Jin C, Reed JC, Tsien RY.** (2004). Bcl-2-mediated alterations in endoplasmic reticulum Ca<sup>2+</sup> analyzed with an improved genetically encoded fluorescent sensor. *Proc Natl Acad Sci U S A* 101: 17404-17409.
- Paredes RM, Bollo M, Holstein D, Lechleiter JD.** (2013). Luminal Ca<sup>2+</sup> depletion during the unfolded protein response in *Xenopus* oocytes: cause and consequence. *Cell Calcium* 53: 286-296.
- Parekh AB, Putney JW, Jr.** (2005). Store-operated calcium channels. *Physiol Rev* 85: 757-810.
- Park MK, Ashby MC, Erdemli G, Petersen OH, Tepikin AV.** (2001). Perinuclear, perigranular and sub-plasmalemmal mitochondria have distinct functions in the regulation of cellular calcium transport. *EMBO J* 20: 1863-1874.
- Periasamy A, Day RN,** eds. (2005). *Molecular imaging: FRET microscopy and spectroscopy*: Oxford University Press, Inc., ISBN-13 978-0-19-517720-6.
- Periasamy M, Bhupathy P, Babu GJ.** (2008). Regulation of sarcoplasmic reticulum Ca<sup>2+</sup> ATPase pump expression and its relevance to cardiac muscle physiology and pathology. *Cardiovasc Res* 77: 265-273.
- Pestka S.** (1971). Inhibitors of ribosome functions. *Annu Rev Microbiol* 25: 487-562.
- Pool MR.** (2005). Signal recognition particles in chloroplasts, bacteria, yeast and mammals (Review). *Molecular Membrane Biology* 22: 3-15.
- Potter MD, Seiser RM, Nicchitta CV.** (2001). Ribosome exchange revisited: a mechanism for translation-coupled ribosome detachment from the ER membrane. *Trends Cell Biol* 11: 112-115.
- Prakriya M.** (2013). Store-Operated Orai Channels: Structure and Function. *Store-Operated Calcium Channels* 71: 1-32.
- Preissler S, Chambers JE, Crespillo-Casado A, Avezov E, Miranda E, Perez J, Hendershot LM, Harding HP, Ron D.** (2015). Physiological modulation of BiP activity by trans-protomer engagement of the interdomain linker. *Elife* 4: e08961.
- Prins D, Michalak M.** (2011). Organellar calcium buffers. *Cold Spring Harb Perspect Biol* 3.
- Rabu C, Wipf P, Brodsky JL, High S.** (2008). A precursor-specific role for Hsp40/Hsc70 during tail-anchored protein integration at the endoplasmic reticulum. *J Biol Chem* 283: 27504-27513.
- Rabu C, Schmid V, Schwappach B, High S.** (2009). Biogenesis of tail-anchored proteins: the beginning for the end? *Journal of Cell Science* 122: 3605-3612.
- Rapiejko PJ, Gilmore R.** (1997). Empty site forms of the SRP54 and SR alpha GTPases mediate targeting of ribosome-nascent chain complexes to the endoplasmic reticulum. *Cell* 89: 703-713.
- Rapoport TA.** (2007). Protein translocation across the eukaryotic endoplasmic reticulum and bacterial plasma membranes. *Nature* 450: 663-669.
- Reid DW, Nicchitta CV.** (2015). Diversity and selectivity in mRNA translation on the endoplasmic reticulum. *Nat Rev Mol Cell Biol* 16: 221-231.
- Reimold AM, Iwakoshi NN, Manis J, Vallabhajosyula P, Szomolanyi-Tsuda E, Gravallesse EM, Friend D, Grusby MJ, Alt F, Glimcher LH.** (2001). Plasma cell differentiation requires the transcription factor XBP-1. *Nature* 412: 300-307.

- Reithinger JH, Kim JE, Kim H.** (2013). Sec62 protein mediates membrane insertion and orientation of moderately hydrophobic signal anchor proteins in the endoplasmic reticulum (ER). *J Biol Chem* 288: 18058-18067.
- Ringer S.** (1883). A further Contribution regarding the influence of the different Constituents of the Blood on the Contraction of the Heart. *J Physiol* 4: 29-42 23.
- Rong Y, Distelhorst CW.** (2008). Bcl-2 protein family members: versatile regulators of calcium signaling in cell survival and apoptosis. *Annu Rev Physiol* 70: 73-91.
- Ruggiano A, Foresti O, Carvalho P.** (2014). Quality control: ER-associated degradation: protein quality control and beyond. *J Cell Biol* 204: 869-879.
- Rutishauser J, Spiess M.** (2002). Endoplasmic reticulum storage diseases. *Swiss Medical Weekly* 132: 211-222.
- Ryu EJ, Harding HP, Angelastro JM, Vitolo OV, Ron D, Greene LA.** (2002). Endoplasmic reticulum stress and the unfolded protein response in cellular models of Parkinson's disease. *J Neurosci* 22: 10690-10698.
- Sarfo FS, Phillips R, Wansbrough-Jones M, Simmonds RE.** (2016). Recent advances: role of mycolactone in the pathogenesis and monitoring of *Mycobacterium ulcerans* infection/Buruli ulcer disease. *Cell Microbiol* 18: 17-29.
- Schauble N, Lang S, Jung M, Cappel S, Schorr S, Ulucan O, Linxweiler J, Dudek J, Blum R, Helms V, Paton AW, Paton JC, Cavalie A, Zimmermann R.** (2012). BiP-mediated closing of the Sec61 channel limits Ca<sup>2+</sup> leakage from the ER. *EMBO J* 31: 3282-3296.
- Scherer WF, Syverton JT, Gey GO.** (1953). Studies on the propagation in vitro of poliomyelitis viruses. IV. Viral multiplication in a stable strain of human malignant epithelial cells (strain HeLa) derived from an epidermoid carcinoma of the cervix. *J Exp Med* 97: 695-710.
- Schneider-Poetsch T, Ju J, Eyler DE, Dang Y, Bhat S, Merrick WC, Green R, Shen B, Liu JO.** (2010). Inhibition of eukaryotic translation elongation by cycloheximide and lactimidomycin. *Nat Chem Biol* 6: 209-217.
- Schorr S, Klein MC, Gamayun I, Melnyk A, Jung M, Schauble N, Wang Q, Hemmis B, Bochen F, Greiner M, Lampel P, Urban SK, Hassdenteufel S, Dudek J, Chen XZ, Wagner R, Cavalie A, Zimmermann R.** (2015). Co-chaperone Specificity in Gating of the Polypeptide Conducting Channel in the Membrane of the Human Endoplasmic Reticulum. *J Biol Chem* 290: 18621-18635.
- Shambharkar PB, Bittinger M, Latario B, Xiong Z, Bandyopadhyay S, Davis V, Lin V, Yang Y, Valdez R, Labow MA.** (2015). TMEM203 Is a Novel Regulator of Intracellular Calcium Homeostasis and Is Required for Spermatogenesis. *PLoS One* 10: e0127480.
- Shannon TR.** (2007). Linking calsequestrin to luminal control of SR Ca<sup>2+</sup> release. *Circulation Research* 101: 539-541.
- Shannon TR, Bers DM.** (1997). Assessment of intra-SR free [Ca] and buffering in rat heart. *Biophys J* 73: 1524-1531.
- Shannon TR, Bers DM.** (2004). Integrated Ca<sup>2+</sup> management in cardiac myocytes. *Cardiac Engineering: From Genes and Cells to Structure and Function* 1015: 28-38.
- Shannon TR, Ginsburg KS, Bers DM.** (2000). Reverse mode of the sarcoplasmic reticulum calcium pump and load-dependent cytosolic calcium decline in voltage-clamped cardiac ventricular myocytes. *Biophys J* 78: 322-333.
- Shannon TR, Ginsburg KS, Bers DM.** (2002). Quantitative assessment of the SR Ca<sup>2+</sup> leak-load relationship. *Circulation Research* 91: 594-600.
- Shannon TR, Wang F, Puglisi J, Weber C, Bers DM.** (2012). A mathematical treatment of integrated Ca dynamics within the ventricular myocyte (vol 87, pg 3351, 2004). *Biophysical Journal* 102: 1996-2001.
- Shao S, Hegde RS.** (2011). A calmodulin-dependent translocation pathway for small secretory proteins. *Cell* 147: 1576-1588.
- Simon SM, Blobel G.** (1991). A protein-conducting channel in the endoplasmic reticulum. *Cell* 65: 371-380.
- Solovyova N, Veselovsky N, Toescu EC, Verkhratsky A.** (2002). Ca<sup>2+</sup> dynamics in the lumen of the endoplasmic reticulum in sensory neurons: direct visualization of Ca<sup>2+</sup>-induced Ca<sup>2+</sup> release triggered by physiological Ca<sup>2+</sup> entry. *EMBO J* 21: 622-630.

- Somogyi R, Stucki JW.** (1991). Hormone-induced calcium oscillations in liver cells can be explained by a simple one pool model. *J Biol Chem* 266: 11068-11077.
- Stathopoulos PB, Ikura M.** (2013). Structure and function of endoplasmic reticulum STIM calcium sensors. *Curr Top Membr* 71: 59-93.
- Stefanovic S, Hegde RS.** (2007). Identification of a targeting factor for posttranslational membrane protein insertion into the ER. *Cell* 128: 1147-1159.
- Stewart AP, Smith GD, Sandford RN, Edwardson JM.** (2010). Atomic force microscopy reveals the alternating subunit arrangement of the TRPP2-TRPV4 heterotetramer. *Biophys J* 99: 790-797.
- Supnet C, Bezprozvanny I.** (2011). Presenilins function in ER calcium leak and Alzheimer's disease pathogenesis. *Cell Calcium* 50: 303-309.
- Suzuki J, Kanemaru K, Ishii K, Ohkura M, Okubo Y, Iino M.** (2014). Imaging intraorganellar Ca<sup>2+</sup> at subcellular resolution using CEPIA. *Nat Commun* 5: 4153.
- Szabadkai G, Simoni AM, Rizzuto R.** (2003). Mitochondrial Ca<sup>2+</sup> uptake requires sustained Ca<sup>2+</sup> release from the endoplasmic reticulum. *J Biol Chem* 278: 15153-15161.
- Tang L, Gamal El-Din TM, Payandeh J, Martinez GQ, Heard TM, Scheuer T, Zheng N, Catterall WA.** (2014). Structural basis for Ca<sup>2+</sup> selectivity of a voltage-gated calcium channel. *Nature* 505: 56-61.
- Taylor CW, Laude AJ.** (2002). IP<sub>3</sub> receptors and their regulation by calmodulin and cytosolic Ca<sup>2+</sup>. *Cell Calcium* 32: 321-334.
- Torrente AG, Zhang R, Zaini A, Giani JF, Kang J, Lamp ST, Philipson KD, Goldhaber JJ.** (2015). Burst pacemaker activity of the sinoatrial node in sodium-calcium exchanger knockout mice. *Proc Natl Acad Sci U S A* 112: 9769-9774.
- Traynelis SF, Wollmuth LP, McBain CJ, Menniti FS, Vance KM, Ogden KK, Hansen KB, Yuan H, Myers SJ, Dingledine R.** (2010). Glutamate receptor ion channels: structure, regulation, and function. *Pharmacol Rev* 62: 405-496.
- Van Coppenolle F, Vanden Abeele F, Slomianny C, Flourakis M, Hesketh J, Dewailly E, Prevarskaya N.** (2004). Ribosome-translocon complex mediates calcium leakage from endoplasmic reticulum stores. *J Cell Sci* 117: 4135-4142.
- Verkhratsky A.** (2005). Physiology and pathophysiology of the calcium store in the endoplasmic reticulum of neurons. *Physiol Rev* 85: 201-279.
- Verkhratsky A, Fernyhough P.** (2008). Mitochondrial malfunction and Ca<sup>2+</sup> dyshomeostasis drive neuronal pathology in diabetes. *Cell Calcium* 44: 112-122.
- Vilardi F, Lorenz H, Dobberstein B.** (2011). WRB is the receptor for TRC40/Asna1-mediated insertion of tail-anchored proteins into the ER membrane. *Journal of Cell Science* 124: 1301-1307.
- Villamil Giraldo AM, Lopez Medus M, Gonzalez Lebrero M, Pagano RS, Labriola CA, Landolfo L, Delfino JM, Parodi AJ, Caramelo JJ.** (2010). The structure of calreticulin C-terminal domain is modulated by physiological variations of calcium concentration. *J Biol Chem* 285: 4544-4553.
- Voeltz GK, Rolls MM, Rapoport TA.** (2002). Structural organization of the endoplasmic reticulum. *EMBO Rep* 3: 944-950.
- Voorhees RM, Fernandez IS, Scheres SHW, Hegde RS.** (2014). Structure of the Mammalian Ribosome-Sec61 Complex to 3.4 angstrom Resolution. *Cell* 157: 1632-1643.
- Walsh DS, Portaels F, Meyers WM.** (2008). Buruli ulcer (*Mycobacterium ulcerans* infection). *Trans R Soc Trop Med Hyg* 102: 969-978.
- Walter P, Blobel G.** (1983). Preparation of microsomal membranes for cotranslational protein translocation. *Methods Enzymol* 96: 84-93.
- Wang M, Kaufman RJ.** (2014). The impact of the endoplasmic reticulum protein-folding environment on cancer development. *Nat Rev Cancer* 14: 581-597.
- Wang Q, Li L, Ye Y.** (2008). Inhibition of p97-dependent protein degradation by Eeyarestatin I. *J Biol Chem* 283: 7445-7454.
- Wang Q, Shinkre BA, Lee JG, Weniger MA, Liu Y, Chen W, Wiestner A, Trenkle WC, Ye Y.** (2010). The ERAD inhibitor Eeyarestatin I is a bifunctional compound with a membrane-binding domain and a p97/VCP inhibitory group. *PLoS One* 5: e15479.

- Wang S, Kaufman RJ.** (2012). The impact of the unfolded protein response on human disease. *J Cell Biol* 197: 857-867.
- Watts C, Wickner W, Zimmermann R.** (1983). M13 procoat and a pre-immunoglobulin share processing specificity but use different membrane receptor mechanisms. *Proc Natl Acad Sci U S A* 80: 2809-2813.
- Weihofen A, Binns K, Lemberg MK, Ashman K, Martoglio B.** (2002). Identification of signal peptide peptidase, a presenilin-type aspartic protease. *Science* 296: 2215-2218.
- Weitzmann A, Baldes C, Dudek J, Zimmermann R.** (2007). The heat shock protein 70 molecular chaperone network in the pancreatic endoplasmic reticulum - a quantitative approach. *FEBS J* 274: 5175-5187.
- Whitaker M.** (2010). Genetically encoded probes for measurement of intracellular calcium. *Methods Cell Biol* 99: 153-182.
- Wonderlin WF.** (2009). Constitutive, translation-independent opening of the protein-conducting channel in the endoplasmic reticulum. *Pflugers Arch* 457: 917-930.
- Wong W, Bai XC, Brown A, Fernandez IS, Hanssen E, Condrón M, Tan YH, Baum J, Scheres SH.** (2014). Cryo-EM structure of the *Plasmodium falciparum* 80S ribosome bound to the anti-protozoan drug emetine. *Elife* 3.
- Yamada T, Ishihara H, Tamura A, Takahashi R, Yamaguchi S, Takei D, Tokita A, Satake C, Tashiro F, Katagiri H, Aburatani H, Miyazaki J, Oka Y.** (2006). WFS1-deficiency increases endoplasmic reticulum stress, impairs cell cycle progression and triggers the apoptotic pathway specifically in pancreatic beta-cells. *Human Molecular Genetics* 15: 1600-1609.
- Yamamoto Y, Sakisaka T.** (2012). Molecular Machinery for Insertion of Tail-Anchored Membrane Proteins into the Endoplasmic Reticulum Membrane in Mammalian Cells. *Molecular Cell* 48: 387-397.
- Zalk R, Lehnert SE, Marks AR.** (2007). Modulation of the ryanodine receptor and intracellular calcium. *Annu Rev Biochem* 76: 367-385.
- Zalk R, Clarke OB, des Georges A, Grassucci RA, Reiken S, Mancina F, Hendrickson WA, Frank J, Marks AR.** (2015). Structure of a mammalian ryanodine receptor. *Nature* 517: 44-49.
- Zhang C, Wu B, Beglopoulos V, Wines-Samuelson M, Zhang D, Dragatsis I, Sudhof TC, Shen J.** (2009). Presenilins are essential for regulating neurotransmitter release. *Nature* 460: 632-636.
- Zhang H, Sun S, Herreman A, De Strooper B, Bezprozvanny I.** (2010). Role of presenilins in neuronal calcium homeostasis. *J Neurosci* 30: 8566-8580.
- Zhou Y, Lee J, Reno CM, Sun C, Park SW, Chung J, Lee J, Fisher SJ, White MF, Biddinger SB, Ozcan U.** (2011). Regulation of glucose homeostasis through a XBP-1-FoxO1 interaction. *Nat Med* 17: 356-365.
- Zimmermann R, Eyrisch S, Ahmad M, Helms V.** (2011). Protein translocation across the ER membrane. *Biochim Biophys Acta* 1808: 912-924.
- Zimmermann R, Zimmermann M, Wiech H, Schlenstedt G, Müller G, Morel F, Klappa P, Jung C, Cobet WW.** (1990). Ribonucleoparticle-independent transport of proteins into mammalian microsomes. *J Bioenerg Biomembr* 22: 711-723.

## 7 Publications

Schorr S, Klein MC, **Gamayun I**, Melnyk A, Jung M, Schauble N, Wang Q, Hemmis B, Bochen F, Greiner M, Lampel P, Urban SK, Hassdenteufel S, Dudek J, Chen XZ, Wagner R, Cavalie A, Zimmermann R. (2015). Co-chaperone Specificity in Gating of the Polypeptide Conducting Channel in the Membrane of the Human Endoplasmic Reticulum. *J Biol Chem* 290: 18621-18635.

**Gamayun, I.**, Klein, M.-Ch., Lee, P.-H., Piacenti, M., Flitsch, S. L., Whitehead, R., Swanton, E., High, S., Helms, V., Zimmermann, R., Cavalié, A. (2017) Eeyarestatins selectively enhance Sec61-mediated  $\text{Ca}^{2+}$  leak from the endoplasmic reticulum. *In preparation.*

**Gamayun, I.**, Schorr, S., Zimmermann, R., Cavalié, A. (2017) Contribution of Sec61 complexes to the  $\text{Ca}^{2+}$  leak from endoplasmic reticulum in non-excitabile cells. *In preparation.*

### Conference abstracts:

- **Gamayun, Igor**; Klein, Marie-Christine; Schorr, Stefan; Dudek, Johanna; Jung, Martin; Zimmermann, Richard; Cavalié, Adolfo; “Modulation of the calcium leak through Sec61 complexes by small molecules” EMBO Conference: Structure and function of the endoplasmic reticulum. 23-27 October 2016, Girona, Spain
- **Gamayun, I.**, Schorr, S., Dudek, J., Zimmermann, R., Cavalié, A. “Mechanism of  $\text{Ca}^{2+}$  leak from endoplasmic reticulum.” Joint German-Israeli Network Meeting March 26th - 27th 2015, Homburg(Saarland), Germany
- **Gamayun, I.**, Schorr, S., Dudek, J., Zimmermann, R., Cavalié, A. “Mechanism of  $\text{Ca}^{2+}$  leak from endoplasmic reticulum.”. Cell Physics 2014, 23.09-26.09.2014, Saarland University, Saarbrücken
- **Gamayun, I.**, Kravchenko, M., Schorr, S., Zimmermann, R., Cavalié, A. “Calcium leak induced by puromycin via opening of the Sec61 channel complex.” SFB894 Meeting 2012 Calcium Signalling: Molecular Mechanisms and Integrative Functions 06.-08. September 2012 Saarland University, Homburg, Germany

## 8 Acknowledgements

I am very happy to acknowledge people who helped me to accomplish this study.

I am very grateful to Prof. Dr. Adolfo Cavalié for inviting me and giving me an opportunity to work in his laboratory, for his supervision, support and suggestions during the whole period of my work.

Also to Prof. Dr. Richard Zimmermann for his support, brilliant ideas, brainstorming and discussions, which made this project comprehensive and relevant.

Dr. Rachel Simmonds and Prof. Stephen High for sharing their ideas and letting me an opportunity to work on very interesting projects with new compounds.

The entire Pharmacology department, where this project was done, and personally to Prof. Veit Flockerzi, Dr. Andreas Beck, PD Dr Stephan Phillipp, and PD Dr. Ulrich Wissenbach for giving me a support and enlightening views on the project.

To the technical assistance of the Pharmacology department for showing me the principles of the fastest achieving of my aims: Martin Simon-Thomas, Karin Wolske, Heidi Löhr, and Stefanie Buchholz, as well as to our secretary Julia Schmidt.

I want to say thank you to my brother Dr. Oleksandr Gamayun for continuous and enormous support during the whole period of my research, for his suggestions and discussions of the critical moments in the study.

My colleagues from the Medical Biochemistry department and the Pharmacology department: Dr. Stefan Schorr, Prof. Martin Jung, Marie-Christine Klein, Dr. Sven Lang, Dr. Nico Scheuble, Armin Melnyk, Tillman Pick and René Tinschert, with you it was really interesting and pleasant to work.

To my dearest friends and also former colleagues who made not only my work pleasant but also my life interesting and bright during this research period: Anna Holderbaum, Dr. Pascal Schalkowsky, Dr. Jessica Welter, Tobi Lüdeke, Andreas Helfer, Dr. Cristof Störger, Dr. Antonio Yarsagaray, Dr. Sandeep Dembla, Oleksandr Rizoun, Dr. Mykola Kravchenko.

Finally my special thanks are to my beloved parents Volodymyr and Natalia Gamayun, who always believe in me and support me on my way. Thanks a lot!